

**MOLECULAR MODELLING AND SCREENING OF
ANDROGEN RECEPTOR LIGANDS TO TREAT PROSTATE
CANCER**



A THESIS

Submitted to

***The Tamil Nadu Dr.MGR Medical University,
Chennai***

*In the partial fulfillment of the requirements for
the award of the degree of*

DOCTOR OF PHILOSOPHY

In

Faculty of Pharmacy & Pharmaceutical Sciences

By

**S. DIVAKAR, M. Pharm.,
(Reg. No. 141340505)**

Under the guidance of

**Dr. M. RAMANATHAN, M.Pharm., Ph.D.
Professor and Head
Department of Pharmacology
PSG College of Pharmacy
Coimbatore**

June 2017

**Dr. M. RAMANATHAN, M.Pharm., PhD.,
Professor and Head,
Department of Pharmacology,
PSG College of Pharmacy,
Coimbatore.**

Certificate

This is to certify that the Ph.D. thesis entitled “**MOLECULAR MODELLING AND SCREENING OF ANDROGEN RECEPTOR LIGANDS TO TREAT PROSTATE CANCER**” being submitted to the Tamil Nadu Dr. MGR Medical University, Chennai, for the award of degree of **DOCTOR OF PHILOSOPHY in PHARMACY & PHARMACEUTICAL SCIENCES** was carried out by **S. DIVAKAR** at PSG College of Pharmacy, Peelamedu, Coimbatore, under my direct supervision and guidance to my fullest satisfaction. The contents of this thesis, in full or in parts, have not been submitted to any other Institute or University for the award of any degree or diploma.

Dr. M. RAMANATHAN, M.Pharm., Ph.D.

(Supervisor & Guide)

Place:Coimbatore

Date:

**Dr. V. Sankar, M. Pharm, PhD.,
Professor and Head,
Department of Pharmaceutics,
PSG College of Pharmacy,
Coimbatore.**

Certificate

This is to certify that the Ph.D. thesis entitled “**MOLECULAR MODELLING AND SCREENING OF ANDROGEN RECEPTOR LIGANDS TO TREAT PROSTATE CANCER**” being submitted to the Tamil Nadu Dr. MGR Medical University, Chennai, for the award of degree of **DOCTOR OF PHILOSOPHY** in **PHARMACY & PHARMACEUTICAL SCIENCES** was carried out by **S. DIVAKAR** at Department of Pharmaceutics, PSG College of Pharmacy, Coimbatore, under the direct supervision and guidance of **Dr. M. RAMANATHAN, M. Pharm., Ph.D.**, Professor & Head, Department of Pharmacology, PSG College of Pharmacy, Coimbatore.

**Dr. V. Sankar, M. Pharm, PhD.,
(Center Head)**

Place:Coimbatore

Date:

DECLARATION

I hereby certify that I am the sole author of this thesis entitled **“MOLECULAR MODELLING AND SCREENING OF ANDROGEN RECEPTOR LIGANDS TO TREAT PROSTATE CANCER”** and that neither any part of this thesis nor the whole of the thesis has been submitted for a degree to any other University or Institution. I certify that, to the best of my knowledge, my thesis does not infringe upon anyone’s copyright nor violate any proprietary rights and that any ideas, techniques, quotations, or any other material from the work of other people included in my thesis, published or, are fully acknowledged in accordance with the standard referencing practices. I declare that this is a true copy of my thesis, including any final revisions, as approved by my thesis review committee.

S. Divakar, M. Pharm.,

Place: Coimbatore

Date:

Acknowledgements

ACKNOWLEDGEMENTS

It is privilege to give my foremost and my special thanks to my Lovable Family, without those unconditional love and support, this process of my learning would have been incomplete and they are the backbone for all successful endeavours in my life.

*I express my sincere guileless and substantive gratitude to my dynamic and cheerful guide **Dr. M. Ramanathan, M.Pharm., Ph.D.**, Principal, PSG College of pharmacy, Coimbatore, for the intellectual focus and pragmatic flavour he has given to initiate this work. I admire the most ultimate freedom he imparts me to put my desire and thoughts into practical works during this project.*

*I am thankful to **Dr. V. Sankar, M.Pharm., Ph.D.**, Head of the Pharmaceutical Departemnt, PSG College of pharmacy, Coimbatore, for providing me necessary facilities to complete my thesis work.*

*I am thankful to **Dr. S. Kabilan, M.Sc, Ph.D.**, Dean, Faculty of Science, Annamalai University, Chidambaram, **Dr. K. K. Balasubramanian, M.Sc, PhD**, Professor, Department of Biotechnology, IIT, Madras and **P. Karthikeyan**, Senior scientist, Shasun Research Centre, Chennai, for providing the synthesized compounds for my thesis work.*

*I extend my heart full thanks to **Dr. R. Ranjith kumar, M.Pharm, Ph.D**, Associate Professor, PSGCOP, Coimbatore, **Dr. Sivaram Hariharan, M.Pharm, Ph.D**, Asst. prof, PSG COP, Coumbatore, **Dr. Shah Darshitkumar Bharatkumar, M.Pharm, PhD**, Research Associate, Aurobindo biologicals, Hyderabad, **Dr. B. Balaji, M. Pharm., Ph.D.**, Assistant Manager, Hospira, Chennai, **Mr. M. Siva Selva Kumar, M.Pharm, Assistant Professor, PSGCOP, Coimbatore**, **Dr. K. Saravanan, M.Sc, PhD.**, Scientist, Gland Pharma, Hyderabad, **Dr. S. Prathap Balaji, M. Tech., Ph.D.**, Post Doctoral Research Fellow Islet Cell lab, Dallas,*

PSG College of Pharmacy, Coimbatore.

Acknowledgements

Texas, **R. Elencheran, M.Sc**, Research Associate, IASST, Guwahati, **Mr. K. Raghavan**, Asst prof, PSGCOP, Coimbatore, and **Mr. G. Venkatesh**, Asst prof, PSGCOP, Coimbatore for their guidance and for their timely suggestions and constant support during the period of work.

I would also like to thank my fellow lab members **Mr. Siram Karthik, Mr. Ravikumar Rajan, Mr. Mrinmoy Gautam, Mr. Abdul Khayum and Mr. Arjun** who have helped and created a wonderful, positive and cheerful working environment together.

I am very much indebted to all Non-teaching staffs specially **Mr. Y. Asadhkumar, Mrs. K. Ambika, Mrs. S. Sugana, and Mrs. S. Chithrapriya** of our college for their timely help and constant support during the entire period of work.

Finally I wish to thank one and all who directly and indirectly helped me for the successful completion of my thesis.

Above all, I humbly submit my dissertation work, into the hands of **Almighty**, who is the source of all wisdom and knowledge for the successful completion of my thesis.

Table of Contents

CHAPTER	CONTENTS	PAGE
1	INTRODUCTION	1
2	AIM AND OBJECTIVES	7
3	LITERATURE REVIEW	8
4	PLAN OF WORK	46
5	MATERIALS	48
6	EXPERIMENTAL METHODS	50
	6.1. Phase 1 - To analyse the ligand/protein interactions between the wild and mutant ARs	50
	6.1.1. Root Mean Square deviation between wild and mutant ARs	50
	6.1.2. Analysis of the ligand binding pocket of wild and mutant ARs	50
	6.1.3. Elucidation of the binding mechanism of AR antagonist	53
	6.2. Phase 2 - To develop a pharmacophore model for wild and mutant AR antagonists and to identify difference between the pharmacophore models	54
	6.2.1. Data set preparation for wild, T877A and full antagonists	54
	6.2.2. Ligand preparation	55
	6.2.3. Pharmacophore generation for wild, T877A and full	55

Table of Contents

	antagonists	
	6.2.4. Selection and validation of the Models	57
	6.3. Phase 3 - Identification of new chemical entities through <i>in-silico</i> drug design methods	58
	6.3.1. <i>In-silico</i> virtual screening (Pharmacophore matching and docking)	58
	6.4. Phase 4: <i>In-vitro</i> anti prostate cancer activity of the new chemical entities to identify the hit molecules	58
	6.4.1. <i>In-vitro</i> anti-proliferation assay	58
	6.4.2. Screening for prostate cancer bio-markers	59
	6.5. Phase 4 - Elucidation of the mechanism of action of the best active molecule	63
	6.5.1. Gene expression	64
	6.5.2. Protein expression of AR and AKT1	65
	6.5.3. Apoptosis assays	66
7	RESULTS	69
	7.1. Phase 1 - To analyse the ligand/protein interactions between the wild and mutant ARs	69
	7.1.1. Purpose of the study	69
	7.1.2. Root Mean Square deviation between wild and mutant ARs	69
	7.1.3. Analysis of the ligand binding pocket of wild and	70

Table of Contents

	mutant ARs	
	7.1.4. Elucidation of the binding mechanism of AR antagonists	76
	7.2. To develop a pharmacophore model for wild and mutant AR antagonists and to identify difference between the pharmacophore models	77
	7.2.1. Purpose of the study	77
	7.2.2. Data set preparation for wild, T877A and full antagonists (wild and T877A)	78
	7.2.3. Pharmacophore generation for wild, T877A and full antagonists (wild and T877A mutant)	79
	7.2.4. Similarities and differences between the wild and T877A mutant pharmacophores	96
	7.3. Phase 3 - Identification of new chemical entities through <i>in-silico</i> drug design methods	98
	7.3.1. Purpose of the study	98
	7.3.2. Drug Design	99
	7.4. <i>In-vitro</i> anti prostate cancer activity of the new chemical entities to identify the hit molecules	105
	7.4.1. Purpose of the study	105
	7.4.2. Structure of different cells and their morphology	106
	7.4.3. Evaluation of anti-proliferation activity in AR	106

Table of Contents

	positive and negative cell lines	
	7.4.4. Structural activity relationship	110
	7.4.5. Gene expression of AR response elements	111
	7.5. Phase 4 - Elucidation of the mechanism of action of the best active molecule	113
	7.5.1. Purpose of the study	113
	7.5.2. Gene expression of androgen induced oncogenes	113
	7.5.3. Protein expression of AR and AKT1	116
	7.5.4. Apoptotic assays	117
8	DISCUSSION	122
9	SUMMARY AND CONCLUSION	136
10	IMPACT OF STUDY	137
	REFERENCES	
	ANNEXURES	
	ANNEXURE 1: Plagiarism report	
	ANNEXURE 2: Conference Certificate	
	ANNEXURE 3: List of publications	
	ANNEXURE 4: Ethical committee certificate	

List Of Tables

LIST OF TABLES

TABLES	TITLE	PAGE
1	AR antagonist and the resistance causing mutation	4
2	Classification of drugs used to treat prostate cancer	13
3	Drugs in clinical trials for the treatment of prostate cancer	14
4	Frequency of AR mutations in AIPC	20
5	Materials list	48
6	Thermal conditions for cDNA synthesis	62
7	Primers for prostate cancer biomarkers	62
8	Thermal conditions for qPCR	62
9	Primers of oncogenes	64
10	Thermal conditions for qPCR	64
11	List of antibodies for western blot	66
12	Primers for apoptosis biomarkers	67
13	Thermal conditions for qPCR	67
14	RMSD between wild and mutant ARs	70
15	Docking score and H-Bond interaction of AR standard ligands	72
16	Validation of training set	79
17	Validation of test set	80
18	Angle and distances between pharmacophore site points of wild type AR antagonist	82

List Of Tables

19	19a: Observed and predicted activity of bicalutamide derivatives	83
	19b: Observed and predicted activity of enzalutamide derivatives	86
20	Angle and distances between T877A mutant pharmacophore site points	89
21	Distance and angle between full antagonist pharmacophore site points	92
22	22a. Observed and predicted activity of 1-arylmethyl-4-phenylpyrrole derivatives	93
	22b. Observed and predicted activity of 4-arylmethyl-1-phenylpyrazole derivatives	94
	22c: Observed and predicted activity of 4-aryloxy-1-phenylpyrazole derivatives	95
	22d: Observed and predicted activity of 3-aryl-3-hydroxy-1-phenylpyrrolidine derivatives	95
23	Docking score and H-Bond interactions of tested and standard ligands	104
24	Bioactivity of tested and standard compounds	108
25	Selectivity of tested and standard compounds	109

List Of Figures

LIST OF FIGURES

FIGURE	TITLE	PAGE
1	Recently identified AR antagonist hit molecules	16
2	<i>De-novo</i> synthesis of androgen	17
3	AR/AKT interaction in prostate cancer	23
4	AR/GSK3 β / β -Catenin signalling in prostate cancer	25
5	AR as central dogma in androgen independent prostate cancer	27
6	Functional domains of AR	29
7	Ligand binding domain of the AR	34
8	Activation of AR by androgens	36
9	Ligand dependant non-genomic pathway of AR	39
10	Classification of non steroidal AR antagonist	40
11	Computer aided drug design methods	43
12	Virtual screening workflow for the identification of HIT molecules	44
13	Scaffolds of the dataset molecules for pharmacophore modelling	55
14	Binding interactions of androgens with AR	71
15	Interactions of flutamide with wild and T877A mutant ARs	74
16	Binding interactions of bicalutamide and enzalutamide with AR	75

List Of Figures

17	Binding conformation of bicalutamide with wild (helix-12 negative) and W741L mutated AR	77
18	Pharmacophore of wild type AR antagonist	81
19	Correlation between observed and predicted activity of wild type AR antagonist	87
20	Pharmacophore of T877A mutant AR antagonist	88
21	Correlation between observed and predicted activity of T877A mutant AR antagonist	90
22	Pharmacophore of wild and T877A AR antagonists	91
23	Correlation between observed and predicted activity of wild and T877A mutant AR antagonists pharmacophore	96
24	2D diagram representing the differences between the pharmacophores	97
25	Figure 25: AR as central dogma in AIPC (From literature review)	99
26	Pharmacophore matched compounds	101
27	<i>In-silico</i> drug design workflow	102
28	Docking interactions of best hit molecules	104
29	Morphology of AR positive and negative cell lines	106
30	Bioactivity of the tested and standard compounds	107
31	Gene expression of AR response elements with melt curves	112
32	Gene expression of oncogenes with melt curves	114

List Of Figures

33	Gene expression of AR and PS2 with melt curves	115
34	Protein expression of AR and AKT1	116
35	BAX/Bcl2 mRNA ratio with melt curves	118
36	Caspase activity	119
37	Fluorescence image of ARA3 treated LNCaP cells	120
38	Phase contrast image of ARA3 treated LNCaP cells	121
39	Anti-prostate cancer mechanism of ARA3 in AIPC cells	134

Abbreviations

ABBREVIATIONS

Dihydrotestosterone (DHT), Androgen receptor (AR), Activation function 1 (AF - 1), Activation function 2 (AF - 2), Steroid receptor co-activator - 1 (SRC-1), Transcriptional intermediary factor-2 (TIF2), p300/cAMP (cyclic adenosine mono-phosphate) response element binding protein (CREB), Castration resistant prostate cancer (CRPC), Androgen independent prostate cancer (AIPC), T877A (threonine to alanine), ETS (erythroblast transformation-specific), ERG (ETS-related gene), ETV1 (ETS translocation variant 1), TMPRSS2 (transmembrane protease serine 2), Protein data bank (PDB), Epithelial mesenchymal transition (EMT), Prostate specific antigen (PSA), Prostate cancer antigen 3 (PCA3), GnRH: Gonadotropin releasing hormone, T877A (threonine to alanine), T877S (threonine to serine), V715M (valine to methionine), A721T (alanine to threonine), N756D (asparagine to aspartic acid), H874Y (histidine to tyrosine), W741C (tryptophan to cysteine), W741L (tryptophan to leucine), D879G (aspartic acid to glycine), F876L (Phenyl alanine to leucine), PTEN (Phosphatase and tensin homolog), PI3K/AKT (Phosphatidylinositol 3-kinase/ Protein kinase B), GSK3 β (Glycogen synthase kinase), T-cell factor (TCF), Lymphoid enhancer factor 1 (LEF1), Variable N-terminal domain (NTD), DNA binding domain (DBD), Ligand binding domain (LBD), C - terminal extension (CTE), Hormone response element (HRE), AR response elements (AREs), Estrogen receptor response element (ERE), Nuclear localization signal (NLS), Nuclear export signal (NES), Heat shock proteins (HSP), protein kinase C (PKC), The mitogen-activated protein kinase (MAPK), Extracellular signal-regulated kinase (ERK), Apalutamide

Abbreviations

(ARN-509), Structure based drug design (SBDD), Ligand based drug design (LBDD), COX (Cyclooxygenase), Root mean square deviation (RMSD), Water molecule (HOH), Glide Score (G Score), Structural analysis and verification server (SAVES), Common pharmacophore hypotheses (CPH), Hydrogen bond acceptors (A), Hydrogen bond donor (D), Hydrophobicity (H), Aromatic rings (R), positively ionizable groups (P), Negatively ionizable groups (N), Partial least squares (PLS), Ethidium bromide/acridine orange (EB/AO) staining, H-Bond (Hydrogen bond), EREs (estrogen receptor response elements).

Chapter 1: Introduction

1. INTRODUCTION

1.1. Prostate cancer

Adenocarcinoma of prostate gland is the second most frequent cancer and sixth leading cause of mortality in males. The growth, development, and homeostasis of the prostate gland are under the control of androgens. Androgens, dihydrotestosterone (DHT) and testosterone bind with the androgen receptor (AR) and stimulate the growth of the prostate gland. The proliferation of the prostate gland occurs significantly during the time of puberty and after that, the androgens continue to play an important role in maintaining the homeostasis of the prostate gland. In some men, with increasing age, androgen dependent proliferation of the prostate gland resumes, resulting in benign prostatic hyperplasia or malignant prostate cancer [1]. The AR antagonists competitively prevent the binding of androgens with AR. So, they are used in the treatment of prostate cancer [2].

1.2. Structure and activation mechanism of AR

The AR has 900-920 amino acids and the variations in the amino acid number are due to the polymorphism in the length of polyglutamine (CAG repeats) and polyglycine (GGN repeats) tracts in the first exon. The AR was also divided into 4 regions such as variable N-terminal domain or activation function 1 (AF - 1), DNA binding domain, hinge region, and ligand binding domain (LBD) or activation function 2 (AF - 2) [3]. The ligand binding domain has twelve α helices and two β sheets that fold to form a hydrophobic ligand binding pocket to which the androgens bind. The helix-12 of the AR is the highly flexible and functions as a gate for the entry of ligands. Helix 3, 4, 5, and 10 are the primary

Chapter 1: Introduction

contact sites for androgens. The helix 3, 4 and 12 are the primary contact sites for co-activators. The binding of androgens with AR largely remains hydrophobic interactions with amino acids Val746, Met742, Gln711, Met745, Leu707, Leu704, and Trp741. The hydrogen bond interactions with amino acids, Arg752, Gln711, Asn705, Asn704 and Thr877 also play a critical role in the specific binding of androgens to AR [4]. The AR agonists and antagonists bind to the same binding pocket but with one major difference between them. The AR antagonists were bulkier molecules than the agonist and because of this the AR antagonists prevent the closing of the helix-12 towards the ligand binding domain [5]. It attains an open and closed conformation in response to antagonist and agonist respectively. The closed conformation (agonist) favours interaction with co-activators. The open conformation (antagonist) prevents the interaction of helix-12 with co-activators and favours the interaction with co-repressors [6].

The Androgen binding causes the helix-12 to lie over the ligand binding pocket, which will reveal the domain for intramolecular AF-1 and AF-2 interaction (N/C terminal interaction). The N/C terminal interaction is specific to AR. The N/C terminal interaction will lead to cascade of events like phosphorylation, dimerization, nuclear translocation, binding to specific AR response elements, co-activator recruitment, and initiation of transcription. Class 1 family of co-activators such as steroid receptor co-activator - 1 (SRC-1) and 3, transcriptional intermediary factor-2 (TIF2) and class 2 family of co-activators such as, p300/cAMP (cyclic adenosine mono-phosphate) response element binding protein (CREB) regulates the transcriptional activity of AR. The co-

Chapter 1: Introduction

activators de-condense the chromatin and facilitate the binding of RNA polymerase for the initiation of transcriptional mechanism [3, 7].

1.3. Castration resistant prostate cancer

The hormonal therapy largely becomes ineffective and most of the prostate cancer relapses after a treatment median of 18-24 months. The relapsed prostate cancer is known as castration resistant prostate cancer (CRPC). The CRPC could be either androgen dependant or androgen independent prostate cancer (AIPC) [8, 9]. In case of androgen dependant CRPC, the enzymes involved in the synthesis of androgens were over expressed which lead to the increase in the intracrine androgen level. The androgen dependant CRPC could be controlled by drugs which inhibit the synthesis of androgens [9, 10]. The AIPC doesn't depend on androgens for proliferation; instead it adapts various mechanisms to neutralize the hormonal therapy. Clinically, AIPC is defined as the ability of the prostate cancer cells to grow in the castrated plasma levels of androgen. The occurrence of point mutation in the ligand binding domain of the AR was one of the major reasons behind the development of AIPC [11].

1.4. AR mutations

The mutation at amino acid Thr877 was frequently expressed in AIPC [11]. This mutant AR could be activated by non-androgens such as AR antagonists (flutamide, cyproterone acetate and nilutamide) and steroidal hormones (estradiol, glucocorticoids, progesterone, etc) [12, 13]. The AR antagonist, bicalutamide antagonizes the T877A (threonine to alanine) mutated AR but another mutation at amino acid Trp741 was identified among bicalutamide

Chapter 1: Introduction

treated patients resulting in relapse. The point mutations were specific to the AR antagonists and convert them into an agonist. This leads to the withdrawal of the antagonist from the treatment regimen [14, 15].

Table 1: AR antagonist and the resistance causing mutation

S. No	Classification	AR antagonist	Resistance
1	Steroidal	Cyproterone acetate, Megestrol, Medroxy progesterone	T877A
2.	Non-steroidal	<u>1st generation</u> Flutamide, Nilutamide	T877A
		<u>2nd generation</u> Bicalutamide	W741L
		<u>3rd generation</u> Enzalutamide, ARN509 (clinical trials)	F876L

1.5. AR mediated activation of TMPRSS2-ETS gene fusion

The fusion of ETS (erythroblast transformation-specific) genes like ERG (ETS-related gene) and ETV1 (ETS translocation variant 1) with TMPRSS2 (transmembrane protease serine 2) were identified in the significant number of AIPC patients. The TMPRSS2 is an AR response element. The ETS family of transcriptional factors is oncogenic and stimulates the cell differentiation, cell division, metastasis, and angiogenesis [16, 17]. The fusion of ETS genes with AR response elements results in the over expression of ETS genes whenever AR is

Chapter 1: Introduction

activated [16, 17]. The hormonal therapy decreases the plasma testosterone level but the mutated AR which is expressed in AIPC does not require androgen for activation. Consequently, the mutated AR could activate the expression of ETS genes without androgen. The AR mutation and ETS chromosomal rearrangement in conjunction could co-ordinate the AIPC progression and drug resistance for AR antagonist and cytotoxic drugs. A novel AR antagonist that resists the mutations and decreases the expression of ETS genes could well be the future for prostate cancer treatment.

1.6. Hypothesis generation and work plan

At present, there are no AR antagonists in either market or in the clinical trials that could tolerate the point mutations. Hence, our aim the study is to identify a novel AR antagonist that could efficiently antagonize mutant ARs. The mechanism of the antagonist binding to either wild type or mutant ARs was yet to be elucidated. This is because there is no antagonist bound AR conformation in the protein data bank (PDB). The available co-crystal structures of AR with antagonist express mutation which converts them into an agonist. Hence the difference in the binding mechanism between the wild and mutant ARs should be elucidated for successful identification of the novel AR antagonist.

The structure based virtual screening could not be used for hits identification due to the lack of AR crystal structure. Hence, the essential functional groups (pharmacophore) of the AR antagonist should be derived through ligand based drug design methods. We also constructed a homology model of AR for docking studies. The homology model was used to visualize the

Chapter 1: Introduction

binding conformation of the identified hit molecules. Combining the outputs from the ligand and structure based drug design methods we had identified novel AR antagonist to treat AIPC. These new chemical entities have 4-nitro-phenyl or 4-methoxy-phenyl or 4-fluoro-phenyl nucleus bearing bulky β -iminoenamine BF₂ group. In this study we identified the functional groups that are essential for an AR antagonist to overcome the resistance with mutant ARs. The anti prostate cancer activity of the new chemical entities was also been elucidated through various *in-vitro* techniques.

Chapter 2: Aim and Objectives

2. AIM AND OBJECTIVES OF THE STUDY

2.1. Aim

To identify novel AR antagonist that could antagonize mutant ARs for the treatment of androgen independent prostate cancer.

2.2. Specific objectives

- To analyse the ligand/protein interactions between the wild and mutant ARs.
- To develop a pharmacophore model for wild and mutant AR antagonists and to identify difference between the pharmacophore models.
- Identification of new chemical entities through *in-silico* drug design methods.
- *In-vitro* anti prostate cancer activity of the new chemical entities to identify the hit molecules.
- To elucidate the anti-cancer mechanism of action of the best active molecule.

Chapter 3: Literature Review

3. LITERATURE REVIEW

3.1. Prostate cancer

Adenocarcinoma of prostate gland is the second most frequent cancer and sixth leading cause of mortality in males. The occurrence rate of prostate cancer is high in developed countries and the occurrence rate is lower in the central Asian countries. In the recent past, the death rates in the western countries were reduced due to improved diagnostic and treatment techniques [18]. The prostate gland is a heart shaped organ that surrounds the neck of the urethra which is presented immediately inferior to the bladder. The prostate gland empties the prostatic fluid into the urethra. The secretary portion of the gland is of epithelial cells, which are supported by fibro muscular stromal cells. The cancer develops in the epithelial cells and the stromal cell may aid in cancer progression and metastasis [19]. The risk factors for the prostate cancer are diverse and depends on

1. Higher age
2. Ethnicity
3. Life style and
4. Environmental factors.

The Japanese men have lower risk for prostate cancer because they have reduced 5 α -reductase enzyme activity. This enzyme catalyzes the conversion of testosterone to dihydrotestosterone in the prostate cells. The pollutants like bisphenol A and other hormone disruptors also increase the risk of prostate cancer. The chemical, bisphenol A was present in plastics. Overweight and

Chapter 3: Literature Review

consumption of animal products also increases the risk while intake of soy products decreases the risk [20].

The growth and development of prostate gland is under the control of androgens, dihydrotestosterone, testosterone and adrenal androgens. Androgen dependent growth of the prostate gland occurs significantly during the time of puberty and after that androgens continue to play an important role in its homeostasis. In some men with increasing age androgen dependent hyperproliferation of the prostate gland resumes resulting in benign prostatic hyperplasia or malignant prostate cancer [21]. Dihydrotestosterone is the major androgen and will be synthesized from testosterone *in-vivo* by an enzyme called 5α -reductase. Dihydrotestosterone have more binding affinity for AR than the testosterone. Adrenal androgen also gets converted into dihydrotestosterone inside prostate cells by prostatic enzymes [22].

The occurrence of prostate cancer could be either hereditary or sporadic. The mutation or variations in the hereditary prostate cancer loci are responsible for the pathogenesis of hereditary prostate cancer. In the hereditary prostate cancer the chances of prostate cancer occurrence is very high and occurs at young age. The genes that codes for proteins which are involved in cell division, cell repair and apoptosis are distorted [23]. Mutations of genes ribonuclease L, macrophage scavenger receptor 1, nibrin 1, checkpoint kinase 2, breast cancer type 2 susceptibility protein, ElaC Ribonuclease Z 2, mismatch repair, and homeobox protein 13, p21, p27 and p53 are some of the reasons for the occurrence for of hereditary prostate cancer [24 - 30]. The sporadic prostate cancer is the most

Chapter 3: Literature Review

common and widely occurring one. This depends on increasing age, ethnicity, environmental factors and life style. The metastatic potential to the cancer cells were guided by the down regulation of E-Cadherin. This results in epithelial mesenchymal transition and over expression of N-Cadherin which increases the heterotypic cell adhesion. This mechanism provides the metastasis and invasiveness to prostate cancer cells [31].

Prostate specific antigen (PSA) is a prostate cancer bio-marker and their serum level is an indicator for prostate cancer patients. Higher levels of PSA possess greater risk of prostate cancer occurrence. However, there is no prescribed PSA level below which the men can be assured no risk of prostate cancer. Prostate cancer antigen 3 (PCA3) and TMPRSS2-ERG fused genes are the new bio-markers for prostate cancer patients. The new biomarkers have higher specificity and sensitivity for prostate cancer detection [32]. The major clinical symptoms experienced by prostate cancer patients are difficulty in urination, painful urination, loss of control over urination, low back pain, painful ejaculation, urethral dysfunction, and cord compression etc.

3.2. Treatment for prostate cancer

3.2.1. Localized prostate cancer

Radical prostatectomy which involves the surgical removal of prostate gland, image guided radiotherapy which includes three-dimensional conformal radiotherapy and intensity modulated radio therapy are widely used to treat localized prostate cancer [33].

Chapter 3: Literature Review

3.2.2. Metastatic prostate cancer

The treatment was aimed at reducing the circulating PSA and androgen level. This can be achieved by androgen deprivation therapy and combined androgen blockade therapy.

The androgen deprivation therapy includes,

- Surgical castration: Bilateral orchiectomy (removal of both the testes) and the standard plasma castrate level of testosterone (≤ 20 ng/dL) would be achieved within 12 hours.
- Pharmacological castration: Gonadotropin releasing hormone receptor agonist or gonadotropin releasing hormone receptor antagonist (Table 2) are used for pharmacological castration. There will be an initial rise in the testosterone concentration while using gonadotropin releasing hormone receptor agonist. However, after 2 to 4 weeks the castration level of testosterone will be achieved.

In the combined androgen blockade therapy, in addition to castration (surgical or pharmacological) AR antagonist were used to prevent the activation of the AR by adrenal androgens [34, 35].

3.2.3. Recurrence of prostate cancer after treatment

The androgen deprivation therapy or the combined androgen blockade therapy initially has beneficial effects in significant number of patients. However, after a median of 18-24 months treatment most of the prostate cancer relapse into more aggressive form of the disease known as CRPC. The CRPC could be either androgen dependant or AIPC. In androgen dependant ones, tumor growth depends

Chapter 3: Literature Review

on androgen for proliferation and so it responds to hormonal therapies. The androgens were synthesized inside the prostate cancer cells from steroids like cholesterol, androstenedione, dehydroepiandrosterone, pregnenolone, progesterone, etc. This is because of the over expression of the enzymes involved in synthesis of dihydrotestosterone was elevated [36, 37]. The synthesis of dihydrotestosterone can be inhibited by abiraterone acetate and ketoconazole. Hence the androgen dependent prostate cancer cell proliferation could be controlled by CYP17 inhibitors. The cells of AIPC do not depend on androgens for proliferation and could not be treated with CYP17 inhibitors. The cytotoxic agent docetaxel and paclitaxel is the stable treatment regimen for AIPC [34, 35].

Chapter 3: Literature Review

Table 2: Classification of drugs used to treat prostate cancer

1. Hormonal therapy	
GnRH agonist	Leuprolide, Goserilin, Triprorelin, Histrelin, Busrelin
GnRH antagonist	Abarelix, Degarelix, Cetrorelix, Ganirelix
Non-steroidal AR antagonist	1st generation: Flutamide and Nilutamide. 2nd generation: Bicalutamide 3rd generation: Enzalutamide
Steroidal AR antagonist	Cyproterone acetate, Megesterol, Medroxyprogesterone, Diethylstilbesterol
CYP17 inhibitors	Ketoconazole, Abiraterone acetate
5 α reductase inhibitors	Finasteride, dutasteride
2. Non hormonal therapy	
Cytotoxic agents	1. Taxane derivatives: Cabazitaxel, Docetaxel, Paclitaxel 2. Anti-tumor antibiotic: Mitoxantrone hydrochloride
Miscellaneous	Sipulencel - T (Immunotherapy), Radium 223 dichloride (Radiopharmaceutical), Denosumab (Monoclonal antibody), Corticosteroid and Zoledonic acid.

GnRH: Gonadotropin releasing hormone; AR: androgen receptor.

Chapter 3: Literature Review

Table 3: Drugs in clinical trials for the treatment of prostate cancer

Phase	Disease status	Treatment	Mechanism of action
Phase 1	Metastatic prostate cancer	PrCa VBIR	Vaccine based immunotherapy
Phase 1	Advanced prostate cancer	AZD8186 + Abiraterone	PI3K inhibitor + CYP17 inhibitor
Phase 1	Recurrent metastatic CRPC	EC1169	Chemotherapy agents similar to taxanes
Phase 1	Metastatic solid tumours	Durvalumab + Monalizumab	mAb to Programmed death ligand-1 + mAb to NKG2A
Phase 1	Metastatic CRPC	TAS3681	AR antagonist
Phase 1	Advanced prostate cancer	IMC-CS4	Triggers immune response against prostate cancer cells
Phase 1	Advanced prostate cancer	¹³¹ I-MIP-1095	Radiopharmaceutical - Attaches to PSMA protein of prostate cancer cells and delivers radioactive iodine
Phase 1	Advanced prostate cancer	ZEN003694	Inhibits bet family of proteins
Phase 1	Metastatic prostate cancer	ZEN003694 + Enzalutamide	Inhibits bet family of proteins + AR antagonist
Phase 1b	Metastatic prostate cancer	Atezolizumab + Radium - 223	mAb to programmed cell death ligand + radiotherapy
Phase 1b	Metastatic CRPC	CC-115 + enzalutamide	mTOR inhibitor + AR antagonist
Phase 2	Metastatic CRPC	Abiraterone + cabazitaxel	CYP 17 inhibitor + Cytotoxic agent
Phase 2	Localized high risk prostate	ARN509 + Abiraterone +	AR antagonist + CYP 17 inhibitor + GnRH receptor

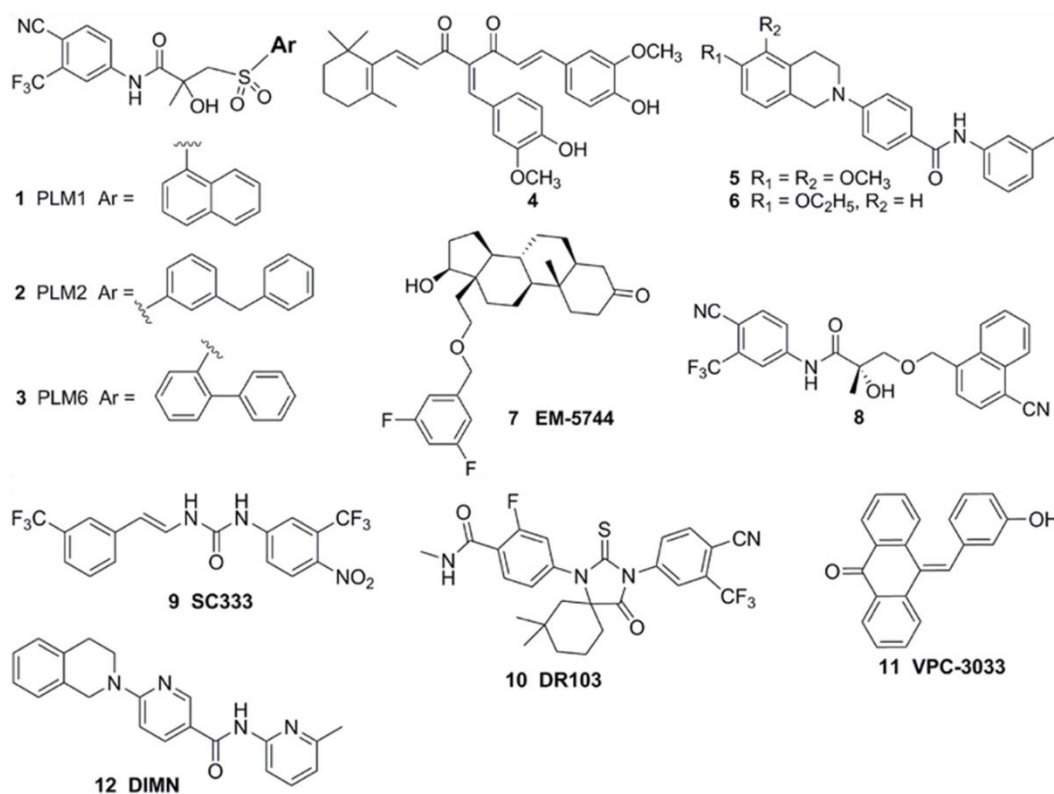
Chapter 3: Literature Review

	cancer	leuprolide + hyperfractionated radiotherapy	agonist
Phase 2	Metastatic prostate cancer	Rucaparib	PARP inhibitor
Phase 3	Metastatic prostate cancer	Abiraterone + predinsone + ARN509	CYP17 inhibitor + Anti-inflammatory + AR antagonist
Phase 3	Localized high risk prostate cancer	Enzalutamide + Leuprolide	AR antagonist + GnRH receptor agonist

Ref: (Memorial Sloan Kettering cancer centre, 2017); PI3K: Phosphatidylinositol-4,5-bisphosphate 3-kinase; mAb: Mono colonel antibody; AR: AR; PSMA: prostate specific membrane antigen; MTOR: mechanistic target of rapamycin; PARP: Poly ADP ribose polymerase; CRPC: castration resistance prostate cancer.

Chapter 3: Literature Review

Figure 1: Recently identified AR antagonist hit molecules [38]

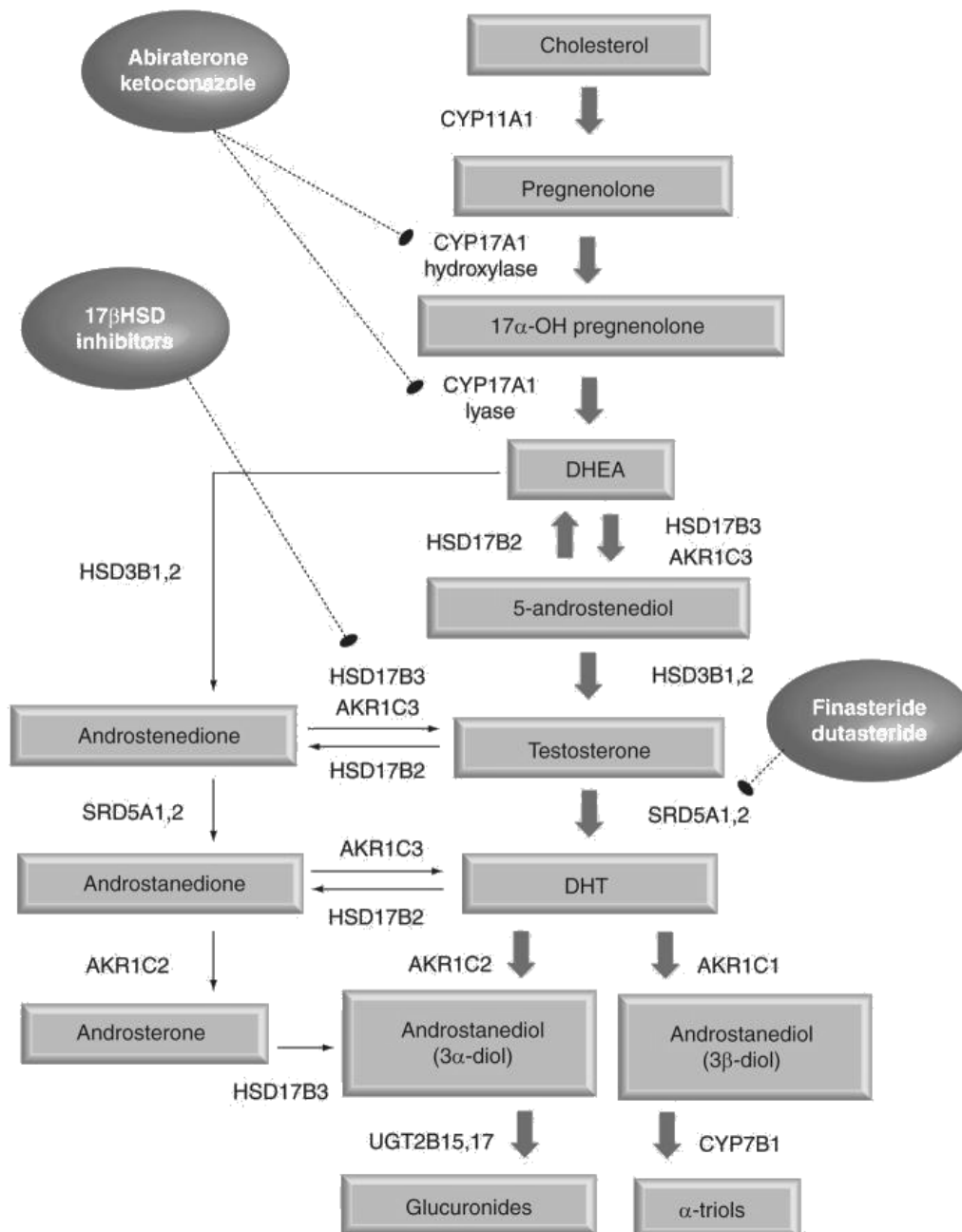


3.3. Castration resistant prostate cancer (androgen dependant)

The pathogenesis involved in the aggressive form of prostate cancers such as androgen dependant and AIPC are different. In androgen dependant prostate cancer, the prostate cancer cells depend on androgen for proliferation. The expression of AR was elevated to utilize the residual androgen efficiently [37]. Additionally, the enzymes involved in the synthesis of dihydrotestosterone are over expressed and the enzymes involved in the catabolism of dihydrotestosterone were down regulated (Figure 2). The above mechanisms work together to the increase the intracrine androgen level [39]. In case of AIPC the prostate growth does not depend on androgens for proliferation. There are many mechanisms behind the development of AIPC.

Chapter 3: Literature Review

Figure 2: *De-novo* synthesis of androgen



The figure 2 represents the synthesis of androgen from cholesterol inside the prostate cancer cells. The androgen synthesis inhibitors could be used to control the aberrant rise in intracrine androgen level.

Chapter 3: Literature Review

3.4. Castration resistant prostate cancer (androgen independent)

The AIPC does not depend on androgen for proliferation and the AIPC cancer cells adapt various mechanisms to evade hormonal therapy. The reasons for prostate cancer cells switching from androgen dependant to independent stage are diverse. In the following section we consider the various reasons behind the AIPC relapse after hormonal therapy failure and new drug discovery strategies for AIPC.

3.4.1. Mutations in the ligand binding domain of AR

The Mutation in the ligand binding domain of the AR is one of the major reasons behind the development of AIPC [40]. The mutations are mostly somatic point mutations which broadens the ligand specificity. The mutation occurs due to the stress given to the AR by antagonist. The somatic point mutations can be broadly classified into three types,

- Mutations expressed in flutamide treated patients

The mutations, T877A (threonine to alanine), T877S (threonine to serine), V715M (valine to methionine), A721T (alanine to threonine), N756D (asparagine to aspartic acid), and H874Y (histidine to tyrosine) were identified in AIPC patients who underwent flutamide containing therapy. These mutations causes resistance to flutamide treatment and these mutant ARs were activated by flutamide [41 - 43].

- Mutations expressed in bicalutamide treated patients

The mutations, W741C (tryptophan to cysteine), W741L (tryptophan to leucine), and D879G (aspartic acid to glycine) were identified in AIPC

Chapter 3: Literature Review

patients who underwent bicalutamide containing therapy. These mutations were responsible for bicalutamide resistance and these mutant ARs were activated by bicalutamide [44, 45].

- Mutations expressed in enzalutamide treatment

F876L (Phenyl alanine to leucine) mutant AR was identified in AIPC cell lines after the treatment with enzalutamide. This mutation converts the enzalutamide into an agonist and causes resistance [45]

The most widely studied mutation and frequently occurring one was T877A mutant AR (Table 4). The replacement with alanine provides additional space within the ligand binding pocket which allows the receptor to bind with variety of ligands. This mutation is specifically expressed in patients who underwent combined androgen blockade therapy in which flutamide is as an AR antagonist [46]. The T877A is activated by non-androgens like cyproterone acetate, hydroxy-flutamide (active form of flutamide), estrogens, glucocorticoids, and progesterone. The bicalutamide antagonizes T877A mutant AR [47, 48]. The crystal structure for T877A mutant AR's ligand binding domain was available (PDB: 2AX6, 2OZ7). This mutated AR was expressed in human prostate cancer LNCaP cell line [49].

The T877S mutant AR was identified in patients who underwent combined androgen blockade therapy in which flutamide is as an AR antagonist [50]. Similar to that of T877A mutant the T877S mutant was also activated by estradiol, progesterone, hydroxy-flutamide, nilutamide and androstenedione. Bicalutamide antagonizes this mutant AR [50]. The W741C/L mutation was identified in

Chapter 3: Literature Review

patients who underwent combined androgen blockade therapy in which bicalutamide is as an AR antagonist. This mutant AR is antagonized by flutamide, cyproterone acetate and nilutamide [42, 44]. The crystal structure of W741L mutant AR's ligand binding domain has been elucidated (PDB: 1Z95).

Table 4: Frequency of AR mutations in AIPC

S. No	Treatment	AR mutation	Frequency identified
1.	Orchiectomy	Q902R	1
2.	Orchiectomy	Wild type	9
3.	Orchiectomy	AR negative	2
4.	Orchiectomy + F	Wild type	1
5.	Orchiectomy + F	AR negative	1
6.	GnRH	Wild type	6
7.	GnRH	AR negative	2
8.	GnRH	D890N	1
9.	DES	AR negative	1
10.	GnRH + F (CAB)	Wild type	10
11.	GnRH + F (CAB)	T877A	18
12.	GnRH + F (CAB)	T877S	2
13.	GnRH + F (CAB)	V715M	2
14.	GnRH + F (CAB)	H874Y	2
15.	GnRH + F (CAB)	A721T	1
16.	GnRH + F (CAB)	N756D	1

Chapter 3: Literature Review

17.	GnRH + B (CAB)	W741C	1
18.	GnRH + B (CAB)	D879G	1
19.	GnRH + B (CAB)	W741L	1

GnRH - Gonadotrophin releasing hormone agonist or antagonist; CAB - Combined androgen blockade therapy; F - Flutamide; B - Bicalutamide; DES - Diethylstilbesterol.

3.4.2. TMPRSS2-ERG gene fusion

Another major identification in CRPC was the discovery of the TMPRSS2 - ETS gene rearrangements. The TMPRSS2 - ETS gene rearrangements were identified in 50% to 70% prostate cancer patients [51]. The ETS families of transcriptional factors are oncogenic and control the cell differentiation, cell division, metastasis and angiogenesis. The fusion between ETS and TMPRSS2 an AR responsive element leads to the over expression of ETS genes. For the ETS to over-express, it requires AR activation because since it was fused with an AR response elements [52]. The hormonal therapy decreases the plasma testosterone level but the mutated AR which is frequently expressed in AIPC does not require androgen for activation. Consequently, the mutated AR could activate the expression of ETS genes without androgen. The AR mutation and ETS chromosomal rearrangement in conjunction could co-ordinate the AIPC progression and drug resistance for AR antagonist and cytotoxic drugs.

3.4.3. AR/TMPRSS2-ETS/PTEN/PI3K/AKT

The TMPRSS2 - ETS gene rearrangements results in the loss of the expression of PTEN (Phosphatase and tensin homolog). About 40% of TMPRSS2

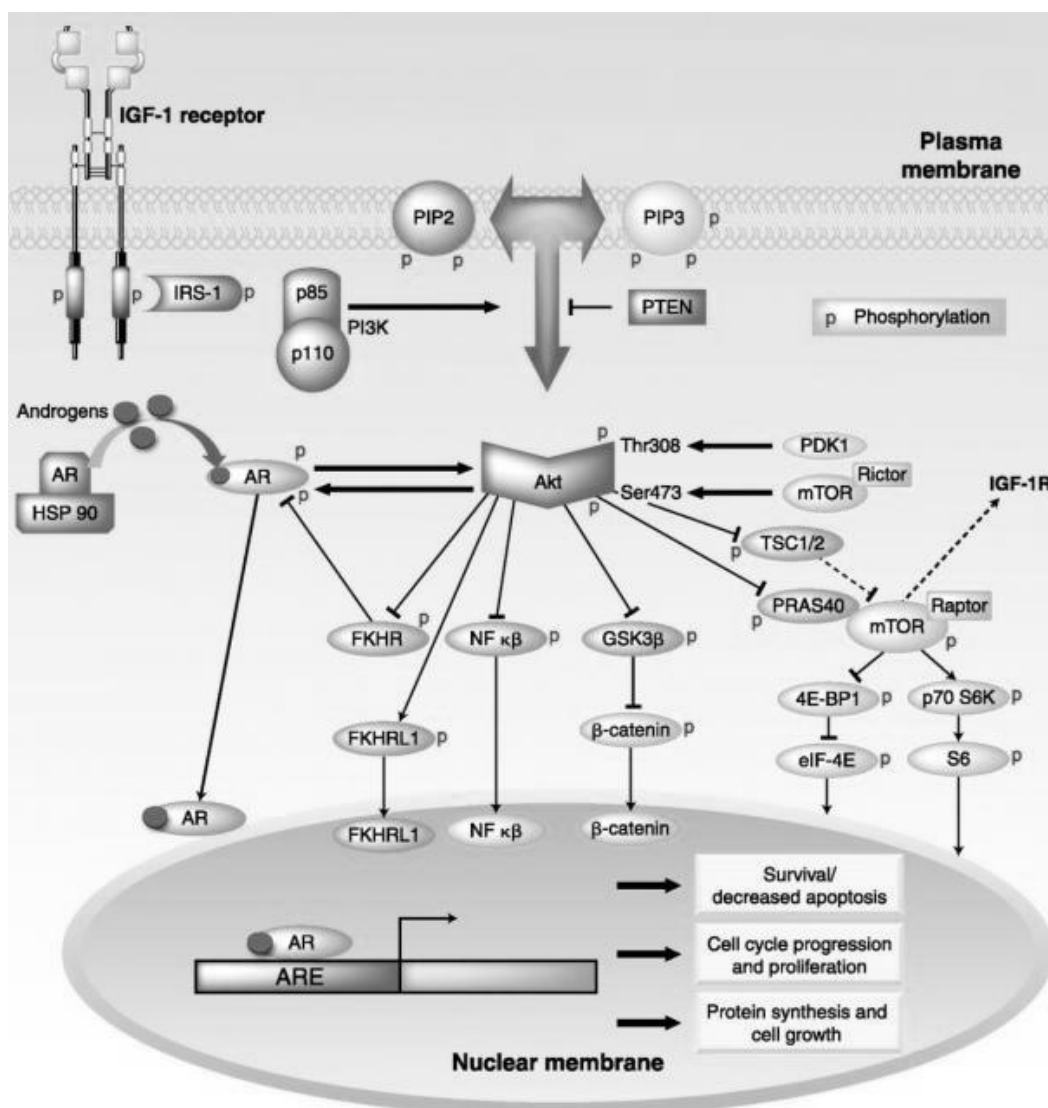
Chapter 3: Literature Review

- ETS gene expressing specimens were associated with the loss of PTEN [53]. This information bring in that the PTEN loss and ETS rearrangements were associated proceedings that act together to uphold the prostate cancer progression. The ETS genes were transcriptional regulators which regulate the transcriptions of the downstream check point genes concerned with promoting cellular proliferation, cell death, and survival. The PTEN is a tumour suppressor gene and has control over PI3K/AKT (Phosphatidylinositol 3-kinase/ Protein kinase B) pathway. Loss of PTEN means the control over the PI3K/AKT pathway was lost that result in the constitutive activation of AKT [53].

The AKT inhibitors decrease the PSA transcription by AR. The AKT phosphorylates the serine residues 213 and 791 of the AR. Phosphorylation of AR by AKT enhances the interaction of AR with the co-activators and increases PSA transcription many fold [54, 55]. Apart from phosphorylation of AR, the AKT is a key signalling protein involved in cell survival and proliferation. They activate the transcription of many proteins necessary for cell survival, proliferation and division. The AKT role in the advancement of cancer has been studied widely. The AKT modulates the effect of wide variety of intracellular proteins by phosphorylation (Figure 3).

Chapter 3: Literature Review

Figure 3: AR/AKT interaction in prostate cancer



The PI3K/AKT pathway and interaction with Androgen Receptor (AR) pathways. AR is bound to heat-shock protein 90 (HSP-90) in the cytoplasm, which stabilizes AR. On binding of androgens, e.g., 5 α -dihydrotestosterone, AR dissociates from HSP-90, allowing AR phosphorylation at multiple sites. The AR-androgen complex translocates to the nucleus, binding to specific androgen response elements on target gene promoters, leading to gene transcription. Activation of the PI3K pathway leads to AKT phosphorylation, triggering a downstream cascade of events that are likely to interact with AR transcriptional activity. These include interaction of the AR with FKHR and FKHL1 transcription factors, cross-talk of AR and AKT with NF κ B; regulation of AR via coactivator Wnt/ β -catenin, and activation of AR via the mTOR pathway.

Chapter 3: Literature Review

3.4.4. AR/TMPRSS2-ETS/PTEN/PI3K/AKT/GSK3 β / β -catenin

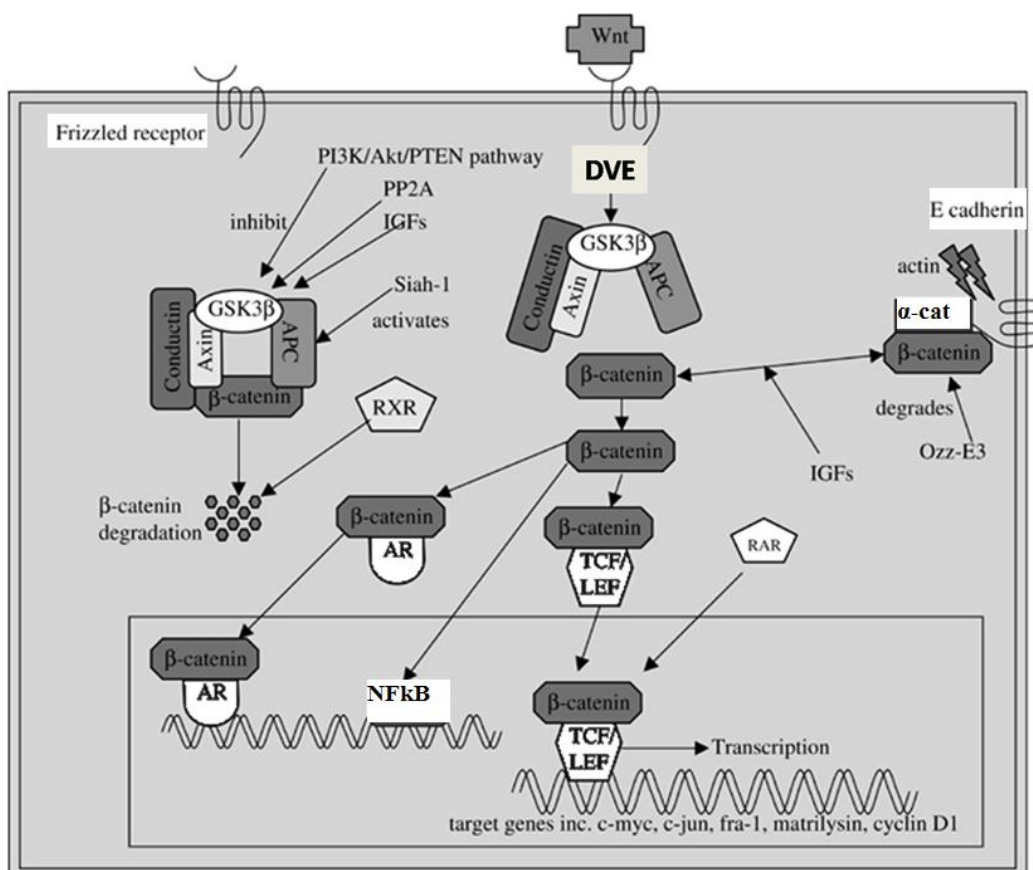
Cross talk between the PI3K/AKT pathway, wnt pathway and AR has been confirmed in prostate cancers (Figure 4) [56]. This was because of the TMPRSS2-ETS gene fusion which results in the subsequent over-expression of ETS genes in AIPC. The ETS genes suppress the expression of the tumour suppressor gene PTEN. Loss of PTEN relieves the control over PI3K/AKT pathway and the pathway becomes constitutively active. A study using synthetic PI3K inhibitor in the transgenic mice expressing PTEN null mutation has indicated that the mechanism indeed involves the GSK3 β / β -catenin pathway. The GSK3 β / β -catenin pathway is a downstream effector of PI3K/AKT pathway. This indicates that the Wnt pathway was also involved in the prostate cancer progression through PTEN and PI3K/AKT pathway [57].

The central particle in the PI3K/AKT/GSK3 β / β -catenin pathway is the protein β -catenin [58]. The β -catenin is responsible for cell proliferation, angiogenesis and metastasis. The β -catenin exists in cell membrane, cytoplasm and nucleus. In the cytoplasm the β -catenin exists as multi-protein complex. Any free β -catenin was phosphorylated by GSK3 β and degraded by ubiquitin. The complex was formed by proteins, GSK3 β (active form), APC (adenomatous polyposis coli), axin and β -catenin [57, 58]. The PI3K/AKT pathway prevents the degradation of β -catenin through inactivating the GSK-3 β . The inactive GSK3 β does not cleave the β -catenin and so the free cytoplasmic β -catenin level increases. The free β -catenin translocates from the cytoplasm into the nucleus and interacts with the T-cell factor (TCF) and lymphoid enhancer factor 1 (LEF1)

Chapter 3: Literature Review

family of transcriptional factors [58, 59]. LEF1 is found to be over expressed in AIPC and hence it has a dominant role in AR over expression. The AR over expression also activates the wnt pathway and sets up a positive feedback for the further expression of AR creating a positive feedback mechanism [60]. The β -catenin–TCF/LEF induces the mRNA transcription of oncogenes like c-myc, cyclin D1 and also increases the ligand dependant AR mediated cellular proliferation (Figure 4).

Figure 4: AR/GSK3 β / β -Catenin signalling in prostate cancer



PP2A: protein phosphatase 2A; IGFs: insulin-like growth factors; Siah-1: human homolog of *Drosophila seven in absentia*; AR: androgen receptor; RAR: retinoic acid receptor A; RXR: retinoid X receptor; NFκB; B: nuclear factor kappa B transcription factor.

Chapter 3: Literature Review

3.4.5. AR co-regulators

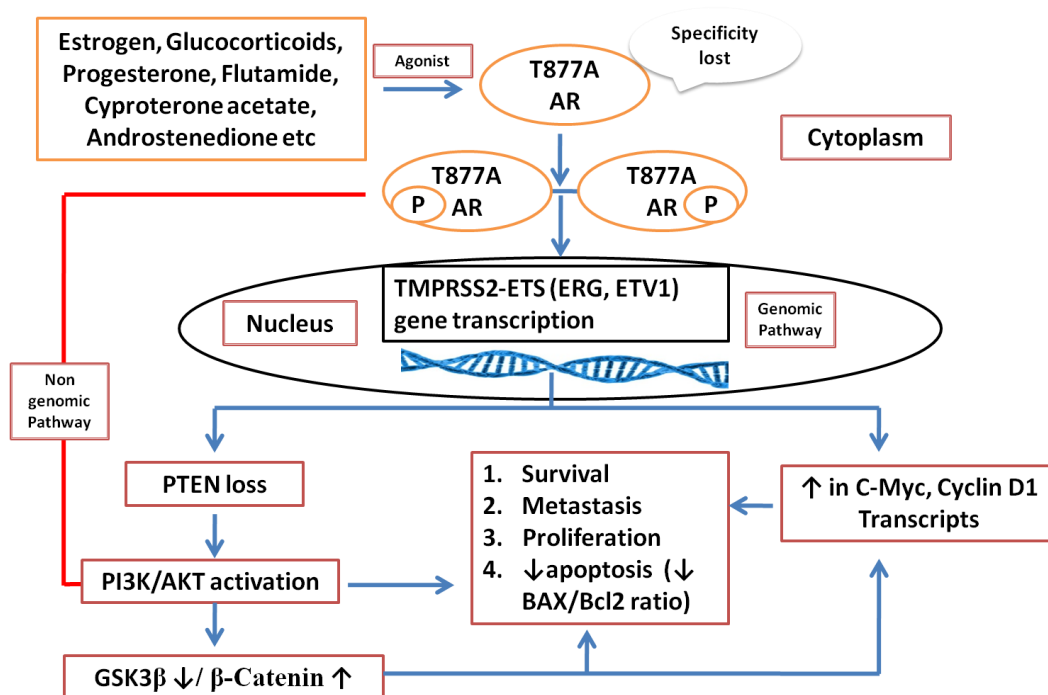
Altered function and over expression of co-regulatory proteins has been implicated in the development of resistance to hormonal therapies leading to prostate cancer relapse. Expression of certain co-regulatory proteins alone confers the activation of AR by anti-androgens. The over expression of class 1 co-activators such as p160/SRC, SRC-1, TIF2 have been well studied [61]. The SRC-1 has histone acetyltransferase activity and relaxes the promoter region of the response elements and increases the transcriptional activity. TIF2 is shown to be regulated by IL-6 and has active role in the development of bicalutamide resistance. The class 2 CBP/p300 family of co-activators are also implicated in AIPC and is involved in the activation of AR in androgen depleted state [62].

The ARA70 is an AR specific response element. The ARA70 was found to activate the androgen deprived cell line in the presence of AR antagonist. This results in the development of resistance towards AR antagonist. Hence it may augment the anti-androgen withdrawal syndrome [63]. The Co-repressors NcoR/SMRT represses the transcriptional activity of androgens in the presence of anti-androgens in normal prostate cells. In relapsed prostate cancers the above mentioned co-repressors are over-expressed and function as a co-activator increasing the transcription of AR response elements [64].

Chapter 3: Literature Review

3.5. Rationale for target selection

Figure 5: AR as central dogma in androgen independent prostate cancer



T887A AR: T877A mutated AR; **TMPRSS2:** Transmembrane protease, serine 2; **ETS:** erythroblast transformation-specific; **ERG:** ETS related genes; **ETV1:** ETS variant 1.

From the evaluation of the molecular pathogenesis of prostate cancer we selected the mutant AR as the target for AIPC. This was because the mutant AR was involved directly or indirectly in the activation cell survival pathways (Figure 5).

- The mutation in AR seems to be the central dogma of AIPC.
- The AR was over expressed and expresses mutation in most of the AIPC.
- The mutant AR was specifically expressed in AIPC cells.

Chapter 3: Literature Review

- The mutant AR was responsible for the over expression of TMPRSS2-ETS gene transcripts. This is because the TMPRSS2 is an AR response element.
- The increased transcripts of ETS were then further responsible for the loss of function of PTEN.
- Loss of PTEN results in the constitutive activation of PI3K/AKT pathway which is a survival pathway. This prevents the prostate cancer cells from apoptosis.
- The PI3K/AKT pathway also inhibits the GSK3 β . The inhibition of GSK3 β increases the activity of β -catenin which increases the expression of oncogenes c-myc, cyclin D1 etc, which leads to increased survival of the AIPC cells.
- Directly targeting the pathways might not be a rational approach because, the enzymes in the pathways are also expressed in non-cancerous cells and could lead to unwanted side effects and toxicity.
- The co-activators of the AR were also an attractive target but there is no crystal structure or any other inhibitors in the clinical or in the clinical trials. Hence it becomes difficult to design novel molecules to specifically inhibit the co-activators.
- Hence to inhibit the TMPRSS2-ETS mediated PI3/AKT activation and to further modulate the GSK3 β / β -catenin pathway a potent AR antagonist that could target mutant AR will be a right choice.

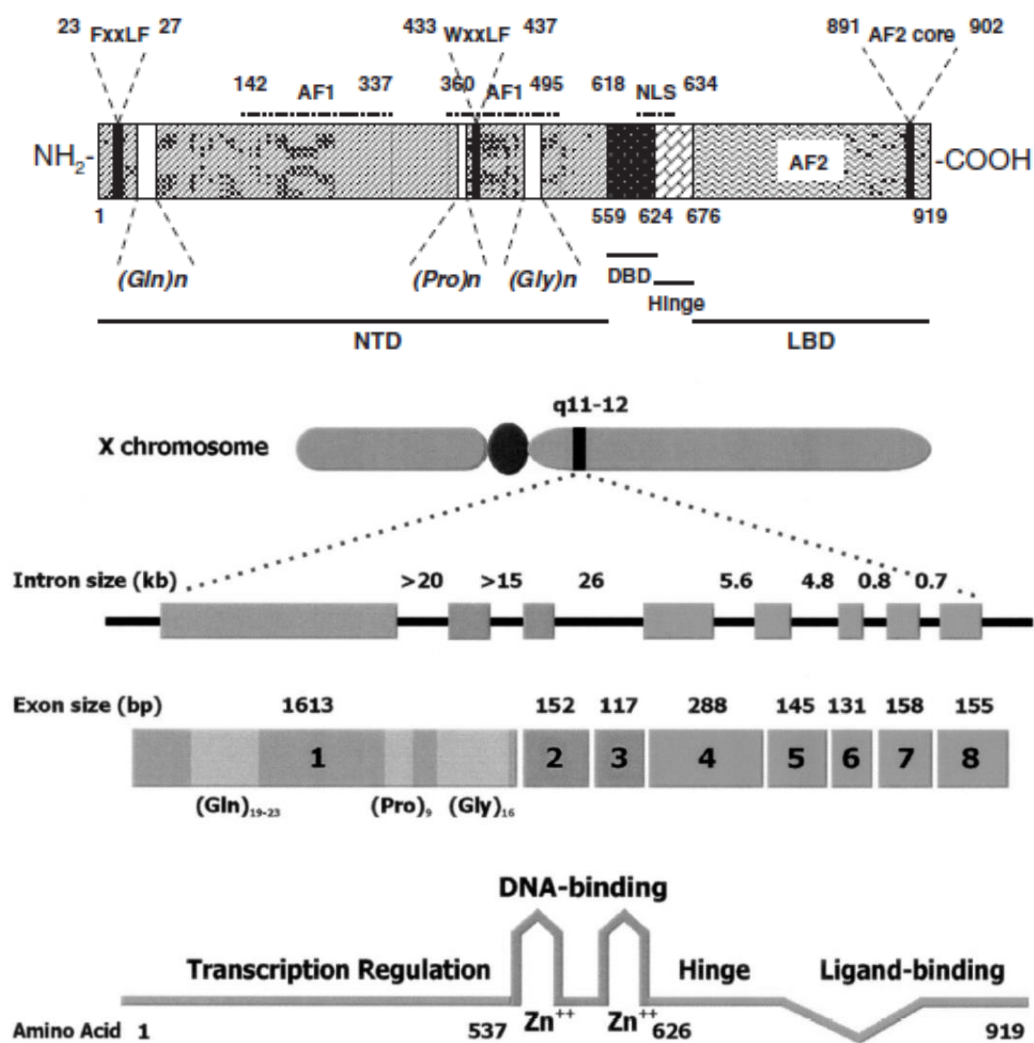
Chapter 3: Literature Review

3.6. AR structure and function

3.6.1. AR gene location

The AR is a nuclear receptor encoded by a single gene located on human X-chromosome at Xq11-12 region that spans more than 90kb and contains 8 exons (Figure 6). The human AR is made of 900-920 amino acids. The variations in the amino acid length are due the polymorphism in the length of polyglutamine (CAG repeats) and polyglycine (GGN repeats) tracts of the first exon [65].

Figure 6: Functional domains of AR



Chapter 3: Literature Review

The AR 4 functional regions

1. Variable N-terminal domain (NTD) or Activation function 1(AF1),
2. DNA binding domain (DBD)
3. Hinge Region
4. Ligand binding domain (LBD) / Activation function 2 (AF2).

There are two isoforms of AR namely AR-A and AR-B. The AR-A and AR-B isoforms are expressed in humans. The N-terminal of the AR-A isoform is produced by translation initiation at alternate site (Met188) and so the amino acid starts from Met188. The AR-B isoform is predominantly expressed one and the ratio of AR-B isoform to AR-A isoform is 10:1 [66].

3.6.2. Structure and function of AR N-terminal domain (NTD)

The first exon codes for NTD. The NTD approximately makes up half of the molecule of AR and is required for full transcriptional activity. Poly glutamine tract (CAG) in the NTD varies from 8 to 33 repeats in normal individual. A rare neuromuscular disorder namely Kennedy's disease is caused by increased CAG repeats [67]. Increased CAG repeats decrease the transactivation potential of AR by p160/SRC family of co-activators. Shorter CAG repeats increase the transcriptional activity of AR but their risk associated with prostate is variable. Recent studies stated that there is no relation between CAG tract length and prostate cancer but a CAG tract length ≤ 21 may have a protective role against prostate cancer [68].

The activity of AR depends on various transactivation domains within the NTD. The NTD of AR contains two activation domains namely TAU-1 and TAU-

Chapter 3: Literature Review

5. TAU-1 (1 to 485) appears to be important in ligand dependant activation and TAU-5 (360 to 528) is responsible for constitutive ligand dependant activation of AR. The ²³FQNLF²⁷ motif is involved in the ligand dependant intramolecular N/C (amino/carboxyl) terminal interaction which is essential for full activation of AR (Figure 6) [69].

This N/C interaction leads to

- Receptor stabilization,
- Prevent the dissociation of ligand from AR
- Increases the binding affinity for DNA
- Creates the surface area for recruitment of the co-activators.

The ligand dependant N/C terminal interaction occurs between the FXXLF motif of NTD with helixes 3, 4 and 12 of AF-2 domain. In addition of mediating intra-molecular interaction, the FXXLF motif also binds to X-chromosome linked melanoma antigen gene product (MAGE-11). MAGE11 is an AR co-activator which enhances the transcriptional activity by allowing the interaction of SRC/p160 family of co-activators with AF-2 domain [70]. The second motif WXXLF is responsible for constitutive activation of AR in the absence of ligand or ligand binding domain. The ⁴³³WXXLF⁴³⁷ motif interacts with ligand binding domain outside of AF-2 domain [70, 71]. The truncated AR lacking ligand binding domain is constitutively activated and has 3/4th of the total transcriptional activity compared to full length AR. These 2 motifs resemble like LXXLF motif in p160 family of co-activators and compete with co-activator binding to carboxyl terminal domain (CTD) or ligand binding domain [71].

Chapter 3: Literature Review

3.6.3. Structure and Function of AR DNA binding domain (DBD)

The DBD is coded by exons 2 and 3. The DBD of AR is highly conserved and plays a major role in

1. AR nuclear localization
2. AR dimerization and
3. DNA binding

The DBD is made of 3 α helices having 2 zinc finger motifs and a short C-terminal extension (Figure 6) (CTE). Each zinc finger consists of 4 cysteine residues and a Zn²⁺ ion [72]. The first zinc finger (P-box) is involved in the sequence recognition and directly binds to major groove of hormone response element (HRE) in the DNA. The HRE consists of the core DNA sequence is 5'-TGTTCT-3'. The class 1 nuclear receptor which includes glucocorticoid, mineralocorticoid and progesterone receptors recognize the inverted repeats of the core sequence separated by 3 nucleotides [73]. A missense mutation in the p-box, K580R resulted in androgen insensitivity syndrome explaining the importance of p-box in AR's transcriptional activity [74]. The second zinc finger (D-box) is responsible for the stabilization of DNA bound AR interactions and mediate DNA dependant intermolecular protein-protein interactions (homo dimerization) [75].

The entire class 1 nuclear receptors bind to the same HRE, the specific physiological function of AR is elicited by carboxyl terminal extension (CTE) amino acids. In AR, CTE amino acids (625 - 636) provide an additional dimer interface along with second zinc finger that is required for selective and high affinity binding of AR to specific AR response elements [76]. Zhong and co-

Chapter 3: Literature Review

workers revealed that the CTE amino acids 617 - 633 have two nuclear targeting sequences (**RKCYEAGMTLGARKLKK**) which import the AR to its nucleus and is called nuclear localization signal (NLS) [77].

3.6.4. Structure and functions of hinge region

The hinge region is coded by exons 4 and a part of 5. It is flexible and separates the DBD from ligand binding domain. The hinge region of AR has a transcriptional inhibiting motif made of highly basic amino acids [629-RKLLKLLGN-636] and has an attenuating effect on AF-2 activity by interfering with the recruitment of co-activators. Deletion of the inhibiting motif enhances the intramolecular N/C terminal interaction which is necessary for AR transcriptional function as discussed in the NTD. However, this impairs the hormone dependant nuclear translocation because of the deletion of NLS and also affects DNA binding and receptor stability [78]. The AR is preferentially acetylated by p300/CBP, Tip60 co-activators in its hinge region of the lysine residues K630, K632, K633 and regulates transcriptional activity [79]. The mutational studies on those amino acids showed that the acetylation enhances the transcriptional activity of the AR. Two missense somatic point mutations R629Q and K630T are identified in prostate cancer patients and have higher transcriptional activity than wild type AR [80].

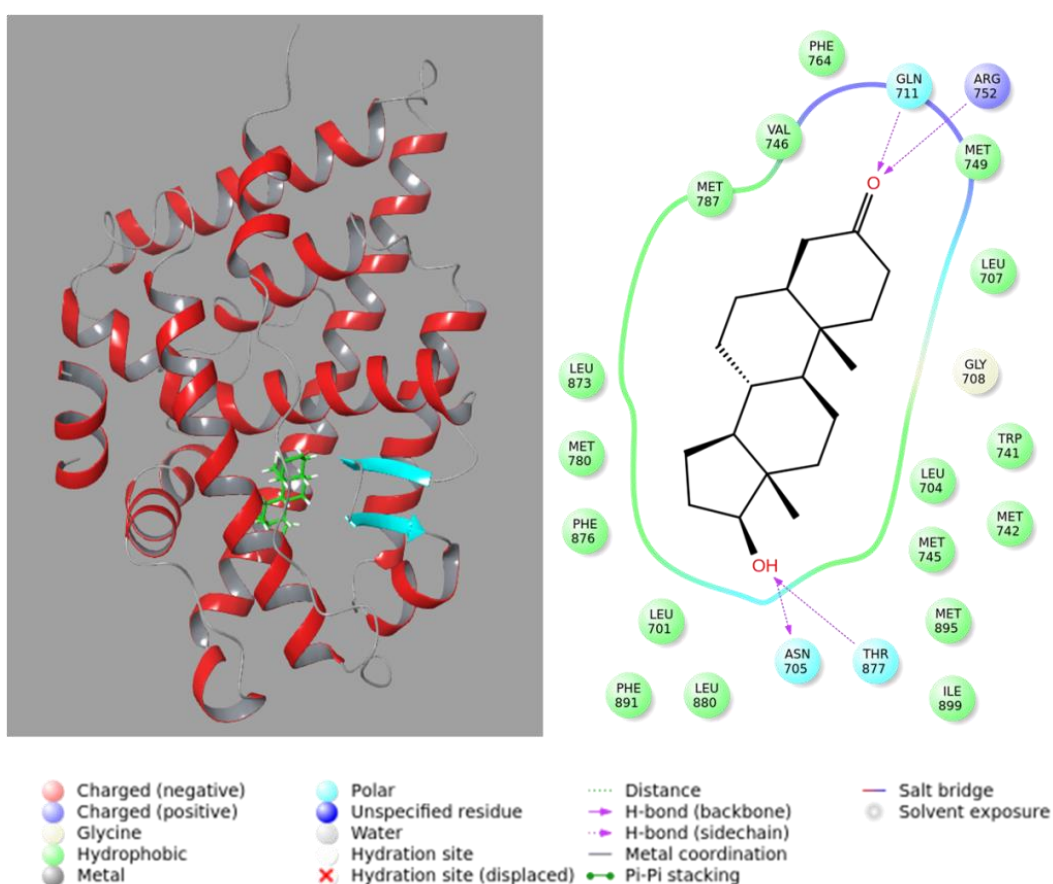
3.6.5. Structure and function of ligand binding domain

The ligand binding domain of AR is coded by exons 6, 7, 8 and C-terminal part of 5. The crystal structures of human AR's ligand binding domain have been elucidated and are available in the PDB. The ligand binding domain of AR

Chapter 3: Literature Review

consists of 12 α -helixes and 2 β -sheets that fold to form triple layered alpha helical sandwich which creates a hydrophobic ligand binding pocket to which the ligand binds [81]. The AR ligand binding domain has a nuclear export signal (NES) in amino acids 742 to 817. This NES keeps the unbound AR in the cytosol. The NES is dominant over nuclear localization signal in the resting state [82].

Figure 7: Ligand binding domain of the AR



The ligand binding domain interacts weakly with LXXLF motifs of co-activators but preferentially with FXXLF and WXXLF motifs in the NTD [83]. Agonist binding to the ligand binding domain causes helix-12 to lie over the ligand binding pocket and exposes the groove necessary for intramolecular N/C

Chapter 3: Literature Review

interaction. Antagonist binding displaces the helix-12 away from ligand binding pocket and unveils the binding surface for co-repressor NcoR/SMRT interaction and inhibition of AR transcriptional activity [84].

The Helix 4, 5 and 10 are the primary contact sites for androgen. The binding of androgens to AR majorly involves hydrophobic interactions with amino acids Val746, Met742, Gln711, Met745, Leu707, Leu704, Leu707 and Trp741. The Hydrogen bond interactions between ligand/receptor also play a key role in specific binding of ligands to AR. The keto group in the ring A of DHT forms H-bonds with Gln711, Arg752 while the 17 β -OH group in the D ring forms H-bond with Thr877 and Asn705 (Figure 7). The AR antagonists also bind to the same ligand binding pocket and prevent the androgens from binding to and activating AR.

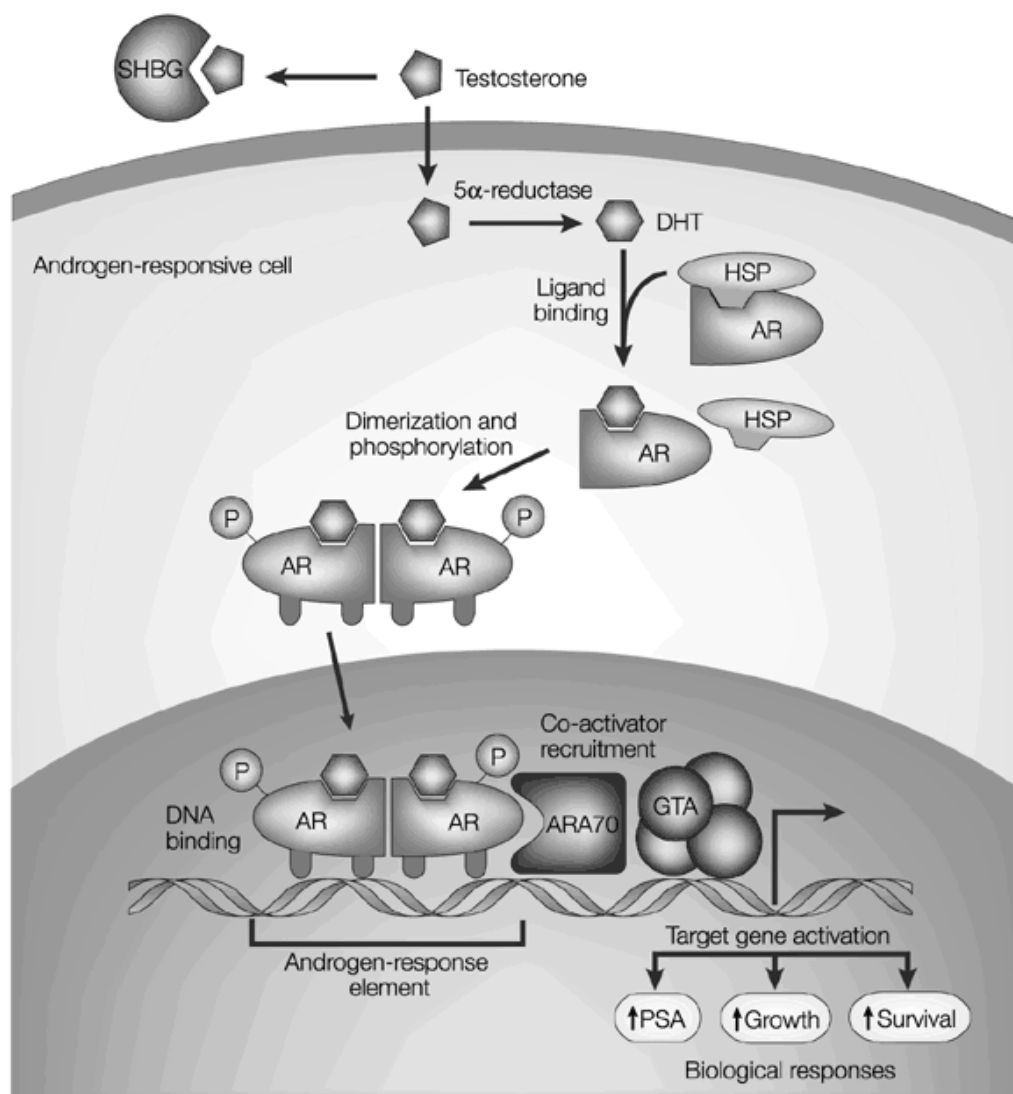
3.6.6. Ligand dependant genomic AR activation

The ligand dependant activation is required for the maximum activation of full length AR. Upon binding of androgens to the AR,

1. The AR dissociates from the heat shock proteins (HSP),
2. Undergoes ligand dependant intramolecular N/C terminal interaction,
3. Phosphorylation,
4. Weakening of NES and increase in Nuclear translocation signal,
5. DNA dependant homodimerization,
6. Co-activator recruitment,
7. Binding to specific AR response elements and initiation of transcription (Figure 8).

Chapter 3: Literature Review

Figure 8: Activation of AR by androgens



Testosterone circulates in the blood bound to albumin (not shown) and sex-hormone-binding globulin (SHBG), and exchanges with free testosterone. Free testosterone enters prostate cells and is converted to dihydrotestosterone (DHT) by the enzyme 5 α -reductase. Binding of DHT to the androgen receptor (AR) induces dissociation from heat-shock proteins (HSPs) and receptor phosphorylation. The AR dimerizes and can bind to androgen-response elements in the promoter regions of target genes. Co-activators (such as ARA70) and corepressors (not shown) also bind the AR complex, facilitating or preventing, respectively, its interaction with the general transcription apparatus (GTA). Activation (or repression) of target genes leads to biological responses including growth, survival and the production of prostate-specific antigen (PSA).

Chapter 3: Literature Review

The AR resides predominantly in cytoplasm and is associated with HSP and chaperons. HSP also have active role in transcriptional activation of the AR because HSP90 binds to the AR and keeps it in an active conformation for androgen binding. Androgen binding to AR results in the dissociation of HSP from AR. The helix 12 folds over the ligand binding pocket and encloses the ligand. This results in the unmasking of the necessary grooves to undergo intramolecular N/C interaction, dimerization and phosphorylation [85]. Phosphorylation of the AR also plays an important role in transcriptional activity.

The newly translated AR is phosphorylated at serine residues 506, 641, 653 as a post-translational modification which increase the ligand acquiring properties. Treatment of LNCaP cells with a synthetic agonist resulted in the phosphorylation of serine residues at 16, 81, 94, 256, 308, 424 and 650 [86]. The phosphorylation of serine 650 is required for full transcriptional activity. Antagonist binding does not enhance receptor phosphorylation. After translocation into the nucleus, the AR undergoes DNA dependant intermolecular homo dimerization. The D-box mediate DNA dependant dimerization and the CTE amino acid provide an additional dimer interface to bind specific AR response elements [87].

Co-activators decondense the chromatin and facilitate the binding of RNA polymerase holoenzyme for initiating transcriptional activity. Class 1 family of co-activators such as SRC-1, TIF2, SRC-3 and class 2 families of co-activators such as p300/ CBP regulate the transcriptional activity of AR [88]. Interaction with NTD seems to be responsible for activation rather than interaction with AF-

Chapter 3: Literature Review

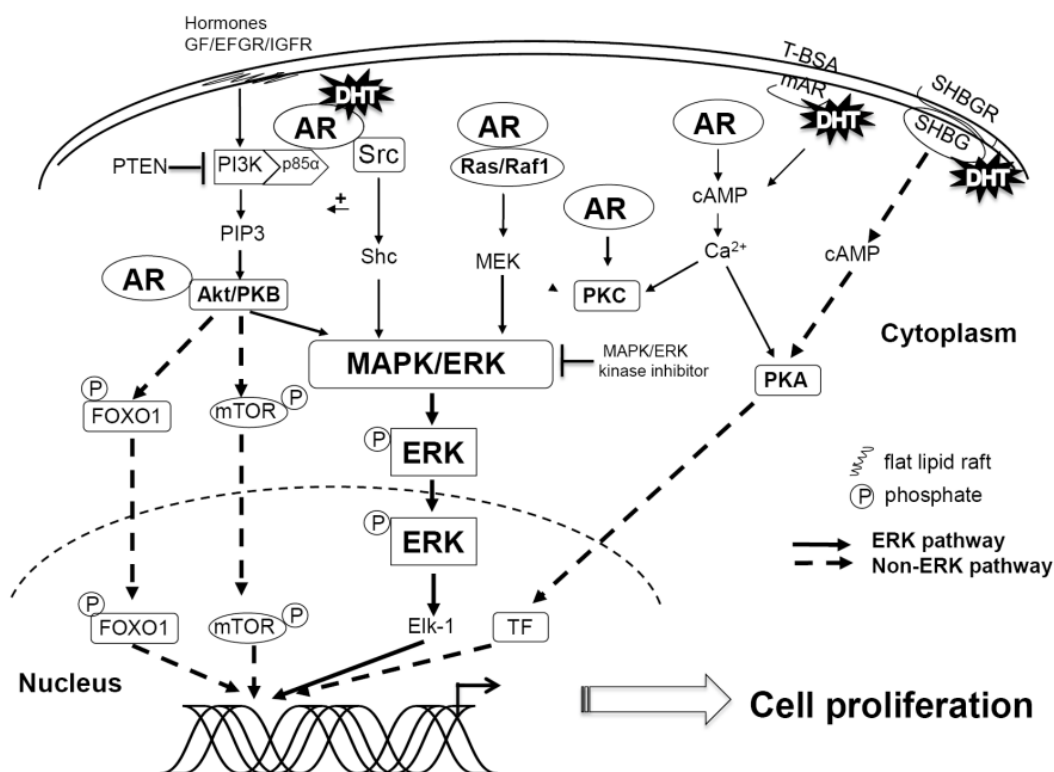
2. The SRC1 interacts with NTD of the AR via a glutamine rich region [1053 – 1123] and mutants lacking this glutamine region are inactive [89].

3.6.7. Ligand dependant non-genomic AR activation

The activated AR in the cytoplasm could also interact with several signalling pathways such as Ras-Raf-1, PI3K/Akt, Src, and protein kinase C (PKC). The mitogen-activated protein kinase (MAPK)/extracellular signal-regulated kinase (ERK) were activated which leads to the proliferation of prostate cancer cells (Figure 9) [90].

Chapter 3: Literature Review

Figure 9: Ligand dependent non-genomic pathway of AR

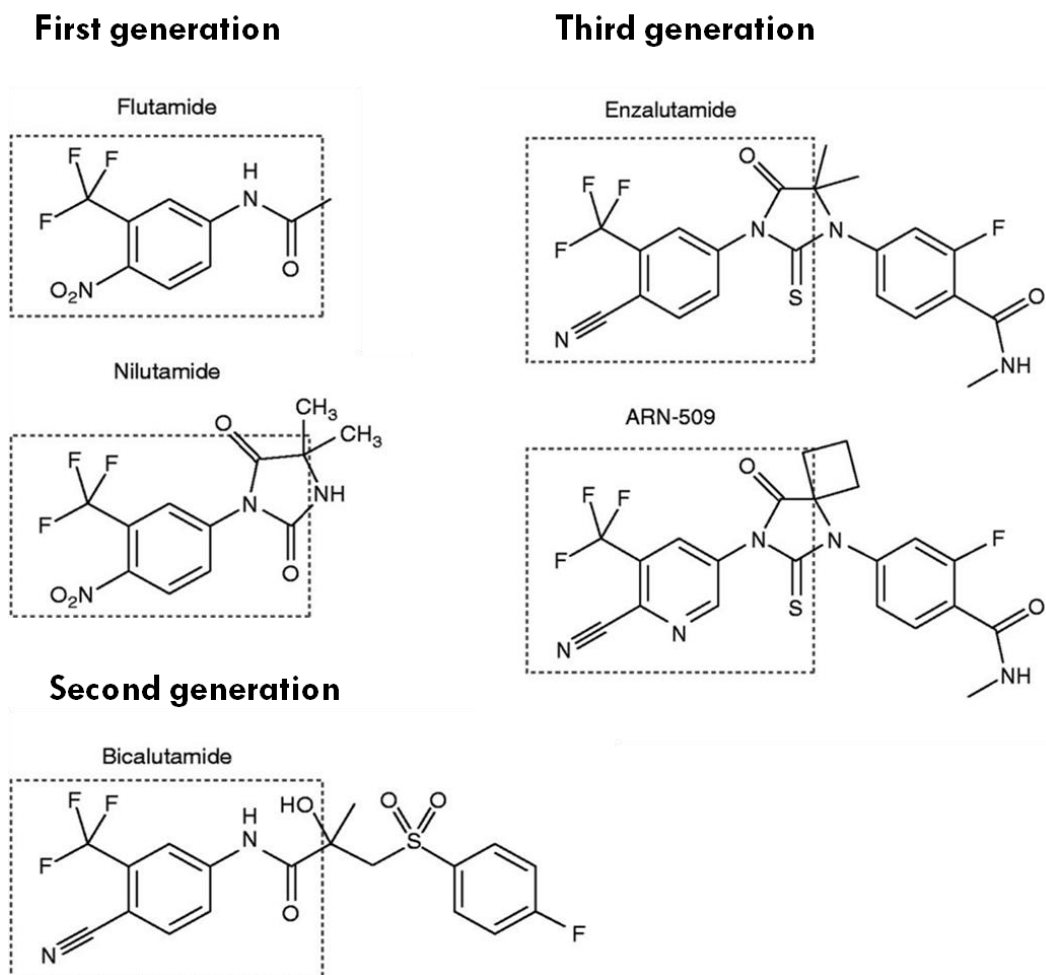


ERK and non-ERK mediated non-genomic AR signaling. ERK mediated non-genomic AR pathways are highlighted in solid line arrows. (I) AR interacts directly with the p85 regulatory subunit of phosphoinositide 3-kinase (PI3K) and activates Akt pathway. (II) AR interacts with Src resulting in Src activation of the adaptor protein, Shc, a known upstream regulator of the MAPK pathway. (III) AR interacts with Ras-Raf leading to sequential activation of Ras, Raf1 and MEK kinase converging on the phosphorylation of ERK. (IV) AR also utilizes PKC as a mediator of MAPK/ERK pathway activation. PKC kinase activity can be regulated by intracellular Ca^{2+} concentrations. Intracellular Ca^{2+} concentration may be modulated through plasma membrane G protein-coupled receptors (GPCRs), the sex hormone binding globulin receptor (SHBGR) and by a membrane-bound AR via up-regulation of cyclic adenosine monophosphate (cAMP) levels. Activated MAPK/ERK translocates to the nucleus, directly interacts with and phosphorylates transcription factors (TFs), such as Elk1, which coordinately regulates the expression of several genes involved in cell proliferation. Non-ERK mediated non-genomic AR pathways are highlighted in dash line arrows and include (V) PI3K/Akt/mTOR or (VI) forkhead box protein O1 (FOXO1) pathway activation. Akt activation may result in FOXO1 phosphorylation resulting in its retention in the cytoplasm and subsequent degradation. In addition, AR interacts with FOXO1 and impairs FOXO1 DNA binding ability and its ability to mediate pro-apoptotic pathways. (VII) Non-ERK signaling can also occur through activation of kinases such as protein kinase A (PKA), whose activation is regulated by intracellular Ca^{2+} concentration

Chapter 3: Literature Review

3.7. AR antagonist

Figure 10: Classification of non steroidal AR antagonist



Non-steroidal antiandrogens. The first, second and third generation AR antagonists that are currently being used in clinical practice share a structural motif consisting of an anilide substituted with a trifluoromethyl group in meta-position and a nitro- or cyano-group in para-position. In nilutamide, enzalutamide, and ARN-509, the amide of the anilide is a part of (thio)hydantoin.

The AR antagonists were broadly classified into steroidal and non-steroidal agents based on the ligand chemistry. Steroidal ligands have steroidal nucleus. The non steroidal ligands possess a similar anilide pharmacophore (Figure 10). The limitations of steroidal anti-androgens are well known because of

Chapter 3: Literature Review

their toxicity. For long term treatment like prostate cancer, the steroidal anti-androgens were not suitable. The 1st generation antagonist, nilutamide and flutamide had developed resistance with mutant ARs. The nilutamide and flutamide functions as an agonist to T877A mutant AR and stimulates the proliferation of prostate cancer cells. The second generation AR antagonist bicalutamide also experiences resistance with W741L/C mutant AR antagonist. The development of resistance among the 1st and 2nd generation AR antagonist lead to the preclinical identification of third generation antagonist, enzalutamide and apalutamide (ARN-509). The ARN-509 and enzalutamide in clinical trials was also found to be resistant to F876L mutation [91]. At present there is no AR antagonist in the clinical trials or in the market without developing resistance against mutant AR. Hence it is essential to develop a novel AR antagonist that could antagonize mutated AR.

The presently available 1st, 2nd and 3rd generation of AR antagonists have common structural features such as an anilide scaffold (Figure 10). In compounds such as nilutamide, enzalutamide and ARAN509 the amide group of the anilide was part of either hydantoin or thiohydantoin. A trifluoromethyl substitution (meta) and either nitro- or nitrile (para) substitution was present in the benzene ring of the anilide group in all the AR antagonists. Hence there is no diverse structural element in the marketed AR antagonist. Hence there is possibility of cross resistance within the molecules and because of that the entire AR antagonist had developed resistance for one or another mutation. Structurally diverse AR

Chapter 3: Literature Review

antagonist could possibly resist those mutations that occur during the course of treatment.

3.8. *In-silico* drug design and discovery

The drug design methods could be classified into two types

- Structure based drug design (SBDD)
- Ligand based drug design (LBDD)

3.8.1. Structure based drug design

In this, the crystal structure of the target (protein) should be available. The hit molecules will be identified based on the binding conformation, binding energy and interactions with the target. The interactions between the ligand and target were particularly important because it decides the affinity and binding energy. Following are some of the major interactions between the ligand and target [92].

- Covalent bond (Irreversible)
- H-Bond interaction
- Hydrophobic interaction
- Ionic interaction
- π - π interaction

The structure of the protein could also be generated by using homology modelling. Here there should be a presence of a template crystal structure that has close similarity with the target protein (Figure 11) [93].

Chapter 3: Literature Review

Figure 11: Computer aided drug design methods

	Known ligand(s)	No known ligand
Known protein structure	<p style="text-align: center;">Structure-based drug design (SBDD)</p> <ul style="list-style-type: none"> •Protein-ligand docking 	<ul style="list-style-type: none"> •<i>De novo</i> design <p style="text-align: center;">Lead grow techniques</p>
Unknown protein structure	<p style="text-align: center;">Ligand-based drug design (LBDD)</p> <p style="text-align: center;"><i>1 or more ligands</i></p> <ul style="list-style-type: none"> • Similarity searching <p style="text-align: center;"><i>Several ligands</i></p> <ul style="list-style-type: none"> • Pharmacophore searching <p style="text-align: center;"><i>Many ligands (20+)</i></p> <ul style="list-style-type: none"> • Quantitative Structure-Activity Relationships (QSAR) 	<ul style="list-style-type: none"> •Homology modelling <p style="text-align: center;">Identification of protein structure from template protein</p>

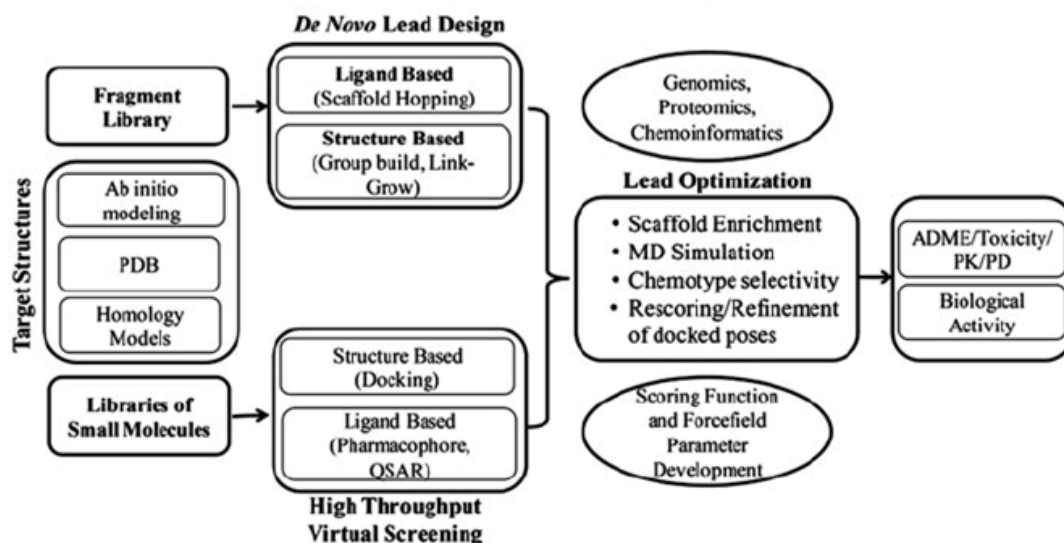
3.8.2. Ligand based drug design

The LBDD is divided into ligand and structure based. In the ligand based, the information about the binding site of the target was not available. In this case a correlation will be obtained between the well-known structures of the ligands and their biological activity. The aim is to construct a pharmacophore (3D-QSAR) which could be used to find matches in the existing chemical databases like, SPECS, ZINC, Cambridge and synthesized molecules. The major drawback in here is the researcher will be unsure of the bio active conformation. The second drawback was to superimpose the different scaffolds of ligands [94]. Hence, a structure based identification of pharmacophore generation is better because this approach will consider the actual binding conformation of the ligand in the

Chapter 3: Literature Review

binding site. Based on bio active binding conformation, a 3D-QSAR (pharmacophore) will be generated. The generated pharmacophore could be used to screen chemical databases for the identification of matches (Figure 12) [94].

Figure 12: Virtual screening workflow for the identification of HIT molecules



The rational drug design had led to the identification of many therapeutically useful drugs. The rational drug design had led to the identification of imatinib. The imatinib is a tyrosine kinase inhibitor and used in treating leukaemia. The successful application of structure based drug design guided to the identification of dorzolamide which is a carbonic anhydrase inhibitor [95 - 99].

Additional examples include:

- Identification of atypical antipsychotics
- Identification of cimetidine which is the prototype of H₂-receptor antagonist which later lead to the identification of many drugs in that series.

Chapter 3: Literature Review

- Selective COX-2 inhibitors which decreased the side effects of COX1 inhibitors.
- Enfuvirtide which is a HIV entry inhibitor for the treatment of AIDS.
- Nonbenzodiazepines like zolpidem and zopiclone
- Zanamivir is a neuraminidase inhibitor for the treatment of influenza
- HIV integrase inhibitor raltegravir for the treatment of AIDS

Chapter 4: Plan Of Work

4. PLAN OF WORK

Phase 1: To analyse the ligand/protein interactions between the wild and mutant ARs

- Collection of wild and mutant androgen receptors from PDB
- Identification of 3D structural difference between wild and mutant ARs
- Analysis of the ligand binding pocket of wild and mutant ARs
- Elucidation of possible ligand/receptor interactions for AR antagonists

Phase 2: To develop a pharmacophore model for wild and mutant AR antagonists and to identify difference between the pharmacophore models

- Dataset preparation for wild and mutant AR antagonists
- Pharmacophore generation and validation of the models
- Elucidation of difference in the pharmacophore between wild and mutant ARs

Phase 3: Identification of new chemical entities through *in-silico* drug design methods

- Identification of novel scaffolds through ligand based drug design
- Evaluation of the ligand/receptor interactions of the hit molecules

Phase 4: *In-vitro* anti prostate cancer activity of the new chemical entities to identify the hit molecules

- *In-vitro* anti-proliferation assay for selected hit molecules in LNCaP (T877A AR), MCF-7 (Wild type AR), MDA MB 453 (Q865H AR), PC3 (AR negative) and 3T3 (non-cancerous) cell lines

Chapter 4: Plan Of Work

- Screening for prostate cancer biomarkers (PSA and TMPRSS2) for potent compounds *in-vitro*

.....
Phase 4: Elucidation of the anti-cancer mechanism of action for the best active molecule
.....

- Gene expression studies for oncogenes such as c-myc, cyclin D1, ETV1, PS2 and AR through qPCR
- Protein expression studies for AR, p-AR²¹³, AKT, and p-AKT⁴⁷³ through western blotting
- Elucidation of apoptotic mechanism through BAX/bcl2 mRNA ratio, procaspase 3 protein expression and caspase 3 activity
- Confirmation of apoptosis through Ethidium bromide/Acridine orange staining

Chapter 5: Materials

5. MATERIALS

5.1. Materials used in this study

Following are the list of materials used in this study (Table 5)

Table 5: Materials list

Chemicals/Softwares/Instruments	Manufacturer
Ligprep, Maestro, Glide XP and SP, PRIME, PHASE and PyMOL	Schrödinger
Chem Draw ultra	Cambridge
ChemSketch	ACD Labs
BIOVIA Discovery Studio	Accelrys
Compounds (ARA1 to ARA9), 9 compounds	Shasun Research Centre
R-Bicalutamide	SantaCruz
Polystyrene culture plates - 96, 24 and 6 well plates, 100mm tissue culture dish, T-25 and T-75 culture flask.	Sigma Aldrich
Cell Bind tissue culture T-25 flask and 96 well plates	Sigma Aldrich
ATCC modified RPMI medium, RPMI, PBS and Fetal bovine serum	Gibco
Trypsin 1X, DHT, Testosterone, TRIZOL, Poly - L - Lysine	Sigma Aldrich
Phosphatase and protease inhibitor cocktail, DEPC water, High capacity cDNA conversion kit.	Thermo Scientific
Primary antibodies and secondary antibodies	SantaCruz

Chapter 5: Materials

Primers - PSA, TMPRSS2, GAPDH, PS2, C-Myc, Cyclin D1, ETV1	Sigma Aldrich
Primers - BAX, Bcl2	Bioline
MTT, Ethanol, DMSO	Hi-Media
Caspase 3 assay kit	BIOVISON
SYBR green, ROX dye	Takara
SDS, TEMED, Agarose, Ammonium per sulfate	Sigma Aldrich
Protein assay kit	BIO-RAD
Class II bio-safety cabinet	ESCO
CO ₂ Incubator, Multimode ELISA reader, Thermal cycler	Thermo Scientific
Step oneplus real time PCR	Applied Biosystems
Semi dry blotting	Hoefer
GEL DOC	Syngene

Chapter 6: Experimental Methods

6. EXPERIMENTAL METHODS

6.1. Phase 1 - To analyse the ligand/protein interactions between the wild and mutant ARs

6.1.1. Root Mean Square deviation between wild and mutant ARs

The AR proteins, wild (PDB ID: 2AMA), T877A (PDB ID: 2AX6) and W741L (PDB ID: 1Z95) were downloaded from PDB. The alignment between the proteins were done using protein alignment tool in Maestro (v9.8), Schrödinger [100]. Each of the mutant proteins were aligned with wild type AR and the root mean square deviation (RMSD) was calculated for the protein backbone. The alignment score was used to validate the RMSD calculation [101].

6.1.2. Analysis of the ligand binding pocket of wild and mutant ARs

6.1.2.1. Ligand preparation

The AR ligands such dihydrotestosterone, testosterone, flutamide, bicalutamide and enzalutamide were downloaded from chemspider. The ligands for docking studies were prepared using LigPrep (v3.1), Schrödinger [102]. The LigPrep does the tasks such as conversion of 2D to 3D structure, energy minimization, addition of missing hydrogen atoms, generation of different ionization state, generation of stereoisomer, neutralization of the charged structures, and generation of potential ionization state at a definite pH of 7.2 ± 2 . The selection of wide pH range (5.2 to 9.2) was essential because of the different pharmacokinetic environment that the ligands undergo in biological system. This wide range of pH led to protonation of certain molecules especially those who have nitro or carboxyl functional groups [103].

Chapter 6: Experimental Methods

6.1.2.2. Protein preparation

The AR proteins, wild (PDB ID: 2AMA), T877A (PDB ID: 2AX6) and W741L (PDB ID: 1Z95) were downloaded from PDB. The crystal structures of the proteins were prepared using Protein Preparation Wizard in Maestro (v9.8), Schrödinger [100]. Preprocessing of the proteins were essential because, the crystal structure of the protein may have multiple chains, missing hydrogen atoms, alternate positions for certain amino acids like histamine and glutamine. In the preprocessing step of the protein, the identical chains were deleted, polar hydrogens were added, water molecules were deleted except those were within 5 Å from the ligand binding site. The tautomers were generated using pH value of 7.2 ± 0.2 . This pH 7.2 ± 0.2 was considered because it is the physiological pH [104].

6.1.2.3. Homology modelling

The homology model was prepared by using PRIME (v3.7), Schrödinger [105]. PRIME was used for

- Protein structure prediction,
- Side chain optimization,
- Loop prediction,
- Active site refinement and
- Energy minimization.

The amino acid sequence of the T877A mutant AR was obtained from NCBI. The T877A mutant AR (PDB ID: 2OZ7) was used as the template. This was co-crystallized with antagonist cyproterone acetate and has a resolution of

Chapter 6: Experimental Methods

1.80 Å. In the homology modelled AR, the ligand binding domain has 671-881 amino acids instead of 671-919 amino acids [106]. The homology modelled AR thereby lacks the helix-12 amino acids. The alignment between the target and template sequence was carried out by Clustalw method. The sequence identity between the target and template was 100%. The ligand (cyproterone acetate) and a water molecule (HOH-108) were retained in the final model. The prepared homology model were optimized for energy minimization using OPLS 2005 and the active site was further refined.

6.1.2.4. Docking

The docking studies were carried out using GLIDE XP (extra precision) (v3.3), Schrödinger. The glide docking considers the ligands as a fully flexible unit and the receptor as a rigid grid representation. The grid space within the protein was generated using receptor grid generation using default parameters. The co-crystal ligand was applied as the central of the docking box with a volume competent of binding with ligands with a length of $\leq 20\text{Å}$. The processed proteins were only used to generate the grid space by considering the co-crystal ligand as the centroid of the grid space. The ligands were ranked by Glide Score (G Score). The least energy is the best ligand [107].

$$\text{G Score} = (a \times \text{vdW}) + (b \times \text{Coul}) + \text{Lipo} + \text{Hbond} + \text{Metal} + \text{BuryP} + \text{RotB} + \text{Site}$$

Where,

vdW – van der Waal energy, Coul – Coulomb energy, Lipo – Lipophilic contact term, Hbond – Hydrogen bond, Metal – Metal binding term, BuryP – penalty for

Chapter 6: Experimental Methods

buried polar groups, RotB – penalty for freezing rotatable bonds, Site – polar interaction of the active site.

6.1.2.5. Validation

The docking studies were validated by superimposing and calculating the RMSD between the bound conformation and docked conformation of the co-crystallized ligand. The deviation should be less than 2Å. This is because; the crystal structures in the PDBs have an average deviation of approximately 2Å [108]. The homology model was validated by the structural analysis and verification server (SAVES). The amino acids in the favourable, allowed and disallowed regions were calculated by Ramachandran plot. The stereochemistry of the amino acids in the homology model was evaluated by PROCHECK. The 3D compatibility of the homology model was validated by VERIFY_3D. The docking was carried out as explained in the previous section [109].

6.1.3. Elucidation of the binding mechanism of AR antagonist

The AR antagonists such as flutamide, bicalutamide and enzalutamide were docked with various types of AR proteins. The AR proteins such as wild type (PDB ID: 2AMA), T877A mutant (PDB ID: 2AX6), W741L (PDB ID: 1Z95) and homology model (truncated helix-12) were used for docking studies. Then the docked conformation of the ligands in the mutant ARs were aligned and superimposed with the conformation in the truncated AR. The difference in the binding conformation was elucidated visually and interpreted.

Chapter 6: Experimental Methods

6.2. Phase 2 - To develop a pharmacophore model for wild and mutant AR antagonists and to identify difference between the pharmacophore models

6.2.1. Data set preparation for wild, T877A and full antagonists

The molecules for the datasets were obtained from literatures [110 - 114]. The ligands were then grouped into three datasets. The first dataset consists of ligands that antagonize the wild type AR. The second dataset consists of ligands that antagonize the T877A mutant AR. The third dataset consists of ligands that antagonize both wild and T877A mutant ARs without any agonist / partial agonist effect on either of these receptors (full antagonist). The methods adopted in these papers were the same and the experiments were conducted in the same laboratory.

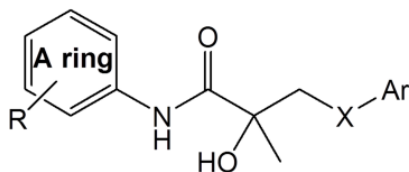
The dataset for wild type has 122 molecules and was randomly split into training (75%) and test (25%) sets [115]. The molecules having $IC_{50} < 4\mu M$ were designated as actives and molecules having $IC_{50} > 50\mu M$ were designated as inactives. The dataset for T877A AR has 132 molecules and the dataset was divided randomly into training (75%) and test (25%) sets. The molecules having $IC_{50} < 3\mu M$ were designated as actives and molecules having $IC_{50} > 32\mu M$ were designated as inactives. The molecules in the wild and T877A mutant ARs dataset represent similarity with AR antagonists, enzalutamide and bicalutamide (Figure 13). The dataset for full antagonist has 42 molecules and the dataset was randomly divided into training (75%) and test (25%) sets. The molecules in the dataset have different types of basic nucleus comprising, 1-arylmethyl-4-phenylpyrrole, 4-arylmethyl-1-phenylpyrazole, 4-aryloxy-1-phenyl pyrazole, and 3-aryl-3-hydroxy-1-phenylpyrrolidine derivatives (Figure 13). The ligands having $IC_{50} < 0.10\mu M$

Chapter 6: Experimental Methods

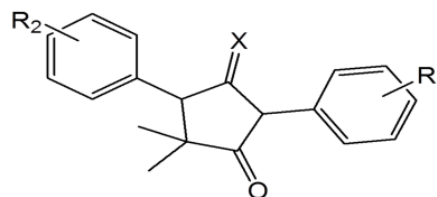
were designated as actives and ligands having $IC_{50} > 3\mu M$ were designated as inactive.

Figure 13: Scaffolds of the dataset molecules for pharmacophore modelling

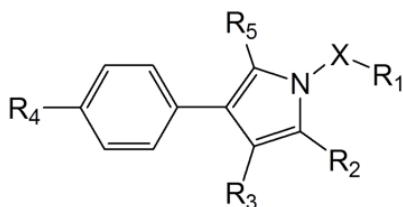
A: Bicalutamide derivatives



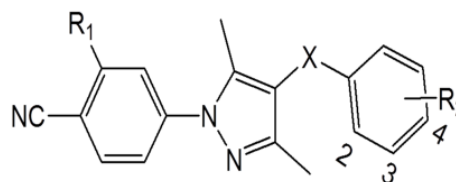
B: Enzalutamide derivatives



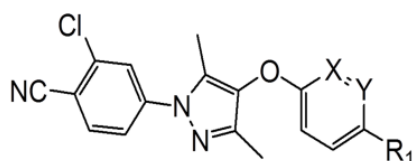
C: 1-arylmethyl-4-phenylpyrrole



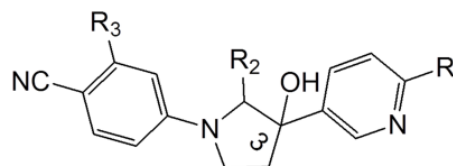
D: 4-arylmethyl-1-phenylpyrazole



E: 4-aryloxy-1-phenylpyrazole



F: 3-aryl-3-hydroxy-1-phenylpyrrolidine



The biological activity of each dataset was obtained in different cell lines. Hence, there is a difference in the biological activity range among the datasets. The active and inactive molecules were selected depending on the activity range among the dataset molecules. The active molecules are the ones which will have the least IC_{50} and the inactive molecules will have the higher IC_{50} values among the dataset molecules. Hence, the inactive molecules are less active rather than absolutely inactive. This method of selection yields an optimal numbers of active and inactive molecules in the training and test set. This is absolutely essential for

Chapter 6: Experimental Methods

validating the 3D-QSAR with an external test set which should have equal activity distribution like training set.

6.2.2. Ligand preparation

The ligands were drawn using Maestro (v9.8), Schrodinger [100]. The LigPrep does the tasks such as conversion of 2D to 3D structure, energy minimization, addition of missing hydrogen atoms, generation of different ionization state, generation of stereoisomer, neutralization of the charged structures, and generation of potential ionization state at a definite pH of 7.2 ± 2 . The selection of wide pH range (5.2 to 9.2) was essential because of the different pharmacokinetic environment that the ligands undergo in biological system. This wide pH range led to protonation of certain molecules especially those who have nitro or carboxyl functional groups. The conformational space for the ligands was explored using a combination of Monte-Carlo Multiple Minimum (MCMM) and Low Mode (LMOD) with a maximum number of conformers set to 1,000 conformers per structure. The energy minimization was performed by OPLS 2005. Each of the energy minimized conformer was filtered by a relative energy window of 10 kJ mol^{-1} . The minimum atomic deviation allowed was set at 1.00 \AA . The conformers that had higher energy than the 10 kJ mol^{-1} thresholds were discarded. For the consideration of identical conformers, the distances between the corresponding heavy atoms should be less than 1.00 \AA [103].

6.2.3. Pharmacophore generation for wild, T877A and full antagonists

Common pharmacophore hypotheses (CPH) identification and 3D-QSAR model were constructed using PHASE, Schrödinger (v3.9) [116]. PHASE give us

Chapter 6: Experimental Methods

a maximum of 7 pharmacophore site points in the 3D-QSAR. The pharmacophore site points includes features such as hydrogen bond acceptors (A), hydrogen bond donor (D), hydrophobicity (H), aromatic rings (R), positively ionisable groups (P), negatively ionisable groups (N) and user defined X, Y, and Z. The Common pharmacophore hypotheses were generated by using a box with a size of 1 Å. All of the common pharmacophore hypotheses were effectively scored by correlating the observed and predicted activity of the training and test sets using partial least squares (PLS) method. The maximum number of partial least square (PLS) factors that could be used for calculations was $N/5$, where N is the number of molecules in the training set. A PLS factor value of 5 was used to validate the wild and T877A mutant AR antagonist. A PLS factor value of 3 was used for full antagonist. Atom based 3D-QSAR method was followed by applying default parameters [117].

6.2.4. Selection and Validation of the Models

The best 3D-QSAR model was selected based on high correlation between the predicted and observed activity (R^2), predictive ability of the model (Q^2), low standard deviation (S.D), and the probability of getting an actual result (P value) of the training set [118]. The model was also validated by predicting a test set having wide range of biological activity. The correlation between the observed and predicted activity of the test set (R^2), Pearson-R, Predictive R^2 (R^2_{pred}), and the correlation between the observed and predicted activity of the test set with intercept set at zero (r^2_m) were used to evaluate the predictive power of the models. The models having the highest (at least >0.5) value for Q^2 , R^2_{pred} , and

Chapter 6: Experimental Methods

r^2_m were considered for selection [119]. From this selection, the model that had the highest R^2 value for training and test set molecules, Q^2 , R^2_{pred} , and r^2_m was considered as the best.

6.3. Phase 3 - Identification of new chemical entities through *in-silico* drug design methods

6.3.1. In-silico virtual screening (Pharmacophore matching and docking)

The generated pharmacophore was used to find matches in the SPECS database and synthesized compounds from Shasun Research Centre, Chennai. The pharmacophore matching was performed by using PHASE (v3.9), Schrodinger [116]. PHASE searches database using sites and geometric arrangements to find molecules that match the hypothesis and then retrieve the relevant conformers from the database for alignment to the hypothesis. The compounds having matching threshold of 2 out of 3 were further processed by docking studies [120].

The AR proteins (PDB ID: 2OZ7) and homology model (helix-12) were used for docking calculations. The Glide SP (standard precision), Schrödinger was followed for docking calculations [107]. The SP method significantly reduces the time taken for docking and hence large number of database ligands could be screened.

6.4. Phase 4: *In-vitro* anti prostate cancer activity of the new chemical entities to identify the hit molecules

6.4.1. In-vitro anti-proliferation assay

The cell lines, LNCaP-FGC, MDA-MB-453, MCF-7, PC3, and 3T3 were purchased from NCCS, Pune. The PC3 and 3T3 cells were cultured in RPMI

Chapter 6: Experimental Methods

medium supplemented with 10% fetal bovine serum (FBS) and 2 mM glutamine. The MDA MB 453 cells were cultured in DMEM F12 medium supplemented with 10% FBS and 2 mM glutamine. The LNCaP cells were cultured in ATCC modified RPMI medium which was supplemented with 10% FBS, 4.5 g/L D-Glucose, 2.383 g/L HEPES buffer, 2M L-Glutamine, 1.5g/L sodium bicarbonate and 110 mg/L sodium pyruvate and. The PC3, MDA MB 453 and 3T3 cells were grown in polystyrene surface (T25 flask & 96 well plate). The LNCaP cells were grown in corning CellBIND surface (T25 flask & 96 well plate). The cells were incubated at 37 °C with 5% CO₂. 0.25 % trypsin was used for detachment of the cells [121, 122].

The entire cell lines were cultured in their respective medium supplemented with charcoal stripped 10% FBS for the proliferation and anti-proliferation assays. The screening was done in a 96 well plate. Each of the 96 wells was seeded with approximately 2000 cells. The anti-proliferative activity was measured by adding standard and test compounds (0.1 µM to 100 µM) in the presence of 1 nM DHT. The proliferative activity of the standard and test compounds (1 µM) was evaluated without 1 nM DHT [123]. The toxicity of the compounds (0.1 µM to 100 µM) was measured in non-cancerous 3T3 cell line. The cells were treated for 48 hours. Post treatment, the culture medium was drained and replaced with fresh medium supplemented with 10 µl of MTT (5 mg/ml) and incubated for 4 hours. The formazon crystals that were formed were dissolved in 100 µl of DMSO/well. The optical density was measured at 570 nm.

Chapter 6: Experimental Methods

The IC₅₀ was calculated by plotting a dose response curve by taking percentage cyto-toxicity in y axis and log dose in x axis.

$$\text{Percentage toxicity} = \{1 - [(At-Ab)/ (Ac-Ab)]\} \times 100$$

Where,

At = Absorbance value of test compound,

Ab = Absorbance value of blank and

Ac = Absorbance value of control.

6.4.2. Screening for prostate cancer bio-markers

6.4.2.1. RNA Isolation

The prostate specific antigen (PSA) and TMPRSS2 were the biomarkers for prostate cancer. The gene expression of the prostate specific antigen and TMPRSS2 were evaluated in LNCaP cell lines by qPCR. The LNCaP cells were cultured in RPMI medium supplemented with charcoal stripped 10% FBS. The cells were treated for 24 hours with bicalutamide (10 μM) or ARA3 (1 μM) in the presence of 1 nM DHT [124]. The total RNA was isolated using trizol (sigma). The treated cells were lysed in the culture plate by using trizol reagent. The quantity of trizol used was 1ml per 10cm² of the surface area. The lysed cells were allowed to rest for 5 minutes at room temperature for the dissociation of nucleoproteins from the RNA. Then, 200μl of chloroform was added to the lysed cells for 1 ml of trizol used. The mixture was shaken intermittently for 15 seconds. Then the samples were allowed to stand for 2–15 minutes. The samples were phase separated by centrifugation at 12,000 × g for 15 minutes at 2–8 °C.

Chapter 6: Experimental Methods

The centrifugation procedure divides the mixture into 3 phases:

- The red colored organic phase contains protein,
- The white ring in the inter phase contains DNA and,
- The colorless supernatant has total RNA.

The supernatant was carefully transferred without disturbing the other layers into a fresh tube. Then, 0.5 ml of 2-propanol was added to the supernatant for 1ml of trizol that was added previously. The supernatant mixture was allowed to stand for 5– 10 minutes. The precipitate RNA is visible in this step. The precipitated RNA was obtained by centrifuging the samples at $12,000 \times g$ for 10 minutes at 2–8 °C. The RNA precipitate was then washed with 1 ml of 75% ethanol. The sample was vortexed and then centrifuged at $7500 \times g$ for 5 minutes at 2–8 °C. The quantity and the quality of the total RNA was identified using Nanodrop (Thermal scientific). The ratio, A260/A280 and A260/A230 of the total RNA was used to assess the quality of the RNA. The RNA samples which had the ratio of >2 were used for gene expression studies [125].

6.4.2.2. Real time PCR (qPCR)

The cDNA was converted from 1 μg of the total RNA using high capacity cDNA conversion kit (Applied Bio-systems). The thermal cycling condition for cDNA synthesis was given in table 6. The amplification of the cDNA and subsequent expressions of the genes were measured using SYBR green master mix (Takara) and step one plus qPCR (Applied Bio-systems). The ROX dye was used as an internal control for SYBR green. The primers were designed by primer 3 software (Table 7). The thermal cycling condition for qPCR was given in table

Chapter 6: Experimental Methods

8. The relative mRNA expression of the test genes (PSA and GAPDH) to GAPDH was calculated by comparative Ct method. The product (amplicon) was confirmed by evaluating the T_m temperature of melt curve [126].

Table 6: Thermal conditions for cDNA synthesis

Settings	Step 1	Step 2	Step 3	Step 4
Temperature	25°C	37°C	85°C	4°C
Time	10 minutes	120 minutes	5 minutes	infinity

Table 7: Primers for prostate cancer biomarkers

Gene	Primers	NCBI	T _m °C
GAPDH	F: 5'-CCATCTTCCAGGAGCGAGATCCC-3',	NM_0020	85.85
	R: 5'-CCCAGCCTTCTCCATGGTGG-3'	46.5	
PSA	F: 5'-CCGGAAGTGGATCAAGGACA-3',	NM_0016	82.92
	R: 5'-GGCCTGGTCATTTCCAAGGT-3',	48.2	
TMPRSS2	F: 5'-GCTTCCCCGTGCATGATTTA-3',	NM_0011	79.35
	R: 5'-ATGGCAGAGAGTGCCAAAGC-3',	35099.1	

Table 8: Thermal conditions for qPCR

Settings	Initial denaturation	PCR condition (40 cycles)	
		Denaturation	Annealing and Elongation
Temperature	95°C	95°C	60°C
Time	30 seconds	5 seconds	30 seconds

Chapter 6: Experimental Methods

6.5. Phase 4 - Elucidation of the mechanism of action of the best active molecule

6.5.1. Gene expression

The mRNA expression of androgen stimulated oncogenes (ETV1, C-MYC & Cyclin D1), AR and oestrogen receptor response element (PS2) were measured in LNCaP cells by qPCR. For the quantification of oncogenes the LNCaP cells were cultured in RPMI medium supplemented with charcoal stripped 10% FBS. The cells were treated for 24 hours with bicalutamide (10 μ M) or ARA3 (1 μ M) in the presence of 1 nM DHT. For the quantification of AR and PS2, the LNCaP cells were treated for 24 hours with bicalutamide (10 μ M) or ARA3 (1 μ M) in the absence of 1nM DHT. The primers were designed by primer 3 software (Table 9). The thermal cycling condition for qPCR was given in table 10. The relative mRNA expression of the test genes to GAPDH was calculated by comparative Ct method. The product (amplicon) was confirmed by evaluating the T_m temperature of melt curve.

Chapter 6: Experimental Methods

Table 9: Primers of oncogenes

Gene	Primers	NCBI	T _m °C
GAPDH	F: 5'-CCATCTTCCAGGAGCGAGATCCC-3', R: 5'-CCCAGCCTTCTCCATGGTGG-3'	NM_00204 6.5	85.85
C-MYC	F: 5'-TAGTGGAAAACCAGCAGCCTCC-3', R: 5'-CGTCGCAGTAGAAATACGGCT-3',	NM_00246 7.4	85.32
Cyclin D1	F: 5'-GCTGCGAAGTGGAAACCATC-3', R: 5'-CCTCCTTCTGCACACATTTGA-3',	NM_05305 6.2	90.02
ETV1	F: 5'-TTAGCCGTTCACTCCGCTAT-3' R: 5'-TATCTGGAAAGGCCATGGAG-3'	NM_00495 6.4	80.83
AR	F: 5'-GCTGCATCAGTTCGCTTTTG-3' R: 5'-CTTGGGCACTTGCACAGAGA-3'	NM_00004 4.3	83.15
PS2	F: 5'-GCCCTCCCAGTGTGCAAATA-3' R: 5'-TGGAGGGACGTTCGATGGTAT-3'	NM_00322 5.2	84.23

Table 10: Thermal conditions for qPCR

Settings	Initial denaturation	PCR condition (40 cycles)	
		Denaturation	Annealing and Elongation
Temperature	95°C	95°C	60°C
Time	30 seconds	5 seconds	30 seconds

Chapter 6: Experimental Methods

6.5.2. Protein expression of AR and AKT1

The LNCaP cells were cultured in medium supplemented with 10% charcoal stripped FBS. The cells were treated for 24 with ARA3 (1 μ M) or bicalutamide (10 μ M) in the presence of 1 nM DHT. The proteins were extracted by adding RIPA buffer supplemented with protease and phosphatase inhibitor cocktail. Protein concentration was determined by Bio-Rad Bradford reagent (Bio-Rad Laboratories, Hercules, CA). The lysate was centrifuged at 16000 g for 20 min. Supernatant equivalent to 40 μ g of protein was subjected to SDS PAGE gel electrophoresis. The antibodies were given in table 11. The resolved proteins were transferred to a PVDF membrane. The transferred proteins were hybridized with primary antibodies. Expression of β -actin was measured as an internal control using β -actin antibody (ab8227). The proteins were detected by horseradish peroxidase labeled anti rabbit or anti-mouse IgG monoclonal or polyclonal antibody and a chemi-luminescence detection kit (ECL, GE healthcare) [127]. The fold expression was calculated by using the formula,

$$\text{Fold ratio} = \frac{\text{Ratio of amount of target protein (treated) normalized with control}}{\text{Ratio of amount } \beta\text{-actin (treated) normalized with control}}$$

Chapter 6: Experimental Methods

Table 11: List of antibodies for western blot

S. No	Antibody	Molecular weight KDa	Dilution
1	AR (sc816)	110	1:1000
2	p-AR ²¹³ (sc135635)	110	1:1000
3	akt1 (sc5289)	62	1:1000
4	p-akt1 ⁴⁷³ (sc293125)	60	1:1000
5	β -actin	41	1:1000

6.5.3. Apoptosis assays

The apoptosis was confirmed in LNCaP cells by quantifying the BAX/Bcl2 mRNA ratio, procaspase-3 protein level, caspase-3 enzyme activity, and ethidium bromide/acridine orange (EB/AO) staining.

6.5.3.1. Gene expression of bax/bcl2

The mRNA expression of BAX and Bcl2 was quantified in LNCaP cells. The LNCaP cells were cultured in RPMI medium supplemented with 10% charcoal stripped FBS. The cells were treated for 48 hours with ARA3 (1 μ M) or bicalutamide (10 μ M) in the absence of 1nM DHT. The cDNA was converted from 1 μ g of the total RNA using high capacity cDNA conversion kit (Applied Bio-systems). The amplification of the cDNA and subsequent expressions of the genes were measured using SYBR green master mix (Takara) and step one plus qPCR (Applied Bio-systems). The ROX dye was used as an internal control for SYBR green. The primers were designed by primer 3 software (Table 12). The thermal cycling conditions for the qPCR were given in table 13. The relative

Chapter 6: Experimental Methods

mRNA expression of the test genes to GAPDH was calculated by comparative Ct method. The product (amplicon) was confirmed by evaluating the T_m temperature of melt curve.

Table 12: Primers for apoptosis biomarkers

Gene	Primers	NCBI	T _m °C
GAPDH	F: 5'-CCATCTTCCAGGAGCGAGATCCC-3',	NM_002	85.85
	R: 5'-CCCAGCCTTCTCCATGGTGG-3'	046.5	
BAX	F: 5'-GGGGACGAACTGGACAGTAA-3'	NM_001	85.45
	R: 5'-CAGTTGAAGTTGCCGTCAGA-3'	291428.1	
Bcl2	F: 5'- CAGGATAACGGAGGCTGGGATG-3'	NM_000	86.94
	R: 5-GACTTCACTTGTGGCCAGAT-3'	633.2	

Table 13: Thermal conditions for qPCR

Settings	Initial denaturation	PCR condition (40 cycles)	
		Denaturation	Annealing and Elongation
Temperature	95°C	95°C	60°C
Time	30 seconds	5 seconds	30 seconds

6.5.3.2. Caspase 3 activity

The protein expression of procaspase was measured as discussed in the earlier section. The LNCaP cells were treated for 48 hours with ARA3 (1 µM) or bicalutamide (10 µM) in the absence 1 nM DHT. The caspase-3 activity was measured in LNCaP cells by a colorimetric caspase assay kit (Bio Vision). Assay

Chapter 6: Experimental Methods

was performed according to instructions given by the manufacturer. The cells were harvested and lysed in 50 μ l of lysis buffer by incubating on ice for 10 minutes. Centrifugation was done to remove cell debris at 10,000 x g for 2 min. This supernatant extract was taken and protein measurement was done by Bradford's method. Total protein (100 μ g) was used in 50 μ l of cell lysis buffer. To that 50 μ l of 2X reaction buffer containing 10 mM DTT and 5 μ l of 4 mM of DEVD-pNA (caspase-3 substrate) was added and incubated at 37°C for 90 min. Absorbance was measured at 405nm by Multiskan™ GO multiplate reader (Thermo Scientific, Waltham, USA). Relative change in enzyme activity was measure

6.5.3.3. Ethidium bromide/Acridine orange (EB/AO) staining

The LNCaP cells were cultured in RPMI medium supplemented with 10% charcoal stripped FBS. The cells were treated for different time points (4 hour, 16 hour and 24 hour) with ARA3 (1 μ M) or bicalutamide (10 μ M) in the absence of 1nM DHT. The method for EB/AO staining was followed as explained in Ribble and co-workers [128]. The cells were cultured in 24well plates. After the treatment period, the EB/AO solution (each 100 μ g/ml) in PBS buffer was added to the wells. The fluorescence was visualized within 10 minutes using Nikon fluorescence microscope and photographed.

Chapter 7: Results and Analysis

7. RESULTS and ANALYSIS

7.1. Phase 1 - To analyse the ligand/protein interactions between the wild and mutant ARs

7.1.1. Purpose of the study

The purpose of the study is to identify the difference between the wild and mutant ARs. The difference in the structure of the wild and mutant AR was identified by computing the root mean square deviation (RMSD) between the protein backbone atoms. The difference in the binding characters of wild and mutant AR was studied using docking studies. The difference in the ligand binding pocket was identified through manual visualization. The entire ARs in the PDB are in agonist conformation. We observed that the bulkiness and rigidity had increased with newer generation of AR antagonist. As discussed earlier, the helix-12 of the AR extends from the ligand binding pocket upon binding with AR antagonist. Hence it may not possible for bulky AR antagonist to fit in the AR in agonist conformation. For the same, we modelled a helix-12 negative AR to fit the bulkier AR antagonist.

7.1.2. Root Mean Square deviation between wild and mutant ARs

The RMSD was calculated between wild and mutant ARs (T877A and W741L) mutant AR's ligand binding domain. The mutant AR proteins (T877A and W741L) were individually aligned with the wild type AR. The wild type AR was in agonist conformation because it was bound with DHT. The mutated ARs were also in agonist conformation but were bound with antagonist (Table 14). The

Chapter 7: Results and Analysis

RMSD of $<1 \text{ \AA}$ indicates that the structures of the mutated ARs are not significantly differ from the wild type AR.

Table 14: RMSD between wild and mutant ARs

AR mutation	RMSD with wild type AR in \AA	Alignment score
T877A	0.399	0.006
W741L	0.276	0.003

7.1.3. Analysis of the ligand binding pocket of wild and mutant ARs

The difference in the ligand-receptor interactions between wild and mutant (T877A and W741L) ARs were evaluated through docking studies. The standard AR agonist such as DHT and testosterone and standard AR antagonist such as bicalutamide, flutamide and enzalutamide were docked with wild, T877A, W741L and homology model (helix-12 negative) ARs (Table 15).

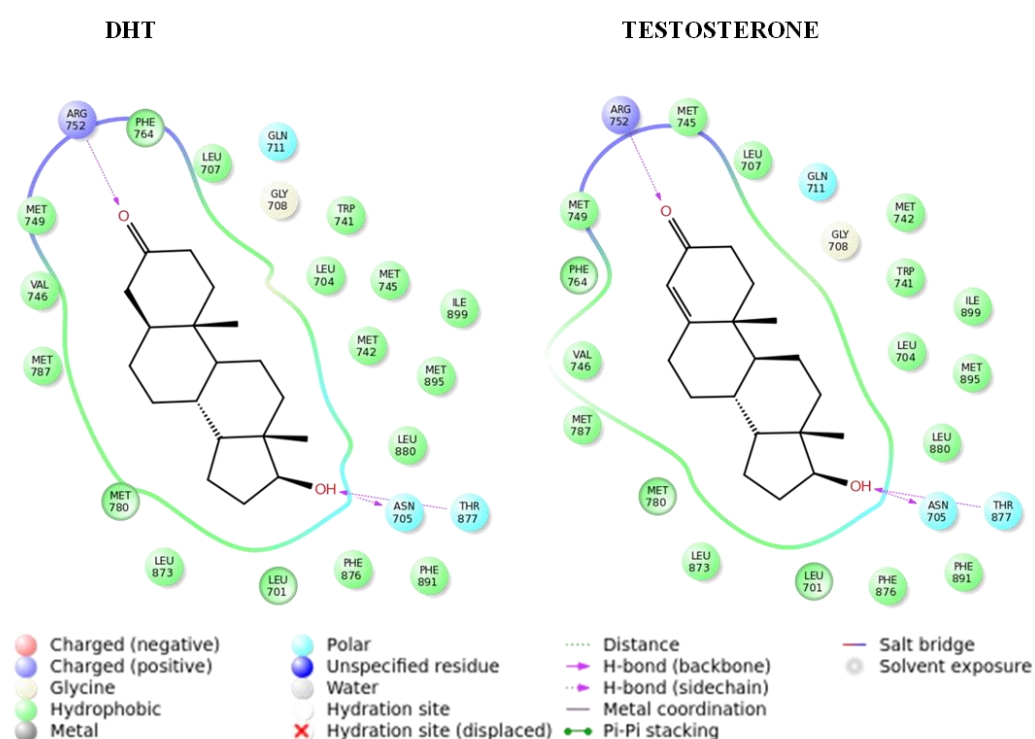
7.1.3.1. Androgen

The androgen DHT has binding affinity towards all the ARs (Table 15). The DHT and testosterone have similar type H-Bond interactions with wild type AR (Figure 14). The ketone group of DHT and testosterone formed H-Bond interaction with Arg752, while the 17β hydroxyl group formed H-Bond interaction with Asn705 and Thr877. Testosterone did not bind with the T877A mutated AR and didn't form any H-Bond interaction with W741L mutated AR. The binding energy of the androgens was less in the mutated ARs than the wild type AR. The DHT has a dock score of -10.80 kcal/mol with wild type AR but the

Chapter 7: Results and Analysis

dock score had decreased with T877A (-7.84 kcal/mol) and W741L (-6.71 kcal/mol) mutated ARs. Similarly the testosterone has a dock score of -10.68 kcal/mol with wild type AR but the dock score had decreased with T877A (no binding) and W741L (-5.95 kcal/mol) mutated ARs. We observed that the AR mutation decreases the binding affinity of the androgens with AR.

Figure 14: Binding interactions of androgens with AR



DHT forms H-Bond interaction with Arg752, Asn705 and Thr877 with wild type AR. Testosterone forms H-Bond interaction with Arg752, Asn705 and Thr877 with wild type AR

Chapter 7: Results and Analysis

Table 15: Docking score and H-Bond interaction of AR standard ligands

Ligands	Wild type		T877A		W741L		Truncated	
	Dock Score ¹	H-Bond	Dock Score	H-Bond	Dock Score	H-Bond	Dock Score	H-Bond
DHT	-10.80	Arg752, Asn705, Thr877	-7.84	Arg752, Gln711, HOH108	-6.71	Arg752, Gln711, Thr877, HOH108	-7.26	HOH108, Asn705
Testosterone	-10.68	Arg752, Asn705, Thr877	×	×	-5.95	×	-7.17	HOH108, Asn705
Flutamide	-7.76	Asn705, Thr877	-8.25	Arg752, Gln711, Asn705, Leu704, HOH108*, HOH213 [#]	-7.22	Arg752, Gln711, Leu704, Asn705, HOH108	-6.22	Arg752, Gln711, Asn705, HOH108
Bicalutamide	-2.54	×	×	×	-10.27	Arg752, Gln711, Leu704, Asn705, HOH108	-7.62	Arg752, Gln711, Asn705
Enzalutamide	×	×	×	×	×	×	-8.42	Arg752, Gln711

¹Dock score in kcal/mol, *HOH108 could form bridged H-Bond interactions with Arg752, Gln711 and Met745, [#]HOH213 could form bridged H-Bond interaction with Leu873

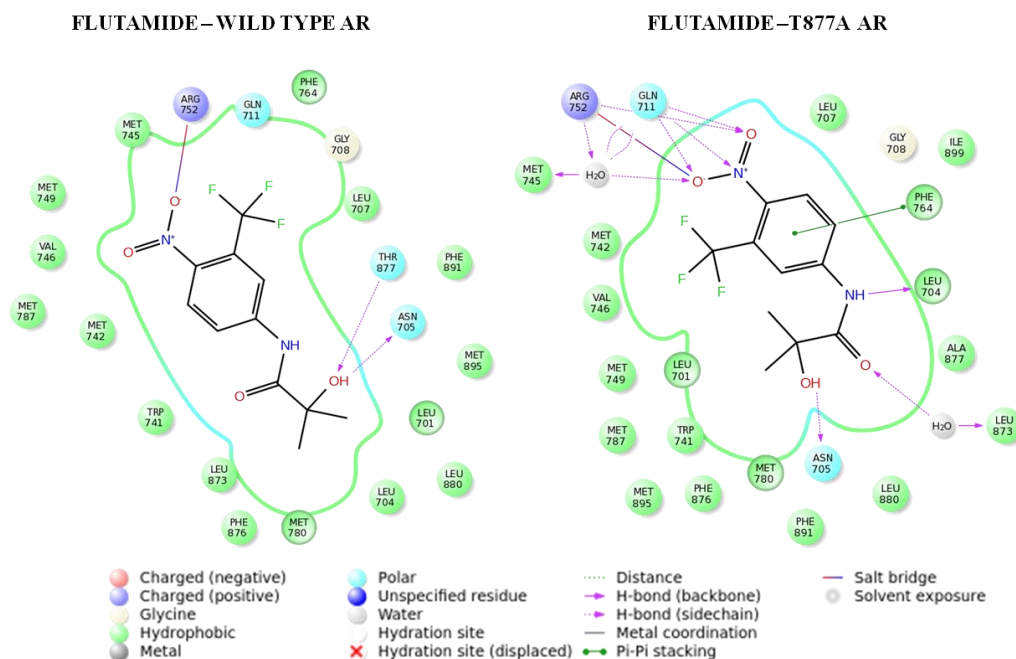
Chapter 7: Results and Analysis

7.1.3.2. Flutamide

Flutamide has binding affinity for all the AR types used in this study. Flutamide has the highest binding energy with T877A mutated AR (dock score = -8.25 kcal/mol). Flutamide has a dock score of -7.76 kcal/mol and -7.22 kcal/mol with wild and W741L mutated ARs respectively. In wild type AR, the hydroxyl group of flutamide forms H-Bond interactions with Thr877 and Asn705 (Figure 15). In T877A mutated AR, the nitro group of flutamide formed H-Bond interactions with Gln711, Arg752, HOH108, and Met745. The hydroxyl group of flutamide, in the absence of Thr877 amino acid, formed H-Bond interaction only with Asn705. The keto group of the amide formed H-Bond interaction with Leu873 mediated through a water molecule (HOH213) and the amino group of the amide formed H-Bond interaction with Leu704. We could observe that the size of the ligand binding pocket in T877A was bigger than the wild type AR (Figure 15). The flutamide displayed two different binding conformations with wild and T877A mutated ARs respectively. Flutamide attained a bent conformation with T877A mutated AR.

Chapter 7: Results and Analysis

Figure 15: Interactions of flutamide with wild and T877A mutant ARs



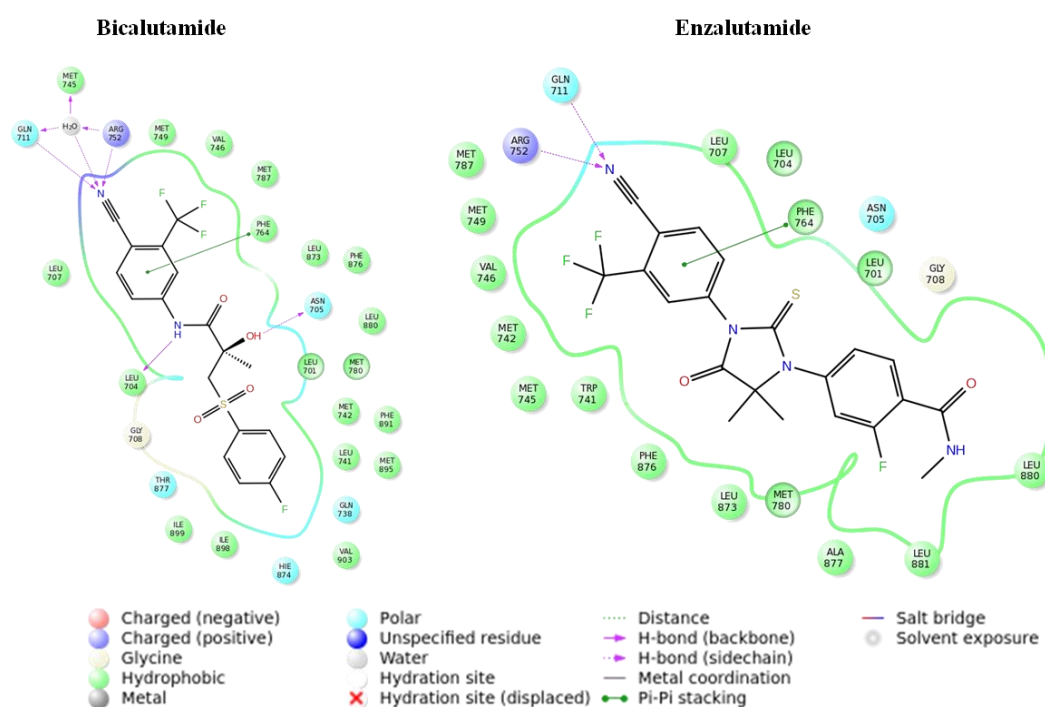
Flutamide forms H-Bond interaction with Thr877, Asn705 and forms ionic interaction with Arg752 in wild type AR. Flutamide forms H-Bond interactions with Arg752 (ionic and H-Bond), Gln711, Leu704, Leu873 (bridged through HOH) and Met745 (bridged through HOH) in T877A mutant AR. Note that the volume of the binding pocket in T877A mutant AR was greater than the wild type.

7.1.3.3. Bicalutamide

The AR antagonist, bicalutamide doesn't bind with T877A AR and has low binding energy with wild type AR (dock score = -2.54 kcal/mol). Bicalutamide has the highest binding energy with W741L mutated AR (dock score = -10.27 kcal/mol). In W741L mutated AR, the nitrile group of bicalutamide formed H-Bond interactions with Arg752, Gln711, HOH108, and Met745. The amine and hydroxyl group formed H-Bond interaction with Leu704 and Asn705 respectively (Figure 16).

Chapter 7: Results and Analysis

Figure 16: Binding interactions of bicalutamide and enzalutamide with AR



Bicalutamide forms H-Bond interaction with Arg752, Gln711, Leu704, Met745 (bridged through HOH) and Asn705 in W741L mutated AR. Enzalutamide forms H-Bond interactions with Arg752 and Gln711 with helix-12 truncated AR.

7.1.3.4. Enzalutamide

Enzalutamide doesn't have binding affinity with wild, T877A and W741L ARs. The enzalutamide has binding affinity only with helix-12 truncated AR (dock score = -8.426 kcal/mol). The nitrile group of enzalutamide forms H-Bond interactions with Arg752 and Gln711 (Figure 16).

7.1.3.4. Validation of docking and homology model

The docking studies were validated by calculating the RMSD between the crystal and docked conformation of co-crystallized ligands. The maximum RMSD between the predicted and crystal structure poses of the ligand was 1.28 Å. The

Chapter 7: Results and Analysis

maximum allowable limit is 2 Å. Hence the docking procedures that were followed were a valid one. The homology model was validated in the structural analysis and verification server (SAVES). The amino acids in the favorable, allowed and disallowed regions were identified by Ramachandran plot. The stereochemistry of the amino acids in the homology model was evaluated by PROCHECK. The 3D compatibility of the homology model was validated by VERIFY_3D. The homology model passed all the criteria for a good protein structure. The percentage of amino acids in the favorable region, allowed region and disallowed regions were 96.2%, 3.8% and zero respectively.

7.1.4. Elucidation of the binding mechanism of AR antagonists

In case of W741L mutant AR, the mutated leucine amino acid (W741L) is much smaller in size than the tryptophan amino acid, so we tried to compare the binding mode of bicalutamide in presence of leucine (W741L AR) and tryptophan. The conformational difference in the bicalutamide was evaluated by superimposing the bicalutamide bound helix -12 negative AR and W741L AR (Figure 17). The helix-12 negative AR has wild type tryptophan amino acid. The B ring of bicalutamide attains a different conformation in the presence of tryptophan and leucine. In the presence of tryptophan, the B ring of bicalutamide was shifted nearer to helix-12 amino acid Ile 899, indicating a possible steric clash with it. In the presence of leucine (mutated AR) the B ring of bicalutamide was well inside the ligand binding pocket and far from the helix-12.

Figure 17: Binding conformation of bicalutamide with wild (helix-12 negative) and W741L mutated AR

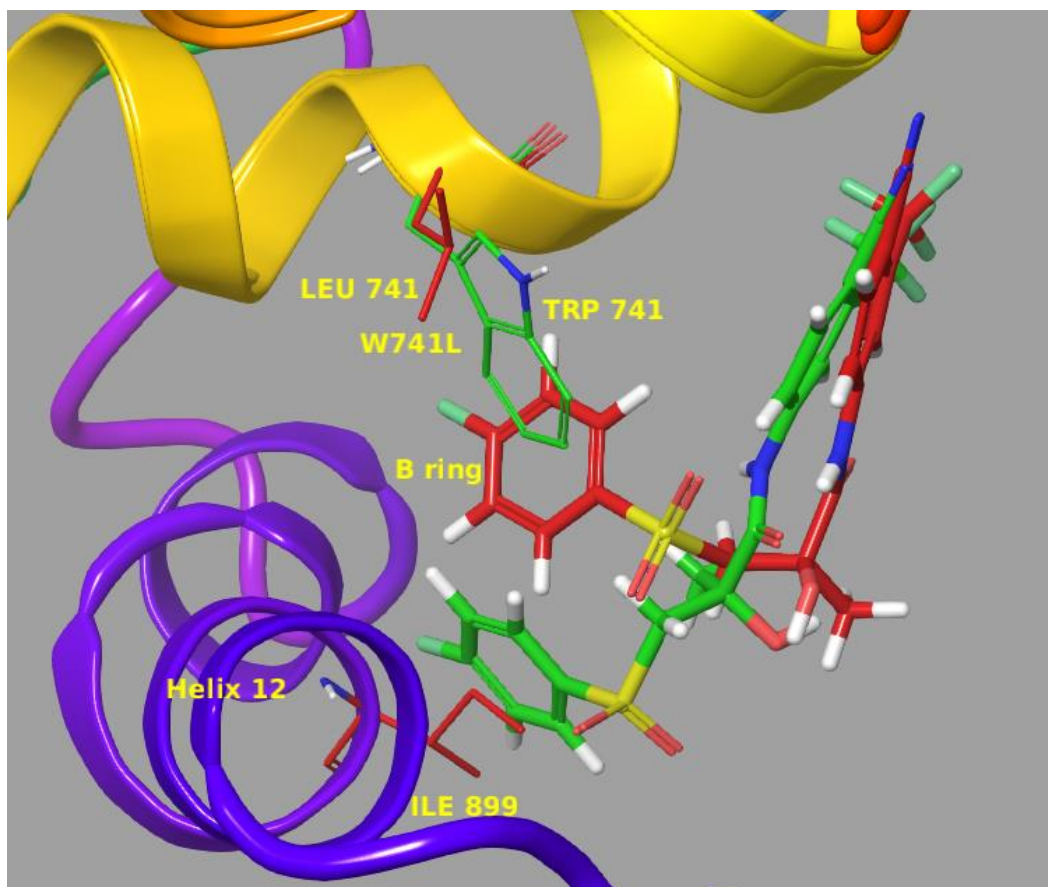


Figure represents the superimposition of the wild (green colored carbon) and W741L mutated (red colored carbon) ARs and the difference in binding mode of bicalutamide. Note the lack of steric clashes of bicalutamide with helix-12 in the mutated type, which in turn leads to resistance.

7.2. To develop a pharmacophore model for wild and mutant AR antagonists and to identify difference between the pharmacophore models

7.2.1. Purpose of the study

The purpose of the study is to construct a pharmacophore (3D-QSAR) for *in-silico* virtual screening and identification of hit molecules. There is no AR in

Chapter 7: Results and Analysis

antagonist bound conformation in PDB. Hence it was not possible to identify hit molecules through structure based virtual screening techniques. Even though a homology model could be built, it would not be a reliable method for the identification of the hit molecule in the first hand. Hence the pharmacophore generation is essential for the identification of the hit molecules. Constructing pharmacophore for wild, T877A and full antagonist was never done before and it could give or augment the results obtained in the docking studies.

7.2.2. Data set preparation for wild, T877A and full antagonists (wild and T877A)

Selection of training molecules is an important step for developing a 3D-QSAR model with good predictive power. The activity (IC_{50}) for wild type AR was evaluated in VCaP cell line. The activity for T877A mutant AR was evaluated in LNCaP cell line. The majority of the molecules were active in wild and T877A mutant AR expressing cell lines. However, the activity of the molecules varied between the cell lines. This is because the molecules exhibit different efficacy with wild and mutant T877A ARs. Hence, the IC_{50} values evaluated in the VCaP cell line was used in developing the 3D-QSAR model for wild type AR. Similarly, the IC_{50} values evaluated in LNCaP cell line was used in developing the 3D-QSAR model for T877A mutant AR. The separation of datasets as mentioned above will lead to the identification of preferential but not absolute 3D-QSAR for respective AR antagonists. Also, the molecules for the first and second datasets were not filtered for resistance. This means that the molecules in the dataset may or may not have agonist/partial agonist activity with either / both wild or T877A mutant AR. The molecules for the dataset of full antagonists were carefully

Chapter 7: Results and Analysis

selected by a two-step process. First, the ligands that could antagonize both wild and T877A mutant ARs were selected. The second step involved the filtering of the molecules for resistance. This means that none of the ligands in the dataset has agonist/partial agonist activity with either / both wild or T877A mutant AR. The activities of the molecules in this dataset were evaluated by luciferase reporter assay.

7.2.3. Pharmacophore generation for wild, T877A and full antagonists (wild and T877A mutant)

7.2.3.1. Wild type AR

The molecules in the dataset were defined by the following pharmacophore site points: hydrogen bond acceptor (A), hydrogen bond donor (D), hydrophobic group (H), and aromatic ring (R). The number of “must match” pharmacophore site points was gradually decreased from 7 to 3 until all the actives were matched and scored successfully. Based on the scoring; ADDHRR.295 was selected as the best model (Tables 16 & 17).

Table 16: Validation of training set

Parameters	3D-QSAR	PLS	SD	R ²	F	P	Q ²
Wild	ADDHRR.295	5	0.13	0.91	171.1	1.918e ⁻⁴³	0.62
T877A	AHHRR.266	5	0.11	0.94	294.5	8.649e ⁻⁵⁶	0.62
Full	AHRR.63	3	0.2	0.94	152.4	7.536e ⁻¹⁸	0.58

Correlation between the predicted and observed activity (R²), predictive ability of the model (Q²), low standard deviation (S.D), and the probability of getting an actual result (P value), Fischer test (F), Partial least square factor (PLS).

Chapter 7: Results and Analysis

Table 17: Validation of test set

Parameters	3D-QSAR	PLS	R ²	r ² m	R ² pred	Pearson-R
Wild	ADDHRR.295	5	0.76	0.76	0.72	0.87
T877A	AHHRR.266	5	0.74	0.74	0.69	0.86
Full	AHRR.63	3	0.80	0.75	0.83	0.89

The correlation between the observed and predicted activity (R²), predictive R² (R²pred), correlation between the observed and predicted activity with intercept set at zero (r²m), Partial least square factor (PLS)

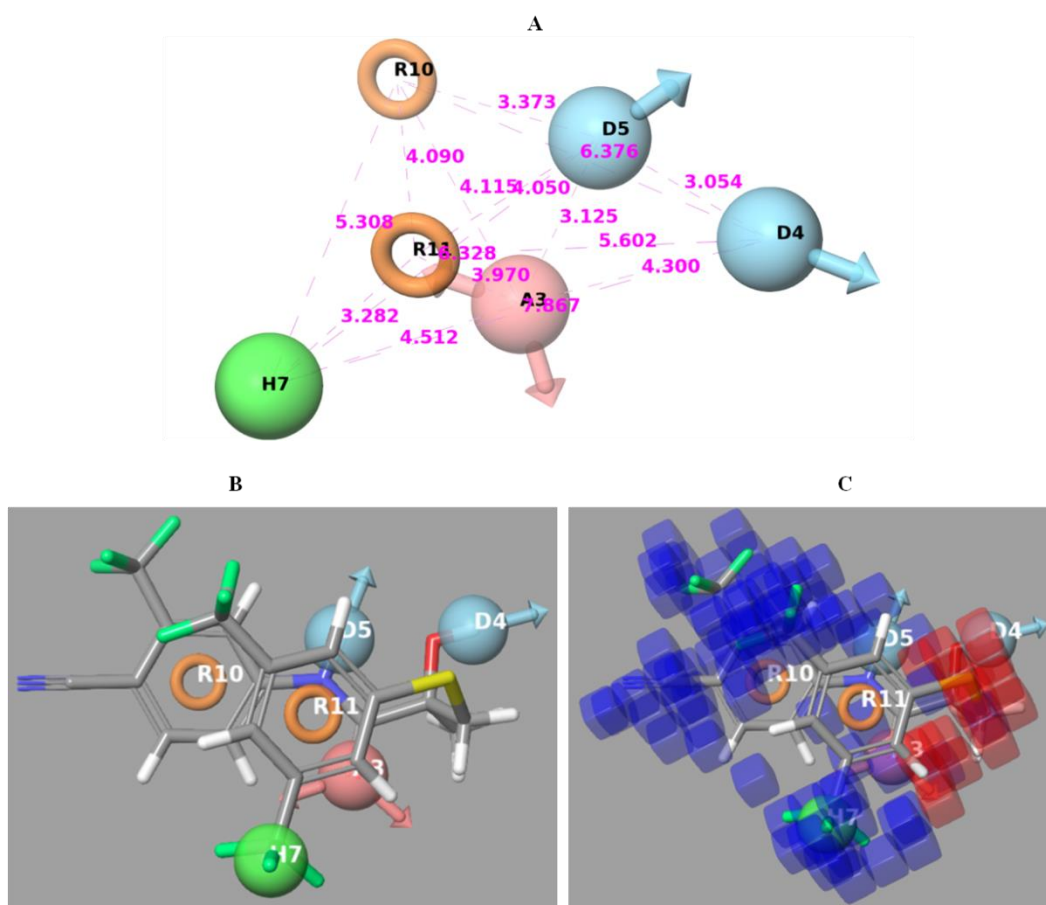
The active groups of the best fit molecules were evaluated by cube models (Figure 18, Table 18). During the construction of the 3D-QSAR, a rectangular grid was applied by PHASE to the aligned training set molecules. The grid includes all the substitutions in the pharmacophore site points. Then by correlating the observed activity and the atoms in the grid space, the PHASE generates the cube models. The cube models have a score value, less than zero means the atoms in the grid space does not favour the activity and greater than 1 will favour the activity. The space occupied by the atoms which does not favour the activity is indicated in red colour. The space occupied by the atoms which favours the activity is indicated in blue colour. Hence, the blue cubes represent the favourable regions for activity and the red cubes represent the unfavourable regions for activity.

The 4-nitrile and 3-CF₃ substitutions in ring R10 were favorable regions for activity. The 3-CF₃ substitution at ring R11, which is the hydrophobic H7 site point, also favors the activity. However, the –OH group and sulphur atom in the

Chapter 7: Results and Analysis

linker region between R10 and R11 were unfavorable for activity. The H atom of the hydroxyl group is the donor D4 site point. This indicates that although it is one among the pharmacophore site points, it decreases the activity. The observed and predicted activities of test and training set molecules are given in the table 19.

Figure 18: Pharmacophore of wild type AR antagonist



A: Represents the distances between the pharmacophore site points. **B:** Represents the best fit molecule with the 3D-QSAR. **C:** Represents the cube model of the best fit active molecule. Blue cubes represent the favourable regions for activity. The red cubes represent the unfavourable regions for activity. The 4-nitrile and 3-CF₃ regions in ring R10, the 3-CF₃ region at ring R11 were favourable regions for activity. The -OH group (D4) site point and sulphur atom was unfavourable for activity. R-ring; D-donor; H-hydrophobic; A-acceptor

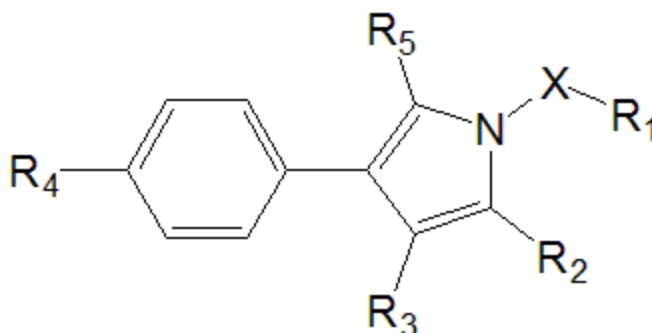
Chapter 7: Results and Analysis

Table 18: Angle and distances between wild type pharmacophore site points

Site1	Site2	Site3	Angle	Site1	Site2	Site3	Angle	Site1	Site2	Distance
D4	A3	D5	45.2	A3	H7	D4	26.1	A3	D4	4.3
D4	A3	H7	126.4	A3	H7	D5	27.5	A3	D5	3.125
D4	A3	R10	98.5	A3	H7	R10	48.7	A3	H7	4.512
D4	A3	R11	85.2	A3	H7	R11	58.7	A3	R10	4.115
D5	A3	H7	110.6	D4	H7	D5	21.5	A3	R11	3.97
D5	A3	R10	53.4	D4	H7	R10	53.7	D4	D5	3.054
D5	A3	R11	68.4	D4	H7	R11	36.9	D4	H7	7.867
H7	A3	R10	75.8	D5	H7	R10	32.2	D4	R10	6.376
H7	A3	R11	45	D5	H7	R11	34.1	D4	R11	5.602
R10	A3	R11	60.8	R10	H7	R11	50.4	D5	H7	6.328
A3	D4	D5	46.6	A3	R10	D4	41.8	D5	R10	3.373
A3	D4	H7	27.5	A3	R10	D5	48.1	D5	R11	4.05
A3	D4	R10	39.7	A3	R10	H7	55.5	H7	R10	5.308
A3	D4	R11	44.9	A3	R10	R11	57.9	H7	R11	3.282
D5	D4	H7	49.5	D4	R10	D5	6.9	R10	R11	4.09
D5	D4	R10	7.6	D4	R10	H7	84.1			
D5	D4	R11	44.7	D4	R10	R11	60.1			
H7	D4	R10	42.2	D5	R10	H7	90.8			
H7	D4	R11	20.6	D5	R10	R11	64.9			
R10	D4	R11	39.3	H7	R10	R11	38.2			
A3	D5	D4	88.2	A3	R11	D4	49.9			
A3	D5	H7	41.9	A3	R11	D5	45.9			
A3	D5	R10	78.5	A3	R11	H7	76.3			
A3	D5	R11	65.7	A3	R11	R10	61.4			
D4	D5	H7	108.9	D4	R11	D5	32.1			
D4	D5	R10	165.5	D4	R11	H7	122.5			
D4	D5	R11	103.2	D4	R11	R10	80.6			
H7	D5	R10	57	D5	R11	H7	118.9			
H7	D5	R11	27	D5	R11	R10	49			
R10	D5	R11	66.1	H7	R11	R10	91.4			

Chapter 7: Results and Analysis

Table 19a: Observed and predicted activity of bicalutamide derivatives



In	Ar (B ring)	X	R (A ring)	Wild (pIC ₅₀)		T877A (pIC ₅₀)	
				Observed	Predicted	Observed	Predicted
Bic	4-F-Ph	SO ₂	4-CN, 3-CF ₃	4.16	4.69	4.34	4.38
44e	4-CN-Ph	O	4-CN, 3-CF ₃	4.61	4.64	4.67	4.57
R-Bic	4-F-Ph	SO ₂	4-CN, 3-CF ₃	4.28	4.29	4.34	4.29
22c	3-CF ₃ -Ph	S	4-CN, 3-CF ₃	5.03	4.91	5.29	5.40
22d	2-CF ₃ -Ph	S	4-CN, 3-CF ₃	5.12	5.18	5.3	5.29
22h	4-OCF ₃ -Ph	S	4-CN, 3-CF ₃	4.39	4.59	4.36	4.36
22o	4-CF ₃ -2-Pyridine	S	4-CN, 3-CF ₃	4.04	4.41	4.09	4.11
23b#	4-CF ₃ -Ph	S	4-NO ₂ , 3-CF ₃	4.67	4.85	4.54	4.61
23c*	3-CF ₃ -Ph	S	4-NO ₂ , 3-CF ₃	5.06	5.19	5.19	5.53
23d*	2-CF ₃ -Ph	S	4-NO ₂ , 3-CF ₃	5.35	5.35	5.32	5.43
24a#	4-F-Ph	S	4-CN, 2-CF ₃	4.34	4.55	4.57	4.65
24c	3-CF ₃ -Ph	S	4-CN, 2-CF ₃	4.62	4.76	4.94	4.85
24d	2-CF ₃ -Ph	S	4-CN, 2-CF ₃	4.73	4.65	4.96	4.81
25a	4-F-Ph	S	4-NO ₂ , 2-CF ₃	4.67	4.68	4.92	4.69
25b#	4-CF ₃ -Ph	S	4-NO ₂ , 2-CF ₃	4.76	4.73	5.06	5.09
25c	3-CF ₃ -Ph	S	4-NO ₂ , 2-CF ₃	4.78	4.65	4.99	5.02
25d	2-CF ₃ -Ph	S	4-NO ₂ , 2-CF ₃	4.89	4.94	4.93	4.87
25f	3,4-F-Ph	S	4-NO ₂ , 2-CF ₃	---	---	4.08	4.66
25g	2,4-F-Ph	S	4-NO ₂ , 2-CF ₃	4.77	4.74	4.95	4.85
25i#	3-OCF ₃ -Ph	S	4-NO ₂ , 2-CF ₃	4.79	4.90	5.03	5.06
25l	2-OCF ₃ -Ph	S	4-NO ₂ , 2-CF ₃	5.27	5.22	5.48	5.42
25o*	4-CF ₃ -2-Pyridine	S	4-NO ₂ , 2-CF ₃	4.76	4.63	4.95	4.84
25p	5-CF ₃ -2-Pyridine	S	4-NO ₂ , 2-CF ₃	4.76	4.93	5.25	5.17
26c	3-CF ₃ -Ph	S	4-CF ₃	4.7	4.62	4.64	4.73
26d*	2-CF ₃ -Ph	S	4-CF ₃	5.23	5.12	5.14	4.83
26i	3-OCF ₃ -Ph	S	4-CF ₃	4.72	4.77	4.85	4.88

Chapter 7: Results and Analysis

27b#	4-CF ₃ -Ph	O	4-CN, 3-CF ₃	5.01	4.69	5.19	5.21
27c#	3-CF ₃ -Ph	O	4-CN, 3-CF ₃	5.04	4.72	5.08	4.94
27d#	2-CF ₃ -Ph	O	4-CN, 3-CF ₃	4.77	4.55	5.01	4.98
27f	3,4-F-Ph	O	4-CN, 3-CF ₃	4.59	4.58	4.72	4.77
27g	2,4-F-Ph	O	4-CN, 3-CF ₃	4.41	4.42	4.42	4.60
27h#	4-OCF ₃ -Ph	O	4-CN, 3-CF ₃	4.75	4.59	4.86	4.74
27i	3-OCF ₃ -Ph	O	4-CN, 3-CF ₃	5	5.02	5	5.03
28b*	4-CF ₃ -Ph	O	4-NO ₂ , 3-CF ₃	4.96	5.02	4.76	5.14
28c*,#	3-CF ₃ -Ph	O	4-NO ₂ , 3-CF ₃	4.98	4.66	5	4.90
28d#	2-CF ₃ -Ph	O	4-NO ₂ , 3-CF ₃	4.56	4.49	4.64	4.63
28e	4-CN-Ph	O	4-NO ₂ , 3-CF ₃	4.57	4.54	4.72	4.80
28f*	3,4-F-Ph	O	4-NO ₂ , 3-CF ₃	4.72	4.75	4.83	4.76
28g	2,4-F-Ph	O	4-NO ₂ , 3-CF ₃	4.67	4.68	4.94	4.87
28h*	4-OCF ₃ -Ph	O	4-NO ₂ , 3-CF ₃	4.7	4.72	4.75	4.91
28i*	3-OCF ₃ -Ph	O	4-NO ₂ , 3-CF ₃	5.01	5.07	5	5.09
28l	2-OCF ₃ -Ph	O	4-NO ₂ , 3-CF ₃	5.01	4.98	5.15	5.11
28m*	4-CN,2-CF ₃ -Ph	O	4-NO ₂ , 3-CF ₃	5.07	5.05	5.24	5.44
28n	4-CN,3-F-Ph	O	4-NO ₂ , 3-CF ₃	4.9	4.97	5.11	5.13
28o	4-CF ₃ -2-Pyridine	O	4-NO ₂ , 3-CF ₃	---	---	4.43	4.51
29b*	4-CF ₃ -Ph	O	4-CN, 2-CF ₃	4.63	4.59	4.54	4.55
29c*,#	3-CF ₃ -Ph	O	4-CN, 2-CF ₃	4.66	4.53	4.81	5.03
29d*	2-CF ₃ -Ph	O	4-CN, 2-CF ₃	4.65	4.79	4.85	4.62
29e	4-CN-Ph	O	4-CN, 2-CF ₃	4.21	4.16	4.45	4.38
29f	3,4-F-Ph	O	4-CN, 2-CF ₃	4.32	4.28	4.45	4.44
29g	2,4-F-Ph	O	4-CN, 2-CF ₃	4.29	4.26	4.51	4.48
29h*	4-OCF ₃ -Ph	O	4-CN, 2-CF ₃	4.65	4.66	4.55	4.58
29i*,#	3-OCF ₃ -Ph	O	4-CN, 2-CF ₃	4.24	4.66	4.19	4.21
29l*,#	2-OCF ₃ -Ph	O	4-CN, 2-CF ₃	4.35	4.77	4.47	4.64
29m*	4-CN,2-CF ₃ -Ph	O	4-CN, 2-CF ₃	4.75	4.64	5.02	5.24
29n	4-CN,3-F-Ph	O	4-CN, 2-CF ₃	4.11	4.07	4.1	4.10
30b*	4-CF ₃ -Ph	O	4-NO ₂ , 2-CF ₃	4.73	4.82	4.86	4.62
30c*	3-CF ₃ -Ph	O	4-NO ₂ , 2-CF ₃	4.71	4.80	4.88	5.08
31c	3-CF ₃ -Ph	O	4-CF ₃	4.72	4.81	4.74	4.96
31d	2-CF ₃ -Ph	O	4-CF ₃	4.93	4.87	5.15	5.03
31i#	3-OCF ₃ -Ph	O	4-CF ₃	5.36	5.41	5.66	5.42
32b	4-CF ₃ -Ph	SO ₂	4-CN, 3-CF ₃	4.53	4.52	4.69	4.63
32c#	3-CF ₃ -Ph	SO ₂	4-CN, 3-CF ₃	4.4	4.41	4.82	4.76
32d#,*	2-CF ₃ -Ph	SO ₂	4-CN, 3-CF ₃	4.23	4.35	4.36	4.42
32h,*	4-OCF ₃ -Ph	SO ₂	4-CN, 3-CF ₃	4.48	4.35	4.49	4.40

Chapter 7: Results and Analysis

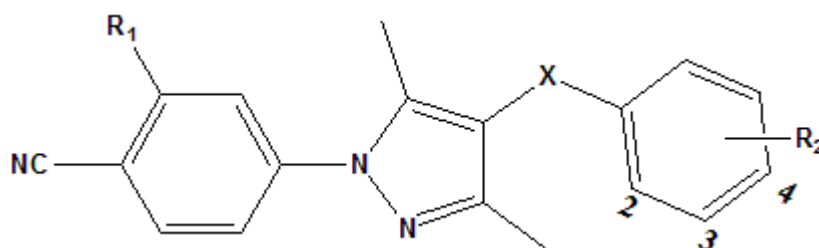
33b	4-CF ₃ -Ph	SO ₂	4-NO ₂ , 3-CF ₃	4.5	4.46	4.74	4.67
33c	3-CF ₃ -Ph	SO ₂	4-NO ₂ , 3-CF ₃	4.51	4.35	4.79	4.74
33d	2-CF ₃ -Ph	SO ₂	4-NO ₂ , 3-CF ₃	4.55	4.56	4.59	4.59
34a	4-F-Ph	SO ₂	4-CN, 2-CF ₃	4.18	4.17	4.03	4.05
34b*	4-CF ₃ -Ph	SO ₂	4-CN, 2-CF ₃	4.36	4.35	4.48	4.73
34c	3-CF ₃ -Ph	SO ₂	4-CN, 2-CF ₃	4.34	4.43	4.49	4.55
34d	2-CF ₃ -Ph	SO ₂	4-CN, 2-CF ₃	---	---	4.13	4.16
35a	4-F-Ph	SO ₂	4-NO ₂ , 2-CF ₃	4.23	4.27	4.41	4.47
35b	4-CF ₃ -Ph	SO ₂	4-NO ₂ , 2-CF ₃	4.32	4.46	4.53	4.51
35c	3-CF ₃ -Ph	SO ₂	4-NO ₂ , 2-CF ₃	4.41	4.37	4.77	4.79
35d	2-CF ₃ -Ph	SO ₂	4-NO ₂ , 2-CF ₃	4.41	4.36	4.68	4.58
35f*	3,4-F-Ph	SO ₂	4-NO ₂ , 2-CF ₃	4.42	4.37	4.71	4.39
35g	2,4-F-Ph	SO ₂	4-NO ₂ , 2-CF ₃	4.23	4.21	4.74	4.57
35i	3-OCF ₃ -Ph	SO ₂	4-NO ₂ , 2-CF ₃	4.69	4.63	4.91	4.77
35l	2-OCF ₃ -Ph	SO ₂	4-NO ₂ , 2-CF ₃	4.28	4.22	4.75	4.83
35p	5-CF ₃ -2-Pyridine	SO ₂	4-NO ₂ , 2-CF ₃	4.23	4.11	4.34	4.37
42b (R)	4-CF ₃ -Ph	S	4-CN, 3-CF ₃	5.03	4.71	4.84	4.74
42c (R)#	3-CF ₃ -Ph	S	4-CN, 3-CF ₃	5.05	4.94	4.84	4.86
42d (R)*	2-CF ₃ -Ph	S	4-CN, 3-CF ₃	5.53	5.52	5.1	4.92
42g (R)	2,4-F-Ph	S	4-CN, 3-CF ₃	4.73	4.70	4.59	4.50
42h (R)	4-OCF ₃ -Ph	S	4-CN, 3-CF ₃	4.75	4.74	4.7	4.72
45b (R)	4-CF ₃ -Ph	SO ₂	4-CN, 3-CF ₃	4.5	4.37	4.75	4.69
45c (R)	3-CF ₃ -Ph	SO ₂	4-CN, 3-CF ₃	4.39	4.56	4.88	4.92
45d (R)#	2-CF ₃ -Ph	SO ₂	4-CN, 3-CF ₃	4.42	4.58	4.49	4.52
45g (R)	2,4-F-Ph	SO ₂	4-CN, 3-CF ₃	4.21	4.15	4.37	4.27
45h (R)#,*	4-OCF ₃ -Ph	SO ₂	4-CN, 3-CF ₃	4.5	4.66	4.72	4.83
46a (R)	4-F-Ph	SO ₂	4-CN, 2-CF ₃	---	---	4.06	4.05
52	2-CF ₃ -Ph	S	4-NO ₂ , 3-CF ₃	5.55	5.32	6.14	6.15
24a*	3,5-CF ₃ -Ph	S	4-CN, 3-CF ₃	5.56	5.81	5.63	5.60
25a*	3,5-CF ₃ -Ph	S	4-NO ₂ , 3-CF ₃	5.81	5.83	5.82	5.68
26a#	3,5-CF ₃ -Ph	S	4-CN, 2-CF ₃	5.17	5.12	5.11	5.01
27a*	3,5-CF ₃ -Ph	S	4-NO ₂ , 2-CF ₃	5.45	5.28	5.5	5.33
28a	3,5-CF ₃ -Ph	S	4-CF ₃	5	5.12	5.01	4.95
29b*	3-CF ₃ -Ph	S	3,5-CF ₃	5	4.97	5.05	4.97
29c	2-CF ₃ -Ph	S	3,5-CF ₃	5.41	5.50	5.44	5.50
29d	3-OCF ₃ -Ph	S	3,5-CF ₃	5.03	5.04	5.11	5.08
29e	2-OCF ₃ -Ph	S	3,5-CF ₃	5.53	5.60	5.53	5.53
30a#	3,5-CF ₃ -Ph	O	4-CN, 3-CF ₃	5.6	5.10	5.52	5.57
30f#	3,5-tBu-Ph	O	4-CN, 3-CF ₃	5.52	5.45	5.57	5.72

Chapter 7: Results and Analysis

31a#,*	3,5-CF ₃ -Ph	S	4-NO ₂ , 3-CF ₃	5.77	5.85	6	5.93
32a#	3,5-CF ₃ -Ph	O	4-CN, 2-CF ₃	5.32	5.02	5.44	5.49
33a*	3,5-CF ₃ -Ph	O	4-NO ₂ , 2-CF ₃	4.82	4.96	4.62	4.83
34a*	3,5-CF ₃ -Ph	O	4-CF ₃	5.38	5.41	5.47	5.11
35a	3,5-CF ₃ -Ph	SO ₂	4-CN, 3-CF ₃	5.2	4.93	5.54	5.59
36a	3,5-CF ₃ -Ph	SO ₂	4-NO ₂ , 3-CF ₃	5.48	5.15	5.67	5.61
38a	3,5-CF ₃ -Ph	SO ₂	4-NO ₂ , 2-CF ₃	5.14	5.11	5.51	5.49
39b	3-CF ₃ -Ph	SO ₂	3,5-CF ₃	5	4.82	5.02	5.04
39c	2-CF ₃ -Ph	SO ₂	3,5-CF ₃	5.06	5.01	5.07	5.20
39d#	3-OCF ₃ -Ph	SO ₂	3,5-CF ₃	5	4.88	5.02	4.98
39e	2-OCF ₃ -Ph	SO ₂	3,5-CF ₃	5	5	5.09	5.15
41	3,5-CF ₃ -Ph	S	4-CN, 3-CF ₃	6.07	5.81	6.1	5.92
42	3,5-CF ₃ -Ph	SO ₂	4-CN, 3-CF ₃	5.38	5.26	5.7	5.76

*Test set = T877A, #Test set = Wild

Table 19b: Observed and predicted activity of enzalutamide derivatives



In	R1	X	R2	Wild (pIC ₅₀)		T877A (pIC ₅₀)	
				Observed	Predicted	Observed	Predicted
61b#	4-CN, 3-CF ₃	O	4-CF ₃	4.52	4.41	5.02	5.19
62b#	4-NO ₂ , 3-CF ₃	O	4-CF ₃	4.13	4.42	5.67	5.60
62c	4-NO ₂ , 3-CF ₃	O	3-CF ₃	---	---	4.81	4.87
63b	4-CN, 2-CF ₃	O	4-CF ₃	---	---	5.07	5.15
63c	4-CN, 2-CF ₃	O	3-CF ₃	---	---	4.73	4.78
64b	4-NO ₂ , 2-CF ₃	O	4-CF ₃	---	---	5.42	5.43
64c	4-NO ₂ , 2-CF ₃	O	3-CF ₃	4.87	5.05	5.39	5.18
65b	3-CF ₃	O	4-CF ₃	4.14	4.26	5.22	5.24
65c	3-CF ₃	O	3-CF ₃	4.12	4.20	5.24	5.09
71b	4-CF ₃	O	3-CF ₃	---	---	4.78	4.90
71d	2-CF ₃	O	3-CF ₃	---	---	4.54	4.80
Enz*,#	4-CN, 3-CF ₃	S	3-F, 4-CONHMe	4.27	4.38	4.94	4.88

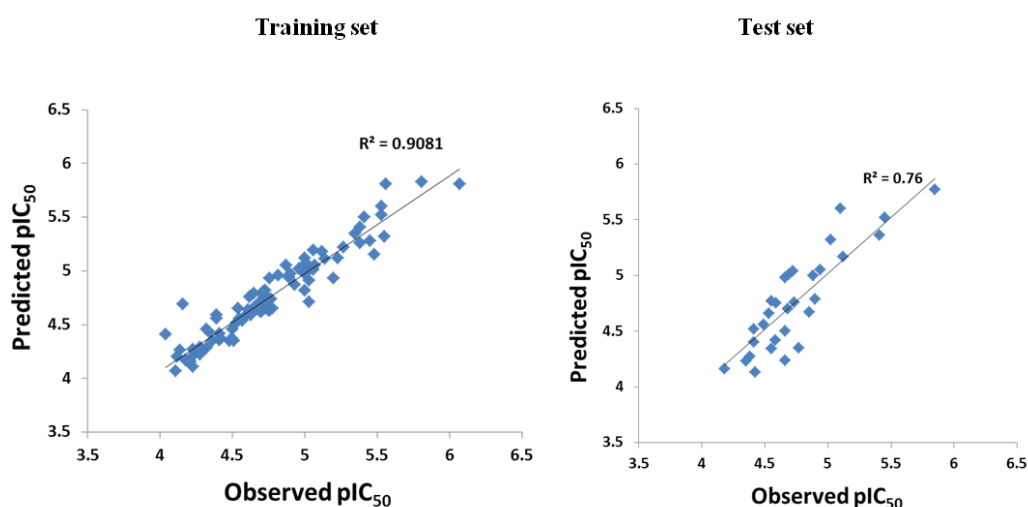
Chapter 7: Results and Analysis

49	4-NO ₂ , 3-CF ₃	S	3,5-CF ₃	4.54	4.65	5	5.05
51	4-NO ₂ , 2-CF ₃	S	3,5-CF ₃	4.73	4.77	5.33	5.40
54#	3,5-CF ₃	S	3-F, 4-CONHMe	4.7	4.68	4.94	4.97

*Test set = T877A, #Test set = Wild

The correlation between the observed and predicted activity of the training set was 0.9. The model was validated by predicting the test set having wide range of biological activity. The correlation between the observed and predicted activity of the test set was 0.76 (Figure 19). Also, the ADDHRR.295 accurately predicted the biological value of AR antagonist, enzalutamide (residual activity =0.14).

Figure 19: Correlation between observed and predicted activity of wild type AR antagonist



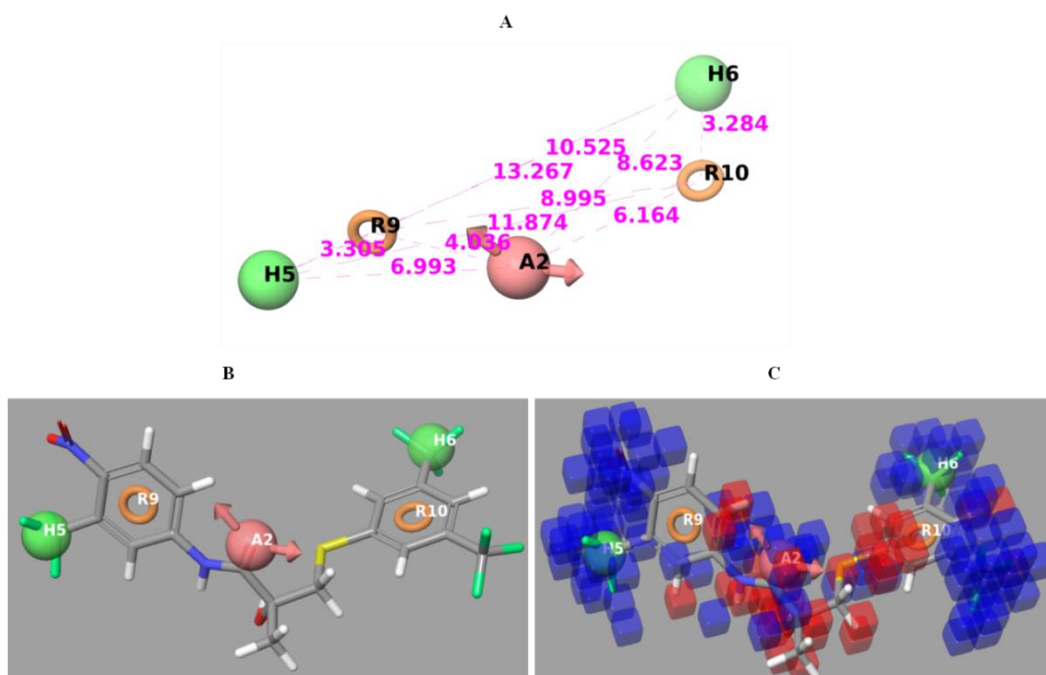
7.2.3.2. T877A mutated AR

The dataset generated A, D, H, and R pharmacophore site points. The hypothesis having five pharmacophore site points survived the scoring functions. Based on the scoring, AHHR.266 was selected as the best model (Table 16 and 17). The pharmacophore has one acceptor group (A), two hydrophobic groups (H) and two aromatic rings (R). The active groups of the best fit molecule were

Chapter 7: Results and Analysis

evaluated by cube models (Figure 20, Table 20). The blue cubes represent the favorable regions for activity and red cubes represent the unfavorable regions for activity.

Figure 20: Pharmacophore of T877A mutant AR antagonist



A. Represents the distances between the pharmacophore site points. **B:** Represents the best fit molecule with the 3D-QSAR. **C:** Represents the cube model of the best fit active molecule. Blue cubes represent the favourable regions for activity. The red cubes represent the unfavourable regions for activity. The 4-nitro and 3-CF₃ (H5 site point) substitution in ring R9, the 3-CF₃ (H6 site point) and 5-CF₃ substitution in ring R10 were favourable regions for activity. The -OH group and sulphur atom was unfavourable for activity. R-ring; D-donor; H-hydrophobic; A-acceptor.

The 4-nitro and 3-CF₃ substitutions in ring R9 are favorable regions for activity. The 3-CF₃ group is the hydrophobic H5 site point. The 3 and 5-CF₃ substitutions at ring R10 also favors the activity. The 3-CF₃ substituent is also the

Chapter 7: Results and Analysis

hydrophobic H6 site point. However, the –OH and sulphur atom in the linker region between R10 and R11 were unfavorable for activity. The observed and predicted activities of all the ligands in the training and test sets are given in Table 19.

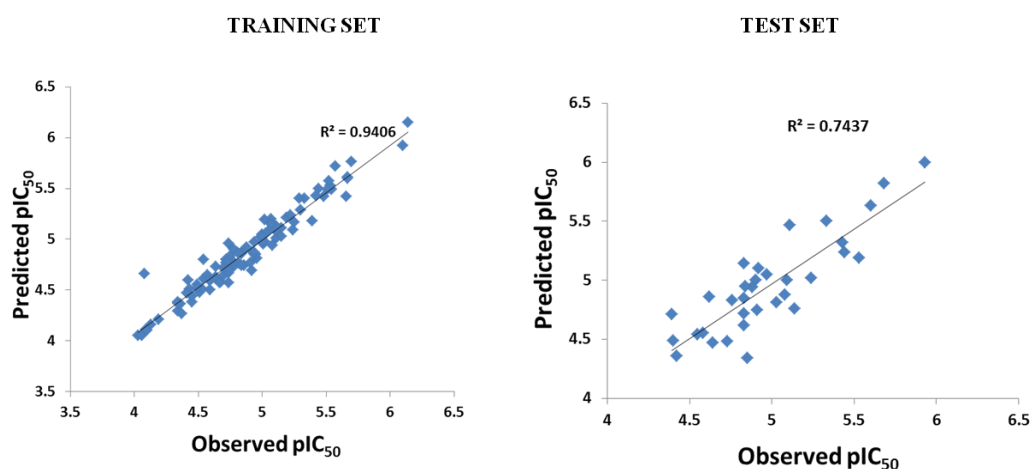
Table 20: Angle and distances between T877A mutant pharmacophore site points

Site1	Site2	Site3	Angle	Site1	Site2	Site3	Angle	Site1	Site2	Distance
H5	A2	H6	115.9	H5	H6	R9	9	A2	H5	6.993
H5	A2	R9	16	H5	H6	R10	58.3	A2	H6	8.623
H5	A2	R10	128.9	R9	H6	R10	54	A2	R9	4.036
H6	A2	R9	106.8	A2	R9	H5	144.4	A2	R10	6.164
H6	A2	R10	17.2	A2	R9	H6	51.7	H5	H6	13.267
R9	A2	R10	122.3	A2	R9	R10	35.4	H5	R9	3.305
A2	H5	H6	35.8	H5	R9	H6	141.3	H5	R10	11.874
A2	H5	R9	19.6	H5	R9	R10	145.8	H6	R9	10.525
A2	H5	R10	23.8	H6	R9	R10	17.2	H6	R10	3.284
H6	H5	R9	29.7	A2	R10	H5	27.3	R9	R10	8.995
H6	H5	R10	13.6	A2	R10	H6	129.2			
R9	H5	R10	25.2	A2	R10	R9	22.3			
A2	H6	H5	28.3	H5	R10	H6	108.1			
A2	H6	R9	21.5	H5	R10	R9	9			
A2	H6	R10	33.6	H6	R10	R9	108.8			

Chapter 7: Results and Analysis

The correlation between the observed and predicted activity of the training set and test set was 0.94 and 0.74, respectively (Figure 21). The model AHHR.266 accurately predicted the biological activity of AR antagonist enzalutamide (residual activity = 0.06). The biological activity of enzalutamide has wide variations between wild and mutant ARs. Enzalutamide is ~5 times selective towards T877A mutant AR. The 3D-QSAR models for wild and T877A mutant AR could identify the differences in the structural features of enzalutamide. This indicates that these models could provide the possible breakthrough needed to overcome AR resistance.

Figure 21: Correlation between observed and predicted activity of T877A mutant AR antagonist



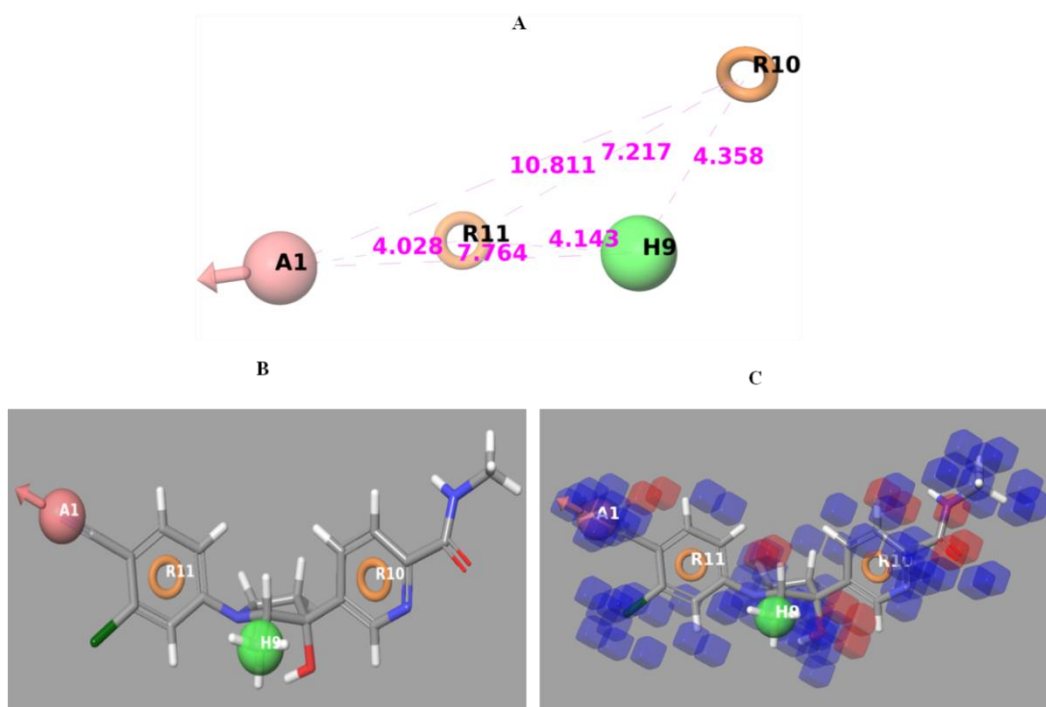
7.2.3.3. Wild and mutant AR antagonist (Full antagonist)

The corresponding dataset of the full antagonists has biological activity for wild type and T877A mutant AR. The dataset generated A, D, H, and R pharmacophore site points. The hypothesis having four pharmacophore site points

Chapter 7: Results and Analysis

survived the scoring functions. Based on scoring; AHRR.63 was selected as the best model (Table 16 and 17).

Figure 22: Pharmacophore of wild and T877A AR antagonists



A: Represents the distances between the pharmacophore site points. **B:** Represents the best fit molecule with the 3D-QSAR. **C:** Represents the cube model of the best fit active molecule. Blue cubes represent the favourable regions for activity. The red cubes represent the unfavourable regions for activity. The nitrile (A1 site point) and 3-Cl substitution in ring R11, the -OH group present between the two rings was favourable for activity. The methyl group of 4-CONHCH₃ in ring R10 was favourable for activity. R-ring; D-donor; H-hydrophobic; A-acceptor.

The pharmacophore has one H-Bond acceptor group (A), one hydrophobic group (H), and two aromatic rings (R). The active groups of the best fit molecule were evaluated by cube models as described above for the wild and mutant modeling (Figure 22, Table 21). The 4-nitrile (A1 site point) and 3-Cl

Chapter 7: Results and Analysis

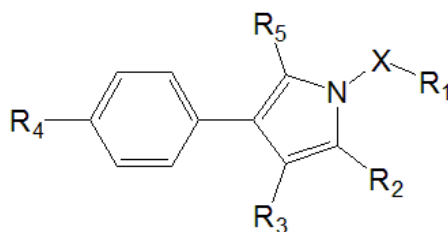
substitutions in ring R11 are favorable regions for activity. These regions are occupied by blue cubes. The methyl group that follows the 4-amide in ring R10 also favors the activity. The N atom in the pyridine ring R10 and the –OH group in the linker region between R11 and R10 were also favorable for activity. The observed and predicted activities of all the molecules in the dataset are given in the tables 22.

Table 21: Distance and angle between full antagonist pharmacophore site points

Site1	Site2	Site3	Angle	Site1	Site2	Site3	Angle	Site1	Site2	Distance
H9	A1	R10	19.6	A1	R10	H9	36.7	A1	H9	7.764
H9	A1	R11	18.4	A1	R10	R11	11.8	A1	R10	10.811
R10	A1	R11	21.5	H9	R10	R11	31	A1	R11	4.028
A1	H9	R10	123.8	A1	R11	H9	143.7	H9	R10	4.358
A1	H9	R11	17.9	A1	R11	R10	146.6	H9	R11	4.143
R10	H9	R11	116.2	H9	R11	R10	32.8	R10	R11	7.217

Chapter 7: Results and Analysis

Table 22a: Observed and predicted activity of 1-arylmethyl-4-phenylpyrrole derivatives



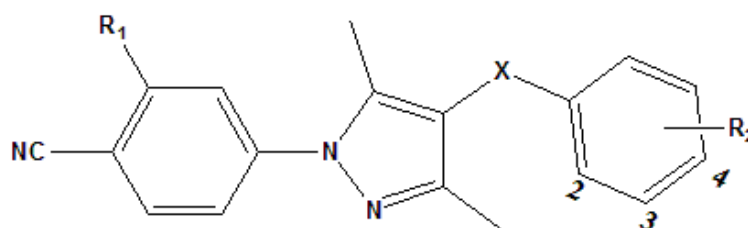
I.D	R1	X	R2	R3	R4	R5	Observed (pIC ₅₀)	Predicted (pIC ₅₀)
1	H	Bond	Me	CO ₂ Et	NO ₂	Me	6.61	6.30
2	Me	Bond	Me	CO ₂ Et	NO ₂	Me	6.30	6.18
3*	Phenyl	Bond	Me	CO ₂ Et	NO ₂	Me	5.36	5.38
4a	Phenyl	CH ₂	Me	CO ₂ Et	NO ₂	Me	6.46	6.42
4b*	Phenyl	CH ₂	Me	CO ₂ Me	NO ₂	Me	6.52	6.43
4d	Phenyl	CH ₂	Me	CH ₂ OH	NO ₂	Me	5.42	5.60
4e	Phenyl	CH ₂	Me	COMe	NO ₂	Me	5.33	5.52
4f	Phenyl	CH ₂	Me	H	NO ₂	Me	6.30	6.25
4g	Phenyl	CH ₂	Me	CO ₂ Me	H	Me	5.58	5.92
4h*	Phenyl	CH ₂	Me	CO ₂ Me	CN	Me	6.56	6.32
4j	Phenyl	CH ₂	Me	CN	CN	Me	7.39	7.24
4l*	2-Chloro-5-Methylpyridine	CH ₂	Me	CN	CN	Me	7.34	6.97
4m*	(5-methylpyridin-3-yl)methanol	CH ₂	Me	CN	CN	Me	7	7.27
4n	(2-chloro-5-methylpyridin-3-yl)methanol	CH ₂	Me	CN	CN	Me	7.60	7.46
4o	(2-chloro-5-methylpyridin-3-yl)methanol	CH ₂	H	CN	CN	Me	6.49	6.90
4p	(2-chloro-5-	CH ₂	Me	CN	CN	H	6.76	6.93

Chapter 7: Results and Analysis

	methylpyridin-3-yl)methanol							
5	Cyclo-hexyl	CH ₂	Me	CO ₂ Et	NO ₂	Me	5.42	5.11
6	Phenyl	(CH ₂) ₂	Me	CO ₂ Et	NO ₂	Me	5.38	5.33
7*	Phenyl	C=O	Me	CO ₂ Et	NO ₂	Me	5.61	5.95
8	Phenyl	SO ₂	Me	CO ₂ Et	NO ₂	Me	5.32	5.32

*Test set

Table 22b: Observed and predicted activity of 4-arylmethyl-1-phenylpyrazole derivatives

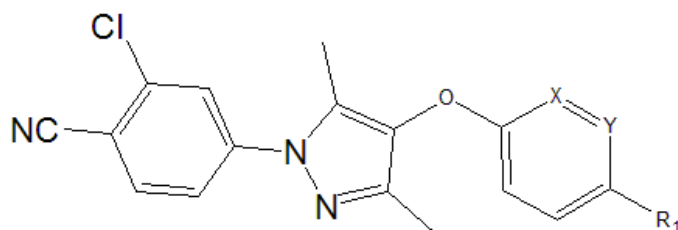


I.D	R1	R2	X	Observed (pIC ₅₀)	Predicted (pIC ₅₀)
3*	H	4- F	CH ₂	6.15	6.30
28b	Cl	3- CONH ₂	CH ₂	6.15	6.04
28c	Cl	4- CONH ₂	CH ₂	6.37	6.44
28d*	Cl	4-CONHMe	CH ₂	5.88	6.24
28e	Cl	4-CONMe ₂	CH ₂	5.39	5.53
28f	Cl	4-CONH <i>t</i> Bu	CH ₂	6.01	6.24
28g	Cl	4-CONH(CH ₂) ₂ OH	CH ₂	5.56	5.60
28h*	Cl	4-CONHCH ₂ C(CH ₂) ₂ OH	CH ₂	6.22	5.71
33	Cl	4-F	Bond	5.20	5.00
36	Cl	4-F	(CH ₂) ₂	5.95	6.10

*Test set

Chapter 7: Results and Analysis

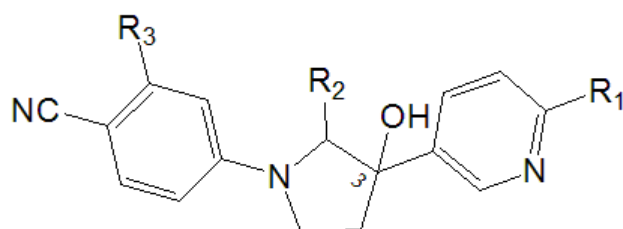
Table 22c: Observed and predicted activity of 4-aryloxy-1-phenylpyrazole derivatives



ID	X	Y	R1	Observed (pIC ₅₀)	Predicted (pIC ₅₀)
25	CH	CH	F	6.17	6.06
29a	CH	CH	N-(2-hydroxy-2-methylpropyl)acetamide	5.74	5.69
29b	CH	CH	1-morpholinoethanone	5.52	5.49
44b	N	CH	N-methylpivalamide	5.39	5.28
45	CH	N	N-methylacetamide	5.14	5.18

Table 22d: Observed and predicted activity of 3-aryl-3-hydroxy-1-

phenylpyrrolidine derivatives



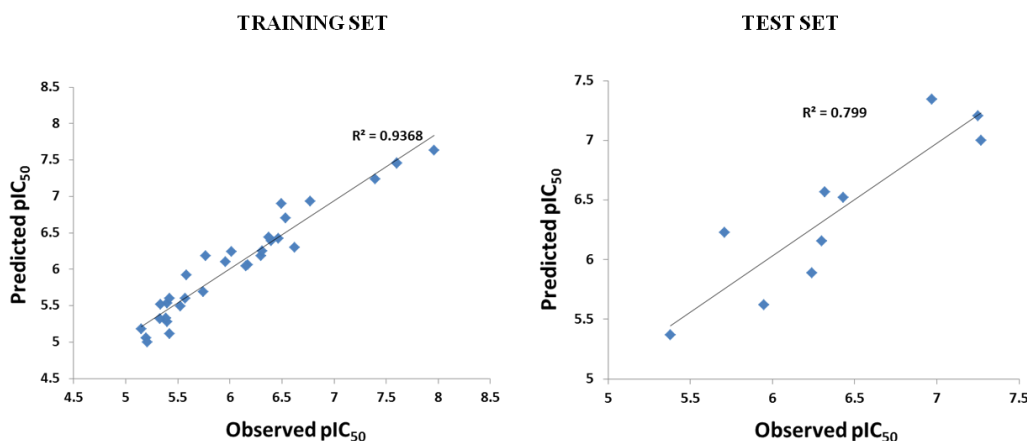
ID	R1	R3	R2	C-3	Observed (pIC ₅₀)	Predicted (pIC ₅₀)
48	CONHMe	Cl	S-Me	R	7.60	7.45
49	CONMe ₂	Cl	S-Me	R	5.76	6.18
50	CONHMe	Cl	R-Me	S	5.19	5.06
51	Pyrrolidin-2-one	Cl	S-Me	R	7.95	7.63
52*	CONHMe	OMe	S-Me	R	7.20	7.25
53	CONHMe	H	S-Me	R	6.39	6.39
54	CONHMe	F	S-Me	R	6.53	6.70

*Test set

Chapter 7: Results and Analysis

The correlation between the observed and predicted activity of the training and test sets were 0.94 and 0.79, respectively (Figure 23). This 3D-QSAR pharmacophore did not match with any of the existing AR antagonists (both wild and mutant). This indicates the hybrid nature of the full antagonist pharmacophore. Recall that all the marketed AR antagonists develop resistance during the course of the treatment.

Figure 23: Correlation between observed and predicted activity of wild and T877A mutant AR antagonist pharmacophore



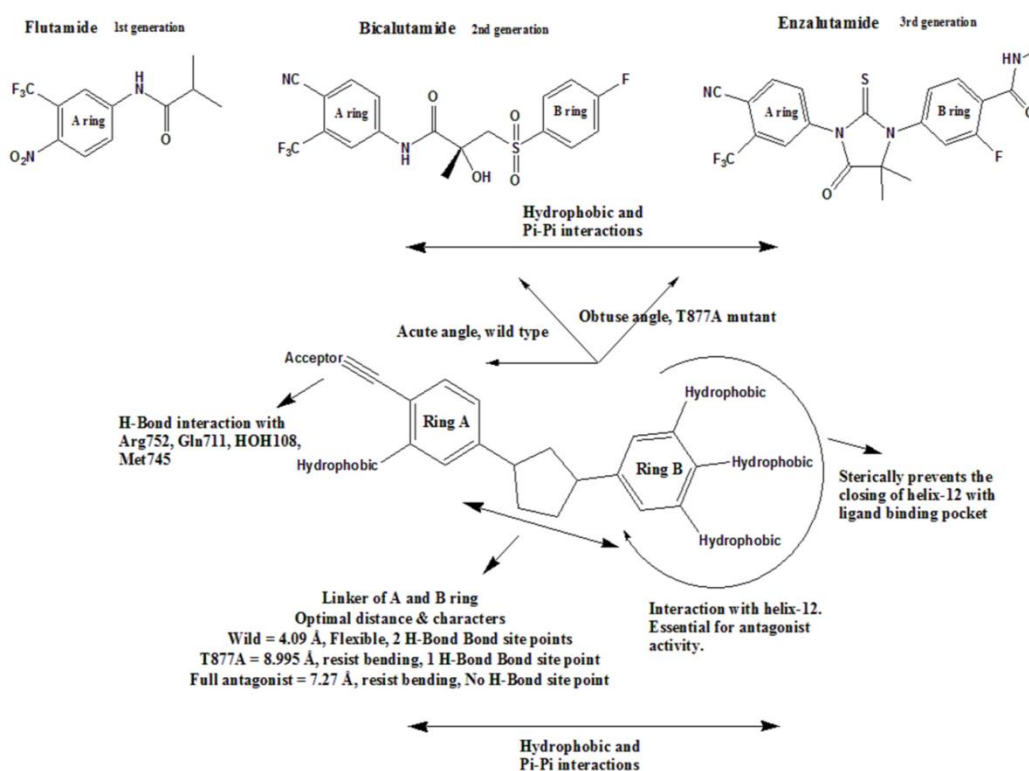
7.2.4. Similarities and differences between the wild and T877A mutant pharmacophores

The molecules in the dataset for the construction of the 3D-QSAR models have common structures, which are also present in the marketed drugs (Figure 24). All the marketed ligands have two rings (A and B) separated by a linker group. These two rings (A and B) were present in all the 3D-QSAR models. Notably, the substitutions of 4-nitro / 4-nitrile groups and 3-CF₃ / 3-Cl groups in the A ring are favorable for activity as explained by the cube models. Similarly,

Chapter 7: Results and Analysis

the hydrophobic substitutions at 3rd, 4th, and 5th position in the B ring also favored the activity. The major difference among the 3D-QSAR models was the distance and angle between the A ring and B ring. Also, there is a difference in the distance between the two extreme pharmacophore site points. These properties describe the variability in the length and flexibility among the active molecules.

Figure 24: 2D diagram representing the differences between the pharmacophores



The shortest distances are for wild type AR antagonist (A ring to B ring: 4.09 Å and D4 to H7: 7.867 Å). The angle between the A ring and B ring is always acute ($<90^\circ$), with the ordinates in the linker region (R10-D4-R11 = 39.3° , R10-D5-R11 = 66° , R10-A3-R11 = 60.8°). The shorter distances and acute angle between the A ring and B ring indicate a flexible linker region among the active

Chapter 7: Results and Analysis

molecules. The longest distances are for the T877A mutant antagonist (ring A to ring B: 8.895 Å and H5 to H6: 13.267 Å). The angle between the A ring and B ring is always obtuse ($>90^\circ$), with the ordinates in the linker region (R10-A2-R9 = 122.3°). The longer distances and obtuse angles between the A and B rings indicate a less flexible linker region among the active molecules. The distances of the full antagonist pharmacophore are marginally less than the T877A mutant 3D-QSAR (ring A to ring B: 7.217 Å and A1 to R10: 10.811 Å). Also, the angle between the A and B rings is always obtuse ($>90^\circ$), with the ordinates in the linker region (R10-H9-R11 = 116.2°).

The relatively longer distances and obtuse angles between the A and B rings indicate a less flexible linker region among the active molecules. Notably, the 3D-QSAR of full antagonists does not represent the site points for H-Bond interaction in the linker region. The 3D-QSAR of wild type AR favors H-bond interaction in the linker region when compared to the other two. This is because it has 3 pharmacophore points (A1, D4 and D5) in the linker region, which could form H-Bond interactions.

7.3. Phase 3 - Identification of new chemical entities through *in-silico* drug design methods

7.3.1. Purpose of the study

The purpose of the study is to identify hit molecules through *in-silico* drug design methods. The ligand based drug design approach was followed for the selection of hit molecules. Then the selected ligands were studied for their interaction with AR through docking studies. *In-silico* virtual screening was very

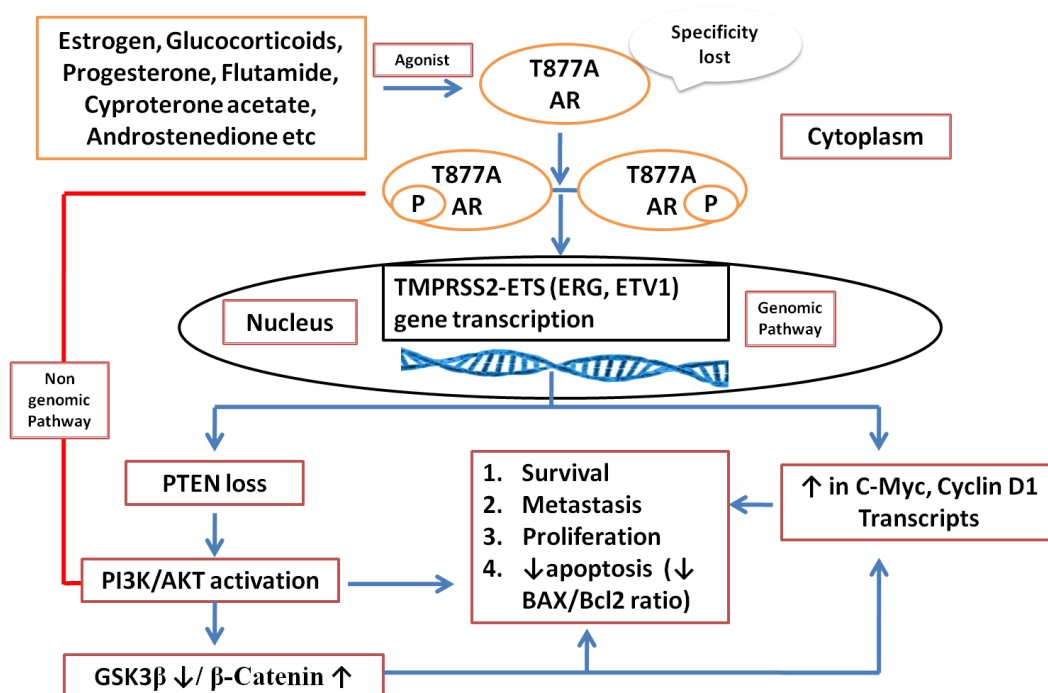
Chapter 7: Results and Analysis

useful method for identification of hit molecules. This is because we can screen millions of molecules in the chemical databases within short period of time. This method was also cost effective. The ADME properties, Lipinski rule of 5 and toxicity parameters were also included in the screening process for the identification of best fit molecule.

7.3.2. Drug Design

7.3.2.1. Target selection

Figure 25: AR as central dogma in AIPC (From literature review)



T887A AR: T877A mutated AR; TMPRSS2: Transmembrane protease, serine 2; ETS: erythroblast transformation-specific; ERG: ETS related genes; ETV1: ETS variant 1.

From the evaluation of the molecular pathogenesis of prostate cancer we selected mutant AR as target for AIPC. The mutant AR was directly modulates

Chapter 7: Results and Analysis

many cellular proliferation pathways. In this study we had used helix-12 negative T877A mutant AR for docking studies. As per literature the evidence, we used helix-12 negative AR to accommodate bulkier AR antagonist.

7.3.2.2. Target validation

The docking studies were validated by calculating the RMSD between the crystal and docked conformation of co-crystallized ligands. The RMSD between the predicted and crystal poses of cypoterone acetate was structure was 1.14 Å. The maximum allowable limit is 2 Å. Hence the docking procedures we were followed was valid one. The homology model was validated in the structural analysis and verification server (SAVES). The amino acids in the favorable, allowed and disallowed regions were identified by Ramachandran plot. The stereochemistry of the amino acids in the homology model was evaluated by PROCHECK. The 3D compatibility of the homology model was validated by VERIFY_3D. The homology model passed all the criteria for a good protein structure. The percentage of amino acids in the favorable region, allowed region and disallowed regions were 96.2%, 3.8% and zero respectively.

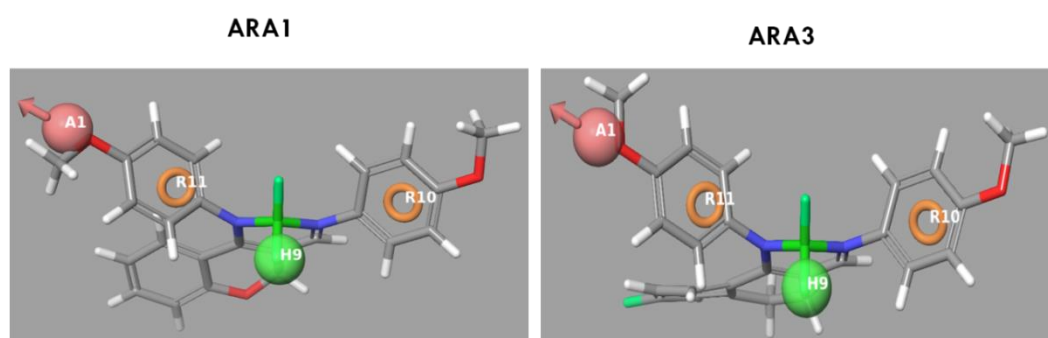
7.3.2.3. Lead identification

The wild and T877A mutated AR antagonist pharmacophore was used to find matches in the SPECS database and synthesized compounds from Shasun Research Center, Chennai (>1 million compounds). The pharmacophore matched ligands (1001 ligands) were ranked according to the fitness score (maximum of 3). The ligands with fitness score >2 (666 ligands) were subjected to structure based screening. Initially, the ligands were screened for optimum bulkiness by docking

Chapter 7: Results and Analysis

with helix-12 positive AR. The ligands that did not have binding affinity for helix-12 positive AR were selected for the next step. This filtering eliminated the less bulky / highly flexible ligands and reduced the total ligands to 192. The remaining ligands were docked with helix-12 negative AR by extra precision (XP) glide docking method. The molecules that form H-Bond interaction with amino acids such as Arg752, Gln711 and Asn705 were selected. Further, the ligands were manually evaluated for ADME and toxicity and we selected the ligands that have β -iminoenamine-BF₂ complex with either 1, 2 dihydronaphthalene or 2H-chromene groups (Figure 26). We obtained a total 9 compounds from the β -iminoenamine-BF₂ series from Shasun Research Centre, Chennai, for *in-vitro* screening.

Figure 26: Pharmacophore matched compounds



ARA1, fitness score - 2.009 3b: ARA3, Fitness score - 2.025

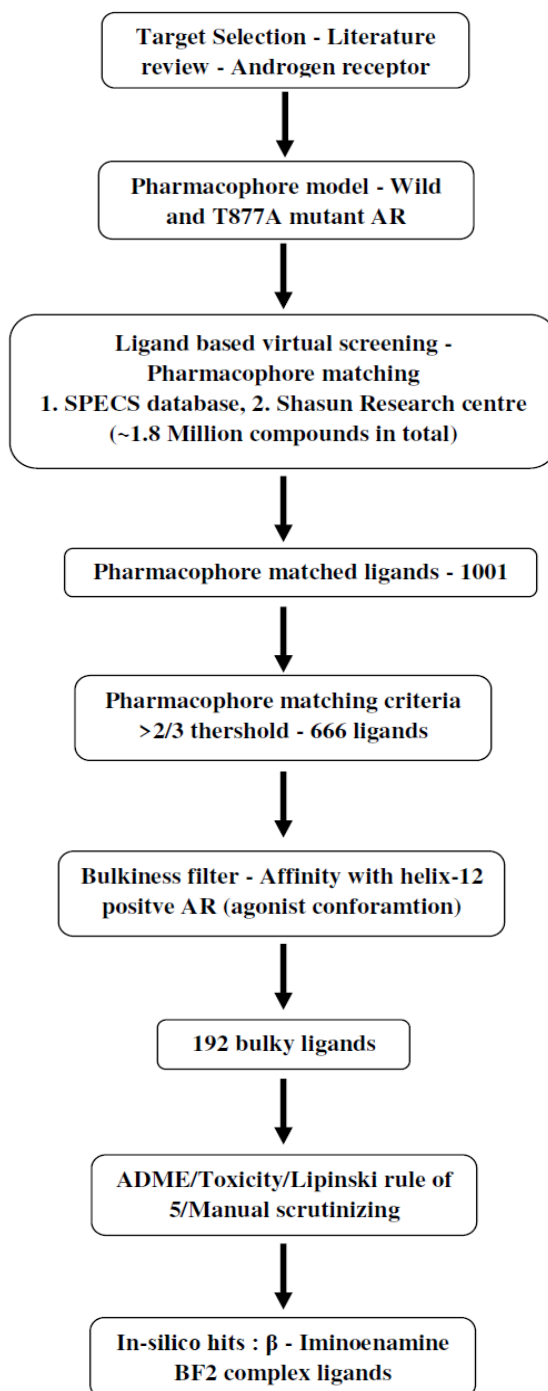
7.3.2.4. β -iminoenamine-BF₂ complex ligands

The β -iminoenamine BF₂ complex ligands also have 4-nitro-phenyl or 4-methoxy-phenyl or 4-fluoro-phenyl nucleus. The bulky ring that makes the β -iminoenamine BF₂ complex is either 2H-chromene or 1, 2-dihydronaphthalene group. These molecules were synthesized and obtained from Shasun Research

Chapter 7: Results and Analysis

Centre [129]. The docking studies have further shown that these molecules have affinity for the AR and formed essential H-Bond interactions with AR.

Figure 27: *In-silico* - Drug design workflow



Chapter 7: Results and Analysis

7.3.2.5. Ligand/AR binding interactions

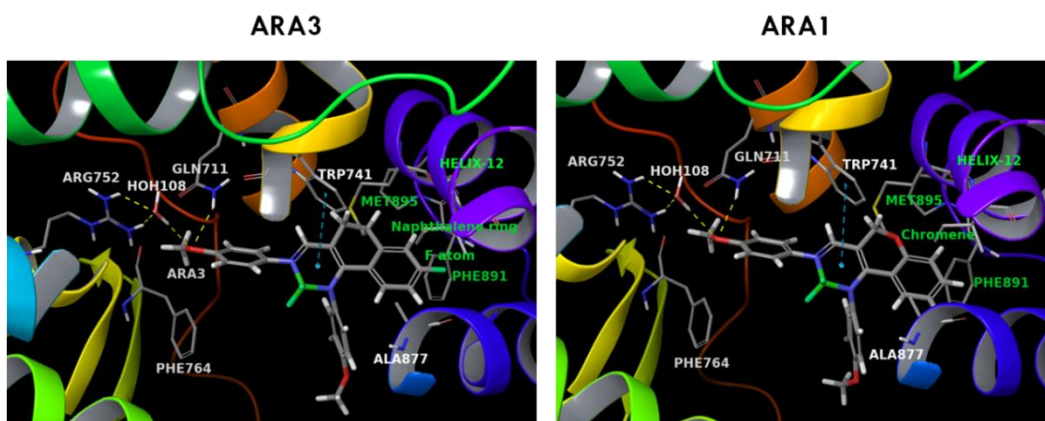
The enzalutamide had the best glide score (-8.426 kcal/mol) followed by test ligand, ARA3 (-8.295 kcal/mol). Most of the test ligands had similar glide scores as of bicalutamide (-7.624 kcal/mol) (Table 23). The enzalutamide and bicalutamide formed H-Bond interactions with Gln711, HOH108, Arg752, and Asn705 with helix-12 truncated AR. Bicalutamide had binding affinity for helix-12 uncut AR (-8.930 kcal/mol) but enzalutamide did not bind with it. Similar to enzalutamide, the test ligands (ARA1-ARA9) had binding affinity for helix-12 truncated AR, but did not bind with helix-12 uncut AR. The ligands (ARA1 - ARA4 and ARA6) formed H-Bond interaction with Gln711, HOH108, and Arg752 (bridged). The oxygen atom of the methoxy-phenyl group in ARA1 and ARA3 functions as H-Bond acceptor and mediates this H-bond interaction (Figure 28). Similarly, the oxygen atom of the nitro-phenyl group in ARA2, ARA4, and ARA6 forms H-Bond interactions with Gln711, HOH-108, and Arg752 (bridged). The ligands ARA5, ARA7 to ARA9 form H-Bond interactions with amino acid Asn705. The oxygen atom of the 2H-chromene group mediates this H-Bond interaction.

Chapter 7: Results and Analysis

Table 23: Docking score and H-Bond interactions of tested and standard ligands

Ligand	H-Bond interaction				Glide score kcal/mol
	Gln711	Arg752	HOH108*	Asn705	
ARA1	✓	✗	✓	✗	-7.869
ARA2	✓	✗	✓	✗	-7.646
ARA3	✓	✗	✓	✗	-8.295
ARA4	✓	✗	✓	✗	-5.367
ARA5	✗	✗	✗	✓	-7.942
ARA6	✓	✗	✓	✗	-6.386
ARA7	✗	✗	✗	✓	-7.737
ARA8	✗	✗	✗	✓	-7.414
ARA9	✗	✗	✗	✓	-7.686
Bicalutamide	✓	✓	✓	✓	-7.624
Enzalutamide	✓	✓	✓	✓	-8.426
Flutamide	✓	✗	✗	✓	-6.591

Figure 28: Docking interactions of best hit molecules



ARA3 forms H-Bond interactions with Gln711, HOH108, and Arg752 (bridged through HOH108). The 1, 2-dihydronaphthalene ring overlaps with Met895 of helix-12. The fluorine atom in 1, 2-dihydronaphthalene ring was closely located near Phe891. 2d: ARA1 forms H-Bond interactions with Gln711, HOH108, and Arg752 (bridged through HOH108). The oxygen atom of the 2H-chromene group was closely located with Met895 of helix-12.

Chapter 7: Results and Analysis

7.4. *In-vitro* anti prostate cancer activity of the new chemical entities to identify the hit molecules

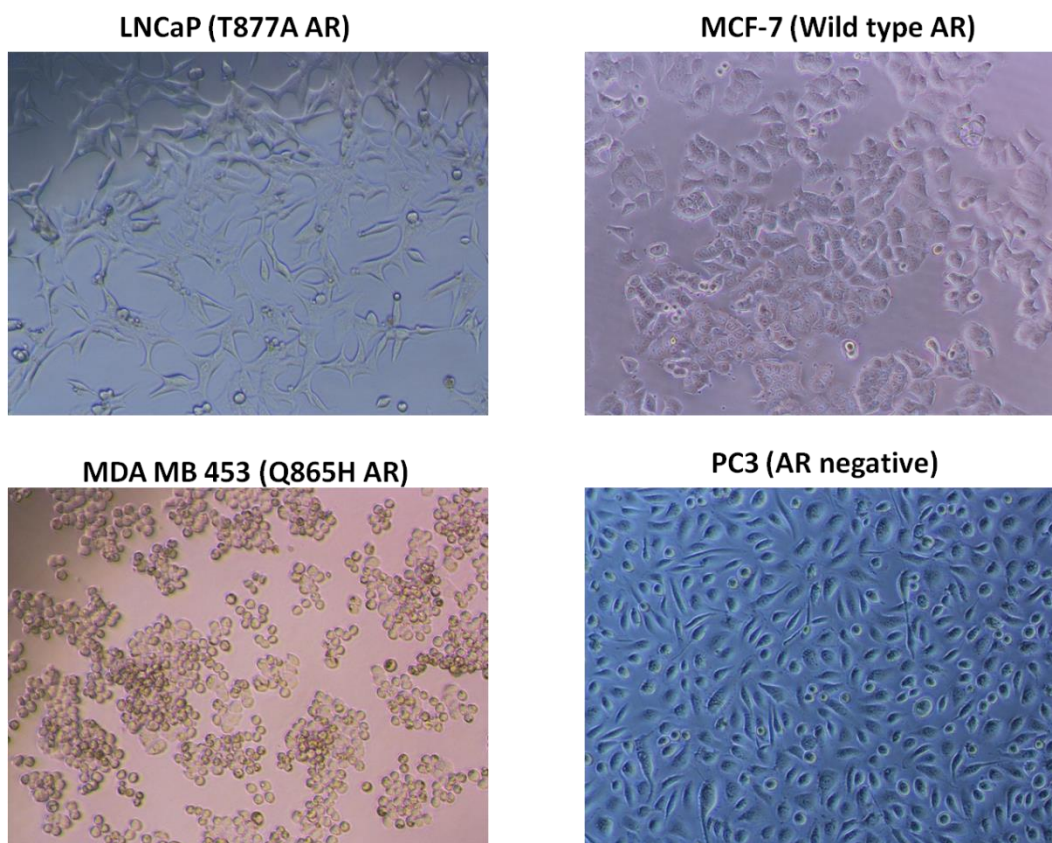
7.4.1. Purpose of the study

The purpose of the study is to select the best hit molecules of the series and to evaluate the anti-prostate cancer activity of the tested (ARA1 -ARA 9) and standard (bicalutamide) ligands. The tested (ARA1-ARA9) and standard molecules were screened in AR positive (LNCaP, MDA MB 453, MCF-7), AR negative (PC3), and non-cancerous (3T3) cell lines through anti-proliferation assay (Modified MTT assay, refer section 7.4.3). This type of screening will identify the ligands which are selective to AR expressing cell line. The measurement of DHT stimulated mRNA expression of AR response elements (PSA, TMPRSS2) by real-time PCR will confirm the anti-prostate activity of the compounds was mediated through AR.

Chapter 7: Results and Analysis

7.4.2. Structure of different cells and their morphology

Figure 29: Morphology of the AR positive and negative cell lines



The figure represents the morphology of AR positive and negative cell lines. The prostate cancer cells LNCaP and PC3 is needle shaped while the breast cancer cells MDA MB 453 and MCF-7 has irregular shape.

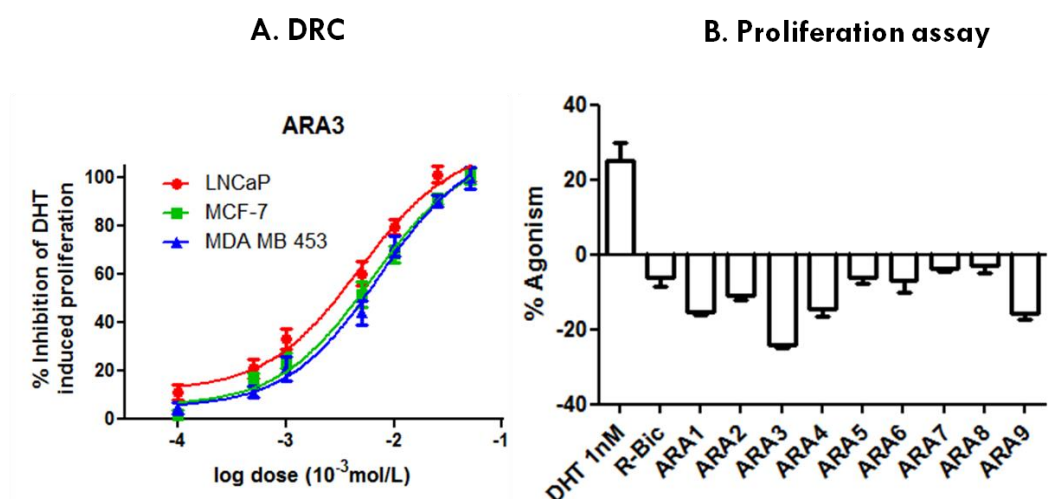
7.4.3. Evaluation of anti-proliferation activity in AR positive and negative cell lines

The bicalutamide was ~1.5 fold selective towards AR positive cell lines (LNCaP, MCF-7, & MDA MB-453) than the AR negative cell line, PC3. The test ligands, ARA1 – ARA4 and ARA6 have better selectivity (>1.5 fold) for AR positive cell lines than bicalutamide (Tables 24 and 25). The ARA3 is the best

Chapter 7: Results and Analysis

active molecule of the series and was ~7.6 fold selective towards AR positive cell lines. The dose response curve of ARA3 is given in figure 30. The test and standard AR antagonist does not have any agonist/partial agonist activity (Figure 30). The best active molecule ARA3 was the most potent molecule and was ~8.8 fold selective towards T877A mutant AR positive cell line than bicalutamide. Selective antagonist to each type of ARs will be intricate because the mutation retains the binding but only changes the activity.

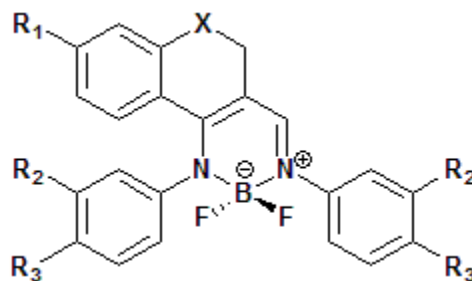
Figure 30: Bioactivity of tested and standard compounds



A: Dose response curve of ARA3. B: Agonist/Partial agonist activity of test and standard compounds treated with $1\mu\text{M}$ for 48 hours. The experiments were conducted in triplicates and the average value was represented as mean \pm S.D.

Chapter 7: Results and Analysis

Table 24: Bioactivity of tested and standard compounds



Ligand	X	R1	R2	R3	LNCaP (T877A AR)	MCF-7 (AR)	MDA MB 453 (Q875H AR)	PC3 (AR -)	3T3 (non-cancer)
ARA1	O	H	H	OMe	14.1 ± 0.64	13.8 ± 2.2	17.7 ± 0.41	51.2 ± 2.87	56.1 ± 0.66
ARA2	CH ₂	F	H	NO ₂	8.4 ± 0.7	12.9 ± 0.45	11.2 ± 0.26	44.6 ± 0.32	47.8 ± 1.26
ARA3	CH ₂	F	H	OMe	4.8 ± 0.03	6.2 ± 0.02	7.4 ± 0.38	45.6 ± 3.56	54.3 ± 0.7
ARA4	CH ₂	H	H	NO ₂	17.5 ± 1.09	16.9 ± 0.43	14.9 ± 1.05	48.2 ± 3.78	54.2 ± 1.68
ARA5	O	H	H	H	33.6 ± 6.15	40.8 ± 5.07	32.1 ± 0.73	56.1 ± 2.48	52.7 ± 1.06
ARA6	O	H	H	NO ₂	21.6 ± 4.84	18.2 ± 1.85	28.5 ± 2.89	42.4 ± 3.88	40.1 ± 2.03
ARA7	O	H	H	F	31.6 ± 1.59	33.5 ± 2.72	34.7 ± 1.90	36.9 ± 2.29	53.6 ± 2.13
ARA8	O	H	F	H	33.1 ± 2.79	38.8 ± 4	36.1 ± 7.87	52.9 ± 1.17	84.3 ± 2.75
ARA9	O	F	H	I	7.1 ± 4.97	8.8 ± 0.39	17.8 ± 1.02	12 ± 0.86	10.8 ± 0.55
(R)-BIC					42.7 ± 3.05	45.5 ± 5	41.6 ± 6.17	66.83 ± 6.9	63.1 ± 5.9

The experiments were conducted in triplicates and the average value was represented as mean ± S.D. The IC₅₀ were represented in μM

Chapter 7: Results and Analysis

Table 25: Selectivity of tested and standard compounds

Ligand	Selectivity for cancer cells				Selectivity for AR+ cells			
	3T3/T877A	3T3/WT AR	3T3/Q865H	3T3/AR (-)	PC3/T877A	PC3/WT AR	PC3/Q865H	Mean
ARA1	3.9	4.1	3.1	1.1	3.6	3.7	2.8	3.3
ARA2	5.6	3.7	4.2	1.07	5.3	3.4	3.9	4.2
ARA3	11.3	8.7	7.3	1.2	9.5	7.3	6.1	7.6
ARA4	3.0	3.2	3.6	1.1	2.7	2.8	3.2	2.9
ARA5	1.5	1.3	1.6	0.9	1.6	1.3	1.7	1.5
ARA6	1.8	2.2	1.4	0.9	1.9	2.3	1.4	1.8
ARA7	1.7	1.6	1.5	1.4	1.1	1.1	1	1
ARA8	2.5	2.2	2.3	1.6	1.5	1.3	1.4	1.4
ARA9	1.5	1.2	0.6	0.9	1.6	1.3	0.6	1.1
(R)-BIC	1.4	1.3	1.5	0.9	1.5	1.4	1.6	1.5

Chapter 7: Results and Analysis

7.4.4. Structural activity relationship

The ARA1 and ARA3 have methoxy substitution at R3 position. The oxygen atom of the methoxy group forms H-Bond interaction with Gln711, HOH108 and Arg752 (bridged). The ARA2, ARA4 and ARA6 have nitro substitution at R3. The oxygen atom of the nitro group forms H-Bond interaction with Gln711, HOH108, and Arg752 (bridged). Substitution of hydrogen or fluorine atom at R3 (ARA5 to ARA8) decreased the activity. Substitution of iodine at R3 (ARA9) was found to be toxic because ARA9 did not have selectivity and inhibited the proliferation of AR negative (PC3) and non-cancerous (3T3) cell lines. The compounds (ARA5 to ARA9) could not form H-Bond interaction with Gln711 and HOH108 because of the absence of H-Bond acceptor group at R3 position. This indicates that H-Bond acceptor group at R3 is essential for activity.

The substitution of fluorine atom at R1 increases the activity. The ligand ARA3 has better activity than ARA1. Similarly, ARA2 has better activity than ARA4 and ARA6. The substitution of oxygen atom at position X decreased the activity. ARA3, which has 1, 2-dihydronaphthalene group ($X = CH_2$), was more potent than ARA1, which has 2H-chromene group ($X = O$). Similarly, the compounds ARA2 and ARA4, which have 1, 2-dihydronaphthalene group, were more potent than ARA6, which has 2H-chromene group. Since the two substitutions were in the bulky region of the ligand and was oriented towards helix-12, we evaluated the binding position of these two substitutions with respect to helix-12 by superimposing helix-12 truncated and uncut AR (Figure 28). The 1,

Chapter 7: Results and Analysis

2-dihydronaphthalene of ARA3 overlaps with the helix-12 amino acid Met895. The fluorine atom was also located nearer to Phe891, which was present in turn before the helix-12. Hence, it might not be possible for the helix-12 to attain agonist conformation when ARA3 binds to the AR (12th helix closed towards the ligand binding pocket for agonist activity). The 1, 2-dihydronaphthalene ring is more bulky than the chromene ring; so the naphthalene ring possibly exhibits better steric clash with helix-12 amino acid Met895.

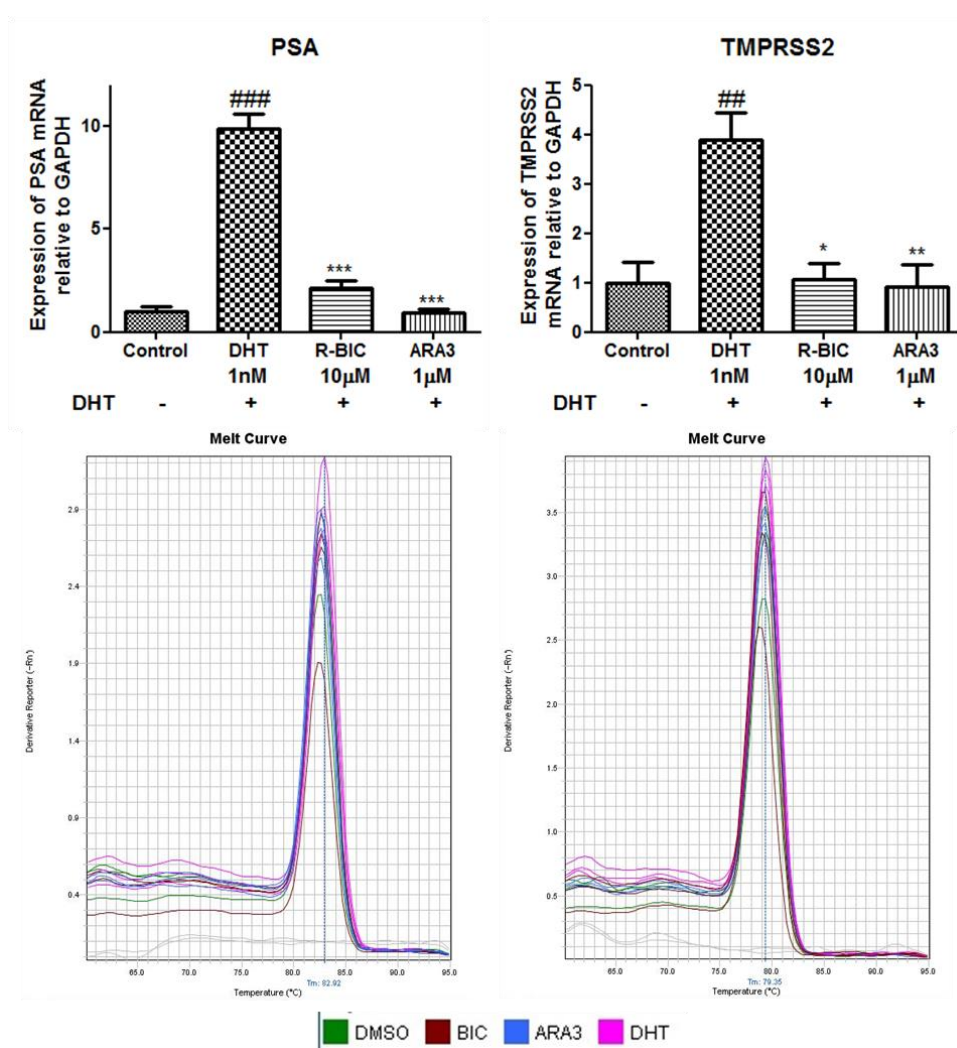
The H-Bond acceptor group at R3 was essential for activity. The bulky substituent should attain optimal conformation in order to push the helix-12 away from the ligand binding domain. Substitution in the bulky groups might augment the steric clash with helix-12 and possibly increase the activity.

7.4.5. Gene expression of AR response elements

The mRNA expression of the androgen receptor response elements PSA and TMPRSS2 genes were evaluated in LNCaP cells. The DHT significantly increased the mRNA expression of PSA (~9.8 fold) and TMPRSS2 (~3.6 fold) genes when compared to solvent treated (control). The Bicalutamide (10 μ M) and ARA3 (1 μ M) treatment significantly decreased the DHT stimulated mRNA expressions of PSA and TMPRSS2 genes (Figure 31).

Chapter 7: Results and Analysis

Figure 31: Gene expression of AR response elements with melt curves



The experiments were conducted in triplicates and the average value was represented as mean \pm S.D. The significance ($P < 0.05$) was obtained by applying one way ANOVA, followed by post hoc turkey test. (***) $P < 0.001$, (**) $P < 0.01$, (*) $P < 0.05$). The # indicates the comparison between control and negative control (1 nM DHT). The * indicates the comparison between 1nM DHT treatment with either ARA3 (1 μ M) or R-BIC (10 μ M) treatment. Single peak indicates the formation of single product (amplicon). There is no amplification in the negative control as observed from the melt curve. This indicates the amplification is because of the mRNA in the sample and not the dimers formed by primers.

Chapter 7: Results and Analysis

7.5. Phase 4 - Elucidation of the mechanism of action of the best active molecule

7.5.1. Purpose of the study

The purpose of the study is to identify the mechanism of action of ARA3. This will help to identify potential novel targets. The AR is a nuclear receptor and increases the transcriptional process of the prostate cells. So, we evaluated the gene expressions of androgen stimulated oncogenes such as c-myc, cyclin d1 and ETV1. The LNCaP cells also express low levels of estrogen receptors. Hence, we quantified the mRNA expression of estrogen receptor response element PS2 to confirm the activity of the ARA3 was mediated through AR. The protein expression of AR, p-AR 213, AKT and p-AKT 473 was also quantified to check the effect of the ARA3 in non-nuclear mediated mechanisms. The apoptosis was confirmed by quantifying bax/bcl2 ratio as well as caspase 3 activities and fluorescence staining techniques.

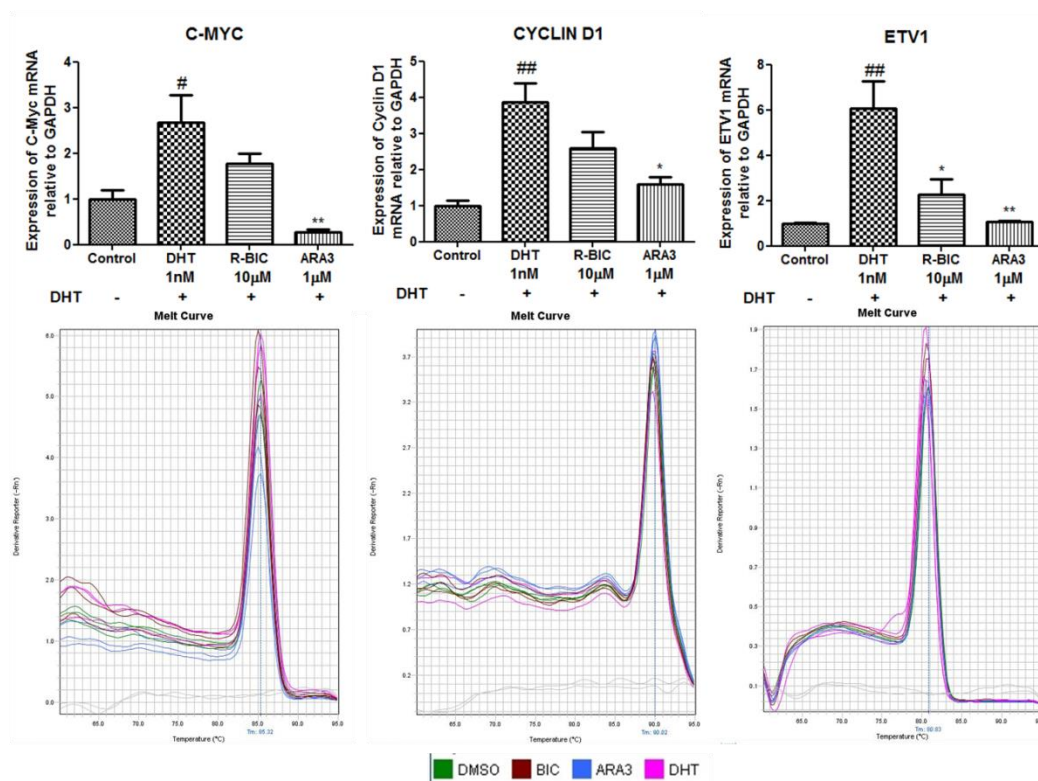
7.5.2. Gene expression of androgen induced oncogenes

The mRNA expression of androgen stimulated oncogenes such as ETV1, c-myc, cyclin d1, AR and PS2 were measured in LNCaP cells by qPCR (Figures 32 and 33). The DHT treatment significantly increased the expression of oncogenes such as cyclin d1 (~3.9 fold), c-myc (~2.6 fold), ETV1 (~6 fold), and PS2 (~2.4 fold) in comparison to the control. The DHT decreased the expression of AR (~0.73 fold) in comparison to the control. The Bicalutamide (10 μ M) did not significantly change the mRNA expression of c-myc, cyclin d1, AR and PS2 genes. The ARA3 (1 μ M) significantly decreased the DHT stimulated mRNA

Chapter 7: Results and Analysis

expression of oncogenes such as c-myc, cyclin d1 and ETV1 genes. Hence, contrary to bicalutamide, ARA3 significantly decreased the androgen stimulated expression of oncogenes such as cyclin d1, and c-myc. ARA3 did not affect the mRNA expression of AR and PS2.

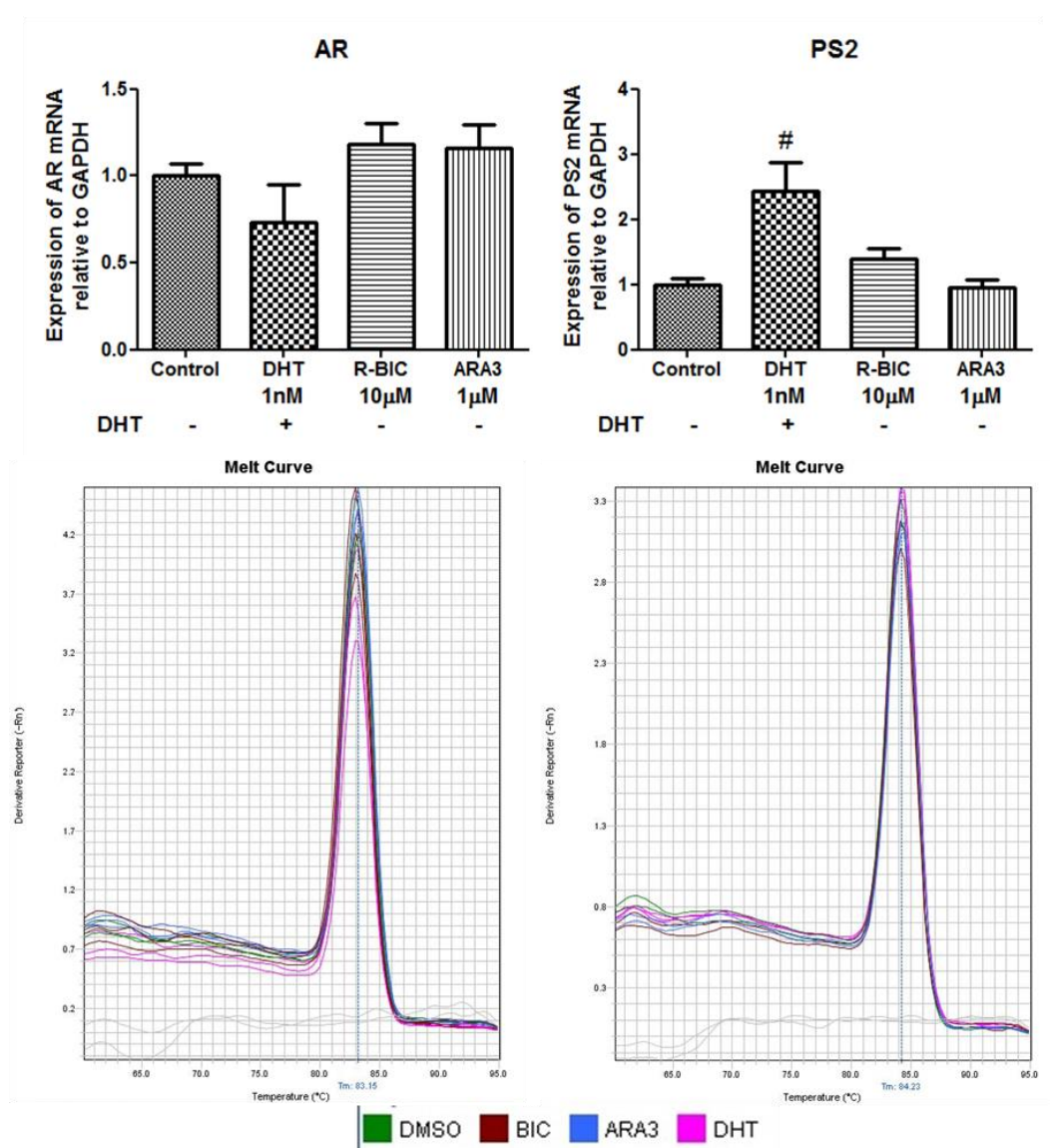
Figure 32: Gene expression of oncogenes with melt curves



The experiments were conducted in triplicates and the average value was represented as mean \pm S.D. The significance ($P < 0.05$) was obtained by applying one way ANOVA, followed by post hoc turkey test. (** $P < 0.01$, *** $P < 0.001$, * $P < 0.05$). The # indicates the comparison between control and negative control (1nM DHT). The * indicates the comparison between 1nM DHT treatment with either ARA3 (1µM) or R-BIC (10µM) treatment. Single peak indicates the formation of single product (amplicon). There is no amplification in the negative control as observed from the melt curve. This indicates the amplification is because of the mRNA in the sample and not the dimers formed by primers.

Chapter 7: Results and Analysis

Figure 33: Gene expression of AR and PS2 with melt curves



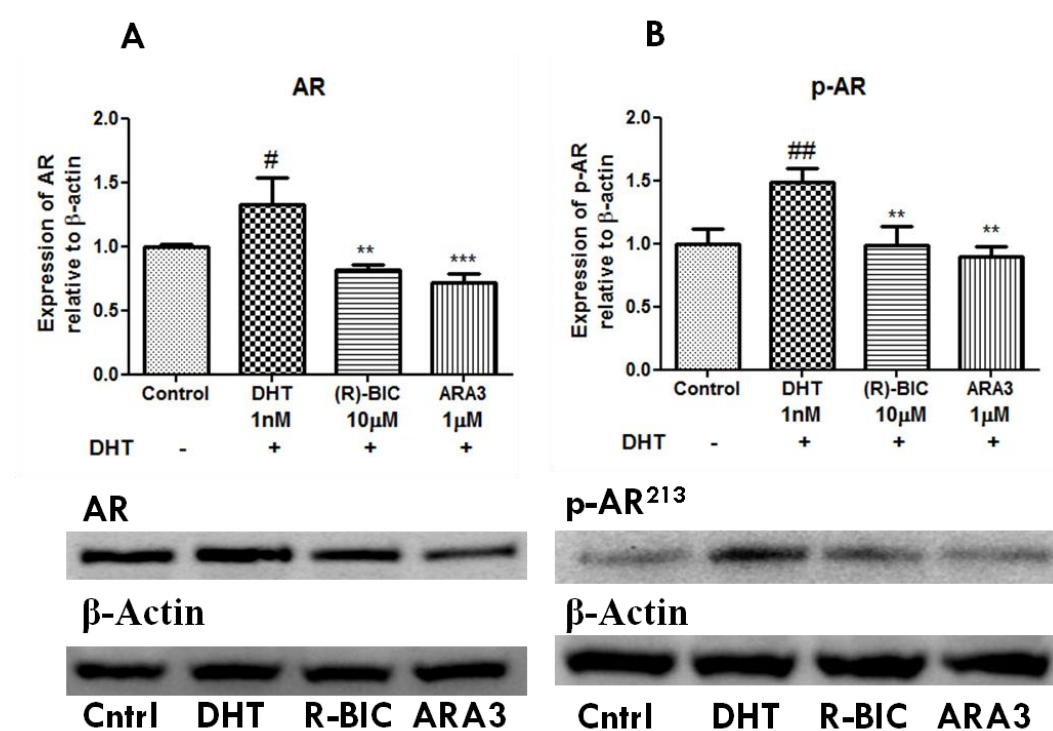
The experiments were conducted in triplicates and the average value was represented as mean \pm S.D. The significance ($P < 0.05$) was obtained by applying one way ANOVA, followed by post hoc turkey test. ($***P < 0.001$, $**P < 0.01$, $*P < 0.05$). The # indicates the comparison between control and negative control (1 nM DHT). The * indicates the comparison between 1 nM DHT treatment with either ARA3 (1 μ M) or R-BIC (10 μ M) treatment. Single peak indicates the formation of single product (amplicon). There is no amplification in the negative control as observed from the melt curve. This indicates the amplification is because of the mRNA in the sample and not the dimers formed by primers.

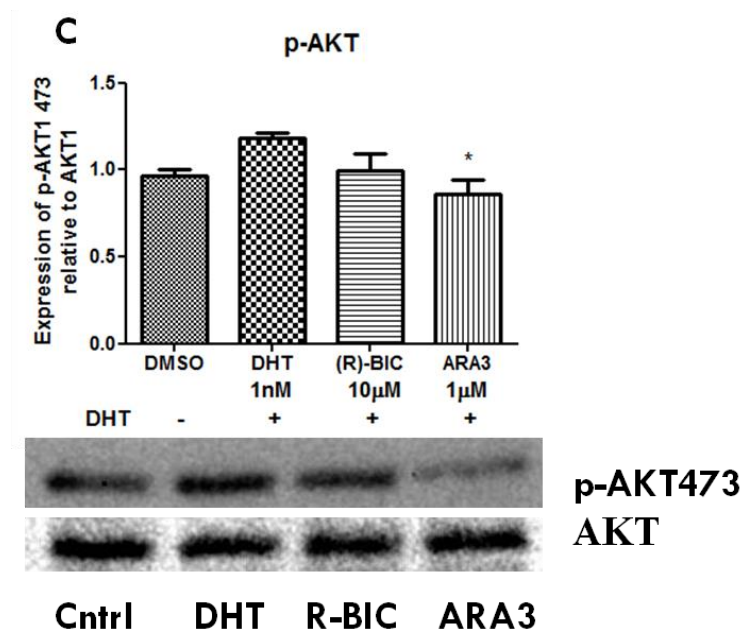
Chapter 7: Results and Analysis

7.5.3. Protein expression of AR and AKT1

The DHT significantly increased the protein expression of AR (~1.3 fold) and p-AR²¹³ (~1.5 fold) compared to control (Figure 34). Bicalutamide (10 μ M) and ARA3 (1 μ M) significantly decreased the DHT stimulated AR and p-AR²¹³ protein expression. The ARA3 significantly decreased the DHT induced protein expression of p-AKT1⁴⁷³ (~0.8 fold). The bicalutamide treatment does not have significant effect on p-AKT1⁴⁷³ (Figure 34).

Figure 34: Protein expression of AR and AKT1





The experiments were conducted in triplicates and the average value was represented as mean \pm S.D. The significance ($P < 0.05$) was obtained by applying one way ANOVA, followed by post hoc turkey test. (** $P < 0.001$, ** $P < 0.01$, * $P < 0.05$). The # indicates the comparison between control and negative control (1 nM DHT). The * indicates the comparison between 1 nM DHT treatment with either ARA3 (1 μ M) or R-BIC (10 μ M) treatment.

7.5.4. Apoptotic assays

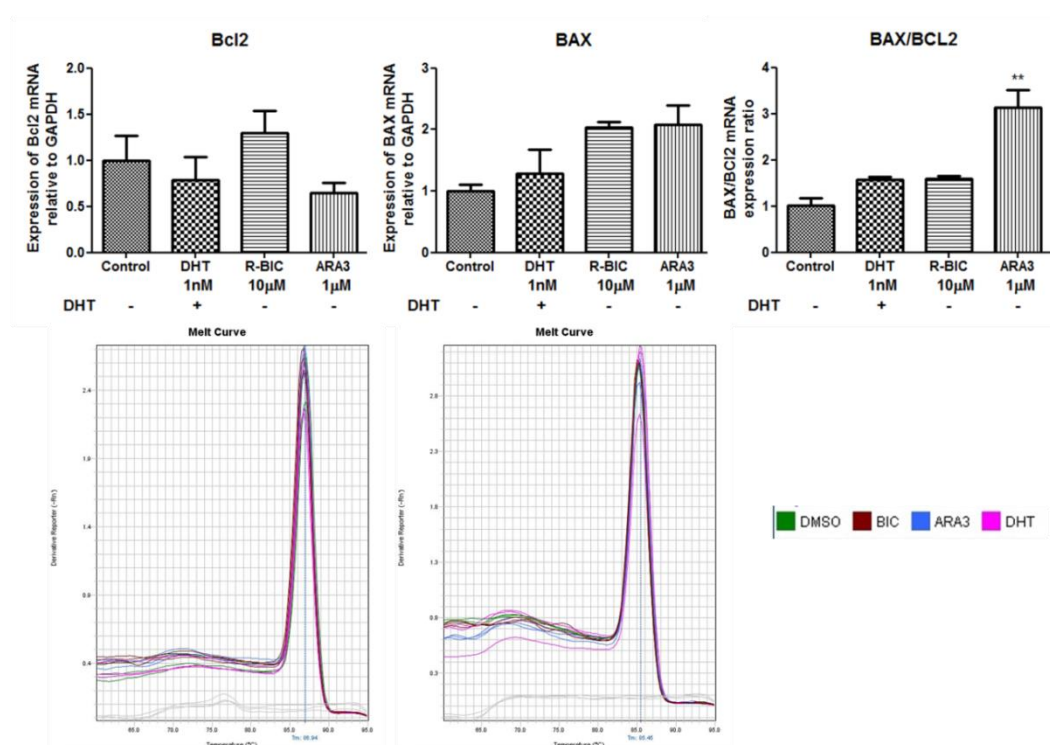
The apoptosis was confirmed in LNCaP cells by quantifying the BAX/Bcl2 mRNA ratio, procaspase-3 protein level, caspase-3 enzyme activity, and ethidium bromide/acridine orange (EB/AO) staining.

7.5.4.1. Gene expression of bax/bcl2

The treatment of LNCaP cells with DHT (1 nM) and bicalutamide (10 μ M) did not affect the mRNA ratio of anti-apoptotic protein, bcl2 and proapoptotic protein BAX. The ARA3 significantly increased (~3 fold) the BAX/Bcl2 ratio when compared to the solvent control [Figure 35].

Chapter 7: Results and Analysis

Figure 35: BAX/Bcl2 mRNA ratio with melt curves



The significance ($P < 0.05$) was obtained by applying one way ANOVA, followed by post hoc turkey test. (** $P < 0.001$, * $P < 0.01$, $P < 0.05$). The # indicates the comparison between control and negative control (1 nM DHT). The * indicates the comparison between 1 nM DHT treatment with either ARA3 (1 µM) or R-BIC (10 µM) treatment. Single peak indicates the formation of single product (amplicon). There is no amplification in the negative control as observed from the melt curve. This indicates the amplification is because of the mRNA in the sample and not the dimers formed by primers. The experiments were conducted in triplicates and the average value was represented as mean \pm S.D.

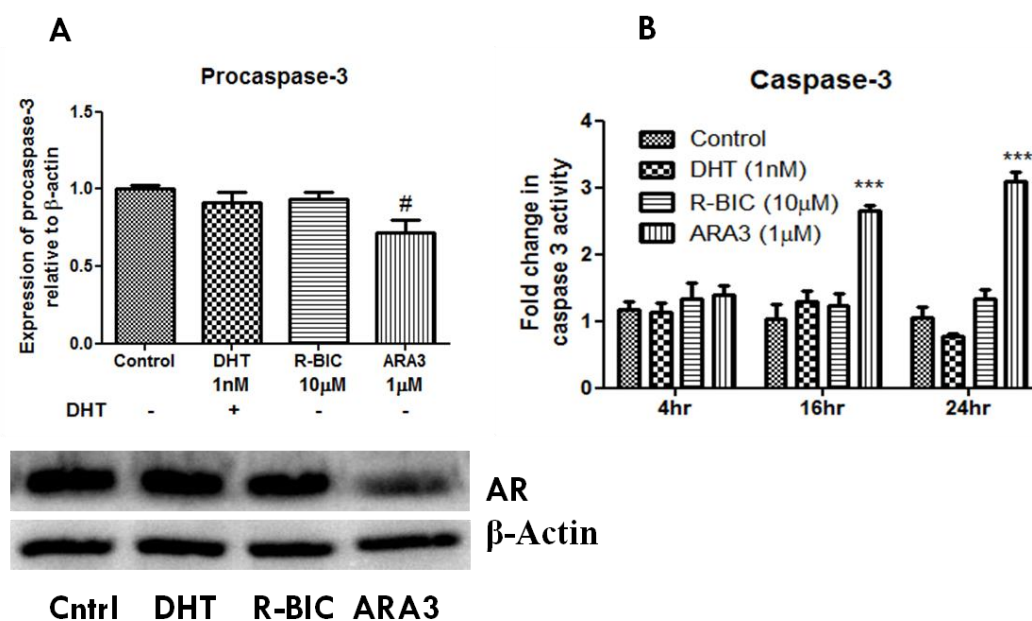
7.5.4.2. Caspase activity

The DHT and bicalutamide did not affect the expression of procaspase-3 and hence there is no significant increase in caspase-3 activity when compared to control. The ARA3 significantly decreased the protein expression procaspase-3

Chapter 7: Results and Analysis

(~0.7 fold) and so the ARA3 significantly increased the caspase 3 activity at 16th and 24th hour (Figure 36).

Figure 36: Caspase activity



The significance ($P < 0.05$) was obtained by applying one way ANOVA, followed by post hoc turkey test. ($***P < 0.001$, $**P < 0.01$, $*P < 0.05$). The # indicates the comparison between control and negative control (1 nM DHT). The * indicates the comparison between 1 nM DHT treatment with either ARA3 (1 μ M) or R-BIC (10 μ M) treatment.

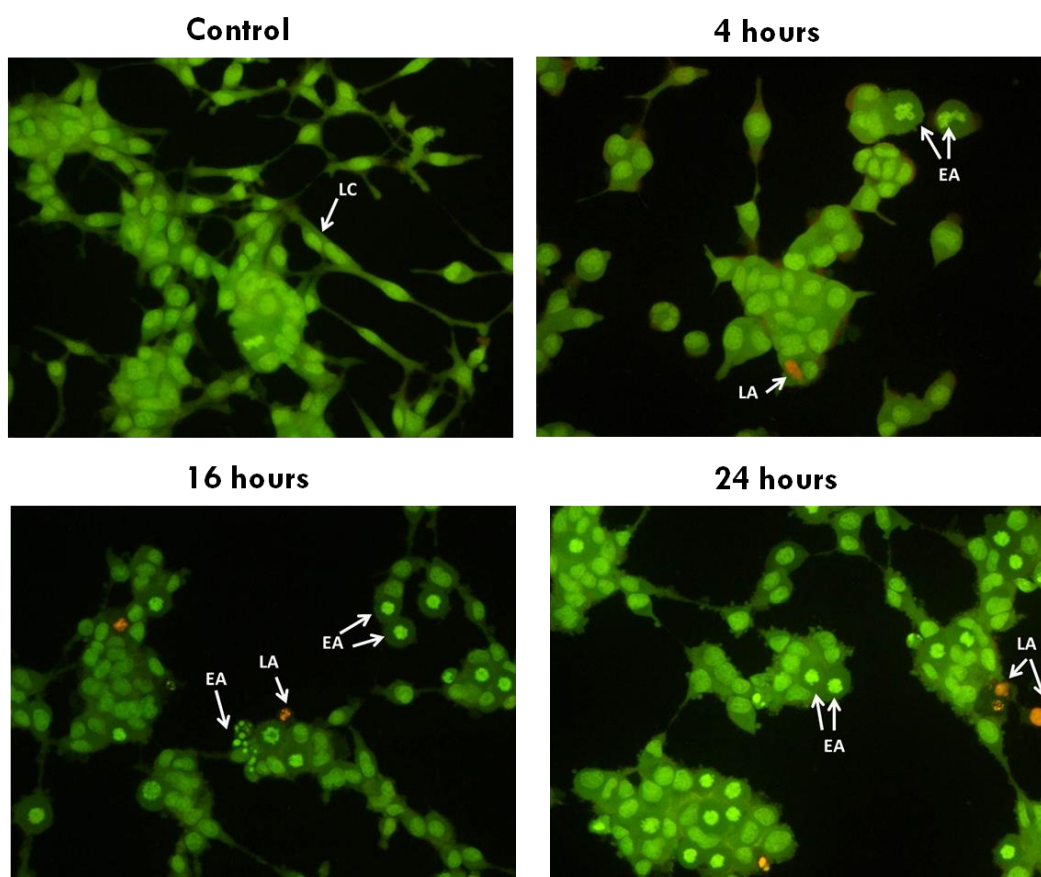
7.5.4.3. Ethidium bromide/Acridine orange staining

The LNCaP cells were cultured in RPMI medium supplemented with 10% charcoal stripped FBS. The cells were treated for different time points (4 hour, 16 hour and 24 hour) with ARA3 (4.8 μ M) in the absence of 1 nM DHT (Figures 37 and 38). The morphology of the ARA3 treated cells was different from the control cells. The density of the cells in the ARA3 treated wells were less when compared to control wells. Further, the cytoplasm of the ARA3 treated cells appear bulged

Chapter 7: Results and Analysis

and the cells have irregular shape when compared to control. The apoptotic nuclei were visible in the 16 and 24 hour treatment. The apoptotic nuclei were condensed and stained bright green. The late apoptotic cells stain bright orange. The late apoptotic cells were seen in 4, 16 and 24 hour treatment.

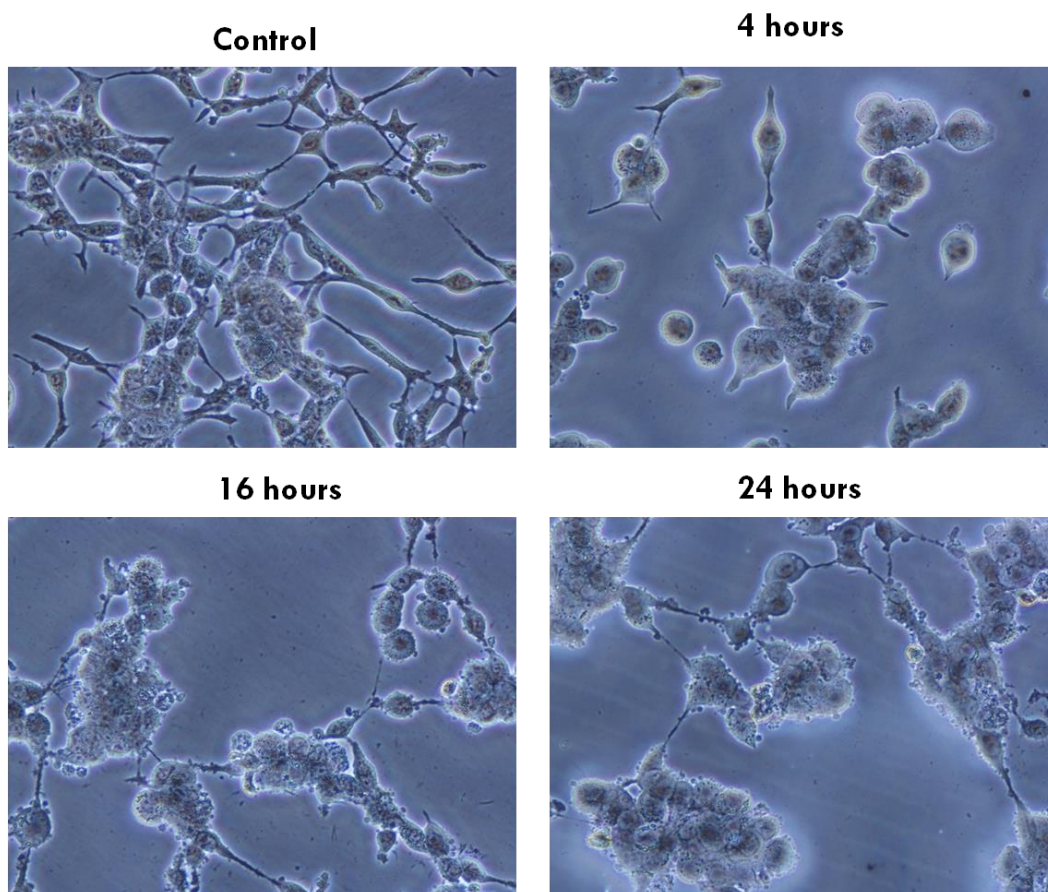
Figure 37: Fluorescence image of ARA3 treated LNCaP cells



The figure (20X) represents the EB/AO fluorescent images of LNCaP cells treated with 4.8 μ M of ARA3. The live cells (LC) stain normal green. The early apoptotic (EA) cells have a condensed or fragmented nucleus and stains bright green. The nucleus of the late apoptotic (LA) cells appears condensed or fragmented and stained yellow-orange. The nucleus of the necrotic cells uniformly stains red.

Chapter 7: Results and Analysis

Figure 38: Phase contrast image of ARA3 treated LNCaP cells



The images (20X) represent the phase contrast images of EB/AO stained cells. The cells were treated with 4.8 μM of ARA3 for 4, 16 and 24 hours. There is a change in the morphology of treated cells when compared to untreated control. The treated cells appear bulged with irregular morphology

Chapter 8: Discussion

8. DISCUSSION

Mutant AR is responsible for androgen independent prostate cancer progression

The expression of the point mutation in the ligand binding domain of the AR was one of the major reasons behind the development of androgen independent prostate cancer [130]. The cells of androgen independent prostate cancer do not dependent on androgens for proliferation [131]. This is because the mutation in the ligand binding domain of the AR widens the ligand specificity such that the steroidal hormones such as oestrogen, progesterone and glucocorticoids activate the mutant AR [132, 133]. Additionally, the mutant AR leads to the withdrawal of AR antagonist from the regimen because the mutant AR converts the AR antagonist into an agonist [134, 135]. The mutations, T877A, W741L/C and F876L are some of the mutations that are identified in androgen independent prostate cancer patients [135]. Recent studies have indicated that the constitutive activation of mutant AR could be reversed by designing a potent AR antagonist that lacks resistance with mutant AR [136, 137]. Hence, we decided to target mutant AR for drug design and development to treat androgen independent prostate cancer.

The entire non-steroidal AR antagonist in clinical use has common anilide pharmacophore. There is no diverse structural element in the marketed non-steroidal AR antagonist. Hence there is possibility of cross resistance within the molecules and because of that the entire AR antagonist had developed resistance for one or another mutation [134, 135]. Structurally diverse AR antagonist could possibly resist those mutations that occur during the course of treatment. In the

Chapter 8: Discussion

preliminary studies we found that the crystal structures of AR ligand binding domain in the protein data bank are in agonist conformation. Therefore we decided to identify novel AR antagonist through ligand based drug design.

Ligand/receptor interactions in wild and mutant AR

As a preliminary investigation we decided to study the interactions of non-steroidal AR antagonist (flutamide, bicalutamide and enzalutamide) with wild, T877A mutant and W741L mutant using docking studies. In the docking studies, we observed that the enzalutamide did not have binding affinity with the wild, T877A and W741L mutant ARs. Similarly the bicalutamide also did not have binding affinity with the wild type and T877A mutant ARs. As discussed earlier the crystal structures of the wild and mutated ARs in the PDB are in agonist conformation. Hence it was not possible for an AR antagonist to have affinity for the ARs in agonist conformation. Altimari and co-workers [138] had indentified novel AR antagonist by rigid docking studies with AR in agonist conformation. The identified triazole derivatives did not have potent activity against mutant AR. Hence, identification of molecules by docking using ARs in agonist conformation might lead to the identification of less potent ligands with partial agonistic type activity.

Another major observation in the docking studies is that the volume of the ligand binding pocket of the mutant ARs (T877A and W741L) was larger than the wild type AR. This is because the mutations were from higher molecular weight amino acids to lower molecular weight ones. It is well established that the AR antagonist are bigger molecules than the agonist [139]. To accommodate the

Chapter 8: Discussion

additional bulkier groups of AR antagonist, the helix-12 of the AR attains an extended conformation from the binding pocket [140]. This new conformation of the AR prevents it from binding with co-activators [141]. Hence the mutations in the AR could be deliberate to prevent the AR antagonist from affecting the agonist conformation of helix-12 (helix-12 closed towards binding pocket). From the docking results and literature review we hypothesized that the bulkier AR antagonist could be fitted in helix-12 negative AR. So, we constructed a homology of AR without the helix-12. We again carried out docking studies using the homology model. The entire non-steroidal AR antagonist including enzalutamide had binding affinity for the helix-12 negative AR. This proves that the bulkiness in AR antagonist prevent it from binding with the AR in agonist conformation. Therefore, to identify a potent AR antagonist, the helix-12 positive AR (agonist conformation) could be used to eliminate the less bulky ligands.

Selection of ligand based drug design method for lead identification

The modelling of a pharmacophore or 3D-QSAR and identification of hits is a ligand based approach. Here, a 3D-representation of the essential descriptors or functional groups will be derived from the reported active molecules [142]. The previous studies from our laboratory had demonstrated that the ligand based drug design methods will more likely provide the hit molecules than the docking studies. This was the direct result of the more amounts of calculations and validation processes involved in 3Q-QSAR generation [143, 144].

In our study we constructed three pharmacophore models. The first pharmacophore was constructed from molecules that antagonize wild type AR.

Chapter 8: Discussion

The second pharmacophore was constructed from molecules that antagonize T877A mutant AR. The dataset molecules in the first two pharmacophore models are bicalutamide and enzalutamide derivatives. The third pharmacophore was constructed from ligands that antagonize wild and T877A mutant AR. The molecules in this dataset do not have any partial agonist/agonist activity with wild and/or T877A mutant AR. The hit molecules were identified from the third pharmacophore because this pharmacophore was derived from molecules that do not have resistance with wild or T877A mutant AR. The first two pharmacophores were compared with each other to identify the difference between wild and T877A mutant AR.

Differences between the wild and T877A mutant AR antagonist pharmacophore

The descriptors such as hydrogen bond acceptor (A), hydrogen bond donor (D), hydrophobic group (H), aromatic ring (R), positively charged group (P) and negatively charged group (N) are used for the construction of pharmacophore [145]. The molecules in the dataset for the construction of the 3D-QSAR models have common structures, which are also present in the marketed drugs. All the marketed ligands have two aromatic rings (A and B) separated by a linker group. These two rings (A and B) were also present in all the 3D-QSAR models. The major difference among the 3D-QSAR models was the distance and angle between the A ring and B ring. Also, there is a difference in the distance between the two extreme pharmacophore site points. These properties describe the variability in the length and flexibility among the active molecules.

Chapter 8: Discussion

The distance between the A and B ring of wild type (A ring to B ring: 4.09 Å) was shorter than the T877A mutant AR (ring A to ring B: 8.895 Å) pharmacophore. Additionally the angle between the A and B ring was acute in wild type and obtuse in T877A mutant AR pharmacophore. The distances and angle for wild and mutant AR pharmacophore was more or less similar to that of T877A mutant AR. The distances between A and B ring was 7.217 Å and the angle between them was obtuse. The relatively longer distances and obtuse angles between the A and B rings indicate a less flexible linker region among the active molecules of T877A mutant AR antagonist. Ohta and co-workers [146] have shown that bulky carborane pharmacophore is essential for AR antagonistic activity in T877A mutant AR. This bulky group is shown to occupy a position in the ligand binding pocket that overlaps with the helix-12 amino acids. The T877A mutant AR pharmacophore from our study also indicates that the rigid and less flexible structures were essential for AR antagonistic activity against T877A mutant AR. From these 3D-QSAR models, we could possibly deduce that smaller and/ or flexible molecules could be sufficient to block wild type AR. For T877A mutant AR, a bigger molecule in length plus less flexibility would be required to block it.

In-silico virtual screening and identification of β -iminoenamine BF₂ ligands as novel AR antagonist

The β -iminoenamine BF₂ ligands were identified through pharmacophore based screening approach. The wild and T877A mutant AR pharmacophore is used for screen the databases for the identification of matches. Voet and co-

Chapter 8: Discussion

workers [147] had followed the pharmacophore based approach for the identification of novel AR antagonist. The pharmacophore in that study was constructed using bio-active conformation of bicalutamide. The identified ligands (ARAN – 4, 51 and 53) were found to be less potent than the standard AR antagonist. The major reason for the decreased activity of the test ligands was because of the selection of bicalutamide for the construction of the pharmacophore. It is well known that the bicalutamide has resistance with W741L mutant AR [148]. In our study, the wild and T877A mutant AR pharmacophore was derived from molecules that does not have resistance with T877A and W741L mutant AR. Hence our pharmacophore is more likely to provide a potent lead molecule against mutant ARs. Additionally, to improve the efficacy of molecules against mutant ARs we included a structure based elimination process to eliminate the flexible and less bulky ligands. Here, we eliminated the pharmacophore matched ligands which has binding affinity for helix-12 positive AR (agonist conformation) and selected the ligands which had binding affinity only with helix-12 negative AR. This process of selection will lead to the elimination of the flexible ligands.

The β -iminoenamine BF2 ligands have 2H-Chromene or 1, 2-Dihydronaphthalene as bulky group. As discussed earlier, the entire standard non-steroidal AR antagonist has a common anilide scaffold which was resistant to one or another mutation. The ARN-509 was a recently approved AR antagonist for phase 4 clinical trials and has the common anilide pharmacophore. Consequently, reports have shown that the ARN-509 exhibits cross resistance with the F876L

Chapter 8: Discussion

mutant AR [149]. The F876L mutation was originally identified in the enzalutamide treated prostate cancer cells. Hence the anilide scaffold could lead to the cross resistance among the AR antagonists. A recently identified clinical trial candidate ODM-201 does not share the common anilide scaffold and was better active than enzalutamide [150]. Therefore, the identification of novel scaffold is essential to avoid cross resistance and to improve the potency against mutant ARs. The β -iminoenamine BF₂ is a novel scaffold and so these ligands might not be affected by cross resistance with mutant ARs.

In-vitro screening and structural activity relationship of β -iminoenamine BF₂ complex ligands

The test ligands (ARA1 - ARA9) and standard bicalutamide were screened in AR positive (LNCaP, MCF-7, & MDA MB-453) and negative cell line (PC3) through anti-proliferative assay. Previous studies have shown that the AR positive and AR negative cell lines could be used in the screening process to identify AR specific ligands [151]. In our study we observed that the ligands, ARA1 – ARA4 and ARA6 have better selectivity towards AR positive cell lines than the bicalutamide. The ligands, ARA1 – ARA4 and ARA6 formed H-Bond interaction with amino acids Gln711 and Arg752 (bridged through HOH108) in docking studies with the helix-12 negative AR. The remaining tested ligands (ARA5, ARA7 – ARA9) have formed H-Bond interaction with Asn705 and have low selectivity to AR positive cell lines than the bicalutamide.

Literature survey has indicated that the H-Bond interactions with the amino acids Arg752, Gln711, HOH108, Leu704, Asn705, and Thr877 is essential

Chapter 8: Discussion

for specific binding of ligands to the AR [152]. The amino acids Arg752, Gln711 and HOH108 are present deep inside the binding pocket. The amino acids Thr877 and Asn705 are present nearer to helix-12. Guo and co-workers [106] had indicated that the molecules that preferentially form H-Bond interaction with the deep residues exhibits better AR antagonist potency than the ones that form H-Bond interaction with Asn705 and Thr877. This is because the amino acids Asn705 and Thr877 are present near to helix-12 and H-Bond interaction with them might prevent the molecules from abutting (steric clash) the helix-12.

The interaction of best hit molecule ARA3 with helix-12 amino acids was evaluated by superimposing the helix-12 negative (ARA3 bound) and helix-12 positive ARs. We observed that the bulky 2H-chromene group of ARA3 was oriented towards the helix-12 of the AR and overlaps with the amino acid Met895 of helix-12. Söderholm and co-workers [153] have identified novel diphenyl and phenylpyridine derivatives and these molecules do not have resistance with mutant ARs. Further, induced fit docking studies had shown that these molecules had interacted with the Met895 of helix-12 and extended the helix-12 away from the binding pocket. Hence, in our case also it may not possible for the helix-12 of the AR to attain an agonist conformation with ARA3. From the structural activity relationship, we conclude that the H-Bond acceptor group should bind deeply into the binding pocket to form H-Bond interaction with Arg752 and Gln711. The proper orientation of the bulky groups towards the helix-12 amino acids, in particular Met895 favors the activity.

Chapter 8: Discussion

The best active molecule ARA3 decreases the androgen dependant protein expression of AR and gene expression of PSA and TMPRSS2

In our study we used the LNCaP cell line for the elucidation of the anti-prostate cancer mechanism of ARA3. This is because the LNCaP cell line expresses T877A mutant AR and TMPRSS2-ETV1 gene fusion, which are the major contributing factors for the development of androgen independent prostate cancer [154]. The androgen dependant activity of the ARA3 was elucidated by measuring the protein expression of AR and p-AR²¹³ and gene expression of PSA and TMPRSS2. The binding of androgens to AR causes phosphorylation of AR at several sites. The p-AR²¹³ is one of the active phosphorylated forms of the AR [155]. We observed that the bicalutamide and ARA3 treatment prevented the activation of AR to p-AR²¹³. The previous reports have shown that the prevention of the phosphorylation of AR is essential to decrease the AR mediated genomic activity [156]. The decrease in the AR mediated genomic activity will subsequently decrease the expression of genes regulated by AR.

The PSA and TMPRSS2 are widely accepted biomarkers for prostate cancer [157]. The expression of these AR response elements is found to be increased in prostate cancer patients [158]. Recently, the TMPRSS2 has gained more attention because of the fusion of ETS (ERG - ETV1) genes with TMPRSS2. This gene fusion has active role in the androgen independent prostate cancer progression [159]. The ETS family of transcriptional factors are oncogenes and stimulates the cell division, metastasis, angiogenesis, etc in cancer cells [160]. We observed that the ARA3 and bicalutamide are almost equipotent in reducing

Chapter 8: Discussion

the DHT stimulated gene expression of PSA and TMPRSS2. Hence our new molecule, ARA3 has anti-prostate cancer activity mediated through AR similar to that of bicalutamide.

The ARA3 reduces the expression of oncogenes and induces apoptosis in LNCaP cells

The LNCaP cells were naturally resistant to apoptosis because of the constitutive activation of PI3K/AKT survival pathway and leads to the over expression of oncogenes such as c-myc and cyclin D1 [161, 162]. The c-myc expression was 50 times higher in LNCaP cell than the normal prostate cells [163]. A recent study has reported that, novel isoindolinediones based AR antagonist decreased the gene expression of c-myc and cyclin d1. Those compounds had prevented the G1/S cell cycle transition and induced apoptosis in LNCaP cells [164]. In our study we quantified the gene expression of oncogenes (c-myc and cyclin d1) in ARA3 and bicalutamide treated LNCaP cells. Here, the ARA3 alone had decreased the gene expression of oncogenes and not the standard bicalutamide. Hence, the ARA3 is better than bicalutamide and could also prevent the G1/S cell cycle transition.

The induction of apoptosis in LNCaP cells by ARA3 was confirmed by measuring the bax/bcl2 mRNA ratio, procaspase-3 protein expressions and caspase-3 enzyme activities. Previous studies have shown that increase in the bax/bcl2 ratio leads to the cleavage of procaspase-3 into active caspase-3 [165]. The activated caspase-3 cleaves many proteins and induces the apoptosis in the normal and cancer cells [166]. In the androgen independent prostate cancer cells

Chapter 8: Discussion

the bax/bcl2 ratio was found to be decreased and it is one of the contributing factors for androgen independent prostate cancer progression [167]. The expression of anti-apoptotic factor bcl2 was found to be elevated in androgen independent prostate cancer cells and this was responsible for the decrease in bax/bcl2 ratio [167]. We observed that the ARA3 increased the bax/bcl2 mRNA ratio but the bicalutamide did not increase the bax/bcl2 mRNA ratio. Browne and co-workers [168] has demonstrated that the bicalutamide had increased the expression of anti-apoptotic factor bcl2 in LNCaP transfected nude mice model. This is exactly the opposite effect that was required for anti-cancer activity. Hence, our new molecule ARA3 was better than the bicalutamide because induction of apoptosis is required to control the cancer cell proliferation.

The anti-cancer activity of ARA3 was mediated through PI3K/AKT pathway

The PI3K/AKT pathway could be activated by AR through genomic and non-genomic pathways in androgen independent prostate cancer cells. In the AR mediated genomic pathway, the transcription of TMPRSS2-ETV1 gene fusion product was responsible for the PI3K/AKT activation [154]. The over expression of ETV1 contributes to the down regulation of PTEN and mitigates the control of PTEN over PI3K/AKT pathway [154]. The PTEN is a tumor suppressor gene and prevents the constitutive activation of PI3K/AKT pathway [169]. In the AR mediated non genomic pathway, the agonist bound AR (AR-DHT/Agonist) directly interacts with the AKT and activates it in the cytoplasm [170]. Therefore we decided to quantify the protein expression of p-AKT1⁴⁷³ (active form of AKT1) and gene expression of ETV1 in LNCaP cells.

Chapter 8: Discussion

We observed that the ARA3 and bicalutamide decreased the DHT induced gene expression of ETV1. However the biological activity of ARA3 and bicalutamide varies with AKT1. The ARA3 decreased the activation of AKT1 to pAKT⁴⁷³ but the bicalutamide did not prevent the activation of AKT1 protein. Therefore, the suppression of AR mediated ETV1 gene expression did not significantly affect the AKT1 activation. As a result of this, the ARA3 could possibly reduce the activation of AKT1 to p-AKT1⁴⁷³ through AR mediated non-genomic pathway. Hence, from the above experimental evidences we propose that the test ligand ARA3 decreases the gene expression of oncogenes (c-myc and cyclin d1) and promotes the apoptosis in LNCaP cells through AR mediated non-genomic inhibition of AKT activation. The bicalutamide prevents the androgen mediated genomic activity but it could not prevent the androgen mediated non-genomic activation of AKT. Hence, the bicalutamide could not decrease the oncogenes of the PI3K/AKT survival pathway to induce the apoptosis. The proposed mechanism of action of ARA3 is given in figure (Figure 39).

Chapter 8: Discussion

Figure 39: Anti-prostate cancer mechanism of ARA3 in AIPC

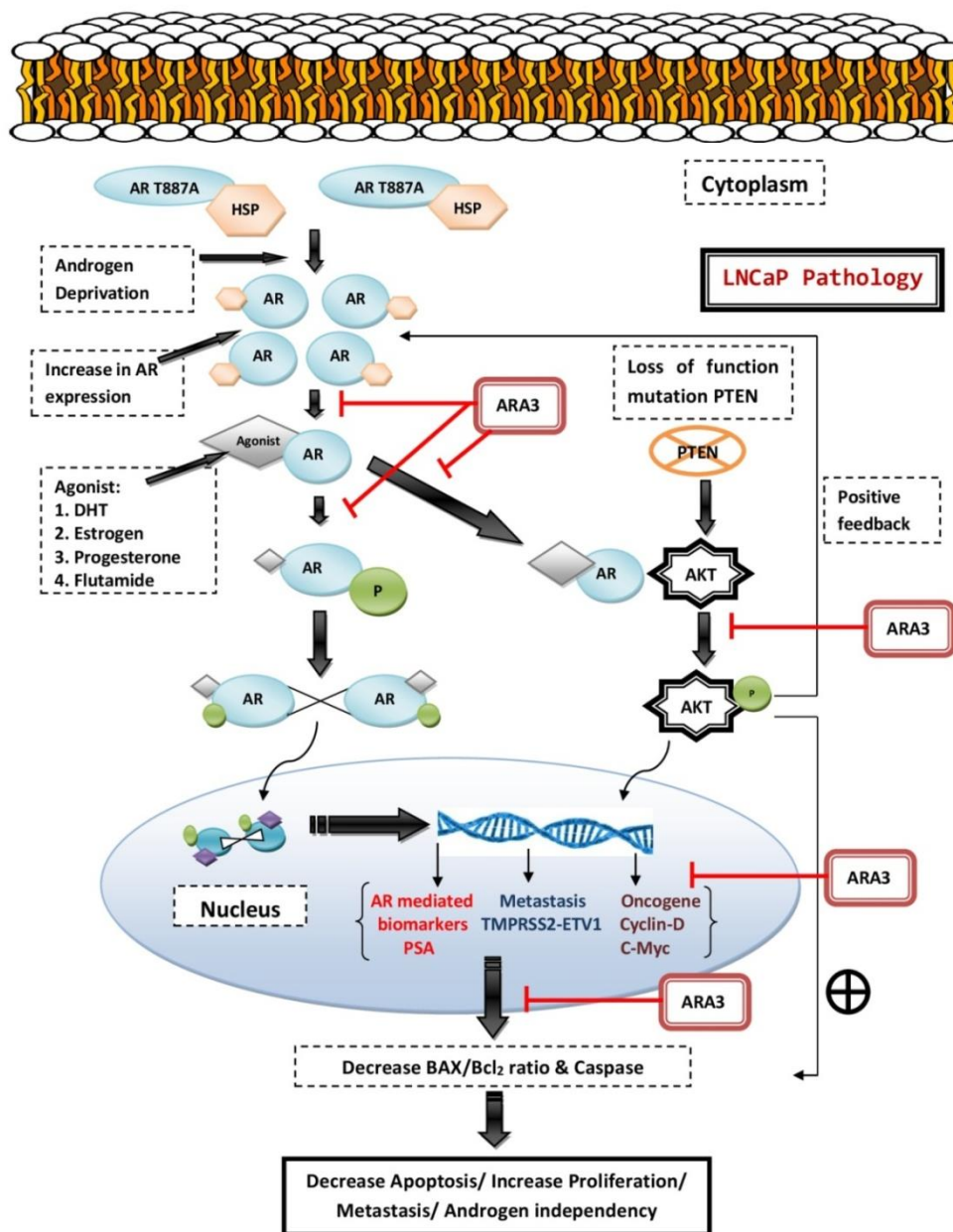


Figure represents the mechanism of action of ARA3. Androgen deprivation increases the expression of AR protein and enzymes involved in the synthesis of androgen. This increases the expression of AR and the intracrine androgen concentration. Since the LNCaP cells express T877A mutant AR, the AR could be activated by androgens and non-androgens (AR antagonist, estrogen, progesterone etc). ARA3 and bicalutamide decreases the DHT stimulated AR and p-AR213 protein expression in LNCaP cells. This

Chapter 8: Discussion

further leads to the decrease in AR mediated genomic activity. The AR-Agonist complex could also activate AKT, which leads to the expression of oncogenes such as c-myc and cyclin D1. The activated AKT also increases the expression of AR which leads to a vicious cycle. ARA3, but not bicalutamide, decreases the AR-Agonist mediated AKT activation. This is the major difference between the bicalutamide and ARA3. The attenuation of AKT activation by ARA3 decreases the transcription of oncogenes and increased the ratio of BAX/Bcl2 mRNA, which leads to the induction of apoptosis in LNCaP cells.

Chapter 9: Summary and Conclusion

9. SUMMARY AND CONCLUSION

The point mutation in the AR increases the volume of the ligand binding pocket to neutralize the bulky functional groups in the AR antagonist. The bulky functional groups of the AR antagonists affect the conformation of the helix-12 of the AR. The helix-12 was essential for the binding with the co-activators. The helix-12 negative and helix-12 positive ARs were used to select new chemical entities among the pharmacophore matched ligands. This led to the identification of ligands having bulky β -iminoenamine groups. The test ligand ARA3 was bulkier and less flexible than the bicalutamide and has improved potency against mutant ARs. The improved potency against mutant AR had led to the effective control of the AR mediated non-genomic phosphorylation and activation of the AKT. The decrease in the activation of AKT had further prevented the over expression of oncogenes such as c-myc, cyclin d1 and bcl2. Bicalutamide did not significantly decrease the gene expression of oncogenes because of its inability to control the phosphorylation and activation of AKT. This is because the bicalutamide has lesser efficacy against mutant AR expressing cell lines. From the study we conclude that, the different handling of AR mediated non-genomic pathway by ARA3 resulted in the induction of apoptosis.

Chapter 10: Impact of the study

10. IMPACT OF THE STUDY

- Adenocarcinoma of prostate gland is the second most frequent cancer and sixth leading cause of mortality in males. The mutation at amino acid Thr877 was frequently expressed in androgen independent prostate cancer patients.
- The point mutations were specific to the AR antagonists and convert them into an agonist, which leads to the withdrawal of the antagonist from the treatment regimen.
- *In-silico* docking and pharmacophore studies had indicated that the interaction with helix-12 of AR was essential to antagonize mutant AR.
- Through *in-silico* drug design methods, we have identified a novel hit AR antagonist bearing β -iminoenamine BF2 complex. The ARA3 is the best hit molecule of the series.
- The mechanism by which the ARA3 induces the apoptosis is novel. The androgen/AR mediated activation of AKT is unexplored and ARA3 induces the apoptosis by preventing the activation of AKT by androgen/AR complex.
- The ARA3 was also active in breast cancer cell lines (MCF-7 & MDA MB 453) that expresses AR. Therefore, the ligands in this chemical class are also eligible candidates for the treatment of prostate cancer.

Bibliography

BIBLIOGRAPHY

1. Watabe T, Lin M, Ide H, Donjacour AA, et al. Growth, regeneration, and tumorigenesis of the prostate activates the PSCA promoter. Proceedings of the National Academy of Sciences. 2002 Jan 8; 99(1):401-6.
2. Gao W. Androgen receptor as a therapeutic target. Advanced drug delivery reviews. 2010 Oct 30; 62(13):1277-84.
3. Dehm SM, Tindall DJ. Androgen receptor structural and functional elements: role and regulation in prostate cancer. Molecular endocrinology. 2007 Dec; 21(12):2855-63.
4. Pereira de Jésus-Tran K, Côté PL, Cantin L, Blanchet J, et al. Comparison of crystal structures of human androgen receptor ligand-binding domain complexed with various agonists reveals molecular determinants responsible for binding affinity. Protein Science. 2006 May 1; 15(5):987-99.
5. Bohl CE, Gao W, Miller DD, Bell CE, et al. Structural basis for antagonism and resistance of bicalutamide in prostate cancer. Proceedings of the National Academy of Sciences. 2005 Apr 26; 102(17):6201-6.
6. Hodgson MC, Shen HC, Hollenberg AN, Balk SP. Structural basis for nuclear receptor corepressor recruitment by antagonist-liganded androgen receptor. Molecular cancer therapeutics. 2008 Oct 1; 7(10):3187-94.
7. Heinlein CA, Chang C. Androgen receptor (AR) coregulators: an overview. Endocrine reviews. 2002 Apr 1; 23(2):175-200.
8. Feldman BJ, Feldman D. The development of androgen-independent prostate cancer. Nature Reviews Cancer. 2001 Oct 1; 1(1):34-45.

Bibliography

9. Yuan X, Balk SP. Mechanisms mediating androgen receptor reactivation after castration. *Urologic Oncology: Seminars and Original Investigations*. 2009 Feb 28; 27(1):36-41.
10. Heidenreich A, Bastian PJ, Bellmunt J, Bolla M, et al. EAU guidelines on prostate cancer. Part II: treatment of advanced, relapsing, and castration-resistant prostate cancer. *European urology*. 2014 Feb 28; 65(2):467-79.
11. Brooke GN, Bevan CL. The role of androgen receptor mutations in prostate cancer progression. *Current genomics*. 2009 Mar 1; 10(1):18-25.
12. Urushibara M, Ishioka J, Hyochi N, Kihara K, et al. Effects of steroidal and non-steroidal antiandrogens on wild-type and mutant androgen receptors. *The Prostate*. 2007 Jun 1; 67(8):799-807.
13. Veldscholte J, Ris-Stalpers C, Kuiper GG, Jenster G, et al. A mutation in the ligand binding domain of the androgen receptor of human LNCaP cells affects steroid binding characteristics and response to anti-androgens. *Biochemical and biophysical research communications*. 1990 Dec 14; 173(2):534-40.
14. Hara T, Miyazaki JI, Araki H, Yamaoka M, et al. Novel mutations of androgen receptor. *Cancer research*. 2003 Jan 1; 63(1):149-53.
15. McCrea E, Sissung TM, Price DK, Chau CH, et al. Androgen receptor variation affects prostate cancer progression and drug resistance. *Pharmacological research*. 2016 Dec 31; 114:152-62.
16. Mehra R, Tomlins SA, Yu J, Cao X, et al. Characterization of TMPRSS2-ETS gene aberrations in androgen-independent metastatic prostate cancer. *Cancer research*. 2008 May 15; 68(10):3584-90.

Bibliography

17. Yu J, Yu J, Mani RS, Cao Q, et al. An integrated network of androgen receptor, polycomb, and TMPRSS2-ERG gene fusions in prostate cancer progression. *Cancer cell*. 2010 May 18; 17(5):443-54.
18. Jemal A, Bray F, Center MM, Ferlay J, et al. Global cancer statistics. *CA: a cancer journal for clinicians*. 2011 Mar 1; 61(2):69-90.
19. Gupta N, Duda DG. Role of stromal cell-derived factor 1 α pathway in bone metastatic prostate cancer. *Journal of biomedical research*. 2016 May; 30(3):181.
20. Key T. Risk factors for prostate cancer. *Cancer surveys*. 1994 Dec 2; 23(3):63-77.
21. Watabe T, Lin M, Ide H, Donjacour AA, et al. Growth, regeneration, and tumorigenesis of the prostate activates the PSCA promoter. *Proceedings of the National Academy of Sciences*. 2002 Jan 8; 99(1):401-6.
22. Askew EB, Gampe RT, Stanley TB, Faggart JL, et al. Modulation of androgen receptor activation function 2 by testosterone and dihydrotestosterone. *Journal of Biological Chemistry*. 2007 Aug 31; 282(35):25801-16.
23. Xu J, Meyers D, Freije D, Isaacs S, et al. Evidence for a prostate cancer susceptibility locus on the X chromosome. *Nature genetics*. 1998 Oct 1; 20(2):175-9.
24. Rökman A, Ikonen T, Seppälä EH, Nupponen N, et al. Germline alterations of the RNASEL gene, a candidate HPC1 gene at 1q25, in patients and families with prostate cancer. *The American Journal of Human Genetics*. 2002 May 31; 70(5):1299-304.

Bibliography

25. Xu J, Zheng SL, Komiya A, Mychaleckyj JC, et al. Germline mutations and sequence variants of the macrophage scavenger receptor 1 gene are associated with prostate cancer risk. *Nature genetics*. 2002 Oct 1; 32(2):321-5.
26. Cybulski C, Gorski B, Dębniak T, Gliniewicz B, et al. NBS1 is a prostate cancer susceptibility gene. *Cancer research*. 2004 Feb 15; 64(4):1215-9.
27. Grönberg H, Åhman AK, Emanuelsson M, Bergh A, et al. BRCA2 mutation in a family with hereditary prostate cancer. *Genes, Chromosomes and Cancer*. 2001 Mar 1; 30(3):299-301.
28. Tavtigian SV, Simard J, Teng DH, Abtin V, et al. A candidate prostate cancer susceptibility gene at chromosome 17p. *Nature genetics*. 2001 Feb 1; 27(2):172-80.
29. Ewing CM, Ray AM, Lange EM, Zuhlke KA, et al. Germline mutations in HOXB13 and prostate-cancer risk. *New England Journal of Medicine*. 2012 Jan 12; 366(2):141-9.
30. Grindedal EM, Møller P, Eeles R, Stormorken AT, et al. Germ-line mutations in mismatch repair genes associated with prostate cancer. *Cancer Epidemiology and Prevention Biomarkers*. 2009 Sep 1; 18(9):2460-7.
31. Jennbacken K, Tešan T, Wang W, Gustavsson H, et al. N-cadherin increases after androgen deprivation and is associated with metastasis in prostate cancer. *Endocrine-related cancer*. 2010 Jun 1; 17(2):469-79.
32. Hessels D, Smit FP, Verhaegh GW, Witjes JA, et al. Detection of TMPRSS2-ERG fusion transcripts and prostate cancer antigen 3 in urinary sediments may

Bibliography

improve diagnosis of prostate cancer. *Clinical Cancer Research*. 2007 Sep 1; 13(17):5103-8.

33. Heidenreich A, Bellmunt J, Bolla M, Joniau S, et al. EAU guidelines on prostate cancer. Part 1: screening, diagnosis, and treatment of clinically localised disease. *European urology*. 2011 Jan 31; 59(1):61-71.

34. Mottet N, Bellmunt J, Bolla M, Joniau S, et al. EAU guidelines on prostate cancer. Part II: Treatment of advanced, relapsing, and castration-resistant prostate cancer. *Actas Urológicas Españolas*. 2011 Dec 31; 35(10):565-79.

35. Denmeade SR, Isaacs JT. A history of prostate cancer treatment. *Nature Reviews Cancer*. 2002 May 1; 2(5):389-96.

36. Montgomery RB, Mostaghel EA, Vessella R, Hess DL, et al. Maintenance of intratumoral androgens in metastatic prostate cancer: a mechanism for castration-resistant tumor growth. *Cancer research*. 2008 Jun 1; 68(11):4447-54.

37. Dutt SS, Gao AC. Molecular mechanisms of castration-resistant prostate cancer progression. *Future Oncology*. 2009 Nov 10; 5(9):1403-13.

38. Tian X, He Y, Zhou J. Progress in antiandrogen design targeting hormone binding pocket to circumvent mutation based resistance. *Frontiers in Pharmacology*. 2015 Mar 1; 6(57):1-11

39. Eisenberger MA. Re: Phase I Clinical Trial of a Selective Inhibitor of CYP17, Abiraterone Acetate, Confirms that Castration-Resistant Prostate Cancer Commonly Remains Hormone Driven. *European urology*. 2009 Jan 31; 55(1):248.

Bibliography

40. Tilley WD, Buchanan G, Hickey TE, Bentel JM. Mutations in the androgen receptor gene are associated with progression of human prostate cancer to androgen independence. *Clinical Cancer Research*. 1996 Feb 1; 2(2):277-85.
41. Taplin ME, Bubley GJ, Shuster TD, Frantz ME, et al. Mutation of the androgen-receptor gene in metastatic androgen-independent prostate cancer. *New England Journal of Medicine*. 1995 May 25; 332(21):1393-8.
42. Taplin ME, Rajeshkumar B, Halabi S, Werner CP, et al. Androgen receptor mutations in androgen-independent prostate cancer: Cancer and Leukemia Group B Study 9663. *Journal of Clinical Oncology*. 2003 Jul 15; 21(14):2673-8.
43. Balk SP. Androgen receptor as a target in androgen-independent prostate cancer. *Urology*. 2002 Sep 30; 60(3):132-8.
44. Hara T, Miyazaki J, Araki H, Yamaoka M, et al. Novel mutations of androgen receptor: a possible mechanism of bicalutamide withdrawal syndrome. *Cancer Research*. 2003 Apr 1; 63(4):149-153.
45. Korpál M, Korn JM, Gao X, Rakiec DP, et al. An F876L mutation in androgen receptor confers genetic and phenotypic resistance to MDV3100 (enzalutamide). *Cancer discovery*. 2013 Sep 1; 3(9):1030-43.
46. Taplin ME, Bubley GJ, Ko YJ, Small EJ, et al. Selection for androgen receptor mutations in prostate cancers treated with androgen antagonist. *Cancer research*. 1999 Jun 1; 59(11):2511-5.
47. Urushibara M, Ishioka J, Hyochi N, Kihara K, et al. Effects of steroidal and non-steroidal antiandrogens on wild-type and mutant androgen receptors. *The Prostate*. 2007 Jun 1; 67(8):799-807.

Bibliography

48. Shi XB, Ma AH, Xia L, Kung HJ, et al. Functional analysis of 44 mutant androgen receptors from human prostate cancer. *Cancer research*. 2002 Mar 1; 62(5):1496-502.
49. Veldscholte J, Berrevoets CA, Ris-Stalpers C, Kuiper GG, et al. The androgen receptor in LNCaP cells contains a mutation in the ligand binding domain which affects steroid binding characteristics and response to antiandrogens. *The Journal of steroid biochemistry and molecular biology*. 1992 Mar 31; 41(3):665-9.
50. Steketee K, Timmerman L, Ziel-van der Made AC, Doesburg P, et al. Broadened ligand responsiveness of androgen receptor mutants obtained by random amino acid substitution of H874 and mutation hot spot T877 in prostate cancer. *International journal of cancer*. 2002 Jul 20; 100(3):309-17.
51. Rahim S, Beauchamp EM, Kong Y, Brown ML, et al. YK-4-279 inhibits ERG and ETV1 mediated prostate cancer cell invasion. *PloS one*. 2011 Apr 29; 6(4):e19343.
52. Farooqi AA, Hou MF, Chen CC, Wang CL, et al. Androgen receptor and gene network: Micromechanics reassemble the signaling machinery of TMPRSS2-ERG positive prostate cancer cells. *Cancer cell international*. 2014 Apr 17; 14(1):34-46.
53. Sarker D, Reid AH, Yap TA, de Bono JS. Targeting the PI3K/AKT pathway for the treatment of prostate cancer. *Clinical Cancer Research*. 2009 Aug 1; 15(15):4799-805.
54. Lee SH, Johnson D, Luong R, Sun Z. Crosstalk between androgen and PI3K/AKT signaling pathways in prostate cancer cells. *Journal of Biological Chemistry*. 2015 Jan 30; 290(5):2759-68.

Bibliography

55. McCall P, Adams CE, Willder JM, Bennett L, et al. Androgen receptor phosphorylation at serine 308 and serine 791 predicts enhanced survival in castrate resistant prostate cancer patients. *International journal of molecular sciences*. 2013 Aug 13; 14(8):16656-71.
56. Schweizer L, Rizzo CA, Spires TE, Platero JS, et al. The androgen receptor can signal through Wnt/ β -Catenin in prostate cancer cells as an adaptation mechanism to castration levels of androgens. *BMC cell biology*. 2008 Jan 24; 9(1):4-16.
57. Robinson DR, Zylstra CR, Williams BO. Wnt signaling and prostate cancer. *Current drug targets*. 2008 Jul 1; 9(7):271-580.
58. Song LN, Herrell R, Byers S, Shah S, et al. β -Catenin binds to the activation function 2 region of the androgen receptor and modulates the effects of the N-terminal domain and TIF2 on ligand-dependent transcription. *Molecular and cellular biology*. 2003 Mar 1; 23(5):1674-87.
59. Desbois-Mouthon C, Cadoret A, Blivet-Van Eggelpeel MJ, et al. Insulin and IGF-1 stimulate the [beta]-catenin pathway through two signalling cascades involving GSK-3 [beta] inhibition and Ras activation. *Oncogene*. 2001 Jan 11; 20(2):252.
60. Li Y, Wang L, Zhang M, Melamed J, et al. LEF1 in androgen-independent prostate cancer: regulation of androgen receptor expression, prostate cancer growth, and invasion. *Cancer research*. 2009 Apr 15; 69(8):3332-8.

Bibliography

61. Gregory CW, He B, Johnson RT, Ford OH, et al. A mechanism for androgen receptor-mediated prostate cancer recurrence after androgen deprivation therapy. *Cancer research*. 2001 Jun 1; 61(11):4315-9.
62. Debes JD, Schmidt LJ, Huang H, Tindall DJ. p300 mediates androgen-independent transactivation of the androgen receptor by interleukin 6. *Cancer research*. 2002 Oct 15; 62(20):5632-6.
63. Miyamoto H, Yeh S, Wilding G, Chang C. Promotion of agonist activity of antiandrogens by the androgen receptor coactivator, ARA70, in human prostate cancer DU145 cells. *Proceedings of the National Academy of Sciences*. 1998 Jun 23; 95(13):7379-84.
64. Laschak M, Bechtel M, Spindler KD, Hessenauer A. Inability of NCoR/SMRT to repress androgen receptor transcriptional activity in prostate cancer cell lines. *International journal of molecular medicine*. 2011 Oct 1; 28(4):645.
65. Brown CJ, Goss SJ, Lubahn DB, Joseph DR, et al. Androgen receptor locus on the human X chromosome: regional localization to Xq11-12 and description of a DNA polymorphism. *American journal of human genetics*. 1989 Feb; 44(2):264.
66. Wilson CM, McPhaul MJ. A and B forms of the androgen receptor are expressed in a variety of human tissues. *Molecular and cellular endocrinology*. 1996 Jun 18; 120(1):51-7.
67. Kouyoumdjian JA, Morita MD, Araújo RG. X-linked spinal and bulbar muscular atrophy (Kennedy's disease) with long-term electrophysiological evaluation: case report. *Arquivos de neuro-psiquiatria*. 2005 Mar; 63(1):154-9.

Bibliography

68. Price DK, Chau CH, Till C, Goodman PJ, et al. Androgen receptor CAG repeat length and association with prostate cancer risk: results from the prostate cancer prevention trial. *The Journal of urology*. 2010 Dec 31; 184(6):2297-302.
69. Dehm SM, Tindall DJ. Androgen receptor structural and functional elements: role and regulation in prostate cancer. *Molecular endocrinology*. 2007 Dec 6; 21(12):2855-63.
70. Bai S, He B, Wilson EM. Melanoma antigen gene protein MAGE-11 regulates androgen receptor function by modulating the interdomain interaction. *Molecular and Cellular Biology*. 2005 Feb 15; 25(4):1238-57.
71. He B, Kempainen JA, Wilson EM. FXXLF and WXXLF sequences mediate the NH₂-terminal interaction with the ligand binding domain of the androgen receptor. *Journal of Biological Chemistry*. 2000 Jul 28; 275(30):22986-94.
72. Gelmann EP. Molecular biology of the androgen receptor. *Journal of Clinical Oncology*. 2002 Jul 1; 20(13):3001-15.
73. Verrijdt G, Haelens A, Claessens F. Selective DNA recognition by the androgen receptor as a mechanism for hormone-specific regulation of gene expression. *Molecular genetics and metabolism*. 2003 Mar 31; 78(3):175-85.
74. Katsumata N, Horikawa R, Tanaka T. Novel missense mutation in the P-box of androgen receptor in a patient with androgen insensitivity syndrome. *Endocrine journal*. 2008 Apr 5; 55(1):225-8.
75. Dahlman-Wright K, Wright A, Gustafsson JA, Carlstedt-Duke J. Interaction of the glucocorticoid receptor DNA-binding domain with DNA as a dimer is

Bibliography

mediated by a short segment of five amino acids. *Journal of Biological Chemistry*. 1991 Feb 15; 266(5):3107-12.

76. Shaffer PL, Jivan A, Dollins DE, Claessens F, et al. Structural basis of androgen receptor binding to selective androgen response elements. *Proceedings of the National Academy of Sciences of the United States of America*. 2004 Apr 6; 101(14):4758-63.

77. Zhou ZX, Sar M, Simental JA, Lane MV, et al. A ligand-dependent bipartite nuclear targeting signal in the human androgen receptor. Requirement for the DNA-binding domain and modulation by NH₂-terminal and carboxyl-terminal sequences. *Journal of Biological Chemistry*. 1994 May 6; 269(18):13115-23.

78. Haelens A, Tanner T, Denayer S, Callewaert L, et al. The hinge region regulates DNA binding, nuclear translocation, and transactivation of the androgen receptor. *Cancer Research*. 2007 May 1; 67(9):4514-23.

79. Fu M, Wang C, Reutens AT, Wang J, et al. p300 and p300/cAMP-response element-binding protein-associated factor acetylate the androgen receptor at sites governing hormone-dependent transactivation. *Journal of Biological Chemistry*. 2000 Jul 7; 275(27):20853-60.

80. Kumar S, Tyagi RK. Androgen receptor association with mitotic chromatin—analysis with introduced deletions and disease-inflicting mutations. *FEBS Journal*. 2012 Dec 1; 279(24):4598-614.

81. Wang F, Liu XQ, Li H, Liang KN, et al. Structure of the ligand-binding domain (LBD) of human androgen receptor in complex with a selective modulator

Bibliography

- LGD2226. Acta Crystallographica Section F: Structural Biology and Crystallization Communications. 2006 Nov 1; 62(11):1067-71.
82. Gong Y, Wang D, Dar JA, Singh P, et al. Nuclear export signal of androgen receptor (NESAR) regulation of androgen receptor level in human prostate cell lines via ubiquitination and proteasome-dependent degradation. Endocrinology. 2012 Oct 5; 153(12):5716-25.
83. Bevan CL, Hoare S, Claessens F, Heery DM, et al. The AF1 and AF2 domains of the androgen receptor interact with distinct regions of SRC1. Molecular and cellular biology. 1999 Dec 1; 19(12):8383-92.
84. Bennett NC, Gardiner RA, Hooper JD, Johnson DW, et al. Molecular cell biology of androgen receptor signalling. The international journal of biochemistry & cell biology. 2010 Jun 30; 42(6):813-27.
85. Li J, Al-Azzawi F. Mechanism of androgen receptor action. Maturitas. 2009 Jun 20; 63(2):142-8.
86. Gioeli D, Ficarro SB, Kwiek JJ, Aaronson D, et al. Androgen receptor phosphorylation Regulation and identification of the phosphorylation sites. Journal of Biological Chemistry. 2002 Aug 9; 277(32):29304-14.
87. van Royen ME, van Cappellen WA, de Vos C, Houtsmuller AB, et al. Stepwise androgen receptor dimerization. J Cell Sci. 2012 Apr 15; 125(8):1970-9.
88. Heemers HV, Tindall DJ. Androgen receptor (AR) coregulators: a diversity of functions converging on and regulating the AR transcriptional complex. Endocrine reviews. 2007 Dec; 28(7):778-808.

Bibliography

89. Powell SM, Christiaens V, Voulgaraki D, Waxman J, et al. Mechanisms of androgen receptor signalling via steroid receptor coactivator-1 in prostate. *Endocrine-related cancer*. 2004 Mar 1; 11(1):117-30.
90. Liao RS, Ma S, Miao L, Li R, et al. Androgen receptor-mediated non-genomic regulation of prostate cancer cell proliferation. *Translational andrology and urology*. 2013 Sep 1; 2(3):187-98.
91. Moilanen AM, Riikonen R, Oksala R, Ravanti L, et al. Discovery of ODM-201, a new-generation androgen receptor inhibitor targeting resistance mechanisms to androgen signaling-directed prostate cancer therapies. *Scientific reports*. 2015 Jul 3; 5(2):12007-19.
92. Kindt T, Morse S, Gotschlich E, Lyons K. Structure-based strategies for drug design and discovery. *Nature*. 1991 Jan 1; 35(2):581-99
93. Sliwoski G, Kothiwale S, Meiler J, Lowe EW. Computational methods in drug discovery. *Pharmacological reviews*. 2014 Jan 1; 66(1):334-95.
94. Divakar S, Hariharan S. 3D-QSAR Studies on Plasmodium falciparum Proteins: A Mini-Review. *Combinatorial chemistry & high throughput screening*. 2015 Feb 1; 18(2):188-98.
95. Greer J, Erickson JW, Baldwin JJ, Varney MD. Application of the three-dimensional structures of protein target molecules in structure-based drug design. *Journal of medicinal chemistry*. 1994 Apr; 37(8):1035-54.
96. Mannhold R, Kubinyi H, Timmerman H, Folkers G, et al. Methods and principles in medicinal chemistry. *Molecular Modeling. Basic Principles and Applications*. 2001 Jan 1; 5(1):23-36.

Bibliography

97. Capdeville R, Buchdunger E, Zimmermann J, Matter A. Glivec (STI571, imatinib), a rationally developed, targeted anticancer drug. *Nature reviews Drug discovery*. 2002 Jul 1; 1(7):493-502.
98. Schames JR, Henchman RH, Siegel JS, Sotriffer CA, et al. Discovery of a novel binding trench in HIV integrase. *Journal of medicinal chemistry*. 2004 Apr 8; 47(8):1879-81.
99. Ekins S, Mestres J, Testa B. In silico pharmacology for drug discovery: methods for virtual ligand screening and profiling. *British journal of pharmacology*. 2007 Sep 1; 152(1):9-20.
100. Maestro version 9.8, Schrödinger, LLC, New York, NY, 2014.
101. Holm L, Sander C. Protein structure comparison by alignment of distance matrices. *Journal of molecular biology*. 1993 Sep 1; 233(1):123-38.
102. LigPrep version 3.1, Schrödinger, LLC, New York, NY, 2014.
103. Chen Z, Li HL, Zhang QJ, Bao XG, et al. Pharmacophore-based virtual screening versus docking-based virtual screening: a benchmark comparison against eight targets. *Acta Pharmacologica Sinica*. 2009 Dec 1; 30(12):1694-708.
104. Antipin RL, Beshnova DA, Petrov RA, Shiryayeva AS, et al. Synthesis, SAR and molecular docking study of novel non- β -lactam inhibitors of TEM type β -lactamase. *Bioorganic & medicinal chemistry letters*. 2017 Apr 1; 27(7):1588-92.
105. PRIME version 3.7, Schrödinger, LLC, New York, NY, 2014.
106. Guo C, Pairish M, Linton A, Kephart S, et al. Design of oxobenzimidazoles and oxindoles as novel androgen receptor antagonists. *Bioorganic & medicinal chemistry letters*. 2012 Apr 1; 22(7):2572-8.

Bibliography

107. Glide, version 3.3, Schrödinger, LLC, New York, NY, 2014.
108. Tripathi SK, Muttineni R, Singh SK. Extra precision docking, free energy calculation and molecular dynamics simulation studies of CDK2 inhibitors. *Journal of theoretical biology*. 2013 Oct 7; 334(12):87-100.
109. Messaoudi A, Belguith H, Hamida JB. Homology modeling and virtual screening approaches to identify potent inhibitors of VEB-1 β -lactamase. *Theoretical Biology and Medical Modelling*. 2013 Apr 2;10(1):22-34.
110. Yamamoto S, Kobayashi H, Kaku T, Aikawa K, et al. Design, synthesis, and biological evaluation of 3-aryl-3-hydroxy-1-phenylpyrrolidine derivatives as novel androgen receptor antagonists. *Bioorganic & medicinal chemistry*. 2013 Jan 1; 21(1):70-83.
111. Yamamoto S, Matsunaga N, Hitaka T, Yamada M, et al. Design, synthesis, and biological evaluation of 4-phenylpyrrole derivatives as novel androgen receptor antagonists. *Bioorganic & medicinal chemistry*. 2012 Jan 1; 20(1):422-34.
112. Yamamoto S, Tomita N, Suzuki Y, Suzaki T, et al. Design, synthesis, and biological evaluation of 4-arylmethyl-1-phenylpyrazole and 4-aryloxy-1-phenylpyrazole derivatives as novel androgen receptor antagonists. *Bioorganic & medicinal chemistry*. 2012 Apr 1 ;20(7):2338-52.
113. Bassetto M, Ferla S, Pertusati F, Kandil S, et al. Design and synthesis of novel bicalutamide and enzalutamide derivatives as antiproliferative agents for the treatment of prostate cancer. *European journal of medicinal chemistry*. 2016 Aug 8; 118:230-43.

Bibliography

114. Ferla S, Bassetto M, Pertusati F, Kandil S, et al. Rational design and synthesis of novel anti-prostate cancer agents bearing a 3, 5-bis-trifluoromethylphenyl moiety. *Bioorganic & Medicinal Chemistry Letters*. 2016 Aug 1; 26(15):3636-40.
115. Durdagi S, Duff HJ, Noskov SY. Combined receptor and ligand-based approach to the universal pharmacophore model development for studies of drug blockade to the hERG1 pore domain. *Journal of chemical information and modeling*. 2011 Jan 11; 51(2):463-74.
116. PHASE version 3.9, Schrödinger, LLC, New York, NY, 2014.
117. Rai A, Raj V, Hodhod Aboumanei M, K Singh A, et al. Pharmacophore, 3D-QSAR models and Dynamic Simulation of 1,4-Benzothiazines for Colorectal Cancer Treatment. *Comb Chem High Throughput Screen*. 2017 Jan 11; 51(2):263-77.
118. Dahiya L, Mahapatra MK, Kaur R, Kumar V, et al. Validation of TZD Scaffold as Potential ARIs: Pharmacophore Modelling, Atom-based 3D QSAR and Docking Studies. *Comb Chem High Throughput Screen*. 2017 Feb 11; 51(2):218-31.
119. Pratim Roy P, Paul S, Mitra I, Roy K. On two novel parameters for validation of predictive QSAR models. *Molecules*. 2009 Apr 29; 14(5):1660-701.
120. Patel P, Singh A, K Patel V, K Jain D, et al. Pharmacophore based 3D-qsar, virtual screening and docking studies on novel series of HDAC inhibitors with thiophen linker as anticancer agents. *Combinatorial Chemistry & High Throughput Screening*. 2016 Nov 1; 19(9):735-51.

Bibliography

121. Rashid S, Unyayar A, Mazmanci MA, McKeown SR, et al. A study of anti-cancer effects of *Funalia trogii* in vitro and in vivo. *Food and chemical toxicology*. 2011 Jul 31; 49(7):1477-83.
122. Nwankwo JO, Robbins ME. Peroxisome proliferator-activated receptor- γ expression in human malignant and normal brain, breast and prostate-derived cells. *Prostaglandins, Leukotrienes and Essential Fatty Acids (PLEFA)*. 2001 Apr 30; 64(4):241-5.
123. Ivachtchenko AV, Ivanenkov YA, Mitkin OD, Vorobiev AA, et al. Design, synthesis and biological evaluation of novel 5-oxo-2-thioxoimidazolidine derivatives as potent androgen receptor antagonists. *European journal of medicinal chemistry*. 2015 Jun 24; 99:51-66.
124. Andrieu T, Bertolini R, Nichols SE, Setoud R, et al. A novel steroidal antiandrogen targeting wild type and mutant androgen receptors. *Biochemical pharmacology*. 2011 Dec 1; 82(11):1651-62.
125. Zhao Y, Hu L, Yang YJ, Niu DL, et al. Improvement on the extraction method of RNA in mites and its quality test. *Parasitology research*. 2016 Feb 1; 115(2):851-8.
126. Von Keyserling H, Bergmann T, Wiesel M, Kaufmann AM. The use of melting curves as a novel approach for validation of real-time PCR instruments. *Biotechniques*. 2011 Sep 1; 51(3):179-84.
127. Mahmood T, Yang PC. Western blot: technique, theory, and trouble shooting. *North American journal of medical sciences*. 2012 Sep 1; 4(9):429.

Bibliography

128. Ribble D, Goldstein NB, Norris DA, Shellman YG. A simple technique for quantifying apoptosis in 96-well plates. *BMC biotechnology*. 2005 May 10; 5(1):12.
129. Perumal K, Garg JA, Blacque O, Saiganesh R, et al. β -Iminoamine-BF₂ Complexes: Aggregation-Induced Emission and Pronounced Effects of Aliphatic Rings on Radiationless Deactivation. *Chemistry—An Asian Journal*. 2012 Nov 1; 7(11):2670-7.
130. Saraon P, Jarvi K, Diamandis EP. Molecular alterations during progression of prostate cancer to androgen independence. *Clinical chemistry*. 2011 Oct 1; 57(10):1366-75.
131. Hoang DT, Iczkowski KA, Kilari D, See W, et al. Androgen receptor-dependent and-independent mechanisms driving prostate cancer progression: Opportunities for therapeutic targeting from multiple angles. *Oncotarget*. 2017 Jan 10; 8(2):3724.
132. Sack JS, Kish KF, Wang C, Attar RM, et al. Crystallographic structures of the ligand-binding domains of the androgen receptor and its T877A mutant complexed with the natural agonist dihydrotestosterone. *Proceedings of the National Academy of Sciences*. 2001 Apr 24; 98(9):4904-9.
133. Zhao XY, Malloy PJ, Krishnan AV, Swami S, et al. Glucocorticoids can promote androgen-independent growth of prostate cancer cells through a mutated androgen receptor. *Nature medicine*. 2000 Jun 1; 6(6):703-6.

Bibliography

134. Bogner J, Zolghadr K, Hickson I, Romer T, et al. The fluorescent two-hybrid assay for live-cell profiling of androgen receptor modulators. *The Journal of steroid biochemistry and molecular biology*. 2017 Feb 28; 166:45-53.
135. Tan ME, Li J, Xu HE, Melcher K, et al. Androgen receptor: structure, role in prostate cancer and drug discovery. *Acta Pharmacologica Sinica*. 2015 Jan 1; 36(1):3-23.
136. Ferroni C, Pepe A, Kim YS, Lee S, et al. 1, 4-Substituted Triazoles as Nonsteroidal Anti-Androgens for Prostate Cancer Treatment. *Journal of Medicinal Chemistry*. 2017 Mar 20; 60(7):3082-93.
137. Fujimaki T, Saito S, Imoto M. Arabilin overcomes resistance to AR-targeted therapy. *The Journal of Antibiotics*. 2017 Jan 11; 70(3):328-330.
138. Altimari JM, Niranjana B, Risbridger GP, Schweiker SS, et al. Synthesis and preliminary investigations into novel 1, 2, 3-triazole-derived androgen receptor antagonists inspired by bicalutamide. *Bioorganic & medicinal chemistry letters*. 2014 Nov 1; 24(21):4948-53.
139. Zhou J, Geng G, Shi Q, Sauriol F, et al. Design and synthesis of androgen receptor antagonists with bulky side chains for overcoming antiandrogen resistance. *Journal of medicinal chemistry*. 2009 Aug 12; 52(17):5546-50.
140. Liu H, Han R, Li J, Liu H, et al. Molecular mechanism of R-bicalutamide switching from androgen receptor antagonist to agonist induced by amino acid mutations using molecular dynamics simulations and free energy calculation. *Journal of Computer-Aided Molecular Design*. 2016 Dec 1; 30(12):1189-200.

Bibliography

141. Hodgson MC, Shen HC, Hollenberg AN, Balk SP. Structural basis for nuclear receptor corepressor recruitment by antagonist-liganded androgen receptor. *Molecular cancer therapeutics*. 2008 Oct 1; 7(10):3187-94.
142. Vrontaki E, Melagraki G, Voskou S, S Phylactides M, et al. Development of a Predictive Pharmacophore Model and a 3D-QSAR Study for an in silico Screening of New Potent Bcr-Abl Kinase Inhibitors. *Mini Reviews in Medicinal Chemistry*. 2017 Feb 1; 17(3):188-204.
143. Balaji B, Hariharan S, Shah DB, Ramanathan M. Discovery of potential and selective COX-1 inhibitory leads using pharmacophore modelling, in silico screening and in vitro evaluation. *European journal of medicinal chemistry*. 2014 Apr 3; 86(3):469-80.
144. Darshit BS, Balaji B, Rani P, Ramanathan M. Identification and in vitro evaluation of new leads as selective and competitive glycogen synthase kinase-3 β inhibitors through ligand and structure based drug design. *Journal of Molecular Graphics and Modelling*. 2014 Jan 1; 53(3):31-47.
145. Dixon SL, Smondyrev AM, Rao SN. PHASE: a novel approach to pharmacophore modeling and 3D database searching. *Chemical biology & drug design*. 2006 May 1; 67(5):370-2.
146. Ohta K, Goto T, Fujii S, Kawahata M, et al. Crystal structure, docking study and structure–activity relationship of carborane-containing androgen receptor antagonist 3-(12-hydroxymethyl-1, 12-dicarba-closo-dodecaboran-1-yl) benzonitrile. *Bioorganic & medicinal chemistry*. 2011 Jun 1; 19(11):3540-8.

Bibliography

147. Voet A, Helsen C, Zhang KY, Claessens F. The discovery of novel human androgen receptor antagonist chemotypes using a combined pharmacophore screening procedure. *ChemMedChem*. 2013 Apr 1; 8(4):644-51.
148. Liu H, Han R, Li J, Liu H, et al. Molecular mechanism of R-bicalutamide switching from androgen receptor antagonist to agonist induced by amino acid mutations using molecular dynamics simulations and free energy calculation. *Journal of Computer-Aided Molecular Design*. 2016 Dec 1; 30(12):1189-200.
149. Joseph JD, Lu N, Qian J, Sensintaffar J, et al. A clinically relevant androgen receptor mutation confers resistance to second-generation antiandrogens enzalutamide and ARN-509. *Cancer discovery*. 2013; 3(9):1020-9.
150. Borgmann H, Ozistanbullu D, Beraldi E, Dalal K, et al. Targeting enzalutamide-resistant prostate cancer using the novel androgen receptor inhibitor ODM-201. *European Urology Supplements*. 2017 Mar 1; 16(3):e1290.
151. Zuo M, Xu X, Xie Z, Ge R, et al. Design and synthesis of indoline thiohydantoin derivatives based on enzalutamide as antiproliferative agents against prostate cancer. *European Journal of Medicinal Chemistry*. 2017 Jan 5; 125:1002-22.
152. Fang H, Tong W, Branham WS, Moland CL, et al. Study of 202 natural, synthetic, and environmental chemicals for binding to the androgen receptor. *Chemical research in toxicology*. 2003 Oct 20; 16(10):1338-58.
153. Söderholm AA, Viiliäinen J, Lehtovuori PT, Eskelinen H, et al. Computationally identified novel diphenyl-and phenylpyridine androgen receptor

Bibliography

antagonist structures. *Journal of chemical information and modeling*. 2008 Aug 20; 48(9):1882-90.

154. Baena E, Shao Z, Linn DE, Glass K, et al. ETV1 directs androgen metabolism and confers aggressive prostate cancer in targeted mice and patients. *Genes & development*. 2013 Mar 15; 27(6):683-98.

155. Taneja SS, Ha S, Swenson NK, Huang HY, et al. Cell-specific regulation of androgen receptor phosphorylation in vivo. *Journal of Biological Chemistry*. 2005 Dec 9; 280(49):40916-24.

156. Wang LG, Liu XM, Kreis W, Budman DR. Phosphorylation/dephosphorylation of androgen receptor as a determinant of androgen agonistic or antagonistic activity. *Biochemical and biophysical research communications*. 1999 May 27; 259(1):21-8.

157. Lee H, Lee D, Park JH, Song SH, et al. High throughput differential identification of TMPRSS2-ERG fusion genes in prostate cancer patient urine. *Biomaterials*. 2017 Aug 31; 135:23-9.

158. Zhou Y, Li Y, Li X, Jiang M. Urinary Biomarker Panel to Improve Accuracy in Predicting Prostate Biopsy Result in Chinese Men with PSA 4–10 ng/mL. *BioMed Research International*. 2017 Feb 15; 9(1):21-8

159. Deplus R, Delliaux C, Marchand N, Flourens A, et al. TMPRSS2-ERG fusion promotes prostate cancer metastases in bone. *Oncotarget*. 2017 Feb 14; 8(7):11827.

160. Liu CY, Yu T, Huang Y, Cui L, et al. ETS (E26 transformation-specific) up-regulation of the transcriptional co-activator TAZ promotes cell migration and

Bibliography

metastasis in prostate cancer. *Journal of Biological Chemistry*. 2017 Jun 2; 292(22):9420-30.

161. Nesterov A, Lu X, Johnson M, Miller GJ, et al. Elevated AKT activity protects the prostate cancer cell line LNCaP from TRAIL-induced apoptosis. *Journal of Biological Chemistry*. 2001 Apr 6; 276(14):10767-74.

162. Yardy GW, Brewster SF. Wnt signalling and prostate cancer. *Prostate cancer and prostatic diseases*. 2005 Jun 1; 8(2):119-26.

163. Nag A, Smith RG. Amplification, rearrangement, and elevated expression of c-myc in the human prostatic carcinoma cell line LNCaP. *The Prostate*. 1989 Jan 1; 15(2):115-22.

164. Saravanan K, Elancheran R, Divakar S, Anand SA, et al. Design, synthesis and biological evaluation of 2-(4-phenylthiazol-2-yl) isoindoline-1, 3-dione derivatives as anti-prostate cancer agents. *Bioorganic & Medicinal Chemistry Letters*. 2017 Mar 1; 27(5):1199-204.

165. Zhang Z, Sun L, Zhou G, Xie P, et al. Sepia ink oligopeptide induces apoptosis and growth inhibition in human lung cancer cells. *Oncotarget*. 2017 Apr 4; 8(14):23202.

166. Seaman JE, Julien O, Lee PS, Rettenmaier TJ, et al. Caspases can cleave after aspartate, glutamate and phosphoserine residues. *Cell Death & Differentiation*. 2016 Oct 1; 23(10):1717-26.

167. Lin Y, Fukuchi J, Hiipakka RA, Kokontis JM, et al. Up-regulation of Bcl-2 is required for the progression of prostate cancer cells from an androgen-dependent to an androgen-independent growth stage. *Cell research*. 2007 Jun 1; 17(6):531-6.

Bibliography

168. Browne G, Nesbitt H, Ming L, Stein GS, et al. Bicalutamide-induced hypoxia potentiates RUNX2-mediated Bcl-2 expression resulting in apoptosis resistance. *British journal of cancer*. 2012 Nov 6; 107(10):1714-21.
169. Lien EC, Dibble CC, Toker A. PI3K signaling in cancer: beyond AKT. *Current Opinion in Cell Biology*. 2017 Apr 30; 45:62-71.
170. Sun M, Yang L, Feldman RI, Sun XM, Bhalla KN, Jove R, Nicosia SV, Cheng JQ. Activation of phosphatidylinositol 3-kinase/Akt pathway by androgen through interaction of p85 α , androgen receptor, and Src. *Journal of Biological Chemistry*. 2003 Oct 31; 278(44):42992-3000.

Urkund Analysis Result

Analysed Document: S. Divakar, 141340505.docx (D27907910)
Submitted: 2017-05-05 13:17:00
Submitted By: diva.niru@gmail.com
Significance: 4 %

Sources included in the report:


1217030014-S.doc (D22075276)
all_chaps.doc (D24163823)

Instances where selected sources appear:

28

Plagiarism

6/21/2017 Gmail - [Urkund] 3% similarity - diva.niru@gmail.com

 Gmail Divakar Selvaraj <diva.niru@gmail.com>

[Urkund] 3% similarity - diva.niru@gmail.com
1 message

report@analysis.urkund.com <report@analysis.urkund.com> Fri, May 5, 2017 at 4:50 PM
To: diva.niru@gmail.com

Document sent by: diva.niru@gmail.com
Document received: 5/5/2017 1:17:00 PM
Report generated 5/5/2017 1:20:45 PM by Urkund's system for automatic control.

Student message: S. Divakar, Reg .No. 141340505

Document : S. Divakar, 141340505.docx [D27907910]

IMPORTANT! The analysis contains 1 warning(s).

About 3% of this document consists of text similar to text found in 23 sources. The largest marking is 40 words long and is 100% similar to its primary source.

PLEASE NOTE that the above figures do not automatically mean that there is plagiarism in the document. There may be good reasons as to why parts of a text also appear in other sources. For a reasonable suspicion of academic dishonesty to present itself, the analysis, possibly found sources and the original document need to be examined closely.

Click here to open the analysis:
<https://secure.urkund.com/view/27637476-334609-733751>

Plagiarism

Secure | <https://secure.orkund.com/account/#284408/0/0>

URKUND Help Upload documents Divakar S

Analysis Address : diva.niru.mgrmu@analysis.orkund.com

diva.niru.mgrmu@analysis.orkund.com (1) New folder Settings

3% D27907910 S. Divakar, 141340505.docx 14 MB 22691 word(s) Divakar S 5/5/2017 1:17 PM

Conference Certificates

Certificate

This is to certify that J. Divakar
Participated and presented a poster entitled
**Androgen receptor mediated drug development
to treat prostate cancer**
and awarded Third prize in the conference on
“Recent Advances in Computational Drug Design”
held at J N Tata Auditorium,
Indian Institute of Science Campus, Bangalore
on 16th - 17th Sep 2013.

Organizers



Indian Institute of Science



SCHRÖDINGER®
Innovations in Computational Drug Design

Conference Certificates



DEPARTMENT OF PHARMACOLOGY PSG COLLEGE OF PHARMACY

COIMBATORE-4

National Conference on EXPERIMENTAL PHARMACOLOGY & DRUG EVALUATION




CO-SPONSORED BY



Certificate

This is to certify that Prof./Dr./Mr./Ms. S. DIVAKAR
has actively participated as ~~resource person~~ / delegate and presented a paper entitled
EVALUATION OF NON- ANDROGENS IN ANDROGEN INDEPENDENT
PROSTATE CANCER - AWARDED THIRD PRIZE -
in oral / ~~poster~~ session of the conference.


Dr. M. Ramanathan
Chairman


G.G. Prasanth
Organizing Secretary

Conference Certificates

Seventh Indo-US Workshop on Mathematical Chemistry
December 4 - 6, 2012

Jointly organized by

PONNAIYAH RAMAJAYAM INSTITUTE OF SCIENCE AND TECHNOLOGY
PRIST UNIVERSITY
Thanjavur – 613403, TN, India.

and

UNIVERSITY OF MINNESOTA DULUTH
Duluth, Minnesota 55812, USA

Certificate

This is to certify that Dr. / Mr. / Ms. S.DIVAKAR, PSG COLLEGE OF PHARMACY
has participated / presented a paper in the Seventh Indo-US Workshop on Mathematical
Chemistry held during December 4-6, 2012 at PRIST University, Thanjavur.


Organizing Secretary


Convener

Conference Certificates

Symposium on Current Trends in Fundamental Biochemical Research: Diverse Applications from Agriculture to Human Health



Certificate of Participation

This certificate is awarded to *Dr./Prof./Mr./Mrs./Ms. S. Divakar*
Research Scholar, PSG College of Pharmacy, Coimbatore

for his/her active participation and oral/poster presentation entitled
*Androgen receptor antagonist to treat Androgen independent
prostate Cancer* in the National Symposium on
**"Current Trends in Fundamental Biochemical Research: Diverse
Applications from Agriculture to Human Health"** held on 13th and 14th
December 2016, organized by PSG Institute of Advanced Studies
and sponsored by SERB (Department of Science & Technology)
and ICMR (New Delhi).

R. R. Bhattacharjee
Dr. Rama R Bhattacharjee
Organizing Secretary

P. Radhakrishnan
Prof. P. Radhakrishnan
Director, PSG IAS

Publications

1. **Divakar S**, Hariharan S and Ramanathan M. Structure Based Drug Design in Identification of Novel Androgen Receptor Antagonist. In: Azat M, editor. Software and Techniques for Bio-Molecular Modelling, New Jersey: Austin Group Open Access eBooks; 2016, p, 183 - 197. (ISBN: 978-0-9971499-4-4).
2. **Divakar S**, Hariharan S, Ramanathan M. Identification of Pharmacophore for Wild and T877A Mutant Androgen Receptor Antagonist: Challenges in Designing 3D-QSAR For Mutant Protein. International Journal of Quantitative Structure-Property Relationships (IJQSPR). 2017 Jul 1;2(2):47-61.
3. Elancheran R, Saravanan K, **Divakar S**, Kumari S, Maruthanila VL, Kabilan S, Ramanathan M, Devi R, Kotoky J. Design, synthesis and biological evaluation of novel 1, 3-thiazolidine-2, 4-diones as anti-prostate cancer agents. Anticancer Agents Med Chem. 2017 Apr 12.
4. Saravanan K, Elancheran R, **Divakar S**, Anand SA, Ramanathan M, Kotoky J, Lokanath NK, Kabilan S. Design, synthesis and biological evaluation of 2-(4-phenylthiazol-2-yl) isoindoline-1,3-dione derivatives as anti-prostate cancer agents. Bioorg Med Chem Lett. 2017 Mar 1;27(5):1199-1204.
5. Elancheran R, Saravanan K, Choudhury B, **Divakar S**, Kabilan S, Ramanathan M, Das B, Devi R, Kotoky J. Design and development of oxobenzimidazoles as novel androgen receptor antagonists. Medicinal Chemistry Research. 2016 Apr 1;25(4):539-52.

Structure Based Drug Design in Identification of Novel Androgen Receptor Antagonist

Divakar S¹, Hariharan S² and Ramanathan M^{1*}

¹Department of Pharmacology, PSG College of Pharmacy, India

²Department of Medicinal Chemistry, PSG College of Pharmacy, India

***Corresponding author:** Ramanathan M, Department of Pharmacology, PSG College of Pharmacy, Coimbatore, India, Tel: +918870009199; Email: muthiah.in@gmail.com

Published Date: May 20, 2016

ABSTRACT

Prostate cancer is the second most frequent and sixth leading cause of mortality among male population. Androgen receptor antagonist is one of the regimens for prostate cancer. The relapsed prostate cancer patients were found to express point mutations in the ligand binding domain of the androgen receptor. The mutations at amino acids, threonine 877 and tryptophan 741 were frequently expressed among the androgen independent prostate cancer patients. These point mutations were responsible for the development of resistance against androgen receptor antagonist. Identification of novel androgen receptor antagonist was hampered because of the expression of different types of point mutation and the lack of insight into the binding mode of the androgen receptor antagonist with the mutated receptor. In this study, we have discussed the method adopted by us in designing a novel androgen receptor antagonist that could tolerate the point mutations. We also discussed the role of the point mutations in the development of resistance against androgen receptor antagonist.

Keywords: Prostate cancer; Androgen receptor; Resistance; T877A; W741L

Abbreviations: Prostate Cancer (**PCa**); Androgen Receptor (**AR**); Castration Resistant Prostate Cancer (**CRPC**); Androgen Independent Prostate Cancer (**AIPC**); Heat Shock Protein (**HSP**); Androgen Receptor Response Elements (**AREs**); Steroid Receptor Co-activator (**SRC**); Transcriptional Intermediary Factor (**TIF**); cAMP Response Element Binding (**CREB**); CREB Binding Protein (**CBP**); Dihydrotestosterone (**DHT**); Androgen Deprivation Therapy (**ADT**); Combined Androgen Blockade (**CAB**); Gonadotropin Releasing Hormone (**GnRH**); Phosphatase and Tensin Homolog (**PTEN**); E26 Transformation Specific (**ETS**); Transmembrane Protease Serine 2 (**TMPRSS2**); Mirror-Image Polyductyly Gene 1 Protein (**MIPOL**); Threonine to Alanine (**T877A**); Threonine to Serine (**T877S**); Valine to Methionine (**V715M**); Alanine to Threonine (**A721T**); Asparagine to Aspartic Acid (**N756D**); Histidine to Tyrosine (**H874Y**); Tryptophan to Cysteine (**W741C**); Tryptophan to Leucine (**W741L**); Aspartic Acid to Glycine (**D879G**); Protein Data Bank (**PDB**); Hydrogen Bond (**H-Bond**).

INTRODUCTION

Prostate Cancer

The growth, development, and homeostasis of the prostate gland are under the control of androgens. The growth of prostate gland occurs significantly during puberty and after that, the androgens continue to play an important role in its function. In some men, with increasing age, androgen dependant proliferation of the prostate gland resumes, resulting in benign prostatic hyperplasia or malignant prostate cancer [1]. Most of the Prostate Cancer (**PCa**) relapses within 18 to 24 months of hormonal therapy. The relapsed PCa would be either Castration Resistant Prostate Cancer (**CRPC**) or Androgen Independent Prostate Cancer (**AIPC**) [2].

The enzymes involved in the synthesis of Dihydrotestosterone (**DHT**) are over expressed in CRPC resulting in the relapse. The CRPC could be controlled by including the drugs which inhibit the enzymes involved in the synthesis of DHT [3]. Unlike CRPC, the AIPC doesn't depend on androgens for proliferation; instead it adapts various mechanisms to neutralize the hormonal therapy. Clinically, AIPC is defined as the ability of the PCa cells to grow in the castrated plasma levels of androgen. Point mutation in the ligand binding domain of the Androgen Receptor (**AR**) is one of the major reasons behind the androgen independent proliferation of the PCa cells [4,5].

Androgen Receptor

Human AR is a nuclear receptor encoded by a single gene located on human X-chromosome at Xq11-12 region that spans more than 90kb and has 8 exons [6]. AR is a 900-920 amino acid protein and its variations are due to the polymorphism in the length of polyglutamine (CAG repeats) and polyglycine (GGN repeats) tracts in the first exon [7]. Like other nuclear receptors, AR is also divided into 4 regions: variable N-terminal domain or Activation Function 1 (**AF-1**), DNA binding domain, hinge region, and ligand binding domain or Activation Function 2 (**AF-2**).

The ligand binding domain of AR is coded by exons 6, 7, 8, and c-terminal part of exon 5. The ligand binding domain of AR has 12 α helices and a β sheet that fold to form a hydrophobic ligand binding pocket to which the androgens bind [8]. Helix 4, 5, and 10 are the primary contact sites for androgens. The binding of androgens with AR majorly involves hydrophobic interactions with amino acids Val746, Met742, Gln711, Met745, Leu707, Leu704, and Trp741. The hydrogen bond interactions also play a critical role in the specific binding of androgens to AR [9].

Androgen Dependant Androgen Receptor Activation

Androgen is required for the maximum activation of the AR. The AR predominantly resides in cytoplasm, associated with Heat Shock Protein (**HSP**) and chaperons. The HSP also has an active role, HSP90 bind to AR and keeps it in an active conformation that is necessary for androgens to bind [10]. The nuclear localization signal of the AR resides within amino acids 742 to 817, which keeps the AR within the cytoplasm in the resting state. The nuclear localization signal is dominant over the nuclear export signal in the resting state [11].

The ligands bind to the ligand binding domain of the AR. The helix-12 of the ligand binding domain attains different conformation with agonist and antagonist. Androgen binding causes the helix-12 to lie over the ligand binding pocket, which will reveal the domain for intramolecular AF-1 and AF-2 interaction (N/C terminal interaction). The N/C terminal interaction is specific to AR. The AF-2 region of the other nuclear receptors will preferentially interact with leucine rich LxxLF motifs in the co-activators. The AF-2 region of the AR interacts with phenylalanine rich FxxLF motifs in the AF-1 region. The N/C terminal interaction will lead to cascade of events like phosphorylation, dimerization, nuclear translocation, binding to specific androgen receptor response elements, co-activator recruitment, and initiation of transcription [12,13]. Class 1 family of co-activators, Steroid Receptor Co-activator (**SRC**)-1, Transcriptional Intermediary Factor-2 (**TIF2**), SRC-3, and class 2 family of co-activators, which are also known as transcriptional integrators, p300/CREB (cAMP Response Element Binding) binding protein, regulate the transcriptional activity of AR [14]. The co-activators decondense the chromatin and facilitate the binding of RNA polymerase for the initiation of transcriptional activity. The AR co-activators preferentially interact with the glutamine rich region (1053 - 1123) in the AF-1. Mutant AR that doesn't have this glutamine region is inactive [13]. Antagonist binding displaces the helix-12 away from the ligand binding pocket and unveils the binding surface for co-repressor NcoR/SMRT interaction, which leads to the inhibition of the AR mediated transcriptional activity [15].

Androgen Independent Androgen Receptor Activation

The aim of the treatment in metastatic PCa is to reduce the plasma levels of prostate specific antigen and androgen. This can be established by either Androgen Deprivation Therapy (**ADT**) or Combined Androgen Blockade Therapy (**CAB**). ADT includes surgical or pharmacological castration. Surgical castration involves bilateral orchiectomy (removal of testes) and the standard castrate level of testosterone could be achieved within 12hr. Pharmacological castration can be

achieved by either Gonadotropin Releasing Hormone (**GnRH**) receptor agonist or GnRH receptor antagonist. There will be an initial rise in the testosterone concentration by using GnRH receptor agonist but after 2 to 4 weeks, castration levels of testosterone will be achieved. In CAB therapy, in addition to castration (surgical or pharmacological), AR antagonist or 5 α reductase inhibitors are used to prevent AR activation by adrenal androgens [16,17].

The hormonal therapy has beneficial outcome for 18-24 months but the PCa relapses because of many other pathological conditions. Some of the major reasons are, over expression of enzymes involved in DHT synthesis and subsequent rise in intracrine androgen level [18], down regulation of enzymes involved in DHT catabolism [19], somatic point mutations in the ligand binding domain of AR [4,5], AR over expression [20], truncation of AR ligand binding domain, and constitutive activation of AF-1 region [21], Phosphatase and Tensin homolog (**PTEN**) loss [22], increased telomerase activity [23], mutations in p53 [24], down regulation of E-Cadherin and over expression of N-Cadherin which increases the heterotypic cell adhesion and metastasis [25], translocation and fusion of E26 Transformation Specific (**ETS**) genes with androgen responsive genes like Transmembrane Protease Serine 2 (**TMPRSS2**) or prostate specific Mirror-Image Polydactyly gene 1 protein (**MIPOL1**) gene [26,27].

The fusion between androgen responsive and ETS genes were identified in 40 to 70% of aggressive PCa cases [27]. The ETS family of transcriptional factors is oncogenic and controls the cell differentiation, cell division, metastasis, angiogenesis etc. The fusion of ETS genes with androgen responsive genes results in the over expression of ETS genes whenever AR is activated. Somatic point mutation in the ligand binding domain of AR was also frequently identified in drug resistance PCa patients [4,5]. The mechanism by which the AR mutates was unknown and many point mutations were identified among AIPC patients. The mutated AR does not depend on androgen for activation; instead it can be activated by other steroidal hormones like estradiol, progesterone, and AR antagonists. For the ETS to over-express, it requires AR activation, since it was fused with an AR responsive genes. The hormonal therapy decreases the plasma testosterone level but the mutated AR does not require androgen for activation. Consequently, the mutated AR could activate the expression of ETS genes without androgen. The AR mutation and ETS chromosomal rearrangement in conjunction could co-ordinate the AIPC progression and drug resistance for AR antagonist and cytotoxic drugs. A novel AR antagonist that resists the mutations and decreases the expression of ETS genes could well be the future for PCa treatment.

Mutations in the Ligand Binding Domain of Androgen Receptor

The somatic point mutations can be broadly classified into two types

Mutations expressed in flutamide treated patients

The mutations, T877A (Threonine to Alanine), T877S (Threonine to Serine), V715M (Valine to Methionine), A721T (Alanine to Threonine), N756D (Asparagine to Aspartic acid), and H874Y

(Histidine to Tyrosine) were identified in AIPC patients who underwent flutamide containing therapy [5,28,29]. These mutations cause resistance to flutamide treatment and these mutant ARs are activated by flutamide.

Mutations expressed in bicalutamide treated patients

The mutations, W741C (Tryptophan to Cysteine), W741L (Tryptophan to Leucine), and D879G (Aspartic acid to Glycine) were identified in AIPC patients who underwent bicalutamide containing therapy [28,30]. These mutations were responsible for bicalutamide resistance and these mutant ARs are activated by bicalutamide.

In general, these mutations broaden the ligand specificity of the receptor. For example, the T877 amino acid mutated AR was activated by non androgens like cyproterone acetate, flutamide, estrogens, glucocorticoids, progesterone etc., whereas, bicalutamide antagonizes the T877 mutant AR. Similarly the W741 amino acid mutated AR was activated by non androgens like bicalutamide, estrogens, glucocorticoids, progesterone etc., whereas, flutamide antagonizes the W741 mutant AR [30,31,32,33,34].

COMPUTATIONAL METHODS

Docking

The ligands for the docking studies were prepared using LigPrep, Schrödinger. The ligands were geometrically refined and assigned appropriate protonation state at pH 7.0 ± 2.0 . The energy minimization was carried out by OPLS 2005 force field [35]. The proteins (PDB: 2AMA, 2AX6, 1Z95 & helix-12 truncated ARs) were prepared using protein preparation wizard in Maestro, Schrödinger [36]. The preprocessed protein was then used to generate the grid for docking. The grid was assigned by picking the ligand as the center of the grid and the grid box was generated by applying default parameters. The docking was carried out using GLIDE, Schrödinger. GLIDE XP (extra precision) method was followed for docking calculations [37].

Homology Modelling

The helix-12 truncated AR was generated using PRIME, Schrodinger [38]. The Prime suite was used for protein structure prediction, side chain optimization, loop prediction, active site refinement and energy minimization. The amino acid sequence of the ligand binding domain of AR was obtained from NCBI (Protein accession No: P10275.2).

The template protein was identified through blast search. The AR crystal structure, 2AMA was the template for wild type AR and 2OZ7 was the template for T877A mutated AR. The alignment between the target and template sequence was carried out by clustalW method. ClustalW could be used when there is a high sequence identity between the target and template. Prime allows us to build the homology model in two different types, either knowledge based or energy based. We used a knowledge based method where it uses the structure information from the template for gaps

and insertions. As default, the side chains were only optimized for the residues that are not from the template. The ligand and a water molecule (HOH-108) were retained in the final model. The homology model was then energy minimized (OPLS 2005) by VSGB solvation and we also refined the active site (5Å from the ligand) of the model.

CASE STUDY

Target Selection

It is impossible to consider all those mutations while designing an AR antagonist. The mutations in T877 amino acid occur frequently among the flutamide treated patients [34]. At present, flutamide was largely replaced with bicalutamide and there was no report of T877A/S mutation among bicalutamide treated patients. Mutations in W741 predominate among the bicalutamide treated patients [28,30]. The T877A mutated AR was expressed in LNCaP cell line. The LNCaP could also express the W741L/C mutation upon incubation with bicalutamide in an androgen depleted medium for 6-13 weeks [30]. So, the mutations are treatment specific and might keep on piling up depending on the antagonist. Targeting the wild type AR for drug designing is essential because the mutations occur during the course of treatment and as discussed above, the mutations are treatment specific. Understanding the mechanism by which these mutations convert an antagonist to agonist is essential because a novel AR antagonist should tolerate these types of mutations that might occur during the course of treatment.

The crystal structure of the wild type and some of the mutated ARs are available in Protein Data Bank (**PDB**). Unfortunately, none of them are in antagonist bound conformation. Generally, the steroidal receptor antagonist has bulkier groups than the endogenous agonist. Antagonist form similar H-Bond interaction like agonist but due to their bulkier nature, they displace the helix-12 away from the ligand binding pocket [39,40]. The helix-12 of the ligand binding domain adapts closed and open conformation in response to agonist and antagonist respectively [41,42]. Consequently, we modelled an AR that lacks helix-12 for the structure based virtual screening. The truncated receptor has 671-881 amino acids instead of 671-919 amino acids.

Docking Studies

Docking studies were carried out to evaluate the role of the point mutation in converting an AR antagonist to agonist. We chose 4 different types of AR: wild type (PDB: 2AMA), T877A (PDB: 2AX6), W741L (PDB: 1Z95), and helix-12 truncated ARs (homology model). The ligands were DHT, testosterone, non steroidal AR antagonist flutamide, bicalutamide, and enzalutamide.

Androgen

The androgen, DHT, has binding affinity towards all the ARs but did not form H-Bond interaction with T877A mutated AR (Table1). The DHT and testosterone have similar type H-Bond interactions with wild type AR (Figure 1). The keto group of DHT and testosterone formed H-Bond interaction with Arg752, while the 17β hydroxyl group formed H-Bond interaction with Asn705

and Thr877. Testosterone did not bind with the T877A mutated AR and didn't form any H-Bond interaction with W741L mutated AR. The binding energy of the androgens was less in the mutated ARs than the wild type AR. The DHT has a dock score of -10.80 kcal/mol with wild type AR but the dock score had decreased with T877A (-5.84 kcal/mol) and W741L (-6.71 kcal/mol) mutated ARs. Similarly the testosterone has a dock score of -10.68 kcal/mol with wild type AR but the dock score had decreased with T877A (no binding) and W741L (-5.95 kcal/mol) mutated ARs. This indicates that the mutations might affect the binding of the androgens with AR. Ligand binding assay also proved that the mutations could decrease the binding affinity of androgens [43].

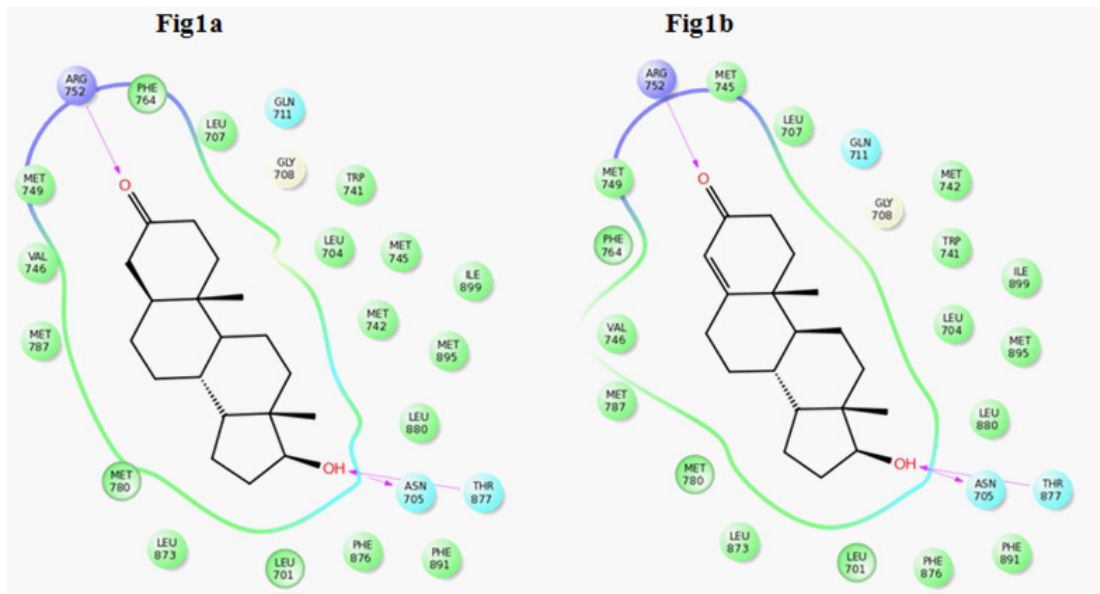


Figure 1: Binding interactions of androgens.

1a: DHT forms H-Bond interaction with Arg752, Asn705 and Thr877 with wild type AR. **1b:** Testosterone forms H-Bond interaction with Arg752, Asn705 and Thr877 with wild type AR.

Table 1: Docking score and H-Bond interaction of androgen receptor ligands.

Ligands	Wild type		T877A		W741L		Truncated	
	Dock Score ¹	H-Bond	Dock Score	H-Bond	Dock Score	H-Bond	Dock Score	H-Bond
DHT	-10.80	Arg752, Asn705, Thr877	-5.84	✘	-6.71	Arg752, Gln711, Thr877, HOH108	-7.26	HOH108, Asn705
Testosterone	-10.68	Arg752, Asn705, Thr877	✘	✘	-5.95	✘	-7.17	HOH108, Asn705
Flutamide	-7.76	Asn705, Thr877	-8.25	Arg752, Gln711, Asn705, Leu704, HOH108 [‡] , HOH213 [#]	-7.22	Arg752, Gln711, Leu704, Asn705, HOH108	-6.22	Arg752, Gln711, Asn705, HOH108
Bicalutamide	-2.548	✘	✘	✘	-10.27	Arg752, Gln711, Leu704, Asn705, HOH108	-9.22	Arg752, Gln711, Asn705
Enzalutamide	✘	✘	✘	✘	✘	✘	-5.87	Arg752, Gln711

¹Dock score in kcal/mol.

*HOH108 could form bridged H-Bond interactions with Arg752, Gln711 and Met745.

#HOH213 could form bridged H-Bond interaction with Leu873.

Flutamide

Flutamide has binding affinity for all the AR types used in this study. Flutamide has the highest binding energy with T877A mutated AR (dock score = -8.25 kcal/mol). Flutamide has a dock score of -7.76 kcal/mol and -7.22 kcal/mol with wild and W741L mutated ARs, respectively. As discussed above, T877A mutation causes resistance specifically to flutamide. In wild type AR, the hydroxyl group of flutamide forms H-Bond interactions with Thr877 and Asn705 (Figure 2). In T877A mutated AR, the nitro group of flutamide formed H-Bond interactions with Gln711, Arg752, HOH108, and Met745. The hydroxyl group of flutamide, in the absence of Thr877 amino acid, formed H-Bond interaction only with Asn705. The keto group of the amide formed H-Bond interaction with Leu873 mediated through a water molecule (HOH213) and the amino group of the amide formed H-Bond interaction with Leu704. The exact mechanism by which the T877A mutation converts the flutamide from antagonist to agonist was unknown, but we could observe that the size of the ligand binding pocket in T877A was bigger than the wild type AR (Figure 2). The binding conformation of flutamide with wild and T877A mutated ARs was also different. Flutamide attained a bent conformation when bound to T877A mutated AR. It is possible that the T877A mutation could increase the space within the ligand binding pocket to accommodate for larger ligands without disturbing the closing of helix-12.

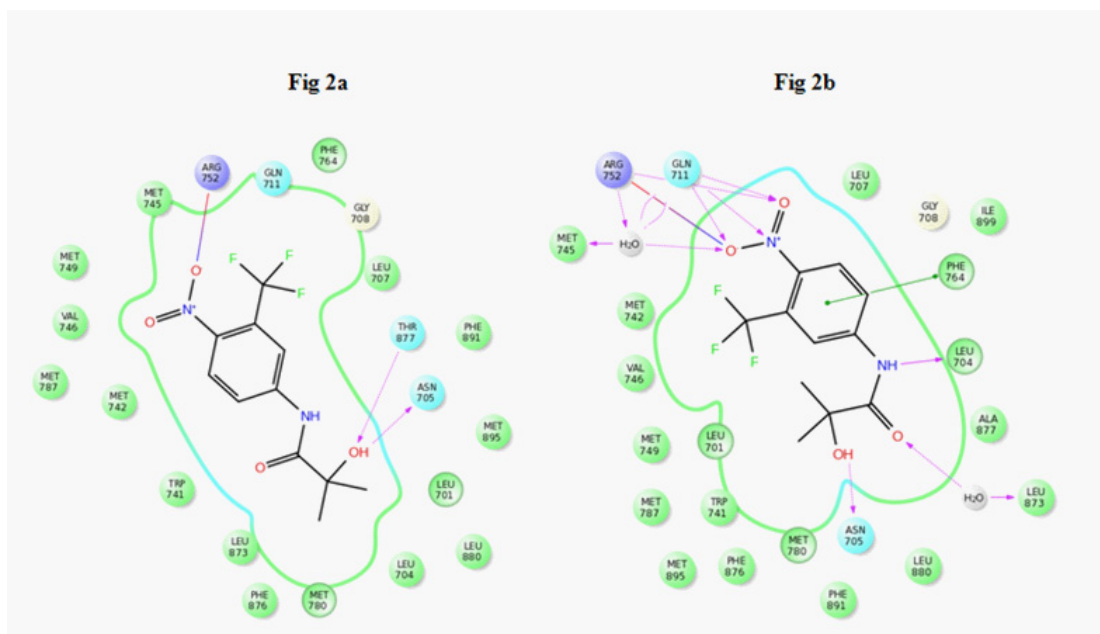


Figure 2: Binding interactions of flutamide.

2a: Flutamide forms H-Bond interaction with Thr877, Asn705 and forms ionic interaction with Arg752 in wild type AR. **2b:** Flutamide forms H-Bond interactions with Arg752 (ionic and H-Bond), Gln711, Leu704, Leu873 (bridged through HOH) and Met745 (bridged through HOH) in T877A mutant AR.

Bicalutamide

The AR antagonist, bicalutamide doesn't bind with T877A AR and has low binding energy with wild type AR (dock score = -2.54 kcal/mol). Bicalutamide is an antagonist to wild and T877A mutated ARs. This reveals that the bicalutamide was bulky enough so that it couldn't bind with AR which has helix-12 in agonist conformation. Bicalutamide has the highest binding energy with W741L mutated AR (dock score = -10.27 kcal/mol) and this mutation causes resistance specifically to bicalutamide. In W741L mutated AR, the nitrile group of bicalutamide formed H-Bond interactions with Arg752, Gln711, HOH108, and Met745. The amine and hydroxyl group formed H-Bond interaction with Leu704 and Asn705 respectively (Figure 3a). It is obvious that the mutated leucine amino acid (W741L) is much smaller in size than the tryptophan amino acid, so we tried to compare the binding mode of bicalutamide in presence of leucine (W741L AR) and tryptophan (wild type AR). The binding comparison was carried out by superimposing the bound conformation of bicalutamide in W741L and wild type (helix-12 truncated) ARs (Figure 3b). The truncated AR has wild type tryptophan amino acid. The B ring of bicalutamide attains a different conformation in the presence of leucine and tryptophan. In the presence of tryptophan, the B ring of bicalutamide was shifted nearer to helix-12 amino acid Ile 899, indicating a possible

steric clash with it. In the presence of leucine (mutated AR) the B ring of bicalutamide was well inside the ligand binding pocket and far from the helix-12. This indicates that the W741L mutation also keeps the bulky B ring of bicalutamide within the binding pocket so that it could switch the antagonist activity of bicalutamide into an agonist.

The unexplained mystery of the mutations T877A and W741L was that flutamide, which is comparatively a smaller ligand than bicalutamide, could antagonize W741L mutated AR but not the T877A AR. Similarly bicalutamide could antagonize T877A mutated AR but not the W741L mutated AR. The possible explanation to this is, the mutations might be specific to the binding conformation of their respective antagonist. For instance, the B ring of bicalutamide was involved in steric interference with helix-12. So, the W741L mutation could be deliberate to keep the B ring of the bicalutamide away from the helix-12. In case of flutamide, there could be some other group involved in the steric interference with helix-12 and hence flutamide works as an antagonist in W741L mutated AR.

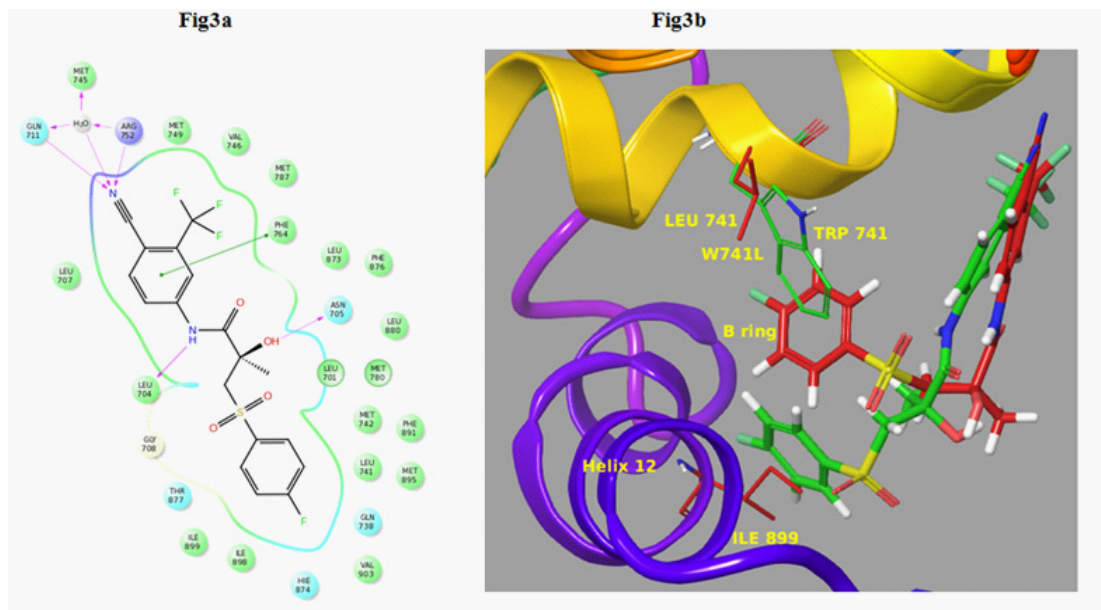


Figure 3: Binding mode of bicalutamide.

3a: Bicalutamide forms H-Bond interaction with Arg752, Gln711, Leu704, Met745 (bridged through HOH) and Asn705 in W741L mutated AR. **3b:** Figure represents the superimposition of the wild (green colored carbon) and W741L mutated (red colored carbon) ARs and the difference in binding mode of bicalutamide. Note the lack of steric clashes of bicalutamide with helix-12 in the mutated type, which in turn leads to resistance.

Enzalutamide

Enzalutamide is a novel AR antagonist which was recently approved and doesn't have the resistance with T877A and W741L mutated ARs. Enzalutamide doesn't have binding affinity with wild, T877A and W741L, which all have helix-12 in agonist conformation. The enzalutamide has binding affinity only with helix-12 truncated AR (dock score = -5.87 kcal/mol). This reveals that enzalutamide has enough bulk that prevents it from binding with ARs that has helix-12 in agonist conformation. The nitrile group of enzalutamide forms H-Bond interactions with Arg752 and Gln711 (Figure 4). This also proves that the truncated helix-12 model is a viable way to identify novel AR antagonists by structure based virtual screening method.

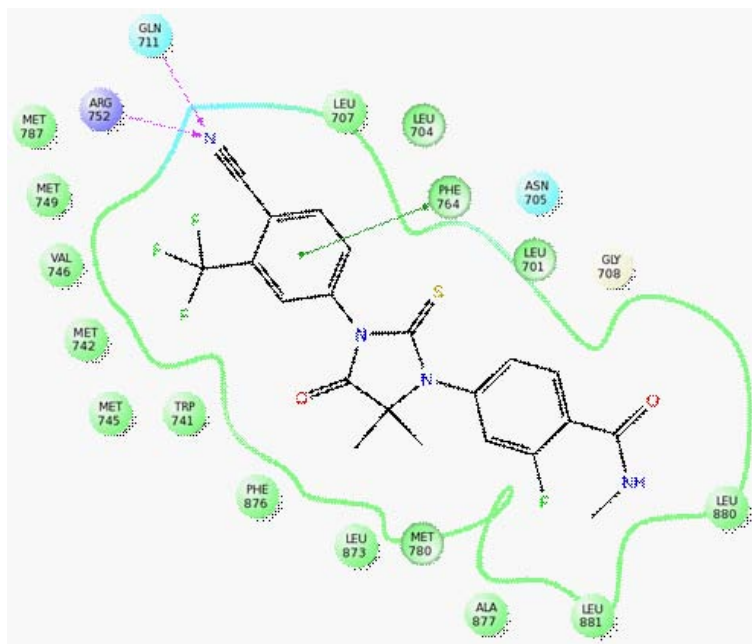


Figure 4: Binding interactions of enzalutamide.

Enzalutamide forms H-Bond interactions with Arg752 and Gln711 with helix-12 truncated AR.

Derivation of Structure Based Drug Design Method

The mutation increases the space within the ligand binding pocket so that it could accommodate for larger molecules without disturbing the helix-12 [44]. The 12th helix truncated AR model could then be used to screen chemical databases (ZINC, SPECS etc) for the identification of novel AR antagonist scaffold. The AR with helix-12 closed conformation could also be included in the docking process to eliminate the ligands that also have good binding score with helix-12 truncated AR. This step will eliminate the less bulk and highly flexible ligands so that the identified ligands might overcome the space increasing mutations that occur in the ligand binding pocket. This way, we can also differentiate between an AR agonist/partial agonist from pure antagonist.

The novel AR antagonist should also form essential H-Bond interactions with the AR for specific binding. In general, the AR ligands could form H-Bond interactions with amino acids Arg752, Gln711, Met745, Leu704, Asn705, and Thr877. The amino acids Arg752, Gln711, and Met745 are present deep inside the binding pocket. The amino acids Thr877 and Asn705 are present nearer to helix-12. An AR antagonist should preferentially form H-Bond with the deep residues, Arg752, Gln711, and Met745 either directly or mediated through a water molecule (bridged H-Bond). The H-Bond interactions with Asn705 and Thr877 might prevent the antagonist from abutting (steric clash) the helix-12 [45]. In the docking studies, flutamide and bicalutamide which exhibit resistance with the mutated AR had formed H-Bond interaction with Asn705 and Thr877 amino acids. Enzalutamide, which doesn't have resistance with Thr877 or W741L mutated ARs, formed H-Bond interaction with Arg752 and Gln711 and didn't form H-Bond interaction with either Asn705 or Thr877.

CONCLUSION

The point mutations in AR increase the binding affinity for the antagonist and decrease the binding affinity for agonist androgens. The mutation converts the antagonist into agonist, which promotes the growth of the cancer cells. Hence, it is essential to design an antagonist that will tolerate the point mutation that may occur during the course of the treatment. This is possible by designing AR antagonists that possess optimal bulk. The bulky groups should also attain optimal conformation in order to abut helix-12. The method described in this manuscript is capable of identifying new chemical entities that remain impervious to mutation in the AR ligand binding domain.

References

1. Watabe T, Lin M, Ide H, Donjacour AA, Cunha GR. Growth, regeneration, and tumorigenesis of the prostate activates the PSCA promoter. *Proc Natl Acad Sci U S A*. 2002; 99: 401-406.
2. Feldman BJ, Feldman D. The development of androgen-independent prostate cancer. *Nat Rev Cancer*. 2001; 1: 34-45.
3. Attard G, Reid AH, Yap TA, Raynaud F, Dowsett M, et al. Phase I clinical trial of a selective inhibitor of CYP17, abiraterone acetate, confirms that castration-resistant prostate cancer commonly remains hormone driven. *J Clin Oncol*. 2008; 26: 4563-4571.
4. Tilley WD, Buchanan G, Hickey TE, Bentel JM. Mutations in the androgen receptor gene are associated with progression of human prostate cancer to androgen independence. *Clin Cancer Res*. 1996; 2: 277-285.
5. Taplin ME, Bubley GJ, Shuster TD, Frantz ME, Spooner AE, Ogata GK, et al. Mutation of the androgen receptor gene in metastatic androgen independent prostate cancer. *N Engl J Med*. 1995; 332: 1393-1398.
6. Brown CJ, Goss SJ, Lubahn DB, Joseph DR, Wilson EM, French FS, et al. Androgen receptor locus on the human X chromosome: regional localization to Xq11-12 and description of a DNA polymorphism. *Am J Hum Genet*. 1989; 44: 264-269.
7. Zeegers MP, Kiemeny LA, Nieder AM, Ostrer H. How strong is the association between CAG and GGN repeat length polymorphisms in the androgen receptor gene and prostate cancer risk? *Cancer Epidemiol Biomarkers Prev*. 2004; 13: 1765-1771.
8. Matias PM, Donner P, Coelho R, Thomaz M, Peixoto C, et al. Structural evidence for ligand specificity in the binding domain of the human androgen receptor. Implications for pathogenic gene mutations. *J Biol Chem*. 2000; 275: 26164-26171.
9. Pereira-de-Jésus-Tran K, Côté PL, Cantin L, Blanchet J, Labrie F, et al. Comparison of crystal structures of human androgen receptor ligand binding domain complexed with various agonists reveals molecular determinants responsible for binding affinity. *Protein Sci*. 2006; 15: 987-999.
10. Fang Y, Fliss AE, Robins DM, Caplan AJ. Hsp90 regulates androgen receptor hormone binding affinity in vivo. *J Biol Chem*. 1996; 271: 28697-28702.

11. Saporita AJ, Zhang Q, Navai N, Dincer Z, Hahn J. Identification and characterization of a ligand-regulated nuclear export signal in androgen receptor. *J Biol Chem.* 2003; 278: 41998-42005.
12. He B, Kempainen JA, Wilson EM. FXXLF and WXXLF sequences mediate the NH2-terminal interaction with the ligand binding domain of the androgen receptor. *J Biol Chem.* 2000; 275: 22986-22994.
13. Bevan CL, Hoare S, Claessens F, Heery DM, Parker MG. The AF1 and AF2 domains of the androgen receptor interact with distinct regions of SRC1. *Mol Cell Biol.* 1999; 19: 8383-8392.
14. Heinlein CA, Chang C. Androgen receptor (AR) coregulators: an overview. *Endocr Rev.* 2002; 23: 175-200.
15. Hodgson MC, Shen HC, Hollenberg AN, Balk SP. Structural basis for nuclear receptor corepressor recruitment by antagonist-liganded androgen receptor. *Mol Cancer Ther.* 2008; 7: 3187-3194.
16. Heidenreich A, Bellmunt J, Bolla M, Joniau S, Mason M, Matveev V, et al. EAU guidelines on prostate cancer. Part 1: screening, diagnosis, and treatment of clinically localised disease. *Eur Urol.* 2011; 59: 61-71.
17. Heidenreich A, Bastian PJ, Bellmunt J, Bolla M, Joniau S, et al. EAU guidelines on prostate cancer. Part II: Treatment of advanced, relapsing, and castration-resistant prostate cancer. *Eur Urol.* 2014; 65: 467-479.
18. Stanbrough M, Bubley GJ, Ross K, Golub TR, Rubin MA, Penning TM, et al. Increased expression of genes converting adrenal androgens to testosterone in androgen-independent prostate cancer. *Cancer Res.* 2006; 66: 2815-2825.
19. Ji Q, Chang L, Stanczyk FZ, Ookhtens M, Sherrod A, et al. Impaired dihydrotestosterone catabolism in human prostate cancer: critical role of AKR1C2 as a pre-receptor regulator of androgen receptor signaling. *Cancer Res.* 2007; 67: 1361-1369.
20. Wang LG, Johnson EM, Kinoshita Y, Babb JS, Buckley MT, et al. Androgen receptor overexpression in prostate cancer linked to Pur alpha loss from a novel repressor complex. *Cancer Res.* 2008; 68: 2678-2688.
21. Dehm SM, Schmidt LJ, Heemers HV, Vessella RL, Tindall DJ. Splicing of a novel androgen receptor exon generates a constitutively active androgen receptor that mediates prostate cancer therapy resistance. *Cancer Res.* 2008; 68: 5469-5477.
22. Sircar K, Yoshimoto M, Monzon FA, Koumakpayi IH, Katz RL, et al. PTEN genomic deletion is associated with p-Akt and AR signalling in poorer outcome, hormone refractory prostate cancer. *J Pathol.* 2009; 218: 505-513.
23. Zhang W, Kapusta LR, Slingerland JM, Klotz LH. Telomerase activity in prostate cancer, prostatic intraepithelial neoplasia, and benign prostatic epithelium. *Cancer Res.* 1998; 58: 619-621.
24. Nesslinger NJ, Shi XB, deVere-White RW. Androgen-independent growth of LNCaP prostate cancer cells is mediated by gain-of-function mutant p53. *Cancer Res.* 2003; 63: 2228-2233.
25. Jennbacken K, Tesan T, Wang W, Gustavsson H, Damber JE, et al. N-cadherin increases after androgen deprivation and is associated with metastasis in prostate cancer. *Endocr Relat Cancer.* 2010; 17: 469-479.
26. Hessels D, Smit FP, Verhaegh GW, Witjes JA, Cornel EB, et al. Detection of TMPRSS2-ERG fusion transcripts and prostate cancer antigen 3 in urinary sediments may improve diagnosis of prostate cancer. *Clin Cancer Res.* 2007; 13: 5103-5108.
27. Rahim S, Beauchamp EM, Kong Y, Brown ML, Toretzky JA, et al. YK-4-279 inhibits ERG and ETV1 mediated prostate cancer cell invasion. *PLoS One.* 2011; 6: e19343.
28. Taplin ME, Rajeshkumar B, Halabi S, Werner CP, Woda BA, et al. Cancer and Leukemia Group B Study 9663. Androgen receptor mutations in androgen-independent prostate cancer: Cancer and Leukemia Group B Study 9663. *J Clin Oncol.* 2003; 21: 2673-2678.
29. Balk SP. Androgen receptor as a target in androgen-independent prostate cancer. *Urology.* 2002; 60: 132-138.
30. Hara T, Miyazaki J, Araki H, Yamaoka M, Kanzaki N, et al. Novel mutations of androgen receptor: a possible mechanism of bicalutamide withdrawal syndrome. *Cancer Res.* 2003; 63: 149-153.
31. Tan J, Sharief Y, Hamil KG, Gregory CW, Zang DY, et al. Dehydroepiandrosterone activates mutant androgen receptors expressed in the androgen-dependent human prostate cancer xenograft CWR22 and LNCaP cells. *Mol Endocrinol.* 1997; 11: 450-459.
32. Urushibara M, Ishioka J, Hyochi N, Kihara K, Hara S. Effects of steroidal and non-steroidal antiandrogens on wild-type and mutant androgen receptors. *Prostate.* 2007; 67: 799-807.
33. Fenton MA, Shuster TD, Fertig AM. Functional characterization of mutant androgen receptors from androgen-independent prostate cancer. *Clin Cancer Res.* 1997; 3: 1383-1388.
34. Taplin ME, Bubley GJ, Ko YJ, Small EJ, Upton M. Selection for androgen receptor mutations in prostate cancers treated with androgen antagonist. *Cancer Res.* 1999; 59: 2511-2515.
35. LigPrep version 3.1, Schrödinger, LLC, New York, NY. 2014.

36. Maestro version 9.8, Schrödinger, LLC, New York, NY. 2014.
37. Glide, version 3.3, Schrödinger, LLC, New York, NY. 2014.
38. PRIME version 3.7, Schrödinger, LLC, New York, NY. 2014.
39. Bohl CE, Gao W, Miller DD, Bell CE, Dalton JT. Structural basis for antagonism and resistance of bicalutamide in prostate cancer. *Proc Natl Acad Sci USA*. 2005; 102: 6201-6206.
40. Bohl CE, Miller DD, Chen J, Bell CE, Dalton JT. Structural basis for accommodation of nonsteroidal ligands in the androgen receptor. *J Biol Chem*. 2005; 280: 37747-37754.
41. Shiau AK, Barstad D, Loria PM, Cheng L, Kushner PJ. The structural basis of estrogen receptor/coactivator recognition and the antagonism of this interaction by tamoxifen. *Cell*. 1998; 95: 927-937.
42. Kauppi B, Jakob C, Färnegårdh M, Yang J, Ahola H, Alarcon M, et al. The three-dimensional structures of antagonistic and agonistic forms of the glucocorticoid receptor ligand-binding domain: RU-486 induces a transconformation that leads to active antagonism. *J Biol Chem*. 2003; 278: 22748-22754.
43. Zhao XY, Boyle B, Krishnan AV, Navone NM, Peehl DM. Two mutations identified in the androgen receptor of the new human prostate cancer cell line MDA PCa 2a. *J Urol*. 1999; 162: 2192-2199.
44. Osguthorpe DJ, Hagler AT. Mechanism of androgen receptor antagonism by bicalutamide in the treatment of prostate cancer. *Biochemistry*. 2011; 50: 4105-4113.
45. Guo C, Pairish M, Linton A, Kephart S, Ornelas M. Design of oxobenzimidazoles and oxindoles as novel androgen receptor antagonists. *Bioorg Med Chem Lett*. 2012; 22: 2572-2578.

Identification of Pharmacophore for Wild and T877A Mutant Androgen Receptor Antagonist: Challenges in Designing 3D-QSAR For Mutant Protein

Divakar Selvaraj, Department of Pharmacology, PSG College of Pharmacy, Coimbatore, India

Sivaram Hariharan, Department of Chemistry, PSG College of Pharmacy, Coimbatore, India

Ramanathan Muthiah, Department of Pharmacology, PSG College of Pharmacy, Coimbatore, India

ABSTRACT

Androgen increases the proliferation of prostate cancer cells by activating the androgen receptor (AR). AR antagonists block the androgen mediated proliferation and are used to treat prostate cancer. Antagonist resistance occurs due to the expression of mutations in AR. One particular mutation, T877A, was frequently expressed in relapsed patients. Presently, there is no antagonist in the market without the problem of resistance developing over the period of treatment. A plausible reason for this shortcoming could be the lack of designing because of the unavailability of AR-crystal structure in antagonist bound conformation. Hence, 3D-QSAR becomes a major tool in identification of novel AR antagonists. Three models, ADDHRR.295, AHHRR.266, and AHRR.63 were designed for wild type, T877A mutant, and full (active at both wild and mutant types) AR antagonists respectively. There is a major difference in the angles and lengths of the pharmacophore site points among the 3D-QSAR models. The generated pharmacophore for full antagonists was then used for screening the SPECS database with filters for identifying hits.

KEYWORDS

3D-QSAR, Androgen Receptor Antagonist, Mutation, Pharmacophore, Prostate Cancer, Resistance, T877A, Virtual Screening

INTRODUCTION

Activation of AR (androgen receptor) by androgen leads to the proliferation of prostate cells. AR antagonists inhibit the binding of androgens with AR and prevent the proliferation of prostate cells (Gao et al., 2010). However, the AR develops resistance for its antagonists after a treatment median of 12-24 months. This is because of the expression of point mutations in the ligand binding domain of the AR (Tilley et al., 1996, Feldman et al., 2001). The T877A mutation was most frequently expressed among prostate cancer patients (Feldman et al., 2001, Balk et al., 2002). The mutant AR converts the antagonist into agonist (Fenton et al., 1997). Furthermore, the mutated AR could also be activated by steroidal hormones, estrogens, progesterone, etc. (Fenton et al., 1997). This leads to the failure of androgen deprivation therapy because of the activation of AR by non-androgens.

DOI: 10.4018/IJQSPR.2017070105

Previously, we had designed and synthesized novel oxbenzimidazole derivatives targeting AR (Elencheran et al., 2016). However, most of the molecules were non selective and inhibited the proliferation of AR negative and positive prostate cancer cell lines. Therefore, in order to overcome this issue, we decided to study the pharmacophoric features of AR antagonists. In this study, we have developed three 3D-QSAR models. These models represent the pharmacophore site points of wild type AR antagonist, T877A mutant AR antagonist, and the full antagonist. The full antagonist, for the purposes of this study, is defined as a molecule that will not function as an agonist or partial agonist with either wild or mutant ARs. The difference between the full antagonist and partial agonist is that the full antagonist will behave as an antagonist irrespective of the AR mutation. The activity of the partial agonist is facultative and depends on the presence of mutation. The partial agonist functions as an agonist in the presence of T877A mutation and acts an antagonist in the absence of the mutation. A good example in this regard is Flutamide. The 3D-QSAR models were compared for differences among them. This study could potentially provide the insight into the necessary structural properties of AR antagonists to avoid resistance developing during treatment.

MATERIALS AND METHODS

Dataset Preparation

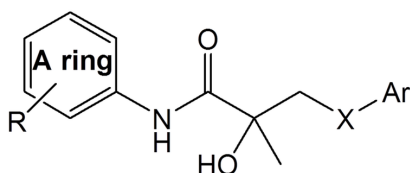
The molecules for the datasets were obtained from literature (Ferla, et al., 2016, Bassetto et al., 2016, Yamamoto et al., 2013, Yamamoto et al., 2012, Yamamoto et al., 2012). The ligands were then grouped into three datasets. The first dataset consists of ligands that antagonize the wild type AR. The ligands for this dataset were obtained from Ferla et al., 2016 and Bassetto et al., 2016. The methods adopted in these papers were the same and the experiments were conducted in the same laboratory. The antagonist activity was measured in VCaP cell line, which expresses wild type AR. The second dataset consists of ligands that antagonize the T877A mutant AR. The ligands for this dataset were also obtained from Ferla et al., 2016 and Bassetto et al., 2016. The methods adopted in these papers were also the same. The antagonist activity was measured in LNCaP cell line, which expresses T877A mutant AR. The third dataset consists of ligands that antagonize both wild and T877A mutant AR without any agonist / partial agonist effect on either of these receptors. The ligands for this dataset were obtained from Yamamoto et al., 2013, Yamamoto et al., 2012, and Yamamoto et al., 2012. The methods adopted in these papers were the same and the experiments were conducted in the same laboratory. The antagonist and partial agonist activity were measured by a transfection assay.

As mentioned above, the biological activity of each dataset was obtained in different cell lines. Hence, there is a difference in the biological activity range among the datasets. The active and inactive molecules were selected depending on the activity range among the dataset molecules. The active molecules are the ones which will have the least IC_{50} and the inactive molecules will have the higher IC_{50} values among the dataset molecules. Hence, the inactive molecules are more precisely described as less actives rather than absolutely inactives. This selection method was followed to yield an optimal numbers of active and inactive molecules in the training and test sets. This is absolutely essential for validating the 3D-QSAR with an external test set which should have equal activity distribution like training set.

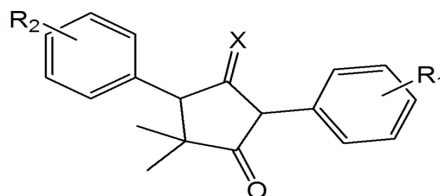
The first dataset (wild type) has 122 molecules and was randomly split into training (75%) and test (25%) sets. The molecules in the dataset represent similarity with AR antagonists enzalutamide and bicalutamide. The molecules having $IC_{50} < 4\mu M$ were designated as actives and molecules having $IC_{50} > 50\mu M$ were designated as inactives. The second dataset (T877A AR) has 132 molecules and the dataset was divided randomly into training (75%) and test (25%) sets. The extra 10 molecules in the mutant (second) dataset do not have any defined activity values in the wild type and consequently were not included in the wild type pharmacophore generation. The molecules in the dataset represent similarity with AR antagonists enzalutamide and bicalutamide (Figure 1). The molecules having $IC_{50} < 3\mu M$ were designated as actives and molecules having $IC_{50} > 32\mu M$ were designated as inactives.

Figure 1. Representation of the scaffolds used in the construction of 3D-QSAR models

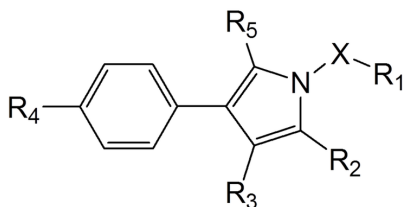
A: Bicalutamide derivatives



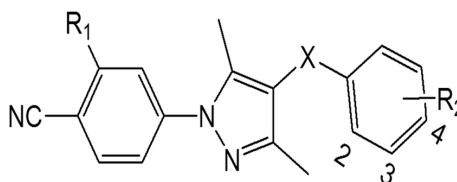
B: Enzalutamide derivatives



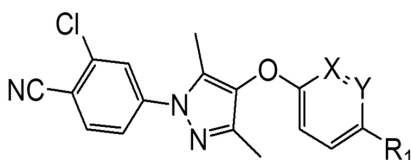
C: 1-arylmethyl-4-phenylpyrrole



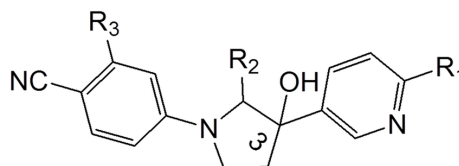
D: 4-arylmethyl-1-phenylpyrazole



E: 4-aryloxy-1-phenylpyrazole



F: 3-aryl-3-hydroxy-1-phenylpyrrolidine



The third data set (full antagonist) had 42 molecules and the dataset was randomly divided into training (75%) and test (25%) sets. The molecules in the dataset have different types of basic nuclei comprising, 1-arylmethyl-4-phenylpyrrole, 4-arylmethyl-1-phenylpyrazole, 4-aryloxy-1-phenylpyrazole, and 3-aryl-3-hydroxy-1-phenylpyrrolidine derivatives (Figure 1). The ligands having $IC_{50} < 0.10 \mu M$ were designated as actives and ligands having $IC_{50} > 3 \mu M$ were designated as inactive.

Common Pharmacophore Hypotheses and 3D-QSAR

Common pharmacophore hypotheses (CPH) identification and 3D-QSAR modelling were performed using PHASE, Schrödinger (v3.9). The ligands were geometrically refined and assigned appropriate protonation states for $pH = 7.0 \pm 0.2$ by LigPrep (v3.1). The IC_{50} values were entered as pIC_{50} . The conformers (maximum of 1000) for each ligand were generated by mixed Monte Carlo Multiple Minimum/Low Mode rapid sampling method. The generated conformers were energy minimized using OPLS 2005 force field (Dixon et al., 2006). The OPLS 2005 force field is one of the preferable force fields for biological systems and organic molecules. It has improved solvation free energies in comparison to other systems like AMBER or CHARMM force fields (Shivakumar et al., 2010). The cutoff value for conformer redundancy was set at 1 Å RMSD. The maximum number of PLS factors that could be used for calculations was $N/5$, where N is the number of molecules in the training set. A PLS factor value of 5 was used to validate the wild and T877A mutant AR antagonist. A PLS factor value of 3 was used for full antagonist. Atom based 3D-QSAR method was followed by applying default parameters.

Homology Modelling and Docking

Schrodinger PRIME (v3.7) was used for protein structure prediction, side chain optimization, loop prediction, active site refinement, and energy minimization. The amino acid sequence of the T877A mutant AR was obtained from NCBI. The T877A mutant AR (PDB: 2OZ7) was used as the template. This was co-crystallized with antagonist cyproterone acetate and has a resolution of 1.80 Å. Regarding the homology modeled AR, its ligand binding domain has 671-881 amino acids instead of 671-919 amino acids (Guo et al., 2012). The homology modelled AR thereby lacks the helix-12 amino acids. The alignment between the target and template sequence was carried out by Clustalw method. The sequence identity between the target and template was 100%. The ligand (cyproterone acetate) and a water molecule (HOH-108) were retained in the final model. The homology model was then energy minimized (OPLS 2005) and the active site was further refined.

The ligands for docking studies were prepared using LigPrep, Schrödinger. The ligands were geometrically refined and assigned appropriate protonation states at pH 7.0 ± 0.2 . The energy minimization was carried out by OPLS 2005 force field. The AR proteins: T877A mutant (2OZ7), and homology model (truncated helix-12) were used for visualizing the dockings into their respective active sites. The proteins were prepared using the protein preparation wizard. The grid was assigned by picking the ligand as the center and applying default parameters. The docking was carried out using GLIDE, Schrödinger. GLIDE XP (extra precision), and SP (standard precision) methods were followed for the docking calculations.

The homology model was validated in the structural analysis and verification server (SAVES) (Messaoudi et al., 2013). The amino acids in the favorable, allowed and disallowed regions were identified by Ramachandran plot. The stereochemistry of the amino acids in the homology model was evaluated by PROCHECK. The 3D compatibility of the homology model was validated by VERIFY_3D. The homology model passed all the criteria for a good protein structure. The percentage of amino acids in the favorable region, allowed region and disallowed regions were 96.2%, 3.8% and zero respectively. The docking studies were validated by calculating the root mean square deviation (RMSD) of the crystal and docked conformation of cyproterone acetate. The RMSD between the predicted and crystal structure was 0.46 Å. The maximum allowable limit is 2 Å (Tripathi et al., 2013).

RESULTS AND DISCUSSION

Dataset Preparation

Selection of training molecules is an important step for developing a 3D-QSAR model with good predictive power. The activity (IC_{50}) for wild type AR was evaluated in VCaP cell line. The activity for T877A mutant AR was evaluated in LNCaP cell line. The majority of the molecules were active in wild and T877A mutant AR expressing cell lines. However, the activity of the molecules varied between the cell lines. This is because the molecules exhibit different efficacy with wild and mutant T877A ARs. Hence, the IC_{50} values evaluated in the VCaP cell line was used in developing the 3D-QSAR model for wild type AR. Similarly, the IC_{50} values evaluated in LNCaP cell line was used in developing the 3D-QSAR model for T877A mutant AR. The separation of datasets as mentioned above will lead to the identification of preferential but not absolute 3D-QSAR for respective AR antagonists. Also, the molecules for the first and second datasets were not filtered for resistance. This means that the molecules in the dataset may or may not have agonist/partial agonist activity with either / both wild or T877A mutant AR. The molecules for the dataset of full antagonists were carefully selected by a two-step process. First, the ligands that could antagonize both wild and T877A mutant ARs were selected. The second step involved the filtering of the molecules for resistance. This means that none of the ligands in the dataset has agonist/partial agonist activity with either / both wild or T877A mutant AR. The activities of the molecules in this dataset were evaluated by luciferase reporter assay.

Selection and Validation of the Models

The best 3D-QSAR model was selected based on high correlation between the predicted and observed activity (R^2), predictive ability of the model (Q^2), low standard deviation (SD), and the probability of getting an actual result (p value) of the training set (Durdagi et al., 2011). The model was also validated by predicting a test set having wide range of biological activity. The correlation between the observed and predicted activity of the test set (R^2), Pearson-R, Predictive R^2 (R^2_{pred}), and the correlation between the observed and predicted activity of the test set with intercept set at zero (r^2_m) were used to evaluate the predictivity of the models. The models having the highest (at least >0.5) value for Q^2 , R^2_{pred} , and r^2_m were considered for selection (Pratim et al., 2009). From this selection, the model that had the highest R^2 value for training and test set molecules, Q^2 , R^2_{pred} , and r^2_m was considered as the best.

Wild Type AR

The molecules in the dataset were defined by the following pharmacophore site points: hydrogen bond acceptor (A), hydrogen bond donor (D), hydrophobic group (H), and aromatic ring (R). The number of “must match” pharmacophore site points were gradually decreased from 7 to 3 until all the actives were matched and scored successfully. The hypothesis having six pharmacophore site points survived the scoring functions. PHASE generates CPH by comparing the pharmacophore site points from two or more active ligands (Almerico et al., 2010). Therefore, the pharmacophore site points in the 3D-QSAR represent the spatial arrangement of the common pharmacophore features that are present among the active ligands. Based on the scoring; ADDHRR.295 was selected as the best model (Table 1). The 3D-QSAR has one acceptor group (A), two hydrogen bond donor groups (D), one hydrophobic group (H), and two aromatic rings (R) (Figure 2).

The active groups of the best fit molecules were evaluated by cube models (Figure 3 and Figure 4). During the construction of the 3D-QSAR, a rectangular grid is applied by PHASE to the aligned training set molecules. The grid comprises all the substitutions in the pharmacophore site points. Then by correlating the observed activity and the atoms in the grid space, the PHASE generates the cube models. The cube models have a score value, which being less than zero means the atoms in the grid space does not favor the activity and greater than 1 will favor the activity. The space occupied by the atoms which does not favor the activity is indicated in red color. The space occupied by the atoms which favors the activity is indicated in blue color (Dixon et al., 2006). Hence, the blue cubes represent the favorable regions for activity and the red cubes represent the unfavorable regions for activity. The 4-nitrile and 3- CF_3 substitutions in ring R10 were favorable regions for activity. The 3- CF_3 substitution at ring R11, which is the hydrophobic H7 site point, also favors the activity. However, the -OH group and sulphur atom in the linker region between R10 and R11 were unfavorable for activity. The H atom of the hydroxyl group is the donor D4 site point. This indicates that although it is one among the pharmacophore site points, it decreases the activity. The observed and predicted activities of test and training set molecules are given in the supplementary data (Tables S1 and S2) (<https://doi.org/10.4018/ijqspr.2017070105>). The correlation between the observed and predicted activity of the training set was 0.9. The model was validated by predicting the test set having wide range of biological activity. The correlation between the observed and predicted activity of the test set was 0.76. Also, the ADDHRR.295 accurately predicted the biological value of AR antagonist, enzalutamide (residual activity = 0.14).

T877A Mutant AR

The dataset generated A, D, H, and R pharmacophore site points. The hypothesis having five pharmacophore site points survived the scoring functions. Based on the scoring, AHHR.266 was selected as the best model (Table 1). The pharmacophore has one acceptor group (A), two hydrophobic groups (H) and two aromatic rings (R) (Figure 5). The active groups of the best fit molecule were evaluated by cube models (Figures 6 and 7). The blue cubes represent the favorable regions for activity

Table 1. Statistics of the 3D-QSAR models

In	ID	Training						Test			
		PLS	SD	R ²	F	P	Q ²	R ²	r ² m	R ² _{pred}	Pearson-R
Wild	ADDHRR.295	5	0.13	0.91	171.1	1.918e ⁻⁴³	0.62	0.76	0.76	0.72	0.87
T877A	AHHRR.266	5	0.11	0.94	294.5	8.649e ⁻⁵⁶	0.62	0.74	0.74	0.69	0.86
Full	AHRR.63	3	0.2	0.94	152.4	7.536e ⁻¹⁸	0.58	0.80	0.75	0.83	0.89

Figure 2. Representation of the distances between the pharmacophore site points of wild type AR

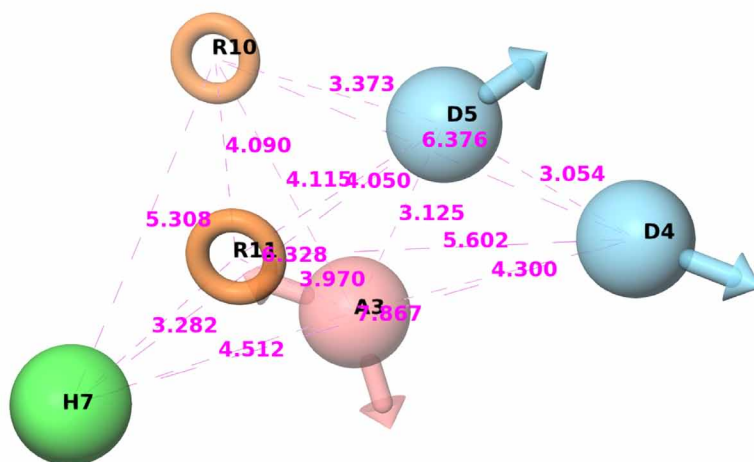


Figure 3. Representation of the best fit molecule with the wild type 3D-QSAR

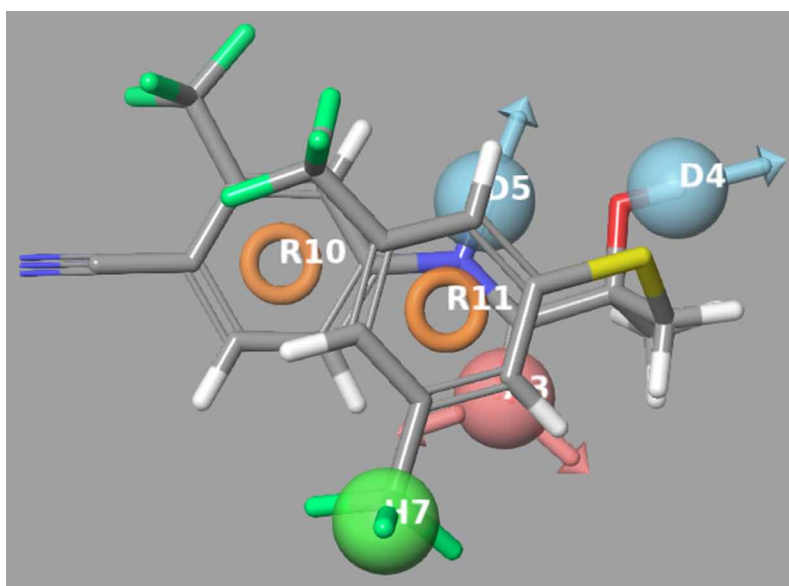


Figure 4. Representation of the cube model of the wild type 3D-QSAR best fit molecule

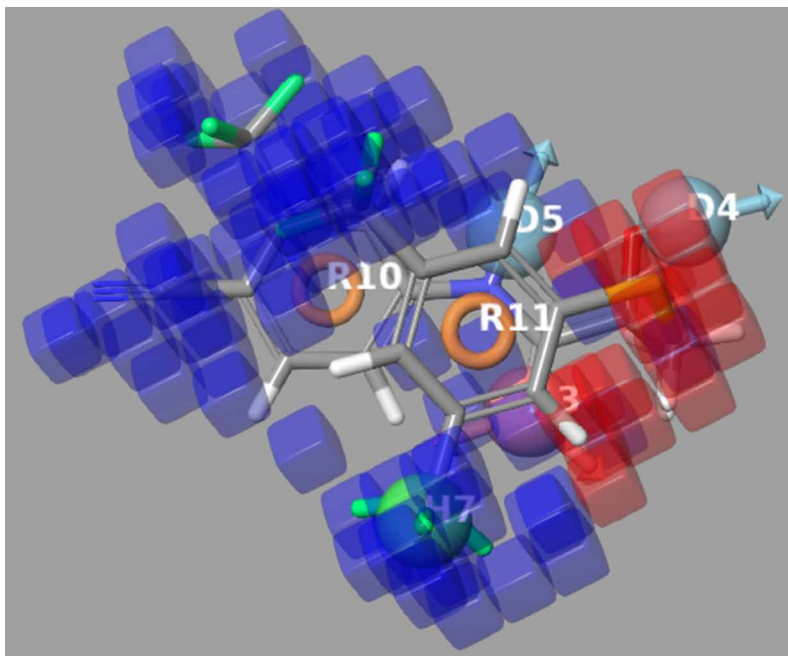
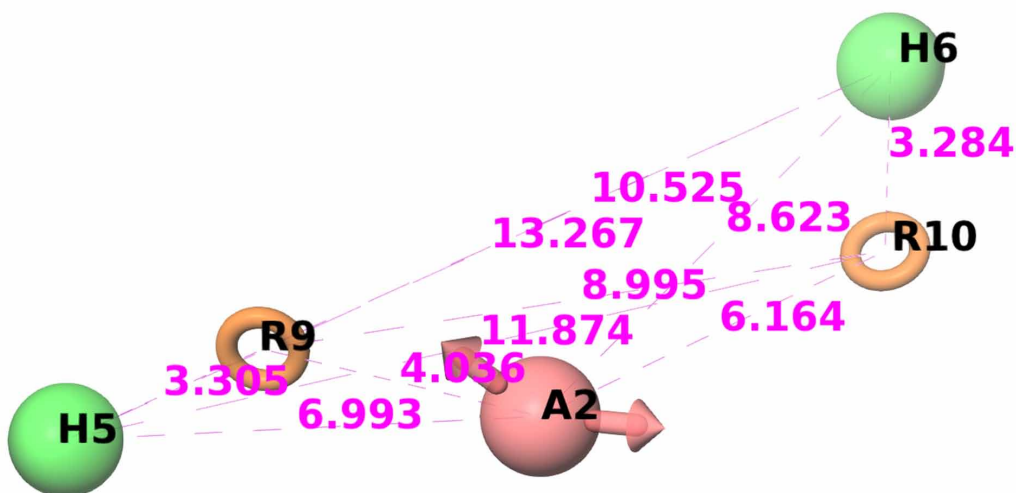


Figure 5. Representation of the distances between the pharmacophore site points of T877A mutant AR



and red cubes represent the unfavorable regions for activity. The 4-nitro and 3-CF₃ substitutions in ring R9 are favorable regions for activity. The 3-CF₃ group is the hydrophobic H5 site point. The 3 and 5-CF₃ substitutions at ring R10 also favors the activity. The 3-CF₃ substituent is also the hydrophobic H6 site point. However, the -OH and sulphur atom in the linker region between R10 and R11 were unfavorable for activity. The observed and predicted activities of all the ligands in the training and test sets are given in Supplementary section (Tables S1 and S2). The correlation between

Figure 6. Representation of the best fit molecule with the T877A mutant 3D-QSAR

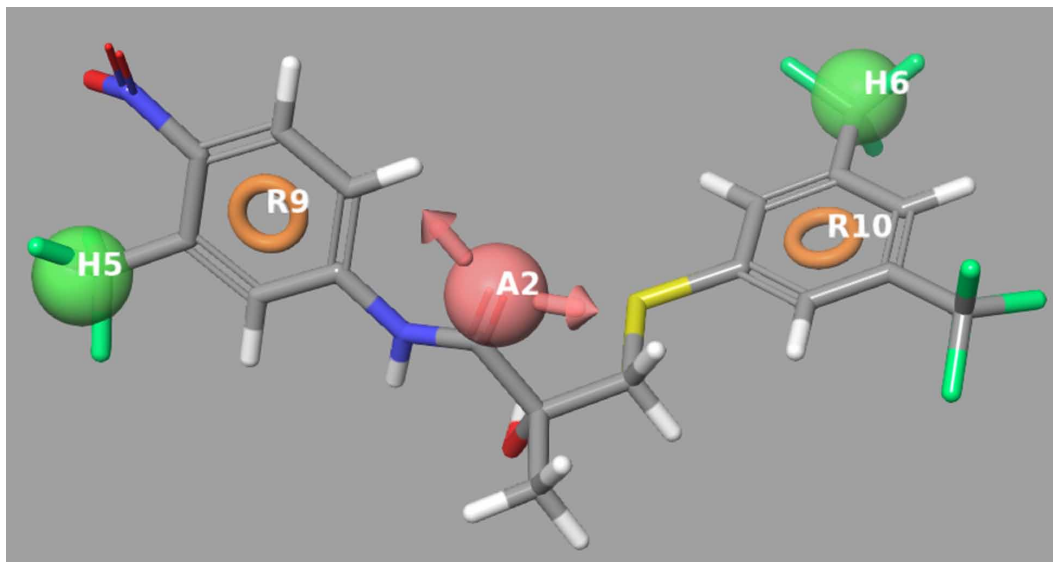
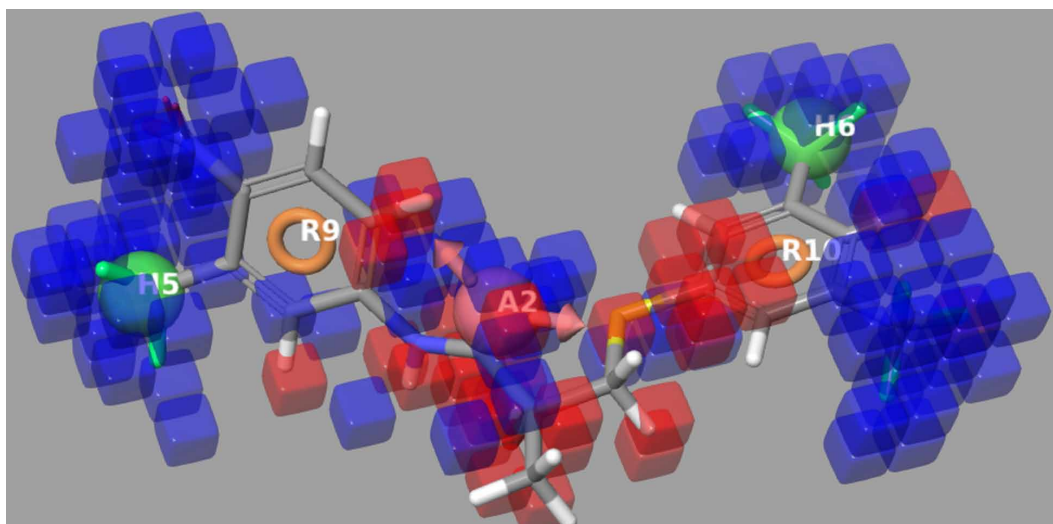


Figure 7. Representation of the cube model of the T877A mutant 3D-QSAR best fit molecule



the observed and predicted activity of the training set and test set was 0.94 and 0.74, respectively. The model AHHRR.266 accurately predicted the biological activity of AR antagonist enzalutamide (residual activity = 0.06). The biological activity of enzalutamide has wide variations between wild and mutant ARs. Enzalutamide is ~5 times selective towards T877A mutant AR. The 3D-QSAR models for wild and T877A mutant AR could identify the differences in the structural features of enzalutamide. This indicates that these models could provide the possible breakthrough needed to overcome AR resistance.

Full Antagonist

The corresponding dataset has activities of the full antagonists listed for both the wild type and the mutant AR. We chose the dataset for the wild type because the resistance develops only during the course of the treatment. The dataset generated A, D, H, and R pharmacophore site points. The hypothesis having four pharmacophore site points survived the scoring functions. The list of the entire CPH in their rank order is given in the Supplementary section. Based on scoring; AHRR.63 was selected as the best model (Table 1). The pharmacophore has one H-Bond acceptor group (A), one hydrophobic group (H), and two aromatic rings (R) (Figure 8). The active groups of the best fit molecule were evaluated by cube models as described above for the wild and mutant modeling (Figure 9 and Figure 10). The 4-nitrile (A1 site point) and 3-Cl substitutions in ring R11 are favorable regions for activity. These regions are occupied by blue cubes. The methyl group that follows the 4-amide in ring R10 also favors the activity. The N atom in the pyridine ring R10 and the -OH group in the linker region between R11 and R10 were also favorable for activity. The observed and predicted activities of all the molecules in the dataset are given in the supplementary data (Tables S3 – S6). The correlation between the observed and predicted activity of the training and test sets were 0.94 and 0.79, respectively. This 3D-QSAR pharmacophore did not match with any of the existing AR antagonists (both wild and mutant). This indicates the hybrid nature of the full antagonist pharmacophore. Recall that all the marketed AR antagonists develop resistance during the course of the treatment.

Similarity and Difference Between the 3D-QSAR Models

The molecules in the dataset for the construction of the 3D-QSAR models have common structures, which are also present in the marketed drugs (Figure 11). All the marketed ligands have two rings (A and B) separated by a linker group. These two rings (A and B) were present in all the 3D-QSAR models. Notably, the substitutions of 4-nitro / 4-nitrile groups and 3-CF₃ / 3-Cl groups in the A ring are favorable for activity as explained by the cube models. Similarly, the hydrophobic substitutions at 3rd, 4th, and 5th position in the B ring also favored the activity. The major difference among the 3D-QSAR models was the distance and angle between the A ring and B ring. Also, there is a difference in the distance between the two extreme pharmacophore site points. These properties describe the variability in the length and flexibility among the active molecules. The shortest distances are for wild type AR antagonist (A ring to B ring: 4.09 Å and D4 to H7: 7.867 Å). The angle between the A ring and B ring is always acute (<90°), with the ordinates in the linker region (R10-D4-R11 = 39.3°, R10-D5-R11 = 66°, R10-A3-R11 = 60.8). The shorter distances and acute angle between the A ring and B ring indicate a flexible linker region among the active molecules. The longest distances are for the T877A mutant antagonist (ring A to ring B: 8.895 Å and H5 to H6: 13.267 Å). The angle between the A ring and B ring is always obtuse (>90°), with the ordinates in the linker

Figure 8. Representation of the distances between the pharmacophore site points of full antagonist

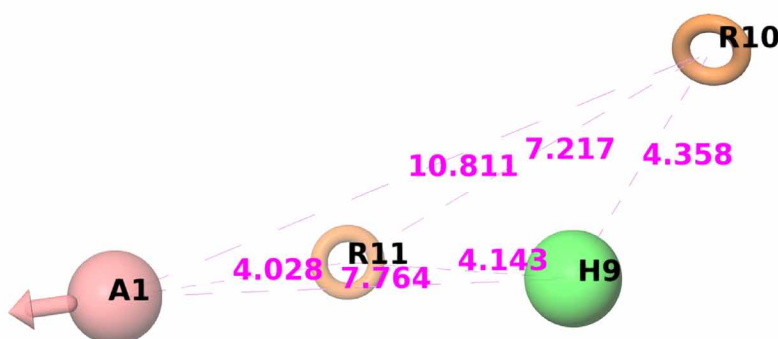


Figure 9. Representation of the best fit molecule with the full antagonist 3D-QSAR

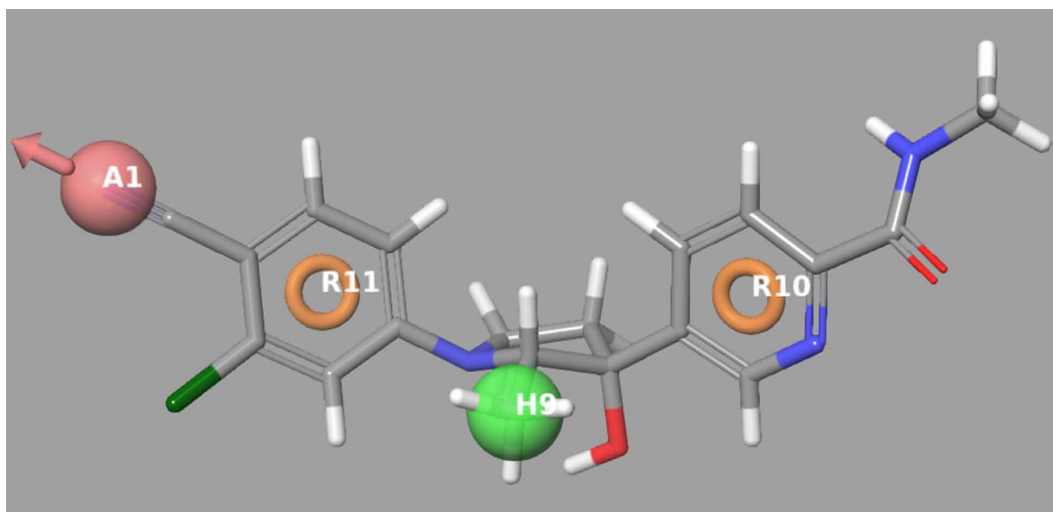
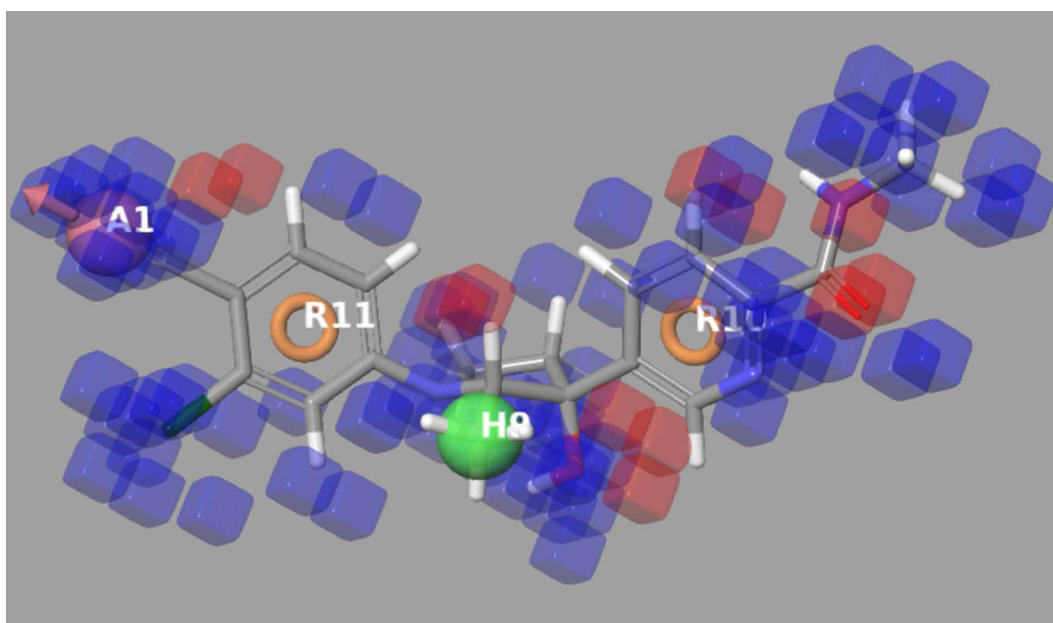


Figure 10. Representation of the cube model of the full antagonist 3D-QSAR best fit molecule

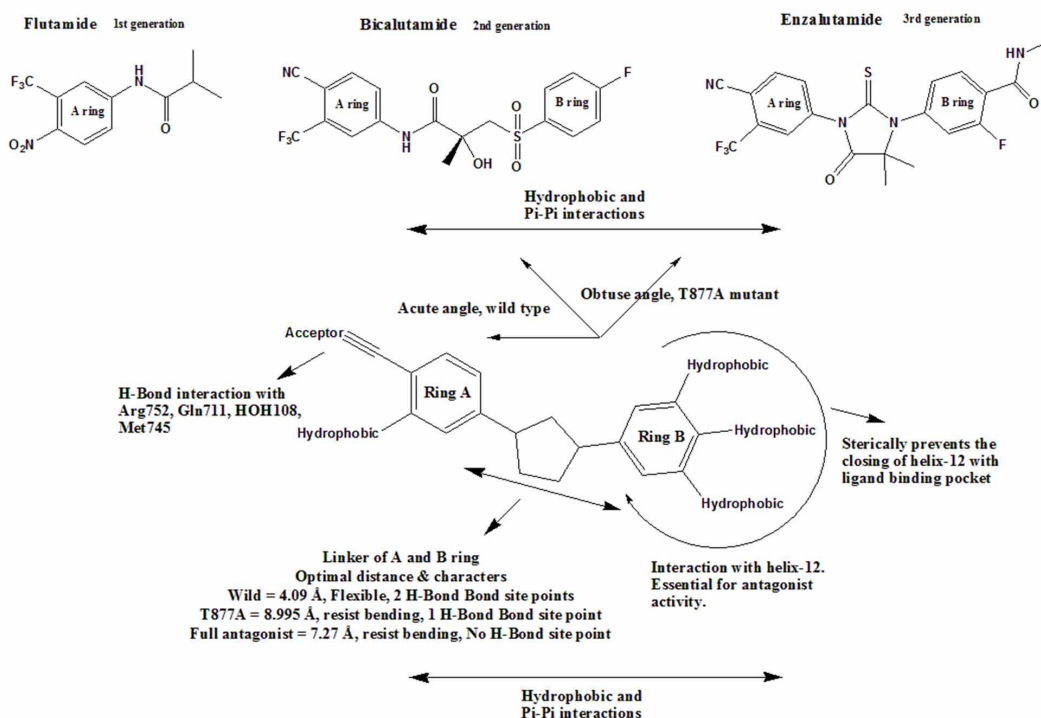


region (R10-A2-R9 = 122.3°). The longer distances and obtuse angles between the A and B rings indicate a less flexible linker region among the active molecules. The distances of the full antagonist pharmacophore are marginally less than the T877A mutant 3D-QSAR (ring A to ring B: 7.217 Å and A1 to R10: 10.811 Å). Also, the angle between the A and B rings is always obtuse (>90°), with the ordinates in the linker region (R10-H9-R11 = 116.2°). The relatively longer distances and obtuse angles between the A and B rings indicate a less flexible linker region among the active molecules. Notably, the 3D-QSAR of full antagonists does not represent the site points for H-Bond interaction in the linker region. The 3D-QSAR of wild type AR favors H-bond interaction in the linker region

when compared to the other two. This is because it has 3 pharmacophore points (A1, D4 and D5) in the linker region, which could form H-Bond interactions.

The identified similarities and differences of the pharmacophore site points and favorable substitutions were evaluated for their interactions with the AR. This is essential because most of the functional groups will be involved in interactions with AR, which decides the efficacy and resistance of the molecules. The favorable regions, 4-nitro or 4-nitrile substitutions in the A ring participate in the H-Bond interaction with amino acids Arg752, Gln711, and HOH108 (Bohl et al., 2005). These interactions with AR are essential for specific binding. The B ring of the AR antagonist interacts with the helix-12 region, which in turn, determines the agonist and antagonist proclivities of the ligands. The ligands, which could displace the helix-12 away from the binding pocket, will block the activation of the AR and function as antagonists. The ligands, which do not affect the conformation of helix-12, will function as an agonist/partial agonist. The mutations in AR increase the space within the ligand binding pocket to accommodate for ligands without the displacement of helix-12 from the binding pocket (Bohl et al., 2005, Osguthorpe et al., 2011). This displacement of helix-12 away from the ligand binding pocket, unveils the binding surface for co-repressor NcoR/SMRT interaction, which leads to the inhibition of the AR mediated transcriptional activity (Hodgson et al., 2008). All our models have shown that the hydrophobic substitution at 3rd or 4th or 5th position in the B ring favored the antagonistic activity. This could be because those ligands could increase the steric clash between the ligand and helix-12 amino acids, thereby favoring the antagonist activity. From these 3D-QSAR models, we could possibly deduce that smaller and/ or flexible molecules could be sufficient to block wild type AR. For T877A mutant AR, a bigger molecule in length plus less flexibility would be required to block it.

Figure 11. The 2D diagram representing the essential features of pharmacophore



Ligand and Structure Based Screening

The 3D-QSAR of full antagonist was used for screening the SPECS database for the identification of possible matches (Darshit et al., 2014). Searching for hits using the 3D-QSAR model generated by the wild type may lead to identification of smaller and / or highly flexible molecules. Those molecules could be kept within the binding pocket when the binding pocket becomes bigger as in the case of mutation. We also chose not to use T877A mutant 3D-QSAR model because the mutation is specific to flutamide treatment (Hara et al., 2003). Moreover, the AR antagonist will be administered when there is no mutation in AR and the mutation only occurs during the treatment. Hence, the hits were identified from full antagonist pharmacophore. This will identify ligands with optimal bulk, which will efficiently antagonize wild type AR and could possibly resist the mutations. The full antagonist cannot access the binding pocket with helix-12 in agonist conformation. The AR antagonist, enzalutamide, did not have binding affinity for with helix-12 positive AR. Therefore, a homology model receptor was built without helix-12. The ligands which could bind with helix-12 positive AR might not be full antagonists. Those ligands could be easily converted into agonist when mutation occurs. The H-Bonding pattern also influences the resistance to some extent. There are two sets of H-Bond interactions that could occur between a ligand and AR. The amino acids Arg752, Gln711 and HOH108 are present deep inside the binding pocket. The amino acids Leu704, Thr877 and Asn705 are present laterally to the helix-12. Preferential H-Bond interaction with amino acids near helix-12 prevents the ligand from clashing with the same (Guo et al., 2012). Hence, the ligands should preferentially form H-Bond interactions only with the deep residues.

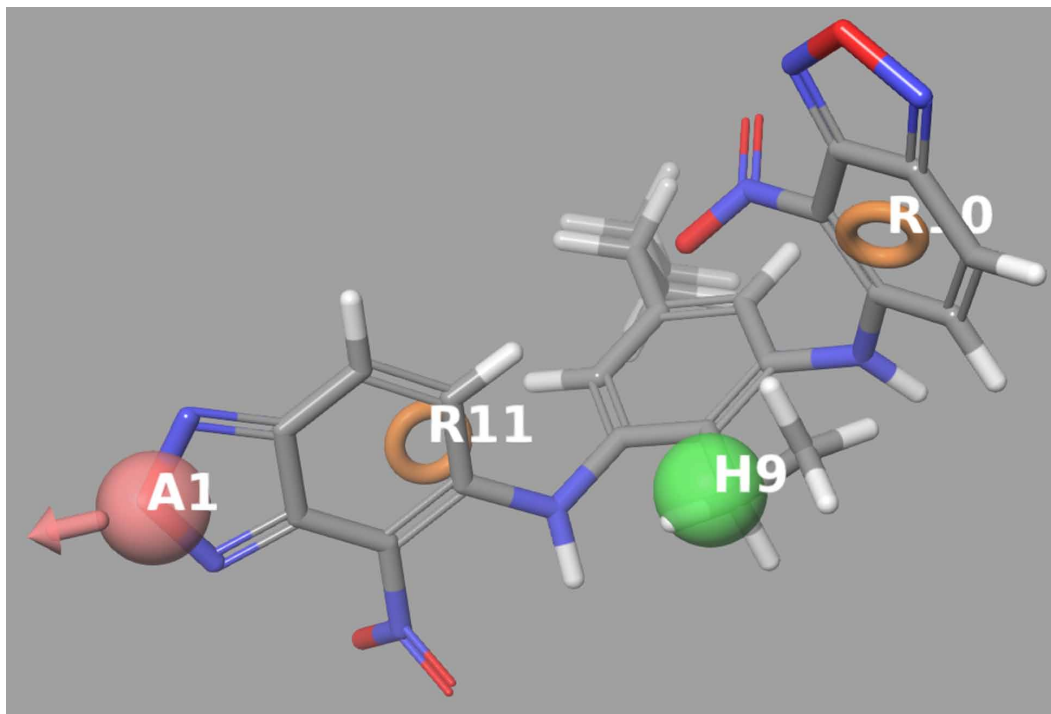
Hits Identification

The 3D-QSAR model of full antagonist was used to find matches in the SPECS database (>1 million compounds). The pharmacophore matched ligands (1001 ligands) were ranked according to the fitness score (maximum of 3). The ligands with fitness score >2 (666 ligands) were subjected to structure based screening. Initially, the ligands were screened for optimum bulkiness by docking with helix-12 positive AR. The ligands that did not have binding affinity for helix-12 positive AR were selected for the next step. This filtering will thus eliminate the less bulky / highly flexible ligands and reduce the total ligands to 192. These remaining ligands were docked with helix-12 negative AR by extra precision (XP) glide docking method. Here we selected molecules that form H-Bond interaction with deep residues (Arg752, Gln711, etc.) and not with ones present near the helix-12 (Asn705, Leu704, etc.). Only one molecule passed the H-Bond query. The ligand (SPECS ID: 88/32738047) has a fitness score of 2.002/3 (Figure 12). The interaction between the hit molecule and AR is given in the Supplementary section (Figure S1). The hit molecule has two nitro groups which may cause toxicity. This is because the nitro-aromatic compounds could be bio-activated in the liver and could cause hepatotoxicity (Boelsterli et al., 2006). The AR antagonist flutamide also exhibited hepatotoxicity possibly because of the presence of nitro-aryl group. We also ran the generated full antagonist pharmacophore with the compounds in the first two data sets (wild and mutant) and also among the compounds from our previous study (Elencheran et al., 2016). But none of the compounds displayed a fitness value over the threshold of 2. Thus, the output generated by this screening should give more clues and directions in designing novel molecules for resistant AR proteins.

CONCLUSION

In this study, we have identified the pharmacophore from three different AR antagonist datasets. The models of wild and T877A mutated ARs could be used to differentiate or identify the structural features of the respective antagonists. The full antagonist 3D-QSAR model could be used to designing aspects for the identification of hit molecules. The differences in the pharmacophore indicate that a major change in the bulk and flexibility of the existing AR antagonist was required to overcome resistance.

Figure 12. Representation of the pharmacophore match of the identified hit



Other relevant filters were also employed for the identification of hits. This led to the identification of only one hit starting with >1 million compounds in the database. Combining the 3D-QSAR and docking studies, we propose that the AR antagonist should preferably form H-Bond interactions with deep amino acid residues (Gln711, Arg752, HOH108) in the active site. Since the mutations increase the space within the ligand binding pocket, the AR antagonist should have additional bulky group(s) and has to attain an optimal conformation in order to push the 12th helix away from the ligand binding pocket. The antagonist that could overcome the mutations will thus be a relatively flat and rigid molecule that resists bending. This is because the flexible ligands might be packed within the mutated receptor binding pocket. Hence, the bulky group(s) in the flexible ligands would not reach the 12th helix to induce the steric clash. The helix-12 positive and negative ARs could be effectively used to differentiate AR antagonists from agonists and partial agonists. Agonists and partial agonists bind to the ligand binding pocket while the 12th helix is in closed conformation. The pure antagonist will not bind to the receptor binding site in 12th helix closed conformation and will only access it in the absence of 12th helix. This hypothesis could then be used in the further structure based screening for AR antagonists that overcomes resistance.

CONFLICT OF INTEREST

The authors report no conflict of interest.

REFERENCES

- Almerico, A. M., Tutone, M., & Lauria, A. (2010). 3D-QSAR pharmacophore modeling and in silico screening of new Bcl-xl inhibitors. *European Journal of Medicinal Chemistry*, 45(11), 4774–4782. doi:10.1016/j.ejmech.2010.07.042 PMID:20728251
- Balk, S. P. (2002). Androgen receptor as a target in androgen-independent prostate cancer. *Urology*, 60(3), 132–138. doi:10.1016/S0090-4295(02)01593-5 PMID:12231070
- Bassetto, M., Ferla, S., Pertusati, F., Kandil, S., Westwell, A. D., Brancale, A., & McGuigan, C. (2016). Design and synthesis of novel bicalutamide and enzalutamide derivatives as anti proliferative agents for the treatment of prostate cancer. *European Journal of Medicinal Chemistry*, 8(118), 230–243. doi:10.1016/j.ejmech.2016.04.052 PMID:27131065
- Boelsterli, U. A., Ho, H. K., Zhou, S., & Leow, K. Y. (2006). Bioactivation and hepatotoxicity of nitroaromatic drugs. *Current Drug Metabolism*, 7(7), 715–727. doi:10.2174/138920006778520606 PMID:17073576
- Bohl, C. E., Gao, W., Miller, D. D., Bell, C. E., & Dalton, J. T. (2005). Structural basis for antagonism and resistance of bicalutamide in prostate cancer. *Proceedings of the National Academy of Sciences of the United States of America*, 102(17), 6201–6206. doi:10.1073/pnas.0500381102 PMID:15833816
- Bohl, C. E., Miller, D. D., Chen, J., Bell, C. E., & Dalton, J. T. (2005). Structural basis for accommodation of nonsteroidal ligands in the androgen receptor. *The Journal of Biological Chemistry*, 280(45), 37747–37754. doi:10.1074/jbc.M507464200 PMID:16129672
- Darshit, B. S., Balaji, B., Rani, P., & Ramanathan, M. (2014). Identification and in vitro evaluation of new leads as selective and competitive glycogen synthase kinase-3 β inhibitors through ligand and structure based drug design. *Journal of Molecular Graphics & Modelling*, 53, 31–47. doi:10.1016/j.jmgm.2014.06.013 PMID:25064440
- Dixon, S. L., Smondyrev, A. M., Knoll, E. H., Rao, S. N., Shaw, D. E., & Friesner, R. A. (2006). PHASE: a new engine for pharmacophore perception, 3D QSAR model development, and 3D database screening: 1. Methodology and preliminary results. *Journal of Computer-Aided Molecular Design*, 20(10-11), 647–671. doi:10.1007/s10822-006-9087-6 PMID:17124629
- Durdagi, S., Duff, H. J., & Noskov, S. Y. (2011). Combined receptor and ligand-based approach to the universal pharmacophore model development for studies of drug blockade to the hERG1 pore domain. *Journal of Chemical Information and Modeling*, 51(2), 463–474. doi:10.1021/ci100409y PMID:21241063
- Elencheran, R., Saravanan, K., Bhaswati, B., Divakar, S., Kabilan, S., & Ramanathan, M. et al.. (2016). Design and development of oxobenzimidazoles as novel androgen receptor antagonists. *Medicinal Chemistry Research*, 25(4), 539–552. doi:10.1007/s00044-016-1504-3
- Feldman, B. J., & Feldman, D. (2001). The development of androgen-independent prostate cancer. *Nature Reviews. Cancer*, 1(1), 34–45. doi:10.1038/35094009 PMID:11900250
- Fenton, M. A., Shuster, T. D., Fertig, A. M., Taplin, M. E., Kolvenbag, G., Bublely, G. J., & Balk, S. P. (1997). Functional characterization of mutant androgen receptors from androgen-independent prostate cancer. *Clinical Cancer Research*, 3(8), 1383–1388. PMID:9815822
- Ferla, S., Bassetto, M., Pertusati, F., Kandil, S., Westwell, A. D., Brancale, A., & McGuigan, C. (2016). Rational design and synthesis of novel anti-prostate cancer agents bearing a 3,5-bis-trifluoromethylphenyl moiety. *Bioorganic & Medicinal Chemistry Letters*, 26(15), 3636–3640. doi:10.1016/j.bmcl.2016.06.001 PMID:27301368
- Gao, W. (2010). Androgen receptor as a therapeutic target. *Advanced Drug Delivery Reviews*, 62(13), 1277–1284. doi:10.1016/j.addr.2010.08.002 PMID:20708648
- Guo, C., Pairish, M., Linton, A., Kephart, S., Ornelas, M., Nagata, A., & Fanjul, A. N. et al. (2012). Design of oxobenzimidazoles and oxindoles as novel androgen receptor antagonists. *Bioorganic & Medicinal Chemistry Letters*, 22(7), 2572–2578. doi:10.1016/j.bmcl.2012.01.116 PMID:22377517
- Hara, T., Miyazaki, J., Araki, H., Yamaoka, M., Kanzaki, N., Kusaka, M., & Miyamoto, M. (2003). Novel mutations of androgen receptor: A possible mechanism of bicalutamide withdrawal syndrome. *Cancer Research*, 63(1), 149–153. PMID:12517791

Hodgson, M. C., Shen, H. C., Hollenberg, A. N., & Balk, S. P. (2008). Structural basis for nuclear receptor corepressor recruitment by antagonist-liganded androgen receptor. *Molecular Cancer Therapeutics*, 7(10), 3187–3194. doi:10.1158/1535-7163.MCT-08-0461 PMID:18852122

Messaoudi, A., Belguith, H., and Ben H. J. (2013). Homology modeling and virtual screening approaches to identify potent inhibitors of VEB-1 β -lactamase. *Theoretical Biology and Medical Modelling*, 2(10), 22. doi:10.1186/1742-4682-10-22

Osguthorpe, D. J., & Hagler, A. T. (2011). Mechanism of androgen receptor antagonism by bicalutamide in the treatment of prostate cancer. *Biochemistry*, 50(19), 4105–4113. doi:10.1021/bi102059z PMID:21466228

Pratim, R. P., Paul, S., Mitra, I., & Roy, K. (2009). On two novel parameters for validation of predictive QSAR models. *Molecules (Basel, Switzerland)*, 14(5), 1660–1701. doi:10.3390/molecules14051660 PMID:19471190

Shivakumar, D., Williams, J., Wu, Y., Damm, W., Shelley, J., & Sherman, W. (2010). Prediction of Absolute Solvation Free Energies using Molecular Dynamics Free Energy Perturbation and the OPLS Force Field. *Journal of Chemical Theory and Computation*, 6(5), 1509–1519. doi:10.1021/ct900587b PMID:26615687

Tilley, W. D., Buchanan, G., Hickey, T. E., & Bentel, J. M. (1996). Mutations in the androgen receptor gene are associated with progression of human prostate cancer to androgen independence. *Clinical Cancer Research*, 2(2), 277–285. PMID:9816170

Tripathi, S. K., Muttineni, R., & Singh, S. K. (2013). Extra precision docking, free energy calculation and molecular dynamics simulation studies of CDK2 inhibitors. *Journal of Theoretical Biology*, 7(334), 87–100. doi:10.1016/j.jtbi.2013.05.014 PMID:23727278

Yamamoto, S., Kobayashi, H., Kaku, T., Aikawa, K., Hara, T., Yamaoka, M., & Ito, M. et al. (2013). Design, synthesis, and biological evaluation of 3-aryl-3-hydroxy-1-phenylpyrrolidine derivatives as novel androgen receptor antagonists. *Bioorganic & Medicinal Chemistry*, 21(1), 70–83. doi:10.1016/j.bmc.2012.11.001 PMID:23199477

Yamamoto, S., Matsunaga, N., Hitaka, T., Yamada, M., Hara, T., Miyazaki, J., & Ito, M. et al. (2012). Design, synthesis, and biological evaluation of 4-phenylpyrrole derivatives as novel androgen receptor antagonists. *Bioorganic & Medicinal Chemistry*, 20(1), 422–434. doi:10.1016/j.bmc.2011.10.067 PMID:22094279

Yamamoto, S., Tomita, N., Suzuki, Y., Suzaki, T., Kaku, T., Hara, T., & Ito, M. et al. (2012). Design, synthesis, and biological evaluation of 4-arylmethyl-1-phenylpyrazole and 4-aryloxy-1-phenylpyrazole derivatives as novel androgen receptor antagonists. *Bioorganic & Medicinal Chemistry*, 20(7), 2338–2352. doi:10.1016/j.bmc.2012.02.005 PMID:22391033

Anti-Cancer Agents in Medicinal Chemistry



Title: Design, synthesis and biological evaluation of novel 1, 3-thiazolidine-2, 4-diones as anti-prostate cancer agents

VOLUME: 17

Author(s): Ramakrishnan Elancheran, Kuppusamy Saravanan, Selvaraj Divakar, Sima Kumari, V. Lenin Maruthanila, Senthamarikannan Kabilan, Muthaiah Ramanathan, Rajlakshmi Devi and Jibon Kotoky

Affiliation: Division of Life Sciences, Institute of Advanced Study in Science and Technology, Guwahati-781035, Assam, Department of Chemistry, Annamalai University, Annamalai Nagar - 608002, Tamil Nadu, Department of Pharmacology, PSG College of Pharmacy, Coimbatore - 641 004, Tamil Nadu, Division of Life Sciences, Institute of Advanced Study in Science and Technology, Guwahati-781035, Assam, Division of Life Sciences, Institute of Advanced Study in Science and Technology, Guwahati-781035, Assam, Department of Chemistry, Annamalai University, Annamalai Nagar - 608002, Tamil Nadu, Department of Pharmacology, PSG College of Pharmacy, Coimbatore - 641 004, Tamil Nadu, Division of Life Sciences, Institute of Advanced Study in Science and Technology, Guwahati-781035, Assam, Division of Life Sciences, Institute of Advanced Study in Science and Technology, Guwahati-781035, Assam

Abstract: Androgen receptor (AR) is an attractive target for the treatment of prostate cancer. Structural modification and molecular docking-based virtual screening approaches were imposed to identify the novel 1,3-thiazolidine-2,4-diones (TZDs) by using Schrödinger (Maestro 9.5). The best fit molecules (3-12 & 23-31) were synthesized and characterized using spectroscopic techniques, then in vitro antioxidant and anti-prostate cancer activities were evaluated. Further, the structure of the intermediate (18) was confirmed by single crystal XRD analysis. Of these compounds, 29, 30 and 31 showed comparatively significant antioxidant activity and better antiproliferative activity against PC-3 & LNCaP cell lines. Also, a very low cytotoxicity was observed in the non-cancerous cell (3T3). The mechanism studies were performed through the gene expression for the compounds, dihydrotestosterone, R-bicalutamide, 29, 30 and 31. The compounds, 29, 30 and 31 significantly decreased the mRNA expression of AR-stimulated genes, PSA and TMPRSS2 which explains their anti-prostate cancer activity. ADME/T properties prediction of the compounds (3-12 & 23-31) showed the promising drug-likeness and pharmacokinetic parameters without any toxicity. Moreover, DFT calculations were apparently confirmed the stable conformer of the compound, 31. These findings may provide the essential information for the development of anti-prostate cancer agents.

Close

Print this page



Design, synthesis and biological evaluation of 2-(4-phenylthiazol-2-yl) isoindoline-1,3-dione derivatives as anti-prostate cancer agents



K. Saravanan^a, R. Elancheran^b, S. Divakar^c, S. Athavan Alias Anand^a, M. Ramanathan^c, Jibon Kotoky^b, N.K. Lokanath^d, S. Kabilan^{a,*}

^aDrug Discovery Lab, Department of Chemistry, Annamalai University, Annamalai Nagar 608002, Tamil Nadu, India

^bDrug Discovery Laboratory, Life Sciences Division, Institute of Advanced Study in Science and Technology, Guwahati 781035, Assam, India

^cDepartment of Pharmacology, PSG College of Pharmacy, Coimbatore 641004, Tamil Nadu, India

^dDepartment of Studies in Physics, University of Mysore, Manasagangotri, Mysuru 570 006, India

ARTICLE INFO

Article history:

Received 22 September 2016

Revised 8 January 2017

Accepted 23 January 2017

Available online 25 January 2017

Keywords:

Androgen receptor

Prostate cancer

AR antagonist

Isoindolinediones

Molecular docking

ABSTRACT

The structural modification and molecular docking-based screening approaches on thiazole-based isoindolinediones were imposed to find the novel 2-(4-phenylthiazol-2-yl) isoindoline-1,3-dione derivatives. The best fit compounds (**6a-n**) were synthesized and evaluated their antiproliferative activities on the prostate cancer cell lines (PC-3 & LNCaP). Among them, the compound, **6m** exhibited good activity, particularly on LNCaP ($IC_{50} = 5.96 \pm 1.6 \mu M$), moderately active against PC-3 cell lines as compared to bicalutamide. The compound, **6m** decreased the androgen-mediated transcription of ARE-mRNA in PSA, TMPRSS2, c-myc and cyclin D1 than R-bicalutamide. The compounds, **6e** and **6f** were reconfirmed through single crystal XRD analysis. The ADME profiling of the test compounds was evaluated to find the drug-likeness and pharmacokinetic parameters. These findings may provide vital information for the development of anti-prostate cancer agents.

© 2017 Elsevier Ltd. All rights reserved.

Prostate cancer (PCa) is the second leading causes of cancer-related deaths in men in the United States. The American Cancer Society has estimated that the diagnosis of 180,890 new cases and 26,120 deaths due to PCa in the United States in 2016¹ and still the incidence is rising. PCa magnification is mainly prompted by androgen and androgen receptor (AR), initially respond to standard androgen deprivation therapies usually relapse into a more truculent, castration-resistant prostate cancer (CRPC). Antiandrogens, such as abiraterone acetate, bicalutamide, cyproterone acetate, flutamide, enzalutamide, galeterone, hydroxyflutamide and nilutamide (Fig. 1) have been utilized for the androgen signal blockage, but they have several side effects.²

Ultimately, AR antagonist therapy is more efficacious for prostate cancer patients, results in castration-resistant due to gene mutations such as T877A mutation is activated by hydroxyflutamide and W741C mutation is found in bicalutamide-resistant PCa patients.^{3,4} Despite these current therapeutic options, CRPC still presents a great clinical challenge due to the inevitably ineluctable development of drug resistance. The drawbacks of

currently available drugs accentuate the desideratum for the development of incipient candidates with high anti-prostate cancer activities and low unpropitious effects. Aforetime, we have reported the design and development of oxobenzimidazoles as novel androgen receptor antagonists.⁵ In recent years, the development of various five-membered heterocyclic predicated scaffolds has been reported as anti-prostate cancer agents.^{6,7} However, the search of incipient novel antiandrogens found that thiazole derivatives were associated with sundry biological activities such as anticonvulsant, antimicrobial, antidiabetic and anticancer activities.^{8–11} Several reports revealed the characteristic properties of thiazole and isoindolinedione scaffolds to attribute various pharmacological properties. In particular, the 4-aromatic substituent on the 1,3-thiazole core could be considered as more potent and selective antitumor agents.¹² Therefore, these findings prompted our further investigations on the anti-tumor effects of thiazole-based isoindolinedione derivatives (Fig. 1).

Taking into account the intriguing properties of these thiazole-based isoindolinedione derivatives and in continuation of our research, we designed a series of novel 2-(5-phenylthiazol-2-yl) isoindoline-1,3-dione utilizing the Schrödinger (Maestro 9.5) software.¹³ The available AR crystal structures were either in agonist or partial agonist conformation which has helix 12 closed towards

* Corresponding author.

E-mail address: profdrskabilanau@gmail.com (S. Kabilan).

Design and development of oxobenzimidazoles as novel androgen receptor antagonists

R. Elancheran¹ · K. Saravanan² · Bhaswati Choudhury¹ ·
S. Divakar³ · S. Kabilan² · M. Ramanathan³ · Babulal Das⁴ ·
R. Devi¹ · Jibon Kotoky¹

Received: 5 February 2015 / Accepted: 6 January 2016 / Published online: 21 January 2016
© Springer Science+Business Media New York 2016

Abstract Antiandrogens are a novel class of anticancer agents that inhibit cancer cell proliferation and induce apoptosis in various cell lines. To find the lead compound from the oxobenzimidazole derivatives, receptor-ligand docking studies were initially performed using Schrödinger software. The best fit molecules were synthesized and characterized through IR, ¹H-NMR, ¹³C-NMR and HRMS analyses. The structure of compound (**9b**) was further confirmed by single-crystal XRD analysis. The cell viability of the compounds was determined by MTT assay to find IC₅₀ values against prostate cancer and breast cancer cell lines (PC-3, LNCaP, MCF-7 and MDA-MB-231). The ADME/T property studies were performed to rationalize the inhibitory properties of these compounds. It can be concluded from the study that **9b** is the most active compound from the series against PC-3 and LNCaP cell lines.

Keywords Androgen receptor · Prostate cancer · Antiandrogen · Breast cancer · Oxobenzimidazoles

Electronic supplementary material The online version of this article (doi:10.1007/s00044-016-1504-3) contains supplementary material, which is available to authorized users.

✉ Jibon Kotoky
jkotoky@gmail.com

- ¹ Drug Discovery Laboratory, Life Sciences Division, Institute of Advanced Study in Science and Technology, Guwahati, Assam 781035, India
- ² Department of Chemistry, Annamalai University, Annamalai Nagar, Tamilnadu 608002, India
- ³ Department of Pharmacology, PSG College of Pharmacy, Coimbatore, Tamilnadu 641 004, India
- ⁴ Department of Chemistry, Indian Institute of Technology, Guwahati, Assam 781035, India

Introduction

Androgen receptor (AR), belongs to the nuclear receptor subfamily, plays an important role in the development, growth, function and homeostasis of the prostate. The National Cancer Institute (NCI) has estimated that 220,800 men will be diagnosed with and 27,540 men will die of prostate cancer in the USA in 2015 (Ferlay *et al.*, 2010; Howlader *et al.*, 2015). Recently, we reported that AR is one of the attractive targets to treat prostate cancer (PCa) (Elancheran *et al.*, 2015b). Although androgens are often considered to be “male” hormones, they are also found at lower levels in women. Recent studies have found that AR is frequently expressed in primary breast tumors, is estimated to be 50–90 %, depending on the subtypes of breast cancer, and could respond to antiandrogen treatment (Fioretti *et al.*, 2014). Antiandrogens, such as bicalutamide (Chen *et al.*, 2005; Gao *et al.*, 2006), cyproterone acetate (Figg *et al.*, 2010; Neumann and Töpert, 1986), flutamide (Cleve *et al.*, 2011; Brogden and Clissold, 1989) and nilutamide (Hsieh and Ryan, 2008; Moguilewsky *et al.*, 1987; Kassouf *et al.*, 2003) have been used to block the androgen signal, but they have several side effects. Recently, novel AR antagonist, enzalutamide (Scher *et al.*, 2010; Tran *et al.*, 2009), has demonstrated efficacy against castration-resistant prostate cancer (CRPC) and estrogen receptor-negative tumors. Among the subtypes, triple-negative breast cancers (ER-, PR-, HER2-) were positive for AR expression and may respond to treatment with antiandrogen drugs (Ni *et al.*, 2011). ARN-509 (IC₅₀ = 16 nmol/L) binds AR with seven to tenfold greater affinity than the clinically approved antiandrogen, bicalutamide (median IC₅₀ = 160 nmol/L), and competes for the same binding site in the ligand-binding pocket of the receptor (Clegg *et al.*, 2012). As a result, there is an



PSG Institute of Medical Sciences & Research

Post Box No. 1674, Peelamedu, Coimbatore 641 004, INDIA
Phone : 91 422-2598822, 2570170 • Fax: 91 422-2594400
E-mail : psgmedschool@gmail.com Website : www.psgimsr.in

19th February, 2013

TO WHOMSOEVER IT MAY CONCERN

Animal Ethical Committee Clearance Certificate for pursuing PhD

This is to certify that, the doctoral work of **Mr S Divakar**, who is currently working as Junior Research Fellow, does not involve animals. His project is entitled "*Molecular modelling and screening of androgen receptor ligands to treat prostate cancer*", and he is working under the guidance of Dr M Ramanathan, PSG College of Pharmacy.

This certificate is given to facilitate the process of registration, for pursuing his Doctor of Philosophy (Ph.D).


Dr S Ramalingam
Principal

Dr. S. Ramalingam, M.D.,
Principal
PSG Institute of Medical
Sciences & Research
Peelamedu, Coimbatore - 641 004.